MODELLING OF THE THERMAL INTERACTIONS OF UNDERGROUND RAILWAYS WITH NEARBY VERTICAL GROUND HEAT EXCHANGERS IN AN URBAN ENVIRONMENT

Prepared by:

Akos Revesz BSc, MSc

A Thesis submitted in partial fulfilment of the requirements for the Degree of Doctor of Philosophy.

May 2017

School of the Built Environment and Architecture

London South Bank University

Supervisors:

Dr Issa Chaer, Professor Graeme Maidment, Dr Jolyon Thompson,

Dr Maria Mavroulidou and Professor Mike Gunn

`

ABSTRACT

Ground source heat pumps (GSHPs) can provide an efficient way of heating and cooling buildings due to their high operating efficiencies. The implementation of these systems in urban environments could have further benefits. In such locations ground source heat is potentially available from alternative sources such as underground railways (URs).

The potential benefits for using the waste heat generated by URs with localised GSHPs are established in this thesis. This was achieved through investigations of UR-GSHP interactions.

The research detailed here was mainly conducted through Finite Element (FE) numerical modelling and analysis. First a preliminary two-dimensional (2D) FE model was developed. This model was highly simplified to enable rapid analysis of the systems. The model was used to establish key parameters and phenomena for more detailed additional research.

Since the operation of the URs and GSHP involves complex, transient, three-dimensional (3D) transport phenomena and extreme geometrical aspect ratios, 3D numerical models of URs and vertical ground heat exchangers (GHEs) were independently developed and validated. These individual models were then built into the same modelling environment for their combined analysis. Initial investigations with the combined 3D model showed that interactions occur between URs and localised GSHPs.

In order to investigate the effect of specific parameter variations on the earlier established UR-GSHP interactions, a parametric analysis was conducted. The analysis included two sets of studies. The first group of studies considered different geometrical arrangements of the systems, and the second group investigated the effect of altered operational characteristics options on the interactions.

Overall the results suggested that the performance of a GSHP can be significantly improved if the GHE array is installed near to the UR tunnel. It was shown that the improvement on the GHEs average heat extraction rate due to the heat load from the UR tunnel can be high as ~ 40%, depending on the size and shape of the GHE array and its proximity to the UR tunnel(s). It was also concluded that if the design aim is to enhance the heat extraction rates of urban GSHP systems, constructing the GHEs as close as possible to the UR tunnel would be essential.

The results gathered from the parametric analysis were used to develop a formula. This formula is one of the key contributions to knowledge from this research. The formula

developed allows approximating the GHEs' heat extraction improvements due to the nearby tunnel(s) heat load(s). The formula makes use of a single variable named as interaction proximity. This variable was found to be one of the key parameters impacting on UR-GSHP interactions.

At the end of the thesis, conclusions are drawn concerning the thermal interactions of URs with nearby vertical GHEs and the numerical modelling of such systems. Recommendations for further research in this field are also suggested.

DECLARATION

The research described in this report is the original work of the author except where otherwise specified, or acknowledgment is made by reference.

It was carried out at The School of Built Environment and Architecture, London South Bank University and under the supervision of Dr Issa Chaer, Dr Jolyon Thompson, Prof. Graeme Maidment, Dr Maria Mavroulidou and Prof. Mike Gunn.

The work has not been submitted for another degree or award of another academic or professional institution during the research program.

Akos Revesz

ACKNOWLEDGEMENTS

The author wishes to express his grateful thanks to Dr Issa Chaer, Prof. Graeme Maidment, Dr Jolyon Thompson, Dr Maria Mavroulidou and Prof. Mike Gunn who have all provided valued help, guidance, encouragement and advice throughout the process of the PhD. Without their much appreciated support, this research would not have been possible.

Completing this PhD research at London South Bank University alongside its helpful and dedicated staff members has been a really positive experience and I would like to thank them. I am also grateful to my fellow PhD colleague Christina. She has not only been a supportive and kind friend but a truly inspirational colleague who I have learned a lot from.

Advice and assistance has been provided throughout by the industrial project partner London Underground Ltd. The support of Nicholas Boot-Handford who has regularly attended progress meetings and provided useful guidance has been greatly appreciated. The support provided by Jamie Burn until he left the company midway through the research is also acknowledged.

My family have always been supportive of my work and I would like to thank you to them for their guidance on my journey. The motivation and support offered by my mum and dad during many years of study has helped me to reach this far. I am also grateful for the support of my friends, in particular James and Ellie who have generously given their time and efforts to proof reading large sections of this thesis on a regular basis.

Finally I must thank my partner Lizzie, whose support, love and inspiration has helped to keep me on track. Completing our PhD journeys together was just the best thing ever…we are lucky!

CONTENTS

LIST OF FIGURES

LIST OF TABLES

NOMENCLATURE

Symbol	Description	Units
a	Amplitude	
A	Area	m^2
$\mathbf{n}$	Boundary Normal Pointing out of the Domain	
z	Coordinate in depth	
f_D	Darcy friction factor	
u	Darcy velocity	m/s
z	depth	m
d	Diameter	m
D	Elevation	m
p	Fluid pressure	Pa
$\mathbf{u}$	Fluid velocity field	m/s
T_p_out	GHE's fluid temperature at the pipe outlet	°C
q	Heat flux	W/m^2
Q	Heat load/source	W/m
h	Heat transfer coefficient	W/m^2*K
$q"$	Heat transfer rate	W/m^2
d_h	Hydraulic diameter of pipe	m
Hd	Hydraulic Head	m
h'	Integrating parameter (FLS)	
L	Length	m
H	Length of the heat exchanger (FLS)	m
g	Magnitude of gravitational acceleration	m/s^2
m	Mass flow rate	kg/s
U_0	Normal inflow speed	m/s
K	Permeability	m^2/s
e	Pipe surface roughness	mm
n	Porosity	
r	Radius	m
S_d	Saturation degree	
T_s_block	Soil block temperature	°C
T_s_tun	Soil temperature surrounding the tunnel	°C

C_p	Specific heat capacity at constant pressure	J/kg*K
T	Temperature	°C
k	Thermal conductivity	W/m*K
t	Time	sec
T_w_tun	Tunnel wall surface temperature	°C
$\dot{V}$	Volume flow rate	m^3/s
Z	Wall wetted perimeter	m
W	Width	m

Greek Symbol	**Description**	**Units**
ρ	Density	kg/m^3
μ	Fluid dynamic viscosity	Pa·s
Ω	Interaction proximity	
τ	Period	s
σ	Ratio between the effective heat capacity per unit volume of the ground and that of groundwater	
α	Thermal diffusivity	m^2/s
∇	Unit vector/gradient/directional change	

Subscripts

If a combination of subscripts is required the sections are strung together using an underscore to show a new section is included. For example if the average soil surface temperature was required the symbol would therefore be T_{S_surf}.

Symbol	**Description**
amb	Ambient
av	Average
eff	Effective
ext	External
f	Fluid

Gr	Ground
$init$	Initial
in	Inlet
i	Inside
int	Internal
$long$	Longitudinal
$Numb$	Number
out	Outlet
o	Outside
pi	Pipe
$plat$	Platform
S	Soil
$surf$	Surface
tun	Tunnel
$wall$	Tunnel wall
var	Variation
wat	Water

List of Abbreviations

BHE	Borehole Heat Exchanger
CoP	Coefficient of Performance
DECC	Department of Energy and Climate Change
DHN	District Heat Network
DST	Duct Storage
ED	Equivalent Diameter
FD	Finite Difference
FE	Finite Element
FLS	Finite Line Source
FV	Finite Volume
GHE	Ground Heat Exchanger
GSHP	Ground Source Heat Pump
HVAC	Heating, Ventilation and Air Conditioning
ICS	Infinite Cylindrical Source
ILS	Infinite Line Source

LS	Line Source
LSBU	London South Bank University
LU	London Underground
LUL	London Underground Limited
NDF	Number of Degrees of Freedom
PDE	Partial Differential Equation
RHI	Renewable Heat Incentive
RANS	Reynolds-averaged Navier-Stokes
SES	Subway Environment Simulation
3D	Three-dimensional
TPH	Trains Per Hour
2D	Two-dimensional
UR	Underground Railway

CHAPTER 1: INTRODUCTION

1.1 BACKGROUND AND IMPORTANCE

A major part of the energy used in the UK and elsewhere is for heating or cooling. In particular, more than 40% of fossil fuels are burnt for low temperature heating of buildings (Committee on Climate Change, 2009). This equates to more than 24% of UK carbon dioxide (CO_2) emissions (DECC, 2013). In March 2007, the European Council made a commitment to reduce greenhouse gas emissions by 20% by 2020 (European Commission, 2009). The UK Government went further and established a target to reduce the nation's CO_2 emissions overall by 80% by 2050 in comparison to a 1990 reference point (The Stationery Office, 2008). Even after major efforts to reduce demand by, for example, optimised industrial processes, improved insulation and reduced infiltration in buildings, a dramatic increase in the energy efficiency of heating and cooling processes through new and innovative low carbon technology will be needed if the 2050 target is to be met. As part of The Renewable Energy Strategy (Secretary of State for Energy and Climate Change, 2009), the UK Government indicated that the target could be achieved with 12% of heat energy demand being met by renewable sources. Financial incentives such as the Renewable Heat Incentive (DECC, 2012) which are designed to encourage the uptake of renewable heat technologies in the UK started to appear in 2014. Heat pumps were one of the technologies incentivised. Common sources of heat for heat pumps include ground, air and water. However, in urban settings, additional heat is accessible from alternative, secondary heat sources, such as sewers or underground railway (UR) tunnels. The London Mayor's 2050 Infrastructure Plan includes supplying a quarter of London's energy from local sources and exploiting the capital's waste heat resource (London City Hall, 2016). It was shown that the total heat which could be delivered from secondary sources in London is of the order of 71 TWh/year, which is more than the city's total estimated heat demand of 66 TWh/yr in 2010 (The Greater London Authority and Buro Happold, 2013).

Some heat sources have the limitation that their location is too far from where the heat is needed or that they are only available at a particular period of the year. However, UR tunnels are often in close proximity to areas of high heat demand and could potentially provide a year-round heat supply. The soil surrounding the tunnels also contains large amount of heat energy which could be extracted through ground source heat pumps (GSHP). However, the potential for this type of heat recovery has not yet been established and first the interactions of UR tunnels with neighbouring GSHPs must be fully understood.

This thesis describes a numerical investigation into this problem. Particular consideration was given to the geothermal heat transfer occurring in the soil which surrounds an UR tunnel and vertical type ground heat exchangers (GHEs) of GSHP systems.

1.2 THESIS CHAPTERS

Chapter 1 - Introduces the investigation that is described in this thesis.

Chapter 2 - Provides a critical literature review showing the need for this research to be undertaken. It explores alternative heat sources for heat pumps and establishes why URs are one of the most attractive secondary heat sources available in urban settings. A suitable modelling approach for the investigation of interactions of URs with localised GSHPs was identified.

Chapter 3 - Details the proposition for the work to be undertaken.

Chapter 4 - Describes the development of a finite element (FE) two-dimensional (2D) model. This preliminary model was highly simplified to enable rapid analysis of the system and establish key phenomena for more detailed additional research. The initial results clearly demonstrated that interactions occur between URs and nearby GHEs. As the operation of the URs and GSHPs involves complex, transient, three-dimensional (3D) transport phenomena and extreme geometrical aspect ratios, the numerical investigations were extended to a more explicit 3D modelling environment.

Chapter 5 - Details the development and validation of two different 3D numerical UR models, which differ in terms of their levels of complexity. The development and validations of these models are discussed in detail, together with their potential applicability.

Chapter 6 - Addresses the development and validation of 3D numerical single and double looped GHE models.

Chapter 7 - Introduces a combined UR and GHEs model, which was used to perform a preliminary study on their interactions.

Chapter 8 - Introduces a parametric study which used the combined 3D numerical model. The aim of this study was to investigate how different geometrical parameters and operational characteristics of the systems would impact on their interactions.

Chapter 9 – Presents conclusions from the literature review and from the 2D and 3D numerical modelling. Finally, the chapter suggests further possible research which would build on the work described in this thesis.

CHAPTER 2: CRITICAL LITERATURE REVIEW

2.1 INTRODUCTION

The critical literature review presented in this chapter explores why heat pumps have become an increasingly common choice for heating and cooling many types of buildings in the UK and elsewhere. It explores conventional and alternative heat sources for heat pumps. The chapter highlights why URs could be considered as one of the most attractive secondary heat sources in urban areas. The chapter explores the typical thermal environment that exists in UR tunnels and justifies using London as a case study for this research as a practical decision. Modelling approaches of both railways and GSHPs were reviewed and conclusions were derived in terms of what method could be used for the combined analysis of the systems.

2.1.1 Chapter Aims

Chapter 2 aimed to review the literature in the following areas:

- Types and operational characteristics of different heat pump systems
- Alternative heat sources are available for heat pumps in urban areas
- Underground railways as a secondary heat sources
- The London Underground as an alternative secondary heat source
- The heat strategy for London

2.1.2 Sources Searched for Relevant Literature

Sources searched for relevant literature are listed below.

- American Society of Heating, Refrigerating and Air-Conditioning Engineers (ASHRAE)
- British Library
- Chartered Institution of Building Services Engineers (CIBSE)
- Google Scholar
- Environmental Agency
- London South Bank University Library including the use of inter-library loans
- Science direct journal listings

These sources have been searched with the following keywords: Analytical, Geothermal, Ground Source Heat Pumps, Ground Heat Exchangers, Groundwater, London, Metro, Modeling, Numerical, Railway, Train, Tunnel, Underground.

The keywords above were also used to search the World Wide Web.

In total over 100 Journal and conference papers were obtained and these were catalogued in a Microsoft Excel spreadsheet. To allow ease of cross-referencing, each paper was categorised in one of the following subject areas:

- Ground and groundwater
- Heat transfer
- Modelling of Underground Railways
- Modelling of Ground Source Heat Pumps

2.2 HEAT PUMPS AND UNDERGROUND RAILWAYS

2.2.1 Heat Pumps and Their Typical Heat Sources

2.2.1.1 Heat pump types

Typically heat pumps use electricity to raise the temperature of low grade heat to high grade. The Coefficient of Performance (CoP), which indicates the efficiency, depends largely on the temperature difference between the heat source and the heat supplied; the greater the difference, the less efficient the heat pump. Common sources of heat for heat pumps include ground, air and water. GSHPs can achieve higher operating efficiencies compared to air source heat pumps. This is because the ground usually has a lower temperature than the outdoor air during the cooling season, and a higher temperature than the outdoor air in the heating season. GSHPs systems typically require between 0.22 and 0.35 kWh of electricity for each kWh of heating or cooling output. This can be 30–50% less than the seasonal power consumption of air-to-air heat pumps (Lund *et al.*, 2004).

2.2.1.2 Ground source heat pumps

The earth is continually absorbing heat from the sun. Although the surface of the earth is subject to seasonal temperature fluctuations, below a depth of 10 to 15 m the ground temperature is approximately equal to the mean annual air temperature (8-11°C in the UK) (BGS, 2017). A GSHP is designed to use this constantly renewed energy resource. The schematics of the two common types of GSHP system configuration, i.e. open and closed-loop systems, are illustrated in Figure 2.1. Open-loop systems extract heat from ground water, usually abstracted from an aquifer via a borehole, which is passed through a heat pump where heat is extracted from the water. This type of system will only work in areas where there is sufficient ground water available. Closed-loop systems pump an anti-freeze solution through pipes buried in the ground. GSHPs commonly serve both small residential houses with only several kW's of heat output as well as large commercial buildings with over a MW of capacity. These systems are commonly installed in rural as well as urban settings.

One great example for a larger sized GSHP installation in an urban area is a hybrid GSHP system which has been installed at the Keyworth 2 building in Keyworth Street, London. The GSHP system consists of four heat pumps linked to energy piles and a dry air cooler. The plant room where the heat pumps are located is on the top floor of the building close to the position of the dry air cooler. The ground loop is composed of a total of 348 geothermal loops placed in 174 foundation piles, with two geothermal loops in each. The piles have a diameter of between 600 and 750 mm, with an average depth of 26 m. Each of the heat pumps has a capacity of 126.6 kW in heating and a capacity of 172.3 kW in cooling serving the entire heating and cooling demand of the building.

2.2.1.3 Typical types of GHEs for GSHPs

The principle of GSHPs is to connect heat pumps to the ground using ground heat exchangers (GHEs). Two of the most common types of vertical GHEs in the UK are boreholes and energy piles. Borehole heat exchangers (BHEs) are typically smaller in diameter and deeper than energy piles. BHEs are usually buried to a depth of about 80–200 m and are typically backfilled with a mixture of sand, bentonite and/or cement (Pahud and Matthey, 2001). Energy piles are typically shorter in depth (typically between 15 and 40 m) and wider in diameter (30 to 45 cm) than conventional BHEs (Brandl, 2006). They are designed to serve as structural foundation elements of buildings as well as for exchanging heat with the ground.

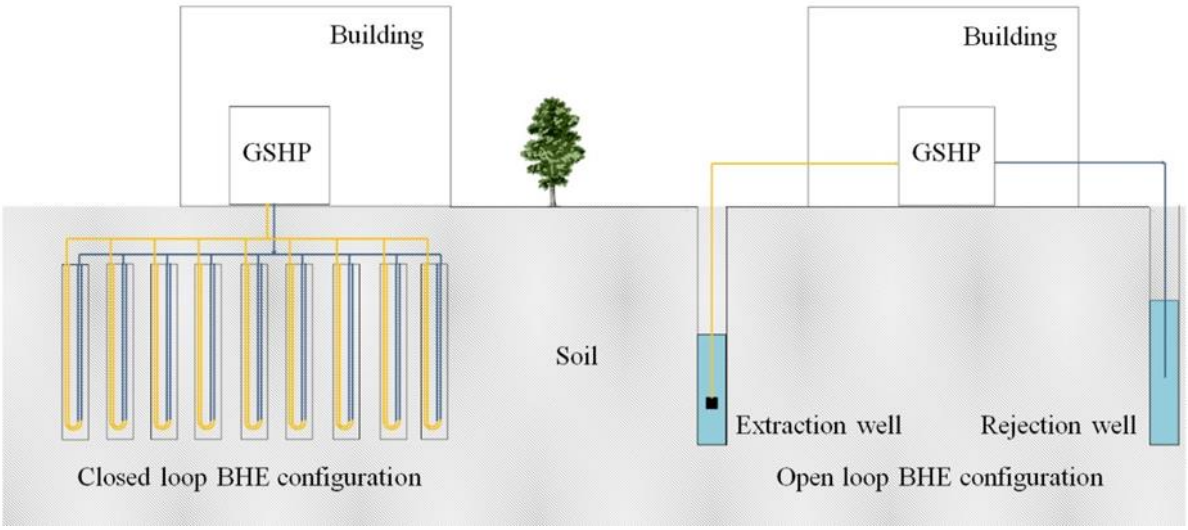

Figure 2.1: Schematic of the closed and open-loop type GSHP configurations

2.2.1.4 Thermal performance of GHEs

Generic rules of thumbs for GHEs thermal capacity are widely cited. These can be a useful starting point prior to more sophisticated analysis and design of GSHP systems. The Verein Deutscher Ingenieure (VDI, 2009) published typical values for GHEs heat extraction rates which are often quoted by both academics as well as in industry. For example, Loveridge (2012) reproduced the VDI data for both small diameter borehole type GHEs as well as for larger diameter energy piles. Results showed a wide range of values, between 18 W/m and 100 W/m depending on the GHE type, the geology, mean undisturbed ground temperature and the hours of system operation. For a moist clay ground type (in which the majority of the London based GSHPs are being installed) values between 30 and 50 W/m were reported.

2.2.1.5 GHE's absorber pipes and the circulated liquid

Absorber pipes of GHEs are commonly made of high-density polyethylene. Pipe diameters typically range from 20 to 38 mm, and their lengths will depend on several factors including borehole/pile length and performance requirements (Pahud and Matthey, 2001). Heat transfer liquid, which is fed through the pipes, serves the purpose of transmitting or receiving heat to or from the ground. For buildings where the cooling loads are much greater than the heating loads, water may be sufficient. Its use is common, but not recommended in colder climates where freezing of the fluid can occur resulting in damage to the pipes. For cooler climates, an antifreeze solution such as a water and glycol mixture is a common substitute.

2.2.2 Alternative Heat Energy Resources in Urban Areas for Heat Pumps

In urban settings heat is potentially more easily accessible through alternative sources. It has been shown that the total heat that could be delivered from secondary sources in London is of the order of 71 TWh/year (The Greater London Authority and Buro Happold, 2013). This was estimated by using heat pumps that delivered heat at 70°C. This was more than the city's total heat demand of 66 TWh/year in 2010. Of this 71 TWh/year around 50 TWh/year (70%) would be from the secondary heat source itself and the remaining 21 TWh/year (30%) would be attributed to the heat pump energy requirements. Some of these secondary heat sources are summarized in Table 2.1 and detailed in the following subsections.

Table 2.1: Alternative heat sources for heat pumps (Adapted from: The Greater London Authority, 2013)

Heat Source	Description	Typical source temperature
Power station heat rejection	Power stations that burn fuel to generate electricity generally operate at electrical efficiencies of around 30-50% depending on fuel type and technology. Considerable energy is lost in the form of waste heat that is generally rejected to the atmosphere.	35°C (in some cases much higher)
Building cooling system heat rejection	Buildings use a range of different cooling systems which typically operate more during summer months and use air or water cooled chillers to reject heat at low temperatures.	28°C
Industrial sources	A number of industrial processes (e.g. chemical industries, clinical waste incinerators and food producers) lead to the rejection of waste heat.	35-70°C Highly variable
Commercial buildings non-HVAC	Some buildings reject heat from equipment other than building cooling systems (e.g. from food refrigeration, IT equipment). Two key commercial operations are supermarkets and data centres.	32-40°C
Underground Railways (Direct through vent shaft)	There is a substantial amount of heat generated through the operation of URs. Recovering that heat through heat exchangers directly linked to the tunnel body is viable.	Can be high as 35°C
Underground Railways (Indirect through ground)	The ground surrounding a typical urban UR tunnel contains a substantial amount of heat energy, which might be extracted with nearby GSHPs.	Typically between 20 and 30°C depending on the distance from the tunnel
Electricity substations	Electricity substations in both the transmission and distribution networks contain transformers to convert power from one voltage to another. Transformer coils are usually cooled and insulated by being immersed in insulating oil.	50°C
Sewer heat mining	Sewage in underground sewers contains heat which can be ‘tapped’ or ‘mined’ in a similar way to the extraction of heat from the ground or rivers.	10-22°C
Roads / Car parks	The exploitation of heat stored in roads and car parks can be recovered through asphalt solar collectors.	25°C

2.2.2.1 Electricity cable tunnels

In London, most electricity is transmitted through underground cables. There are many miles of cable tunnels in London which are warm year round. Currently National Grid is working on housing new electricity cables in tunnels deep below the road surface and these London Power Tunnels will eventually stretch 32 km across the capital (National Grid, 2017). These long cable tunnel segments are all potential sources of heat, however the feasibility of heat recovery from these structures has not yet been evaluated.

2.2.2.2 Sewers and water mains

Another latent energy source is the network of sewers beneath London that run for many hundreds of kilometres (Halliday, 2013). Wastewater derived from buildings is characterized by a higher temperature because around 60% of it has been heated and typically its temperature ranges from 10 and 22°C. Due to the increasing carrying capacity requirements of the sewerage system, a new development called the Thames Tideway scheme has been proposed. This includes large (7.2 m) diameter storage and transfer tunnel of 35 km length (Tideway, 2016).

The water supply network is also a major part of the subterranean infrastructure system in London. For example, the Thames Water ring main is approximately 80 km long with 2.5 m diameter concrete pipes (HAL, 2016). The ring main supplies over 1,300 million litres of water a day with the mains water temperature varying between 5 and 20°C during the year.

Consequently, mains water provides a large energy resource. The work of Paurine and Maidment (2015) showed that the ring main could potentially be used as a heat network enabling different buildings to exchange heat and cold with it as required. Critical to the performance of the water network is how the thermal coupling between the water mains and heat recovery mechanism can best take place, and this should be a subject for further research.

2.2.3 Underground Railways – A Continuous Heat Source

2.2.3.1 Heat generation in UR tunnels

In many capital and large cities, an UR is a major public transport system and serves millions of passengers every day. In 2012 the Paris Metro carried nearly 1.5 billion passengers per year, the London Underground Metro system approximately 1.1 billion, and the Madrid Metro nearly 700 million passengers (ERRAC and UITP, 2012). Commuters are demanding more frequent and faster trains that are likely to result in a rising energy

consumption, a large proportion of which will ultimately be rejected into the tunnel as heat. Often a large quantity of kinetic energy is generated when the trains brake. A good proportion of this energy can be regenerated, but the remainder still presents a great thermal stress on the tunnel environment.

Bendelius (1976) categorised the major heat sources within a typical UR tunnel environment during the operational periods of the trains. These were breaking, carriage accessories, air conditioning and third rail losses. Shortly after (Cockram and Birnie, 1976) reported that the traction energy, train internal lighting, passengers, station lighting and machinery are all major contributors of heat energy generated.

It was much later when Ampofo *et al.* (2004) estimated that for a generic deep UR such as the LU railway, with no air conditioning, the major contributor of heat to the tunnel is the braking system, contributing 85% of the heat load, while the major contributor of heat to the train are the passengers contributing 74% of the heat load. This is illustrated in Figure 2.2. These values were estimated based on steady state energy calculations on the UR tunnel and its surroundings. The different heat loads within the system as categorised by Ampofo *et al.* (2004) are illustrated in Figure 2.3.

Gilbey and Thompson (2009) have also detailed the major heat sources, referring to actual heat dissipation values of the LU railway. For example, the authors published that in trains a standing person is estimated to have a metabolic heat production of approximately 150 W, and during peak-hours passenger heat gain could be equating to approximately 4.5 kW sensible and 10.5 kW latent. In terms of the heat gains in the tunnels and platforms due to the operation of the trains, the authors suggested an equivalent continuous steady state heating effect of between 300 and 350 W/m depending on the train type, speed, loading and service frequency. However, it was highlighted that trains are not the only sources of heat in the system: station lighting systems, advertising and occasionally the heat from air conditioning condensers serving non-public areas can all affect conditions. Despite this, most of other heat gains are small in comparison to the heat released from the trains.

Another factor contributing to rising temperatures is the climate change. Railway infrastructure has a lifespan of over 100 years, and over this period climate change could potentially cause several degrees Celsius of warming. Globally-averaged temperatures in 2016 were 0.99˚C warmer than the mid-20th century mean (Northon, 2017).

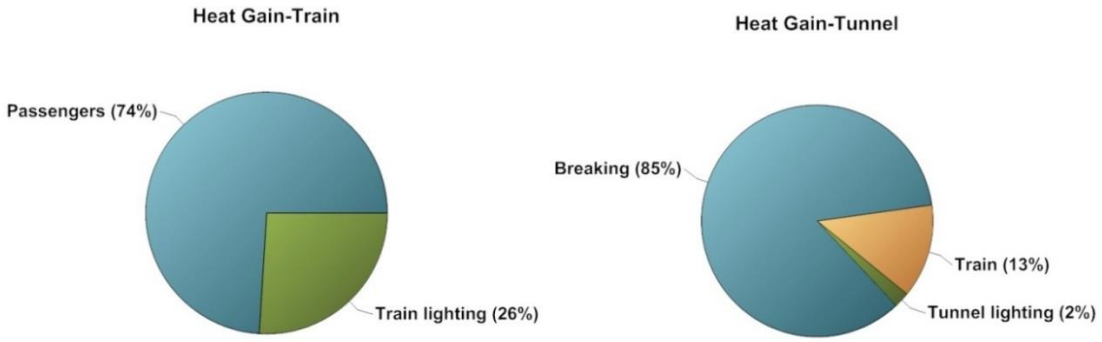

Figure 2.2: Heat gains in a typical UR environment (Adapted from: Ampofo *et al.* 2004)

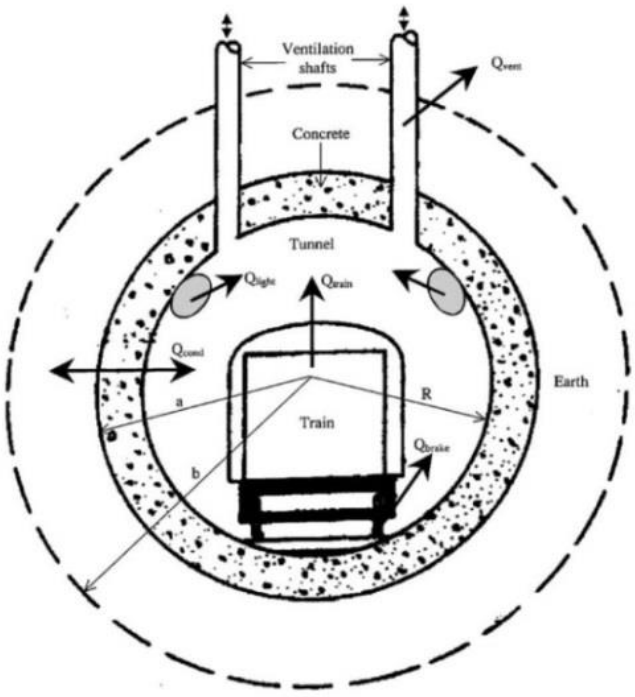

Figure 2.3: UR heat loads as presented by Ampofo *et al.* (2004)

2.2.3.2 Heat mitigation

Failure to manage increasing temperatures in tunnels can drive up operating costs, by increasing the amount of energy required to cool the trains and stations. Energy efficiency is the first and foremost measure that can be employed to take on the challenges. This tackles the heat release at its source. Optimizing rolling stock and traction power specifications, train speed operating profiles, and maximizing regenerative breaking all play a major role in reducing energy usage, which could lead to a reduction in tunnel air temperature. However, the additional heat does give an opportunity for year round heat recovery.

2.2.3.3 Heat Recovery from URs

The heat energy provided by URs could potentially be captured, transferred and utilised by nearby users of heat. This can be achieved through using different methods. Some of the methods have the limitation that they could only be implemented to newly built tunnels, however some have a potential for retrofit into older structures. This section of the thesis lists a number of heat recovery methods which have already been implemented or investigated in some European metro systems.

2.2.3.3.1 Embedded tunnel liner heat exchangers

Embedded tunnel liner heat exchangers could be viable solutions for newly constructed tunnels, which are routinely built as part of city and infrastructure planning. Tunnels are designed to last for more than 100 years, and installing geothermal systems within them adds to their value. However, tunnel liner heat exchanger systems have the limitation that they can not be retrofitted to old tunnel segments, such as the deep level UR lines in London.

Early examples of this form of heat recovery from URs are reported in Austria, where geothermal energy systems have been installed in tunnels lined with sprayed concrete (Adam and Markiewicz, 2009). An example of an activated floor slab solution is the Messe-Prater metro station of the U2 metro line in Vienna. The absorber pipes were deployed like a heating floor as shown in Figure 2.4.

Figure 2.4: Absorber pipes deployed above the floor slab of the U2 Messe-Prater metro station (Vienna, Austria). From Adam and Markiewicz (2009)

Another example is a portion of the Lainzer tunnel in Austria, which was equipped with energy geotextile. This new generation of geotextile is equipped with absorber pipes so that prefabrication is possible. The geotextile is placed between the primary and secondary linings of the tunnel. This is illustrated in Figure 2.5.

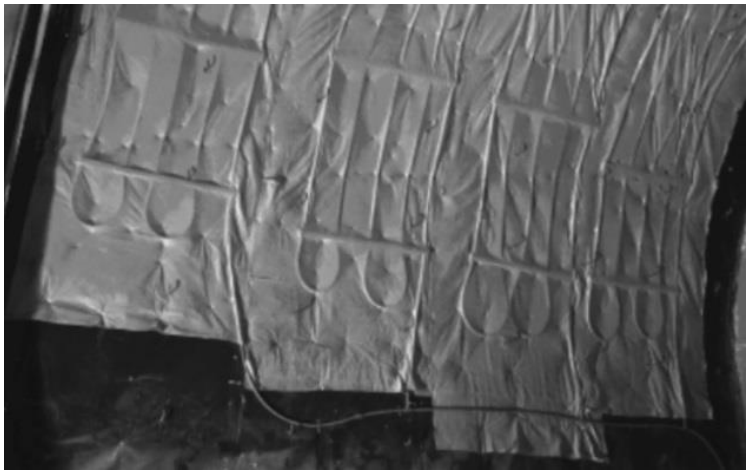

Figure 2.5: Example of an energy geotextile with the prefabricated sections and the collector pipe at the bottom. From Adam and Markiewicz (2009)

In Germany, segmental tunnel linings equipped with heat exchangers have been installed to supply a municipal building with heating energy. The CO_2 emission savings compared with gas-fired boilers were estimated at between 25-35% (Franzius and Pralle, 2011). The 3D schematic of this technology is illustrated in Figure 2.6.

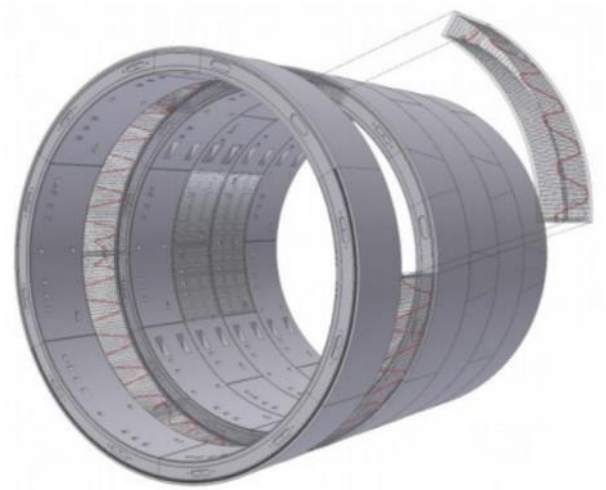

Figure 2.6: Example of an Energy Lining Element. From Franzius and Pralle (2011)

In the UK, the work of Winterling *et al.* (2014) provided an overview of a tunnel energy segment system for Crossrail. The authors highlighted that in the Crossrail tunnel environment the heat is generated by the trains all year round. The system proposed included embedded closed-loop water-filled pipework in tunnel segments to extract heat. It was shown that this could provide both cooling to the tunnels and heating for adjacent buildings.

2.2.3.3.2 Tunnel anchors

The use of tunnel anchors (structural support elements) as heat exchanger was investigated by Mimouni *et al.* (2013). Their study addressed the geothermal potential of long anchors, which are used to maintain the diaphragm walls during the construction of the cut and cover type tunnels. In addition, numerous short nails were distributed around bored tunnel lining as heat exchangers with the ground for seasonal heat storage. As a conclusion, it was highlighted that using the anchors or nails as heat exchangers with the soil was thermally efficient and could provide a great amount of heat for GSHP systems. The estimated extractible heat ranged from 0.6 to 1.2 MWh per year per metre of tunnel for the cut and cover tunnel, and from 2.8 to 4.2 MWh per year and per metre of tunnel for the bored tunnel.

2.2.3.3.3 Ventilation system of the railway

Heat utilisation through the ventilation system of an UR, has also been a focus of a number of studies. The method uses a heat exchanger in the tunnel which may capture the heat and a water circuit then transfers it to a heat pump. This is shown on the left side of Figure 2.7. The heat pump may be connected to a third party's building or small-scale district heating system. The work of Thompson and Maidment (2010) showed that air source recovery through the ventilation system of an UR was viable. This was further supported by Gilbey *et al.* (2011) and more recently by Ninikas *et al.* (2016).

2.2.3.3.4 Railway cooling system integration

All metros including LU require cooling to ensure that the temperatures within the tunnels are maintained at a safe level. Due to the planned upgrade of the Piccadilly, Bakerloo and Central lines, temperatures are predicted to rise significantly. Therefore, a number of mechanical cooling schemes are due to be introduced on the network. An InnovateUK funded project called Metropolitan Integrated Cooling and Heating (MICAH) is currently developing a concept for integrating LU cooling systems with an Islington Council District Heating Network (DHN). In winter months (when cooling of the underground network is not required), Islington will capture the waste heat in the air discharged from the LU ventilation

shaft. In summer months (when cooling of the underground network is required), chilled water will be delivered into the LU ventilation shaft, generated from the removal of heat from outside air which is then used by Islington district heating system. This significantly reduces the energy required by both parties, when compared to a non-integrated scheme.

2.2.3.3.5 Localised GSHP system

The opportunity of heat recovery via an external ground loop as illustrated on the right side of Figure 2.7 has not been widely reported in the literature. A group of researchers at Cambridge University investigated the potential impact of GSHP systems on an UR tunnel. The work of Mortada *et al.* (2015) suggested that using GSHPs in the vicinity of the tunnels could potentially lower the tunnel wall and air temperatures by extracting heat from the ground. However, this conclusion was driven based on the assumption that the soil temperature was lowered by placing the GHEs at a close vicinity of the UR tunnel at 0.4 m. This is well within the 3 m range that LUL does not allow to cross for any structures to be built near the tunnels (TfL, 2013). Also, the potential benefits on the GSHP performance were not addressed by the authors, only the potential cooling impact on the railway.

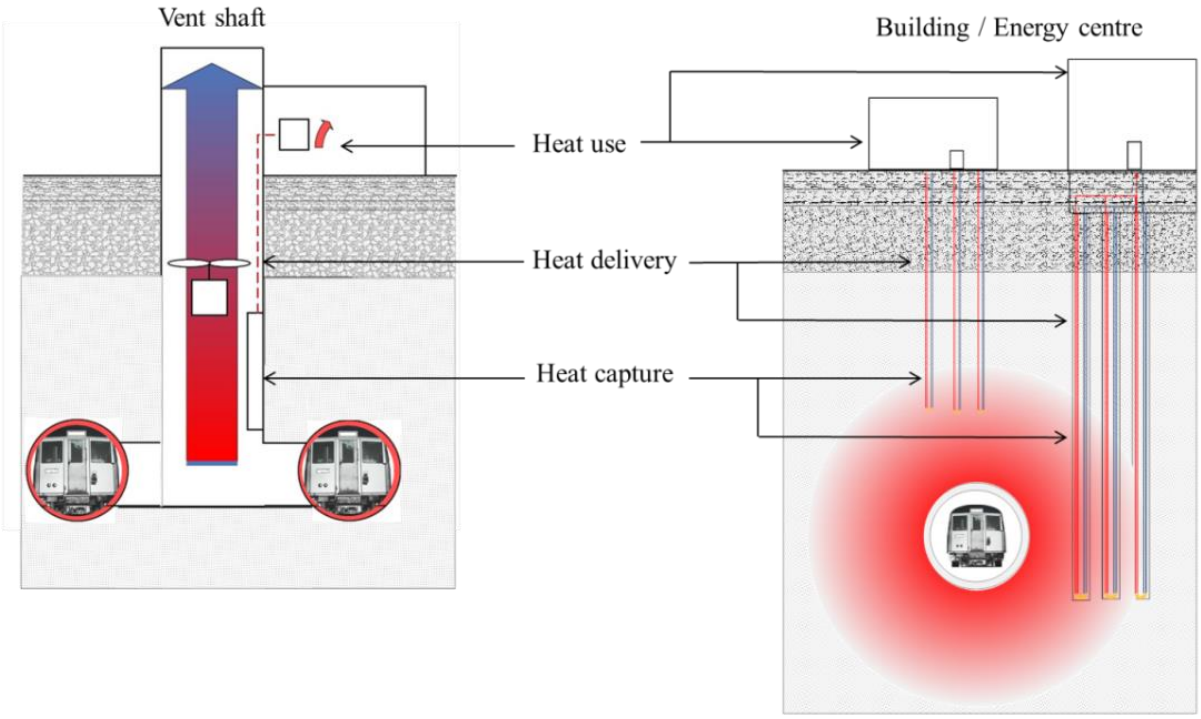

Figure 2.7: Heat recovery from URs through ventilation shaft (left) and heat recovery through GHEs (right) From Revesz *et al.* (2016)

2.3 MODELLING URs AND GSHPs

2.3.1 Modelling Basics

A wide range of models for both URs and GSHPs have been developed, with different capabilities depending on the modelling objectives and methodology which were adopted during the development phase. Typical objectives for both UR and GSHP models are summarised in Figure 2.8. Mathematical models of URs are either custom models (i.e. small models for specific sections of railway) or developed to provide a complete thermo-fluid analysis of an UR environment (Thompson, 2006). GSHP models can also be divided into different categories. Some models focus only on the processes within and in the surroundings of the ground heat exchangers. Other models are of integrated building simulations, whereby the entire GSHP system is coupled to heating, ventilation and air conditioning (HVAC) and thermal models are built to study overall system performance. A common feature of GSHP and UR models is that their level of detail and complexity mostly depends on the modelling objectives that are set and the timescales under consideration.

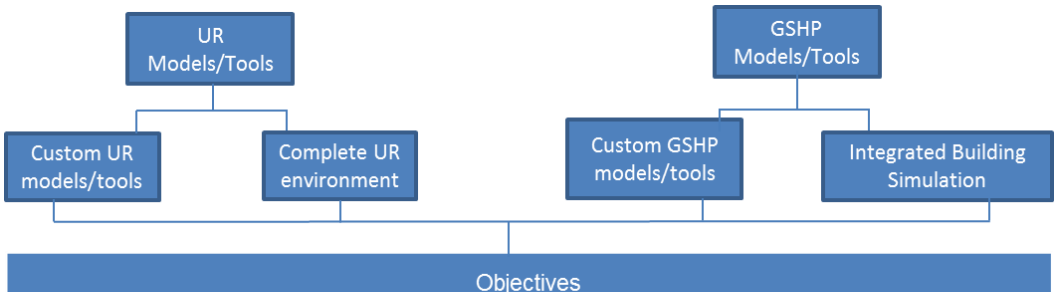

UR		GSHP
• Determine cooling requirements • Investigate cooling strategies	Design	• Size the GHE array • Analyse of in situ ground thermal conductivity test
• Study air velocity, temperature and humidity throughout the stations • Study the effect of temperature rise due to various heat loads on thermal comforts of passengers	Operation / Performance	• Determine the temperature of the fluid running in the pipes under certain operating conditions • Investigate in heating or cooling dominated climates whether an annual energy imbalance is placed on the ground loop
• Analyse the range of heat transfer and heat transfer characteristics of soil surrounding tunnels	Environmental aspects	• Evaluate the temperature rise in the soil surrounding the BHEs and the migration of thermal plumes away from them

Figure 2.8: Typical objectives of UR and GSHP Models/Tools

2.3.2 Modelling Approaches

Numerical methods are common; however analytical solutions are also used to predict UR or GSHP operations. Although analytical solutions that can readily be solved do have limitations, they are often used to provide data for validation purposes of numerical modelling results for both URs and GHEs. The main reason for this is that it is difficult to gather experimental data of sufficient quality and reliability in deep ground.

Numerical methods solve the fundamental engineering equations using established numerical differential-equation solving techniques, such as a finite-difference (FD), finite-element (FE) or finite-volume (FV) methods. These numerical solution methodologies are particularly useful when modelling URs and GHEs. This is because there are complex, transient, 3D transport phenomena and extreme geometrical aspect ratios involved within both schemes. Numerical approaches, if designed correctly, can provide solutions for phenomena with very different time scales (e.g. the system response of coupled low and high inertia systems) and also consider a variety of transient boundary conditions. Accounting for moisture migration in the soil and ground stratification, is also typically less complicated in numerical models, because they can operate with larger degrees of freedom than analytical solutions. A common disadvantage of fully discretized 3D numerical models is that even when using modern and powerful computers, extensive computation times can result.

2.3.3 Analytical Solutions for GHEs and URs

One of the earliest analytical approaches to modelling vertical GHEs is the Line Source (LS) method. This relies on the principle of superposition where a line consists of a combination of sequentially positioned points. The model is called the Infinite Line Source (ILS) model. In the ILS model, which was developed by Ingersoll and Plass (1948), the integral of the point source formula is performed on a line with an infinite length. Another approach based on Fourier's law of heat conduction is the Infinite Cylindrical Source (ICS) method developed by Carslaw and Jaeger (1946). The ICS method can be used to model both GHEs and UR tunnels. This method is based on a cylinder with infinite length, surrounded by a homogeneous medium with constant properties, and considers heat transfers only by conduction. Also it only considers a single cross-section of a cylinder and neglects axial heat conduction effects.

The first method accounting for the finite length of the GHE was developed by Eskilson (1987). The approach was based on a combination of analytical and numerical solution techniques and it is called the Finite Line Source (FLS) model. Based on Eskilson's model,

Zeng et al. (2002) presented a full analytical solution to the FLS problem, considering the soil as a homogeneous semi-infinite medium with constant thermo-physical properties. The ground surface was presented as a boundary with constant temperature throughout the time period considered. The heat flow rate per unit length of the borehole was assumed to be constant along the borehole.

The FLS models have been proven as acceptable approximation, especially in the case of single GHEs and extended time scales. However, its implications for large GHE fields are also possible through the process of superposition. This method invokes the linearity of the heat transport equation with known or constrained heat extraction rates at the borehole wall and it was used by a number of researchers. For example (Lee and Lam, 2008) used solutions from a superimposed FLS method to validate numerically generated results of ground temperatures surrounding of a large GHE array. Also Rivera *et al.* (2017) used this method when investigated the effect of increased ground temperatures in urban areas on a large borehole field thermal performance.

Table 2.2 categorises some of the work, improvements and alternative applications of analytical GHE models. Enhancement of the ICS model used to model UR tunnels was initiated by several researchers including Brown *et al.* (2005), Brown and Vardy (2006), Sadokierski and Thiffeault (2008) and (Thompson *et al.*, 2009).

Table 2.2: Improvement and alternative use of analytical models

Varying heat rate of the GHE	Groundwater movement	Ground surface temp changes	Multi-layered soil profile
Deerman and Kavanaugh, (1991) [ICS] Bernier, (2001) [ICS] (Weibo *et al.*, 2009) [ILS] (Ozudogru *et al.*, 2014) [FLS]	Diao *et al.*, (2004) [ILS] Molina-Giraldo *et al.*, (2011) [FLS]	Bandos *et al.*, (2009) [FLS] (Rivera *et al.*, 2017)	(Abdelaziz *et al.*, 2014) [FLS]

2.3.4 Numerical Models for GHEs and URs

2.3.4.1 GHE models

A number of numerical GHEs models with different features have been developed. One of the earliest is the Duct Storage model (DST), which is a two-dimensional FD scheme. The

DST model was first described by Hellström (1991) and further developed by Thornton *et al.* (1997). The DST code was built in as a component in a simulation environment called TRNSYS (TRNSYS, 2017). The software is a modular system simulation package where users can describe the components that compose the system and the manner in which these components are interconnected.

Alongside TRNSYS a number of other design tools for GHEs based on some typical heat transfer models have been developed over the past decades. One example is a tool which was developed by Gaia Geothermal and is called Ground Loop Design (Thermal Dynamics Inc., 2017). The software is capable to modelling rectangular GHE arrays, as well irregular shapes, by using the theories developed by Hellström (1991).

Numerical models were developed for not only design purposes but for investigating other aspects of GHE operation. Important efforts include the work of Lei (1993) and Muraya *et al.* (1996), who studied the thermal interference which occurs between adjacent legs of a BHE field. Most of these early numerical models were associated with low computational efficiency. In order to overcome this barrier, Al-Khoury *et al.* (2005) developed an FE model for the analysis of 3D steady state heat flow. Shortly after that a transient version of the model was presented in Al-Khoury and Bonnier (2006). More recently a 3D numerical approach was developed by Rees and He (2013). The Al-Khoury and Bonnier's as well as Rees and He's approaches are suitable for the investigation of 3D dynamic heat transfer and fluid flow physical phenomena.

Another important aspect of numerical GHE modelling is the investigation of the groundwater flow and its effect on the energy extraction of the GSHP system. Fan *et al.* (2007) found that moving groundwater influences the heat transfer significantly between the GHE and soil. Zanchini *et al.* (2012) has also studied the effects of groundwater flow on the thermal performance of large GHE fields, and their numerical results show that the groundwater flow yields an important improvement of the long-term performance.

In addition, the heat extraction rates of GHEs in different types of soils and under different operating conditions are also commonly investigated. Recent numerical investigations in these type of studies include the work of Hein *et al.* (2016), Chen *et al.* (2016) and Stylianou *et al.* (2017). These investigations studied the effects of different parameter and operational characteristics such as soil thermal conductivity, volumetric heat capacity, the fluid's inlet flow rate into the GHE pipes, and its temperature. Soil porosity, Darcy velocity magnitude and borehole depth on the heat flux of GHEs were also investigated within these studies.

2.3.4.2 UR models

Numerical models aiming to study heat transfers in and around URs have also been developed. A few examples include the work of Hu *et al.* (2008), Ting *et al.* (2009), Mimouni *et al.* (2013) and Barla and Perino (2014). The descriptions of the implemented numerical strategies detailed within these studies however are somewhat lacking in explanation of the selected validation methodology.

The most common simulation tool used in the railway industry is called the Subway Environment Simulation (SES), which was developed in the 1970s. SES is an industry standard tool in the field of tunnel ventilation. It allows engineers to mathematically model aspects of a subway environment.

IDA Tunnel is a more recent one-dimensional Modelica based tunnel environment simulation program that was developed by EQUA (1995). Multiple geometrical thermal parameters can be inputted into the IDA Tunnel model to simulate the environmental conditions and airflows including pollutant dispersal.

Another supplement to the SES has been developed by Parsons Brinckerhoff to enhance the capabilities of SES. This supplement is called Dynamo, which is a one-dimensional FD model of a single length of tunnel. It uses an energy balance approach to determine the thermofluid interactions. The tool can be used for the analysis of recovery of waste heat from railway tunnels (Thompson, 2014).

ThermoTun (DTR, 2017) is another commonly used railway tunnel ventilation and aerodynamics software application. The software can be used over the internet to perform calculations based on a selection of pre-built tunnel configurations. ThermoTun was developed by Professor Alan Vardy of Dundee University, UK (Vardy, 2001). ThermoTun employs the one-dimensional approaches to model tunnel networks, and allows train traffic to be specified. The programme has been extensively validated against experimental data for several rail tunnel projects, including London Transport‟s Victoria Line, the Mühlberg and Einmalberg tunnels in Germany, and the Grauholz Tunnel in Switzerland. In all of the above cases, it was found that a high degree of accuracy for the maximum pressure transients was obtained if the appropriate tunnel and train parameters were entered into the programme.

Mott MacDonald (2017) has developed a FE model to assess the feasibility of UR systems. The model assumes that the system is radially symmetric and there is radial heat transfer only (Thompson, 2006). The model is a two stage; aerodynamic and thermodynamic model. The reason for this is the time step required for each part. The aerodynamics is a very short

time step process due to the large variation of the aerodynamics over a short time period. The thermodynamics model uses a longer time step due to the longer period of variation when compared to the aerodynamics. The model has been validated with real life data. Mott MacDonald has used its model extensively both for feasibility studies and calculations on existing metro systems. These studies have been undertaken throughout the world and with notable projects in Beijing, Taiwan, Bangkok, Delhi, Taipei, Los Angeles and Singapore. More recently, there have also been studies on the London Jubilee line extension and on the London Crossrail (Mott MacDonald, 2017).

To date, there are limited number of models reported that allow the combined analysis of URs and nearby heat sources/heat sinks e.g. GHEs.

2.3.5 Simulation Platforms for the Combined Analysis of URs and GHEs

At present a number of simulation tools are available commercially and through open source. Those that are capable of simulating heat and mass transports in the ground include commercial FE software such as FEFLOW (MIKE, 2016), ANSYS (ANSYS, 2017) and COMSOL Multiphysics (COMSOL, 2017), amongst others. Most of these simulation tools offer a user-programmable interface, allow the input of user-defined equations and enable linkage with other software such as CAD tools or Matlab (MathWorks, 2017).

These tools allow the building of geometries within either a one, two or three-dimensional modelling domain, thus allowing the complex geometrical aspects of URs and GHEs to be easily represented. These platforms usually also allow the use of a wide variety of boundary and initial conditions that would typically exist during the operation of URs and GHEs. Thus the above-mentioned simulation platforms would allow the detailed investigation of the interactions of URs and GHEs within the same simulation environment. For building a model using such a tool it is essential to become familiar first with the parameters, variables, properties and operating conditions involved.

2.4 LONDON – THE LINKAGE BETWEEN URs AND GHEs

2.4.1 Why London as a Case Study

London has grown to become one of the most significant financial and cultural capitals of the world. Due to this position, more people than ever are using the LU. Simultaneously, GSHP installations are becoming increasingly common in the city and thus GHEs eventually could get closer in proximity to the running tunnels. Investigating the viability of the heat recovery from the ground surrounding the tunnels through these ground loops will therefore become increasingly important. Following a brief introduction to London's geology, this section

reviews the infrastructure of the LU railway and its thermal environment. The potential benefits of the interactions between the tunnels and nearby GHEs are also summarised.

2.4.2 London Basin

The centre of the city of London is part of the London Basin. Of all the lithology of the Basin, the London Clay formation hosts many types of subterranean structures including the majority of the LU railway. A typical geology and a section of the LU railway network are illustrated in Figure 2.9. The London Clay's generally low permeability and good load-bearing characteristics are some of the principal reasons for the comparatively early development of the LU (Paul, 2009). The mean thickness of the London Clay beneath central London, calculated from the borehole data, is 32 m. However, thicknesses are known to vary widely across the London Basin, from ~ 150 m under Hampstead Heath, thinning to zero farther east (Wilson and Grace, 1942). Historically, engineers have planned LU railway tunnels to fully remain within the London Clay. For instance, a quick glance at the Tube map reveals a lack of underground tunnels in eastern and southern regions, where the London Clay is thin or absent (Paul, 2009).

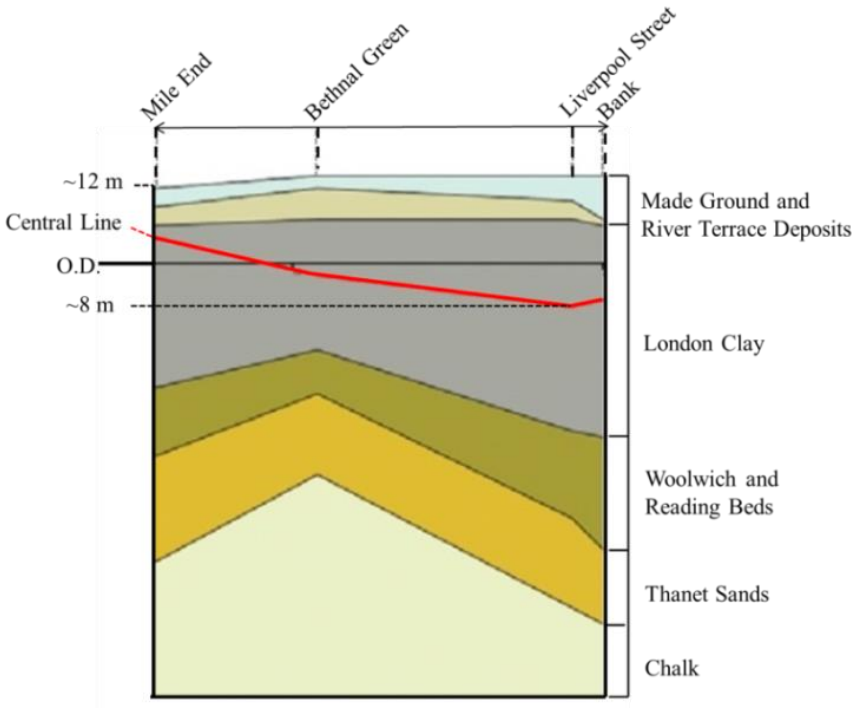

Figure 2.9: A short geological section following the path of the Central line of the LU railway (Adapted from: Paul, 2009)

2.4.2.1 Groundwater

The level of the water table beneath central London has fluctuated greatly over the past few centuries. The major aquifer of the London Basin is the chalk aquifer (Environment Agency,

2014). In the early nineteenth century, heavy water abstractions led to a fall in groundwater levels, increasing the strength of the London Clay. Legislation from the 1960s led to the slow recharge of groundwater levels. For London, the initial average rate of groundwater level rise was 1 m/year but more recently rates of as much as 1.88 to 2.5 m/year were reported (Mavroulidou *et al.*, 2005). Since then, increased pumping has been required in some areas of the LU network as old tunnels are threatened by changes in the pore water pressure in the London Clay. This may lead to increased leakage of water into the tunnel and pressure on the tunnel linings as well as a decrease in the effective stress of the soil. The shallower tunnels, often called "sub-surface" lines, are typically at a depth consistent in location with the River Terrace Gravel strata. These are known to be porous strata often containing ground water flowing to the nearby River Thames basin.

2.4.3 The LU Railway

2.4.3.1 History of the LU

The Metropolitan Railway was the first section of the LU railway. It was constructed from Paddington to Farringdon in 1860-1862 using the cut and cover technique (see in Figure 2.10 left). The railway was a great success from the beginning, attracting 11.8 million passengers in the first year. The railway was soon extended to South Kensington in the west and Tower Hill in the east. The "full circle" (today known as the Circle Line) was completed in 1884. The first "deep tube" line on the LU was the "City and South London Railway" with tunnels and stations now forming the Bank Branch of the Northern Line from Camden Town to Kennington and the southern leg of the line from Kennington to Morden (see in Figure 2.10 right).

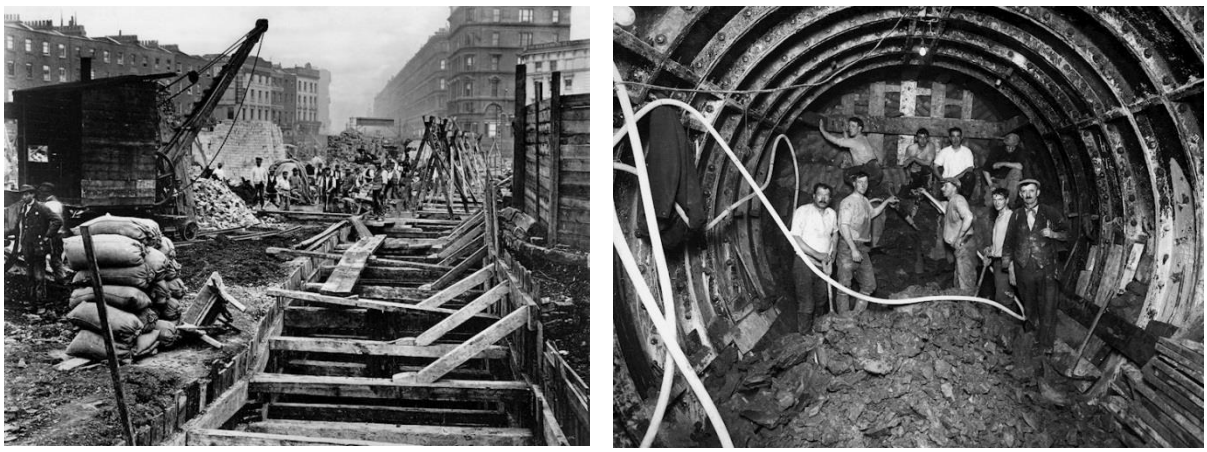

Figure 2.10: Cut and cover trenches built for the District Line (left) and the construction of a deep level line (right) (source: The History Press UK)

2.4.3.2 Current LU tunnel and train characteristics

Since the 1860s the LU network has broadly extended and currently contains approximately 35 km of the "sub surface lines" and about 136 km of the deeper tube tunnels. The average depth of the bored deep tube tunnels is 24 m with a maximum of 67 m (Thompson *et al.,* 2008). The extension of the Northern line was recently announced that will add an extra 5 km to the tunnel network (Constructionenquirer, 2014). The cut and cover tunnel sections (collectively referred to as the sub-surface lines) are mostly bi-directional tunnels created from brick-lined arches and are used by the Metropolitan, District, Circle and Hammersmith and City lines. These lines share the tunnel and station infrastructure at their busiest sections and include a peak-hour train frequency of 30 trains per hour (TPH) of predominantly six-car trains. The six-car trains have an approximate total length of 91 m and are the largest on the network with a height from rails of 3.687 m and a width of 2.92 m. Each six-car train weighs approximately 160 tons with a full load of around 870 passengers (Gilbey and Thompson, 2009).

The deep tube tunnelled sections are mostly single-directional. They are cast iron-lined with a typical diameter of 3.8 m and a free cross sectional area of 10.2 m^2. The different lines have a train frequency of between 19 and 30 TPH and have between six and eight-car trains. A six-car train has an approximate total length of 106 m and a height of about 2.9 m from the top of the rails and a width of about 2.6 m. The trains have a frontal area of approximately 6.3 m^2 with a curved profile along the roof to fit within the tunnels. The blockage ratio of train to tunnel is around 67 percent, a factor which causes considerable aerodynamic drag. Each six-car train weighs approximately 157 tons with a full load of around 800 passengers (Gilbey and Thompson, 2009).

All of the LU's trains are provided with electric motors. Three of the lines include modern traction drives featuring some form of inverter control and regenerative braking, with plans for all trains to be converted to regenerative braking systems in the future. The train speeds vary line by line and along each line, with a maximum of around 80 km/h and a moving average of closer to 35 km/h. There is a mixture of automatic and driver controlled trains, with a future preference for automatic control.

2.4.3.3 The thermal environment of the LU railway

The LU was originally ventilated by platform supply fans, each with a capacity of around 9.44 m^3/s (Cockram and Birnie, 1976). Temperatures were quite low in the early years of the railway; records indicate summer time temperatures on platforms and in carriages of around 15°C and 17°C, respectively. Ventilation improvements continued in the 1920's and 30's with

opportunities for new fan shafts and draught relief shafts arising from the modification of many stations to include escalators rather than elevators (thus making available a number of former elevator shafts). By 1930 there were 73 ventilation shafts in operation with an average capacity of 13.7 m³/s (Gilbey and Thompson, 2009). Between 1930 and the second world war a number of lines were extended and even more ventilation improvements made. Throughout this period ventilation improvements were just able to keep pace with increases in train service and energy usage (Mount, 1947). The line extensions up to the 1980s saw the introduction of mid-tunnel exhaust ventilation shafts, with capacities of approximately 35 m³/s, complimented by station supply ventilation facilities with capacities of around 9.5 m³/s.

LUL presently has more than 120 ventilation assets with an average capacity of 32 m³/s (Gilbey and Thompson, 2009). However, the amount of heat rejected onto the railway has been increasing year-on-year due to increases in service frequency. Figure 2.11 illustrates an energy trend between 1980 and 2005 for the estimated heat inputs to some of the LU tunnels. It can be seen in the figure that in 2005 the highest tunnel heat input was on the Victoria Line, approximately 3 million kWh/year/single track tunnel mile. Some energy saving measures have been implemented by the introduction of lighter trains and regenerative braking, but it is still difficult of keeping pace with the increases in train frequency and the increasing intensity of service throughout the day.

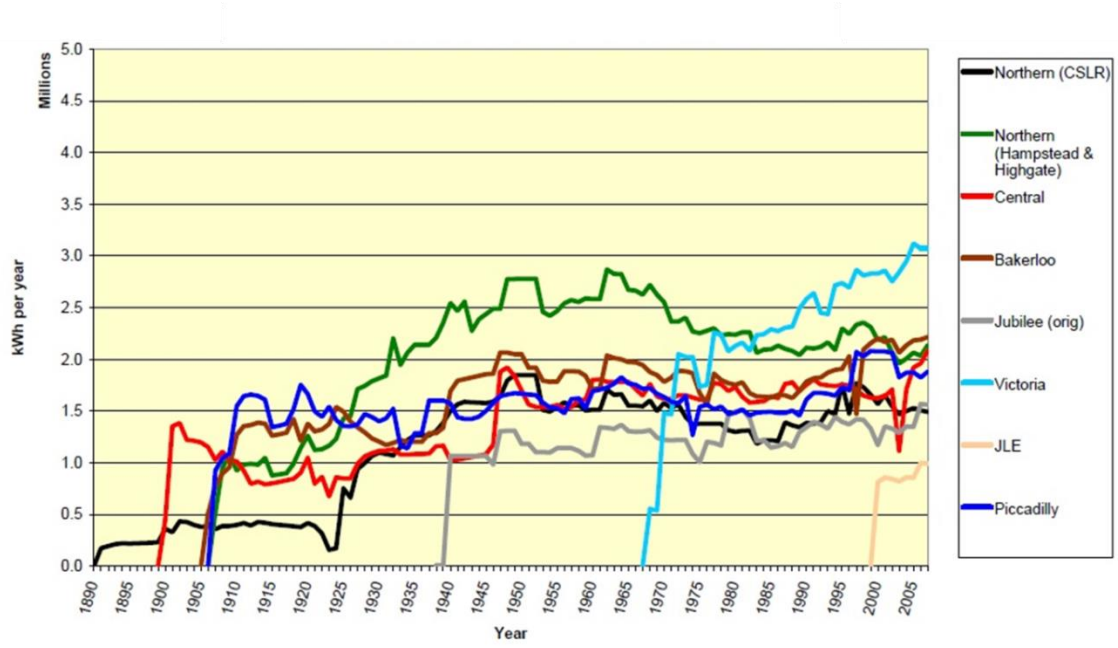

Figure 2.11: Normalised LU network heat input (Heat (kWh per year) per single track tunnel-mile) (Gilbey and Thompson, 2009)

Since 2005, LU has used temperature sensors and data loggers to record the air temperatures at numerous platforms and stations. The recorded data showed that during

summer peak-hour operation temperatures can reach as high as 32°C (Gilbey *et al.,* 2011). Due to the high thermal capacitance of the underground system the tunnel air temperature in winter is in excess of 20°C (Thompson *et al.*, 2008). The work of Gilbey *et al.* (2011) showed that there is an approximate linear relationship between platform and outside air temperatures and it can be expressed as $T_{plat} = 0.36 \times T_{amb\_air} + 19.5$. The authors work also showed that tunnel temperatures are typically 2 to 3°C cooler than platform air temperatures. This was explained as being a result of the heat produced by the braking mechanism concentrating at the platforms. The warmest parts of the LU network for the year of 2008 have been revealed in a map compiled by Transport for London (TfL) in 2009 (BBC, 2009). This map is shown in Figure 2.12.

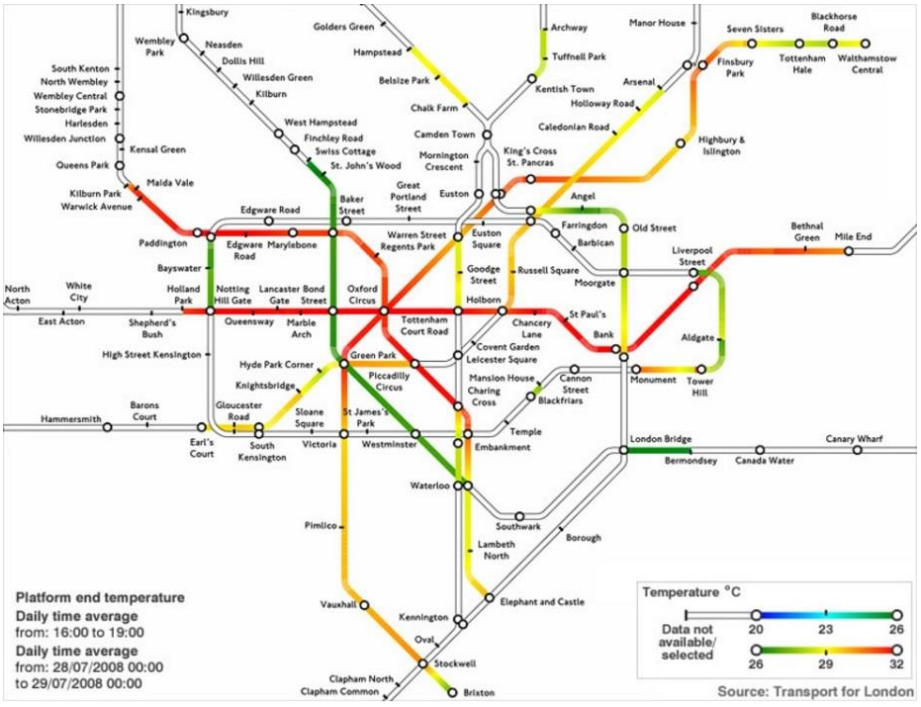

Figure 2.12: The LU heat map monitored in zones one and two on 28 July 2008

It can be seen that the Central Line was the hottest, with temperatures of 32˚C between Holland Park and Mile End. The coolest sections were recorded on the Jubilee Line which was still relatively warm with most stations recording temperatures of 25˚C.

2.4.3.4 Tunnel wall and the surrounding soil's heat sink effect

Deep level tube lines have dissipated heat into surrounding strata for over 100 years, with heat exchange to the tunnel walls forming a major heat sink in summer, and in turn a heat

source during winter. Gilbey and Thompson (2009) showed with some simple calculations that around 80 percent of the heat generated in the tunnel is transferred to the tunnel walls during a summer peak operating hour. The authors have also highlighted that despite the relatively high proportion of heat entering the tunnel walls, the temperature difference between the air and tunnel walls is relatively small. With the train piston-effect generating an average air velocity of about 4 m/s in the tunnels, the average convective surface heat transfer coefficient can be expected to be close to 20 W/m^2*K, giving an average temperature difference between the walls and tunnel air of approximately 1.2°C.

The soil surrounding a typical deep UR tunnel also contains a large amount of heat energy due to the heat sink effect that the ground provides the tunnel. Ampofo *et al.* (2004) have shown that the heat absorbed by the earth surrounding an UR accounts for 30% of the total heat release, and contains approximately 4,500 GJ of heat energy per km of tunnel. This energy is low-grade and ranges in temperature from approximately 20 to 30°C (Thompson *et al.*, 2008). It is important to note that Ampofo *et al.* (2004) only used steady state calculations with a constant convective heat transfer coefficient. The transient balance is somewhat different and would depend on the air volume being moved within the tunnel, and so the percentage of the heat absorbed by the ground can vary significantly depending on the prevailing circumstances.

2.4.4 LU Tunnels and Nearby GSHPs: The Opportunity for Improved Heat Extraction

The low grade thermal energy dissipated into the ground through the tunnel wall could potentially be extracted by nearby GHEs. As these ground loops eventually get closer in proximity to the tunnels the potential for heat recovery will become greater. However, there is a limit to how close structures can be constructed to the tunnels. The minimum proximity that LU allows is about 3 m in horizontal and 6 m in vertical directions. The literature suggests that beyond approximately 20 m from the wall of an UR tunnel built in clay the thermal effects are negligible (Thompson *et al.*, 2008). This means that the 136 km long deep bored tunnel sections with a diameter of 3.7 m, could potentially provide significant volume of earth, perhaps over 200 million m^3 containing a significant amount of low grade energy for potential exploitation by nearby GHEs connected to a heat pump. The heat pump may be connected to a third party's building or small-scale district heating system.

As the GSHP installations are becoming increasingly common in the city, the GHEs eventually get closer in proximity to the running tunnels. A great example of a GSHP installation in close proximity to LU tunnels is the building called One New Change. The building consists of 52,000 m^2 of offices and retail spaces on eight floors. The geothermal

scheme includes 219 energy piles of up to 38 m deep and 2.5 m in diameter. To complete the hybrid GSHP system, there is a pair of deep water wells extending to 140 m into the chalk. The GSHP system's total heating and cooling capacity is respectively 1.6 MW and 1.7 MW. The nearby LU Central Line tunnels run parallel to the northern boundary of the site. The tunnels run approximately 20-25 m below ground level. The piles are located at least 7 m clear distance from the south of the tunnel, closer to the site boundary. Some other GSHP installations in central London and their approximate distances from the LU tunnels are shown in Figure 2.13.

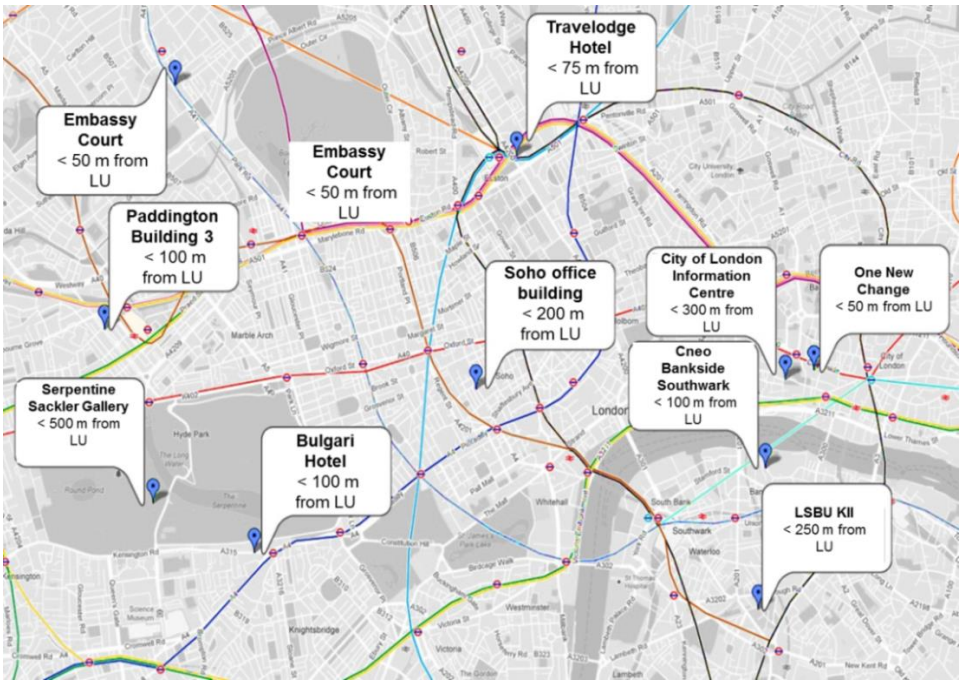

Figure 2.13: The map of the LU network and nearby GSHPs in central London (source: BBC)

2.4.4.1 The benefits of re-using the heat energy stored in the ground

Conventional GSHPs in London typically extract heat from earth which is at about 13-14°C (The Greater London Authority and Buro Happold, 2013). Utilizing source temperatures of 20-30°C which exist in the earth surrounding the deep bored tunnels of the LU network (Thompson *et al.*, 2008) could substantially enhance the performance of GSHPs. An operating characteristics rule of thumb for GSHPs is that the heating CoP is improved by approximately 3% for each degree Celsius that the evaporating temperate is raised (Cengel and Boles, 2001). Improved CoP figures would result in savings in running costs of the heat pumps, smaller heat pumps and reductions in heating related carbon emissions.

2.4.5 The Heat Demand in London and the London Underground

The London Energy Plan (London.gov.uk, 2016) explores how much energy London would need in the future, where it might be needed and the different ways of supplying that energy. It is a set of interconnected data models for building demand, power, heat, decentralised energy and transport, which have been developed using the best available data and with input from a range of stakeholders. One part of it is the London heat map which shows heat demand density across London. It is an interactive online tool which was assembled from data collected across all London boroughs for a number of typical building types. The map is populated with individual building data as well as a raster overlay based on benchmarked predictions for the heating demand of all buildings. The darkest colour schemes on the map show the highest heat demand densities of the capital. This is shown in Figure 2.14. It can be seen in the figure that the areas with the highest heat demand are the central and northern parts of capital. These are the same areas where the majority of the LU railway was built and is in operation today. This shows that the heat generated by the URs are close to the heat demand in London and therefore the railway could contribute towards supplying the heating needs of London. One way of distributing heat to users is through DHNs. One example of heat supply from the LU to a DHN is the scheme already underway in the London Borrow of Islington.

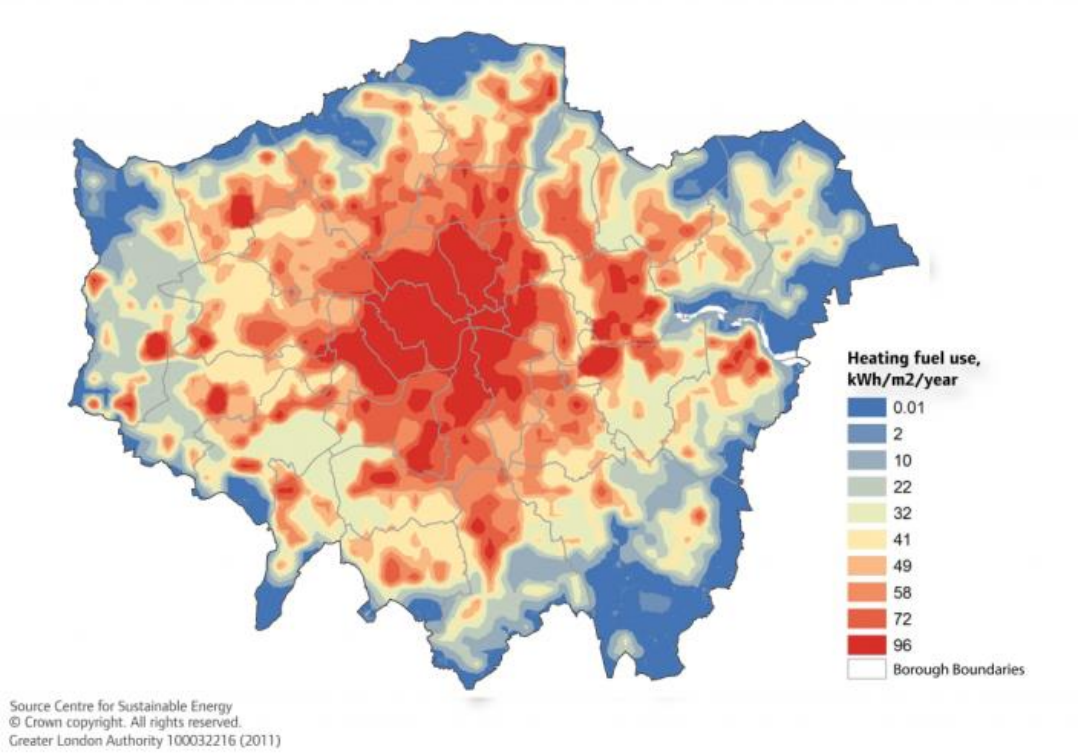

Figure 2.14: The London heat demand map (source: London.gov.uk)

2.4.5.1 The benefits of DHNs and their potential in London

District heating is a future proof technology that can offer local authorities and end-users significant benefits over individual heating solutions. DHNs could significantly reduce CO_2 emissions through the local generation of heat. It is an environmentally friendly technology as renewable energy or waste heat can be used to heat the network. Maintenance costs for the network operator are lower as there is only one central boiler to maintain. As there are also cost savings to the end users and local authorities, district heating can be used to help reduce fuel poverty. The Mayor in London supports the greater use of renewable and low carbon generation technologies, and has set a target for London to generate 25% of its heat and power requirements through the use of local, decentralised energy systems by 2025 (GOV.UK, 2015). It was shown that shifting 25% of London's energy demand to be supplied through DHNs could save up to 2.57 million tonnes of CO_2 a year (GOV.UK, 2015). Renewable decentralised energy opportunities including the use of energy from waste such as URs are also supported in London (See section 2.4.7.2).

2.4.5.2 Heat pump based DHNs

DECC published a report in February 2016 which recognised the value of using heat pumps in DHNs to lower carbon emissions in place of central gas boilers or gas based combined heat and power (CHP). The following is an extract of some of the key findings:

- Alongside a decarbonising grid, integrating heat pumps into district heating offers large CO_2 emissions reduction potential.
- Analysis showed that incorporating heat pumps into district heating schemes has the potential, in the context of a rapidly decarbonising electricity grid, to offer large CO_2 savings relative to district heating based on either gas-CHP (for large schemes) or gas boilers (for small schemes). Assuming the current trajectory towards low carbon electricity generation, the report found CO_2 savings versus gas burning schemes in the range 48-84%.

The report also showed that the CO_2 savings are greater where the following scheme characteristics are combined:

- Heat pumps provide a larger fraction of the heating.
- Heat pumps operate with a lower source-sink temperature difference, leading to increased efficiency.
- Network thermal losses are lower, especially for lower temperature distribution networks with building integrated heat pumps.

2.4.5.3 Bunhill Energy Centre in Islington, London

Islington Council completed the first phase of Bunhill Heat & Power Scheme in September 2012; comprising a temporary energy centre containing a 1.9MWe/2.3MWth CHP scheme, a 115m^3 thermal store and ancillary equipment. The system supplies base load heat to over 850 homes on three estates (Stafford Cripps, Redbrick and St Luke's estates) and two leisure facilities (Finsbury Leisure Centre and Ironmonger Row Baths). Islington Council have secured funding to extend the Phase 1 scheme to include Phase 2. Phase 2 is intended to extend from Phase 1 connecting a minimum of 500 homes that form the King's Estate. The extension to the network will include using heat pumps to utilise heat from two low temperature waste heat sources: a UK Power Network Ltd's transformer and a LU ventilation shaft. As part of Phase 2 these heat sources, along with the new heat loads will be connected back to the existing Phase 1 network. The vision for the Islington scheme is for the eventual expansion of the current network to a wider area network that may also include the inter-connection of the scheme to the existing Shoreditch DHN.

2.4.5.4 The potential of GHSPs in DHNs

The application of GSHPs in DHNs is somewhat limited in the UK. Currently there is only a Code of Practice for surface water source heat pumps in DHNs. It has been produced as a joint project between the Chartered Institution of Building Services Engineers (CIBSE), the Heat Pump Association (HPA) and the Ground Source Heat Pump Association (GSHPA). The work has been supported by the UK Department for Energy and Climate Change (DECC) (now Department for Business, Energy and Industrial Strategy (BEIS)). It is expected that in the future a Code of Practice will be developed for the applicability of GSHPs in DHNs as well.

2.5 CONCLUSIONS

Due to their high operating efficiencies, concerns about carbon emissions, and the highly incentivised nature of GSHPs, the technology has become an increasingly common choice for heating and cooling many types of buildings. In addition to the conventional heat sources, there are alternative options, such as the low-grade heat generated by URs. The soil that surrounds the railway tunnels also contains significant quantities of heat energy. This low grade energy could give an opportunity for a year-round heat supply for nearby users of heat. There is comprehensive literature available regarding how to extract heat directly from URs, for example by placing heat exchangers within existing ventilation shafts. The literature however lacks exploration of the potential for recovering heat through the ground surrounding the tunnels via nearby GHEs. In order to explore this potential in detail, the

interactions of GSHPs with neighbouring UR tunnels must first be fully understood. Investigation of such interactions requires mathematical modelling. A number of modelling approaches have been developed separately for schemes with a different level of complexity. These approaches could potentially be used for the combined analysis of the two systems. Since both URs and GHEs modelling involves complex geometrical aspect ratios and transient phenomena, the use of numerical solution methodologies are preferable. A number of numerical simulation platforms exist that would be suitable for such combined analysis. Investigating the thermal interactions using London as a case study is a practical choice since the tunnels of the LU railway are running beneath a significant part of the central area of the city. Simultaneously, GSHP installations are becoming increasingly common in the city, thus GHEs will eventually get closer in proximity to the tunnels. Understanding the thermal interactions between URs and nearby GSHPs would help to identify how the energy generated and eventually dissipated in the ground by urban railway systems could contribute to sustainable city planning.

CHAPTER 3: PROPOSITION AND CONTRIBUTION TO KNOWLEDGE

3.1 OVERVIEW

The critical review has shown that the low grade heat energy provided by URs could give an opportunity for a year-round heat supply for nearby users of heat. There is a comprehensive literature available regarding how to extract heat directly from URs, for example by placing heat exchangers within existing ventilation shafts.

The literature however lacks exploration of the potential for recovering heat through the ground surrounding the tunnels via nearby GHEs. In order to explore this potential in detail, the interactions of GSHPs with neighbouring UR tunnels must first be fully understood.

Investigation of such interactions requires mathematical modelling. The literature survey has shown that a number of models related to URs and GSHPs have been previously reported. Also several tools exist that allow engineers to mathematically model aspects of the subway environment or the operation of a GSHP system. However, the literature lacks a combined analysis of the two schemes. Implementing previously developed modelling approaches for GSHPs and URs within the same simulation environment would make it possible to study the interactions of the two systems.

The research presented in this thesis will include 2D and 3D numerical simulations of URs and GHEs. The simulation platform selected to carry out the investigations is COMSOL Multiphysics (COMSOL, 2017). The tool is a general-purpose software platform, based on advanced FE numerical methods, for modeling and simulating physics-based problems. The models presented in this thesis will use the language of mathematics to describe the laws of physics, which – for space and time-dependent descriptions – result in partial differential equations (PDEs). The solution to the PDEs is represented by dependent variables, such as velocity fields and temperature fields. The solution is described in space and time, along the independent variables x, y, z, and t.

Within the proposed UR-GHE models the key physical phenomena will include fluid flow in the GHE pipes, air flow within the UR tunnel and heat and mass transfer for entire model domain. For such physical phenomena the descriptions are based on the laws for conservation of momentum, mass and energy. The fluxes in these conservation laws are typically composed of advection and dissipation. The laws governing the proposed model will be combined to describe their interactions within the same simulation environment.

The literature review revealed that a number of analytical solutions were developed in the past which can describe some aspects of the operation of URs and vertical GHEs. Some of these solutions (such as the FLS, and ICS) as well as data from the literature will be used to validate the numerical models developed. Once the model is built and validated, investigations will be conducted with the aim of identifying key parameters influencing the interactions. Additionally, the development of rules-of-thumb and designer aids are also proposed, which will provide guidance to engineers working in fields where these interactions occur.

3.2 ORIGINAL CONTRIBUTION TO KNOWLEDGE

The original contribution to knowlede centres on the development of a mathematical model that: (i) Enables the analysis of interactions between URs and GSHPs; (ii) Identifies the key parameters effecting the interactions; (iii) Allows various design options to be considered that may enhance the cooling and heating effect of GSHPs and URs.

3.3 METHODOLOGY

The research detailed in this thesis will mainly include numerical modelling work which will be broken up into different stages, with the individual systems (e.g. GHEs and URs) modelled and validated separately. Figure 3.1 illustrates the proposed strategical framework for these works and the highlights the specific chapters where these specific stages are detailed. The model development and validation strategies including their limitations are detailed in Table 3.1.

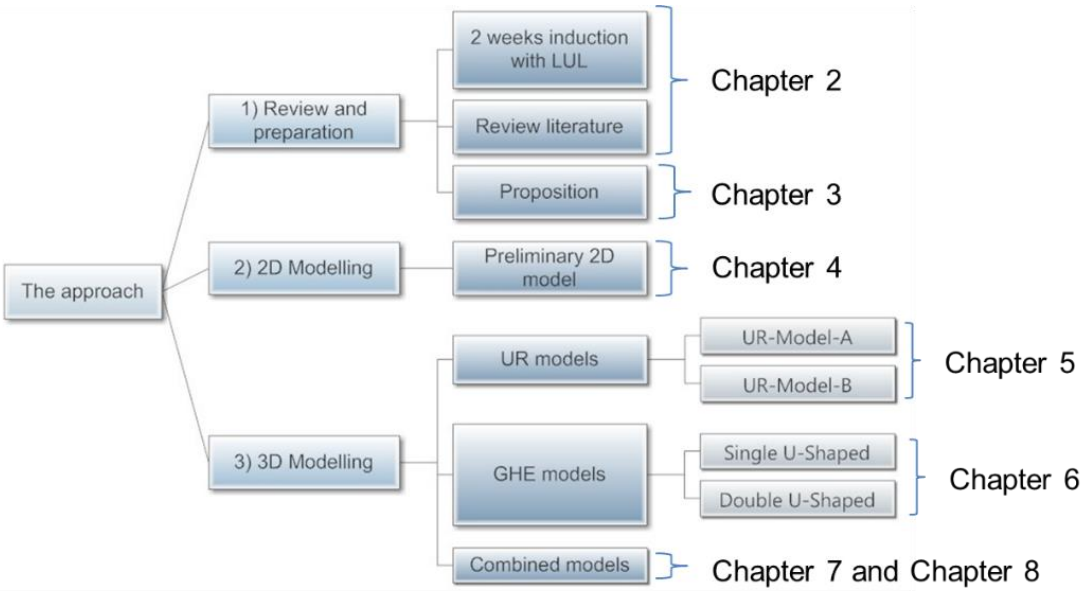

Figure 3.1: The strategical framework for the research

Table 3.1: Model development and validation strategies

2D numerical models				3D numerical models			
Boundary condition	Physical phenomena	Validation Approach	Assumptions/ Limitations	Boundary condition	Physical phenomena	Approach	Assumptions/ Limitations
Time dependent temperature boundary on the soil surface	Heat transfer from surface to deep ground	Numerical results compared to - Analytical equation presented by Brandl (2006)	Homogenous soil Radiation effects and geothermal temperature gradient are neglected	UR tunnel boundary conditions: (i) Time dependent temperature and velocity at the tunnel inlet; (ii) Line heat source at the centre of the tunnel; (iii) outflow condition at the tunnel outlet	Heat transfers and turbulent air flow	Numerical results of averaged tunnel air temperatures compared to platform air temperatures provided by LUL	The train is represented as a line source at the centre of the tunnel with a constant heat dissipation rate Airflow in the tunnel is constant at a fixed rate
Temperature boundary on the tunnel wall	Radial heat transfer from the wall of the tunnel into the soil	Numerical results compared to - results of the 1D steady state heat equation for cylindrical sources (Incropera and Lavine, 2011)	Homogeneous soil Constant temperature at tunnel wall Constant temperature at a far-field distance	GHE boundary conditions: (i) Constant temperature and volume flow rate at the pipe inlet; (ii) Outflow at the pipe outlet	Non-isothermal pipe flow and heat transfers from pipe to soil	Numerical results of temperature excess of soil surrounding the GHEs compared to - Finite Line Source (FLS) analytical solution (Zeng et al., 2002)	GHE pipes and fluid flow are represented as linear 1D elements Borehole/energy pile material and physical geometry is neglected. Homogeneous soil Constant heat rate of the GHE
Time dependent heat flux boundary on the wall of the GHE	Heat transfer at the wall of the GHE	Numerical GHE wall temperatures compared to - data obtained from thermocouples at the installation at LSBU (Yebiyo et al., 2016)	Fluid flow within the GHEs are neglected. The flux on the GHE wall is applied based on the data reported by (Yebiyo et al., 2016)				

CHAPTER 4: TWO DIMENSIONAL MODEL DEVELOPMENT AND INVESTIGATIONS

4.1 INTRODUCTION

The critical literature review identified that there has been limited exploration related to the thermal interactions of GSHPs and URs. In order to establish the potential for such interactions, an initial 2D modelling methodology was developed and is described in this chapter. The numerical model was built with the software package COMSOL Multiphysics. The 2D model was highly simplified to enable rapid analysis of the systems. The results of this preliminary investigation revealed that interactions occur between URs and nearby GHSPs. It was established that as the separation distance between the two systems becomes smaller, the interactions between them become greater. Therefore, it was shown that the proximity at which the GHE is built from an UR tunnel is an important factor. In addition, the 2D model was used to explore the potential influence of other parameters on the interactions, including groundwater movement, parallel running tunnels, earth flux and tunnel wall material. Those that were found to have an effect on the interactions could then be modelled within a more detailed 3D analysis which would evolve out of the work detailed here.

4.2 A PRELIMINARY TWO-DIMENSIONAL MODEL

4.2.1 Model Introduction

A time dependent FE model was built with the software package COMSOL Multiphysics. For the built 2D model, London was chosen as a case study, since an UR network runs beneath the majority of the city. Thus the geometrical parameters, material properties, initial, boundary and operating conditions implemented within the model were based on typical conditions for the UK capital city. In most locations in London, UR tunnels run through the London Clay, a soil of very low permeability (Hight *et al.,* 2003). For this reason, the preliminary model assumes negligible groundwater movement and a soil which is typically fully saturated with water. Consequently, the time dependent simulation process for the whole soil domain was performed using the Fourier equation without heat generation shown by Equation 4.1. This equation is based on applying conversation of energy to a differential control volume through which energy transfer is exclusively by conduction. The left side of the equation describes the change in thermal energy storage whilst the right side defines the net transfer of thermal energy into the control volume, i.e. the model domain.

$$\rho C_p \frac{\partial T}{\partial t} = k\nabla^2 T \tag{4.1}$$

A detailed breakdown of the 2D model constriction is attached as Appendix A and the key model features are detailed in the following sections.

4.2.2 Domain and Geometries

Figure 4.1 shows the modelling domain. The domain was developed so that the dimensions of the ground were much larger than the GHE and UR tunnel dimensions that would be placed in the domain. This was to minimize the effects introduced by the boundary conditions.

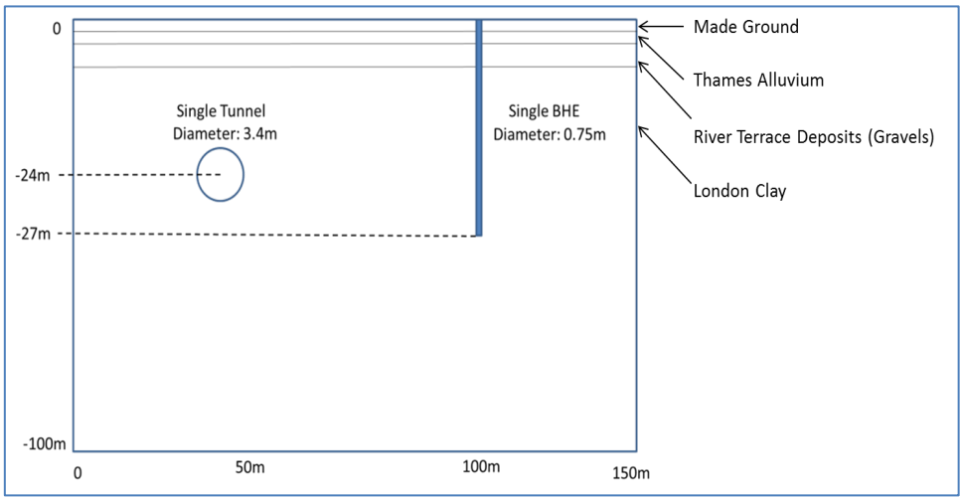

Figure 4.1: Geometrical domain of the 2D model

The literature review suggested that after about 20 m from the wall of an UR tunnel the thermal effects are negligible (HU *et al.*, 2008), whilst for a vertical GHE a distance of 10 m is suggested (Koohi-Fayegh and Rosen, 2012). The model domain was deliberately larger than those values so that different configurations could be investigated within the same overall computational domain.

The GHE dimensions were taken from an existing GSHP installation at London South Bank University (LSBU). The closest running LU tunnels; the Northern and Bakerloo lines, are approximately 50 m away from this specific GSHP installation with an average depth of 24 m. The preliminary model considers a single tunnel and borehole to allow the initial interaction to be identified without overcomplicating the analysis.

The different ground conditions that typically exist down to 100 m below the surface within the central London area were taken into account in the building of the model. The thermo-physical properties of the different soil layers are summarized in Table 4.1. It can be seen that the Made Ground has the highest thermal diffusivity (because of its relatively high thermal conductivity) whilst the London Clay the lowest.

Table 4.1 also summarises the thicknesses of the different soil layers with the 2D model domain. It can be seen that the thickness of the London Clay was chosen to be as 92 m, while the thickness of the top soil layers are significantly smaller. These specified thickness and material properties of the soil layers of the soil domain were set based on typical values reported in literature, in particular by Paul (2009), CTP (2009), Diao *et al.* (2004) and Thompson (2006).

Table 4.1: Thickness and thermo-physical properties of the specified layers

Soil layer	Thickness	Thermal conductivity	Thermal diffusivity	Density
	[m]	[W/m*K]	[m^2/s]	[kg/m^3]
Made Ground	2	3.2	2.5E-07	1800
Thames Alluvium	2	1.25	6.4E-07	1800
River Terrace Deposits (Gravels)	4	0.95	5.1E-07	2000
London Clay	92	1.3	8.5E-07	1920

4.2.3 Boundary Conditions

4.2.3.1 Soil and lateral boundaries

Headon *et al.* (2009) reported that in central London average monthly air temperatures vary between 6 to 19°C between January and December, with an annual average of around 11.7°C. On the other hand, the daily low temperatures in December and January are sometimes falling under -3˚C. For example in January 2016 the lowest temperature recorded was -4˚C (AccuWeather, 2017). Also in summer time temperatures could peak in London at around 32˚C (BBC, 2016). Based on this information a simplified temperature boundary condition was applied for the soil surface which follows Equation 4.2. The formula represents a periodic annual cycle which starts in the month of May. The formula neglects the daily variation of the soil temperature. The validity of this assumption rests in the fact that the soil

heat transfer is fairly slow and therefore the effect of the daily transfer is minimal. A similar method was used by Busby *et al.* (2009) as well as by Lazzari *et al.* (2010).

$$T_{S\_surf} = a_{air} * sin\left(\frac{2\pi t}{\tau}\right) + T_{av\_air} \quad (4.2)$$

Where:

$\tau = 1\ year = 31{,}536{,}000\ s$

The initial ground temperature of the soil domain was set according to Equation 4.3 where the average UK geothermal gradient is 0.026°C m^{-1}(Busby *et al.*, 2009).

$$T_{Gr\_init} = T_{av\_air} - 0.026 * z \quad (4.3)$$

The lateral boundary of the domain was assumed to be adiabatic therefore a Neumann boundary condition was applied that can be expressed as Equation 4.4. Intuitively, this equation says that the temperature gradient across the boundary is zero. This is a commonly used boundary condition in GHE models which reduces model complexity e.g. as used by Cui *et al.* (2008), Florides and Kalogirou (2007) and Bortoloni *et al.* (2017). Its application in the model could also be justified by findings from the literature review of this thesis that highlighted that beyond the far-field radius of 20 m there are no heat exchanges occurring.

$$q" = (-k\nabla T) = 0 \quad (4.4)$$

4.2.3.2 GHE

In order to simplify the model further, the fluid flow within the pipes of the GHE was neglected and instead a time periodic heat flux boundary was applied on the entire wall surface of the GHE, similarly to the method described by Lazzari *et al.* (2010). A time periodic heat load was created with a period of 1 year representing a GSHP system operating in both heating and cooling modes using Equation 4.5. The period which the formula represents is the same as described with Equation 4.2. The maximum heat load per unit GHE length was taken to be 18 W/m. This value matched the operational performance of the central London GSHP installation site at LSBU (Yebiyo *et al.*, 2016). The time periodic

heat load was then applied to the wall of the GHE as a time periodic heat flux boundary condition per unit length as in Equation 4.6.

$$Q_{GHE_{Wall}} = a\_load * \sin\left(\frac{2 * \pi * t}{\tau}\right) \quad (4.5)$$

$$q_{GHE_{wall}} = Q_{GHE_{wall}}/(2 * \pi * r_{GHE}) \quad (4.6)$$

4.2.3.3 UR tunnel

Heat exchange between the tunnel air flows and the surrounding ground depends on many factors, including traffic and ground related phenomena as well as the temperature of the incoming air. For this preliminary 2D study, the entire air domain of the tunnel has been neglected. Instead, a simplified temperature boundary was applied directly to the inner wall surface of the tunnel based upon the work of Gilbey *et al.* (2011). The formulation of the temperature boundary is shown in Equation 4.7. Although this fixed temperature boundary limits the interactions between the tunnel and the GHE, it was considered to be appropriate to establish whether an UR tunnel could have an impact on a nearby GHE. Gilbey *et al.* (2011) also reported that the tunnel air temperatures are typically 2 to 3°C cooler than platform air temperatures, and to reflect this in the model a tunnel surface temperature boundary was modified as shown in Equation 4.8. The surface boundary condition used in this initial model did not require an ambient air temperature. To prevent the inclusion of an additional parameter the model assumes that the outside air temperature (ambient as used by Gilbey *et al.* (2011)) can be approximated as the soil surface temperature from Equation 4.2.

$$T_{plat} = 0.36 * T_{S\_surf} + 19.5 \quad (4.7)$$

$$T_{tun} = 0.36 * T_{S\_surf} + 17.5 \quad (4.8)$$

4.2.4 Results and Validations

4.2.4.1 Soil

Initially the soil temperatures were investigated excluding the load of the tunnel and the GHE. In order to ensure that the applied temperature boundary on the soil surface was

applicable, the model was validated against the work of Brandl (2006). The results of this validation are illustrated in Figure 4.2. The analytical solution presented by Brandl (2006) ignores radiation effects and the geothermal gradient and assumes a homogeneous soil profile. For the purpose of the validation, the layered soil profile in the numerical model was reduced to a single stratum, which consisted of London Clay. Figure 4.2 shows a good correlation between the analytical predictions and the model for a homogeneous simulation. It can be seen that the surface temperature variation has an effect down to about 10-12 m below the surface, which corresponds well with what is detailed in the literature. It can be seen in Figure 4.2 that in winter the surface is cooler than the deep ground, and in summer conversely it is warmer. In spring, the surface warms faster than the deeper ground because of the thermal capacitance of the soil at those depths. However, after a certain depth (approximately 4 m) the ground gets warmer again. In autumn, there is a similar trend however process is reversed.

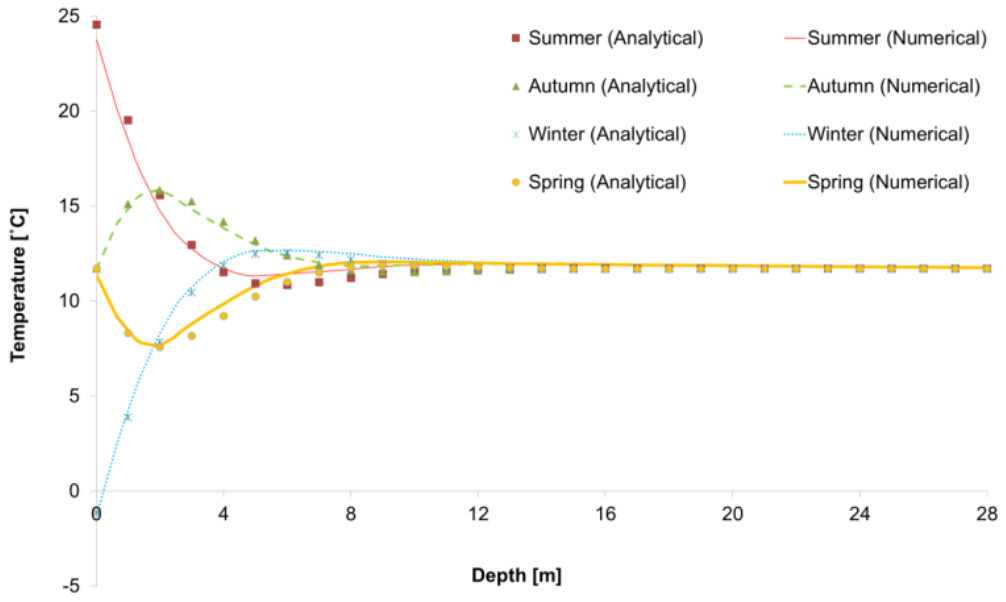

Figure 4.2: Annual temperature distribution within soil. Numerical results compared with results from an analytical solution (Brandl, 2006)

4.2.4.2 GHE

To validate the performance of the GHE heat flux, the simulated temperature figures at the wall of the GHE were compared to data obtained from thermocouples at the installation at LSBU. The thermocouples, from which the data was obtained and were then used to

validate the 2D model, were installed at depths of 3, 14 and 26 m on the wall of the GHEs (Yebiyo *et al.*, 2016). For multiple year time intervals (August 2010 to August 2013) the monthly averaged GHE wall temperatures at those depths were observed by Yebiyo *et al.*, 2016. During those site measurements at LSBU, the values of the GHEs' average wall temperature during the cooling and heating seasons were found to be between 20 and 5˚C respectively (Yebiyo *et al.*, 2016). These values have been compared well with the model generated figures of ~ 21 and 6˚C, hence the modelling assumption related to the GHEs operation was maintained for the preliminary investigation.

4.2.4.3 UR Tunnel wall surface temperature

The model predictions of the tunnel wall surface temperatures and the ground surface temperatures are plotted in Figure 4.3. The maximum and minimum values of the sinusoidal wave represent the summer and winter conditions respectively throughout.

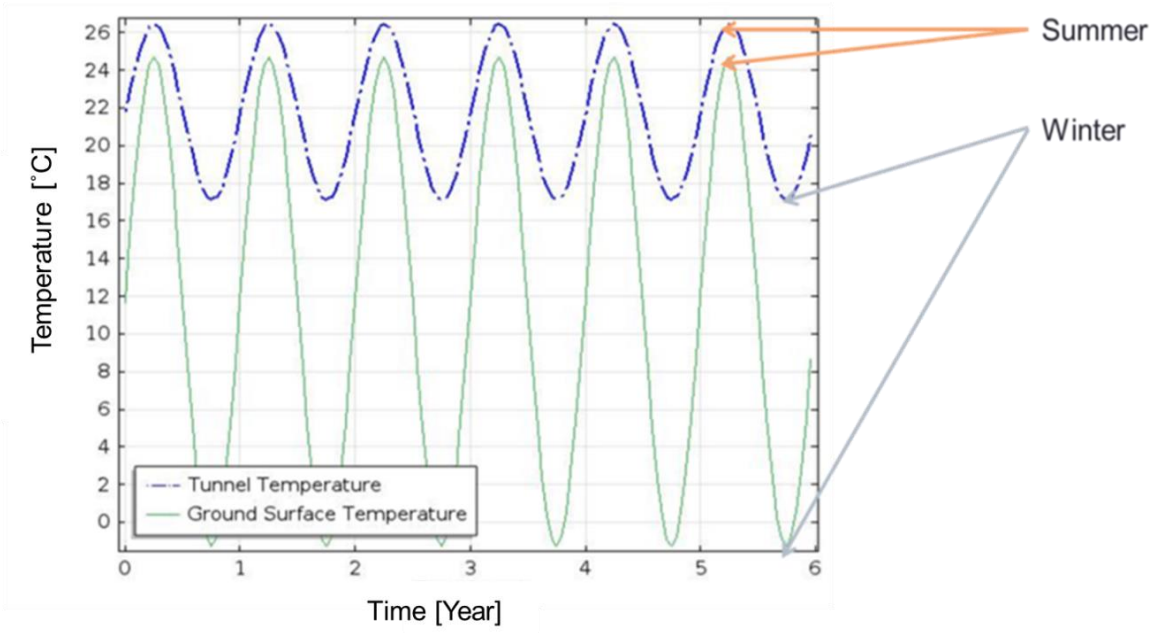

Figure 4.3: Numerically simulated tunnel and ground surface temperatures

A periodic stationary load was applied through the simulation period, such that the same cycle pattern appears throughout. The figure clearly illustrates that the annual temperature fluctuation in the tunnels is significantly lower than the fluctuation at the surface of the ground. Gilbey *et al*. (2011) reported that current winter-temperature on LU platforms can be up to 20°C even on operational cold winter days. They also noted that tunnel temperatures are approximately 2 to 3°C cooler than the platforms. Therefore, the 17°C tunnel

temperatures obtained from the simulation during the winter season were considered to be appropriate for the analysis of a London based interaction. The summer months are also considered to be reasonable due to matching conditions reported by Thompson *et al*. (2008).

4.2.4.4 Heat transfer in the ground from the wall of the UR tunnel

In order to validate the heat transfer process from the UR tunnel wall into the ground, the model generated numerical results were compared with the results gained from the analytical solution of the 1D steady state heat equation for cylindrical sources as Equation 4.9.

$$\frac{1}{r}\frac{d}{dr}\left(k.r\frac{dT}{dr}\right) = 0 \qquad (4.9)$$

It can be seen in Figure 4.4 that the numerical results and the results of the analytical solution are nearly identical (~ plus or minus 0.02˚C temperature difference), thus the tool is capable to accurately simulating the impact of an UR on its surroundings.

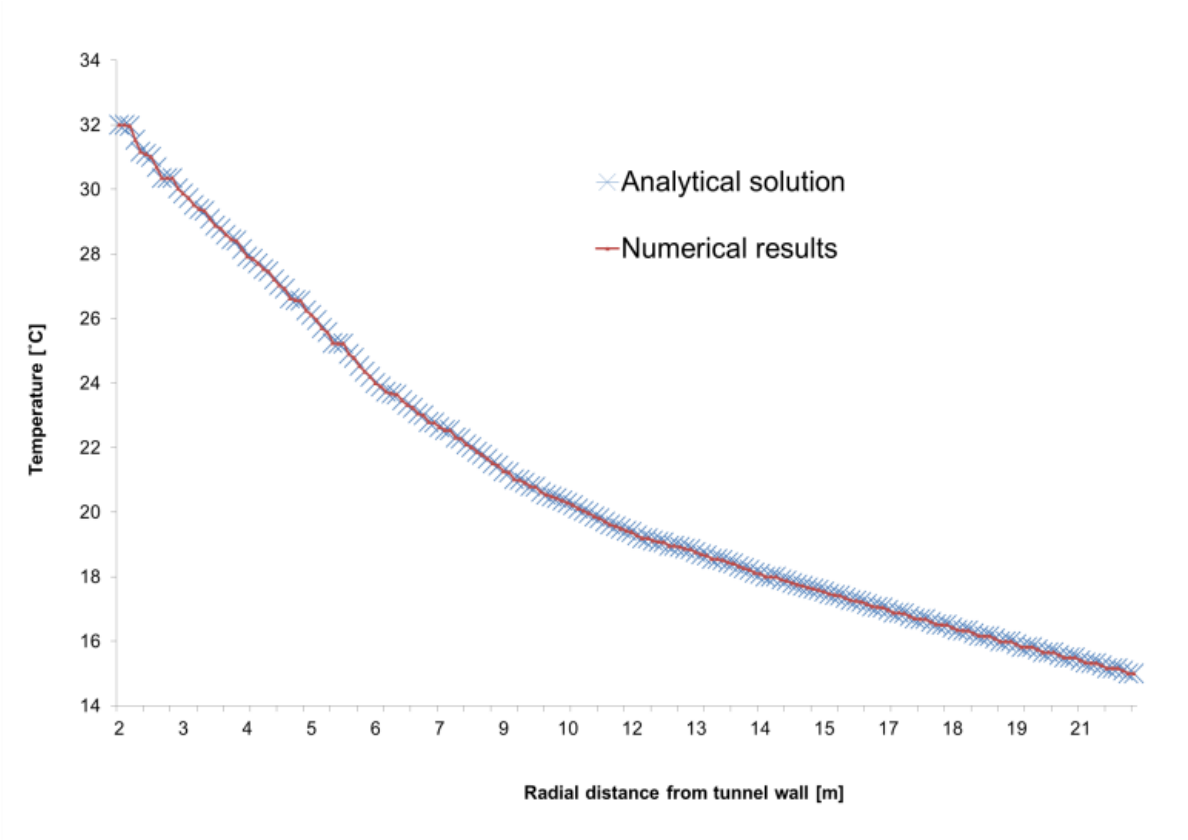

Figure 4.4: Steady state temperature distribution by radius (numerical results vs analytical solution)

4.2.5 Mesh Independency Analysis

In order to establish the mesh independency of the numerically generated results, four unstructured meshes made of triangular elements were tested. The finest mesh contained 5926 domain elements while the coarsest mesh included 426. Temperature values at a specific point (middle point between the tunnel and GHE walls) were compared for the different mesh configurations. For the preliminary study introduced in this chapter, the second finest configuration was selected with 1807 domain elements. Results from a model with such mesh configuration converged to nearly the same values as the model with the finest mesh, but being able to achieve that 2 seconds faster. The mesh analysis of the preliminary 2D model is attached in Appendix B.

4.3 INITIAL INVESTIGATIONS WITH THE 2D MODEL

4.3.1 Introduction

The preliminary model was used to perform a study of the impact of separation of the UR and GHE. This study considered two key locations. The first consideration (Investigation 1) was the impact that the two systems had on each other, which was considered via the ground temperature at the midpoint between the UR and the GHE. The second effect considered (Investigation 2) was the impact that the UR had upon the GHE as the distance between the two systems decreased.

4.3.2 Investigation 1

The effect of heat loads on an initial ground temperature of 12.3°C at a specific depth of 24 m was investigated through three different setups as follows:

Option (a) only GHE heat load
Option (b) only tunnel heat load
Option (c) both heat loads

For these options different scenarios were set whereby the horizontal distance between the wall of the UR tunnel and the GHE was reduced gradually by moving the UR tunnel towards the GHE. The simulated temperature was monitored at the midpoint between the UR and GHE. The temperature rise at the midpoints during the 6 year simulation period was considered and is reported in Table 4.2 and Figure 4.5. Note that the coordinate of the GHE was fixed throughout the analysis and only the UR location was varied in the model domain. The results are shown in Figure 4.6.

Table 4.2: Investigation 1 - The different scenarios investigated

	Horizontal distance between tunnel and GHE wall	Midpoint "x" coordinates	Midpoint "y" coordinates	GHE left wall "x" coordinate
	[m]	[m]	[m]	[m]
Scenario 1	50	75	-24	100
Scenario 2	40	80		
Scenario 3	30	85		
Scenario 4	20	90		
Scenario 5	15	92.5		
Scenario 6	10	95		
Scenario 7	8	96		
Scenario 8	3	98.5		

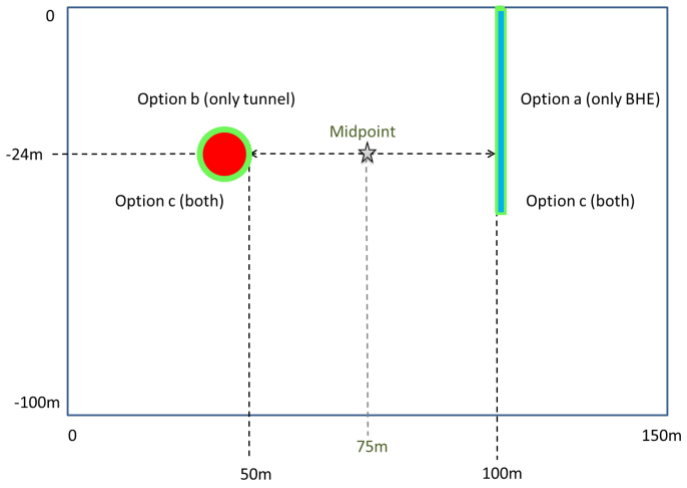

Figure 4.5: Investigation 1 - Scenario 1

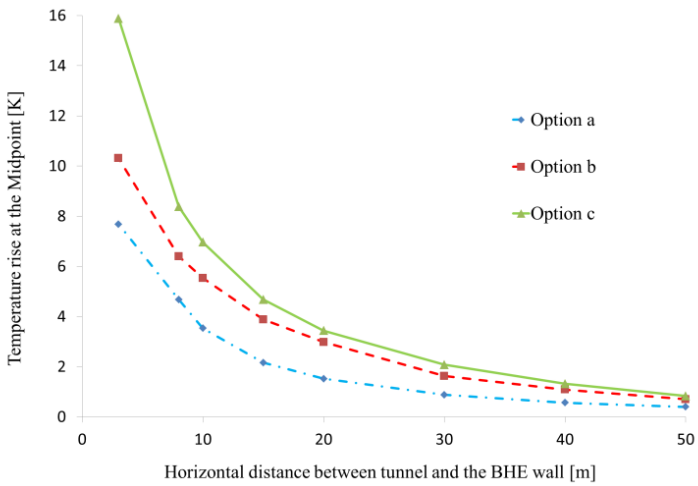

Figure 4.6: Investigation 1 – Results

Figure 4.6 shows that, as the tunnel get closer to the GHE the effects of heat loads on initial ground temperatures are more significant. When both loads are considered simultaneously (Option c) the resulting temperatures are the highest. In addition, it is also notable that the UR tunnel heat load (Option b) has a greater effect on the initial ground temperatures than the GHE heat load (Option a). Therefore, the heat load of the UR is likely to have a stronger impact on the GHE than the GHE's impact upon the UR. This could be beneficial depending on the application requirements. Utilizing higher than expected source temperatures could substantially enhance performance of GSHPs operating in heating mode. On the other hand, high ground temperatures are likely to cause negative effects on GSHPs operating in a cooling cycle. If the soil temperature rose and thermally saturated the GHE it is likely to be unable to reject heat to the ground. This may eventually lead to the GSHP not working effectively in all operating modes.

4.3.3 Investigation 2

The second investigation aimed to study the interactions of the GHE and the UR tunnel by examining the temperatures at a point on the wall of the GHE in response to the closer proximity of the tunnel. The point of interest was selected at a depth of 24 m while the horizontal distance between the tunnel and the GHE wall was varied between 3 and 50 m. The resulting GHE wall temperatures are plotted in Figure 4.7.

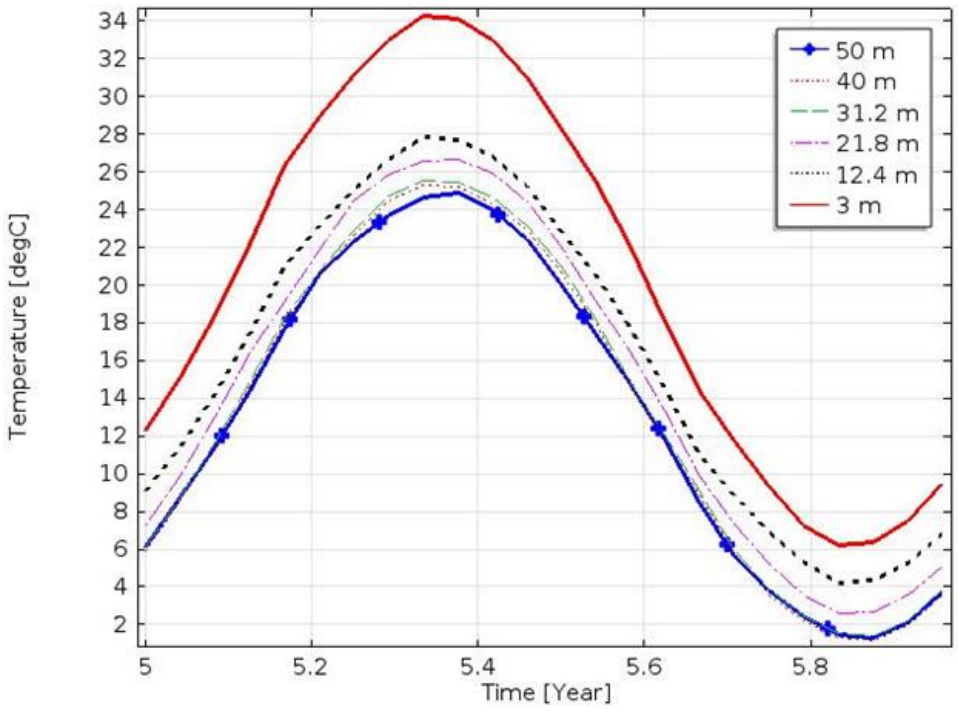

Figure 4.7: GHE wall temperature versus tunnel proximity

Figure 4.7 shows that as the tunnel get closer to the GHE the temperature changes at the wall of the GHE are more significant. A maximum temperature, 34°C at the GHE wall, was seen when the proximity between the tunnel and the BHE was reduced to 3 m. As previously noted, increased GHE wall temperatures are beneficial for heating solutions. The heating CoP is improved by approximately 3% for each degree Celsius that the evaporating temperature is raised (Cengel and Boles, 2001).

4.3.4 Conclusions from the Initial Investigations

Results of the initial investigations showed that both the operation of URs and GHEs have an impact on their surroundings. It was also shown that the operation of the railway was likely to have a significant impact on the performance of the GHE. The next section investigates additional characteristics using the 2D model to further establish the parameters which may impact on the interactions between URs and nearby GHEs. The parameters which were fund to have a potential impact on the interactions were used when the complex 3D numerical model was developed.

4.4 ADDITIONAL INVESTIGATIONS WITH THE 2D MODEL

4.4.1 Introduction

The preliminary 2D model was used to perform five additional investigations with the main objective of identifying parameters or physical phenomena, which could potentially have an effect on the interactions between GSHPs and URs. The parameters which were identified to have a potential effect on the interactions, were then implemented within the more complex 3D models introduced in Chapters 5, 6, 7 and 8. Throughout these additional investigations, the 2D model geometry presented in Figure 4.1 was further simplified by neglecting the Thames Alluvium and only considering the Thames Gravels as a geological section between the Made Ground and London Clay. This new assumption was made on the basis of some historical information referring to geological cross sections at the location of Kennington station. This is illustrated in Figure 4.8. By neglecting the Thames Alluvium, the thickness of the Made Ground layer was increased. It can be seen on Figure 4.8, that the layer thickness of the Made Ground and the gravels beneath that are similar. The thermo-physical properties of the Made Ground layer were changed by averaging its properties with the properties of the Alluvium shown in Table 4.1. This way, the complication of the model was reduced whilst maintaining the applicability of the model to the London case study.

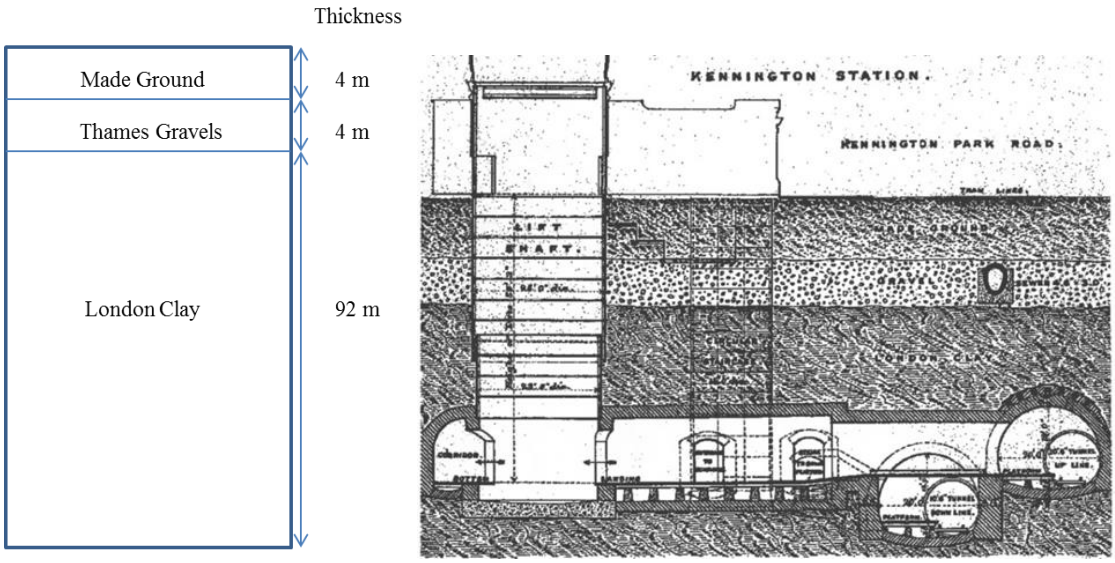

Figure 4.8: New soil layer profile based on some historical data (Gunn, 2015)

4.4.2 Groundwater Movement

4.4.2.1 Introduction

Where groundwater is present, flow will occur in response to hydraulic gradients, and the physical process affecting the heat transfer in the ground is inherently a coupled one of heat diffusion (conduction) and heat advection by moving groundwater (Chiasson *et al.*, 2000). Thus the presence of groundwater flow changes the heat transfer problem from one of purely heat conduction to one of coupled flow and advective-diffusive heat transfer. Two investigations were conducted with the aim of establishing the potential impact of groundwater movement on UR-GSHP interactions whilst considering different soil types (clay and sands). The preliminary 2D model capabilities were extended to be able to take account of flow through porous media.

4.4.2.2 Darcy's law

The governing equation describing flow through porous media is Darcy's law. Darcy's law states that the velocity field is determined by the pressure gradient (hydraulic heads), the fluid viscosity, and the structure of the porous medium. The net flow across the porous medium follows Equation 4.10.

$$u = -\frac{K}{\mu}(\nabla p + \rho g \nabla D) \tag{4.10}$$

If the gravity effects are neglected, that is, the elevation "D" is set to zero, then Equation 4.10 becomes Equation 4.11.

$$u = -\frac{K}{\mu}\nabla p \tag{4.11}$$

The energy balance equation describing the coupled heat and groundwater flow is Equation 4.12.

$$\rho_{wat} C_{p_{wat}} \left(\sigma \frac{\partial T}{\partial \tau} + u \cdot \nabla T\right) = k_{Gr} \nabla^2 T \tag{4.12}$$

4.4.2.3 Investigation 1 – Groundwater movement in Thames Gravels and London Clay and its potential impact on UR and GSHP interactions

The first investigation with the 2D model aimed to investigate potential Darcy velocity magnitudes within the different soil layers of the model domain. It also aimed to establish whether the velocity magnitude of groundwater movement in those specific soil layers would have an effect of UR and GSHP interactions. The hydraulic properties assigned to the soil layers in Figure 4.8 are the same values that were used by Diao *et al.* (2004) for gravel and clay. These are summarised in Table 4.3. The values for clay are within the same range as the values reported by Hight *et al.* (2003).

Table 4.3: Hydraulic properties of the specific soil layers

Porous medium	**Hydraulic properties**	
	Hydraulic conductivity [m/s]	**Porosity**
Thames Gravels	3E-3	0.31
London Clay	2.2E-10	0.47

Three different scenarios were considered as boundary conditions during the simulation of the groundwater movement. These options are illustrated in Figure 4.9, Figure 10 and in Figure 4.11, where the green lines; Hd1 and Hd2 are the hydraulic heads.

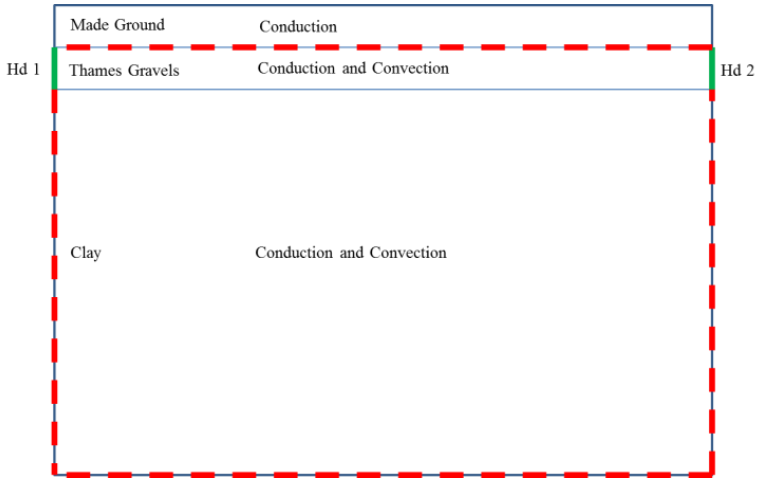

Figure 4.9: Scenario 1 - Hydraulic head in Thames Gravels only

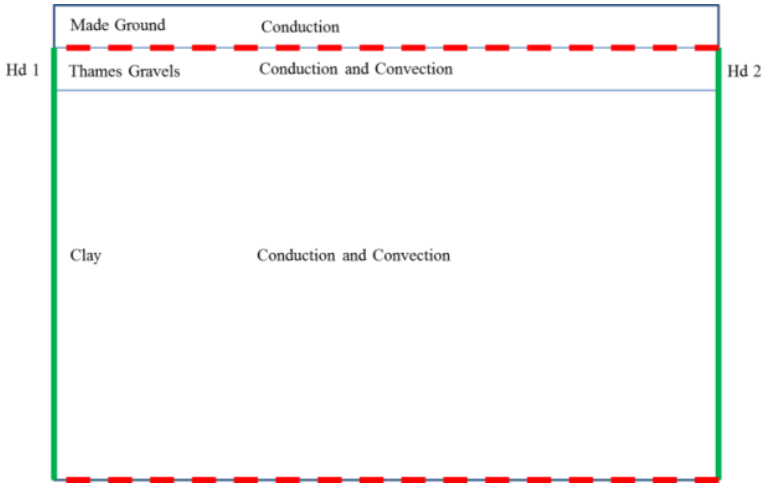

Figure 4.10: Scenario 2 - Hydraulic head in Thames Gravels and Clay

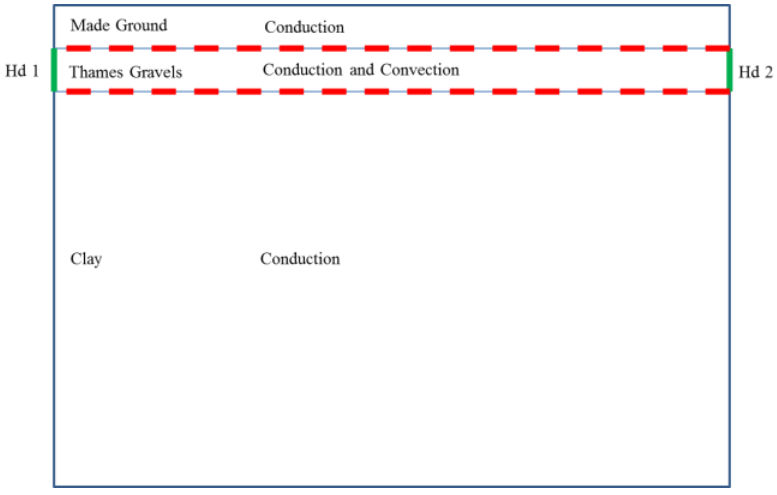

Figure 4.11: Scenario 3 - Hydraulic head in Thames Gravels only (no flow in Clay)

It can be seen in the figures that in Scenario 1 and 3 the heads were imposed only within the Thames Gravels layer. In Scenario 2 the heads were placed throughout the Thames Gravels as well as the layer of the London Clay. The red dotted lines indicate boundaries where no flow conditions were applied. The temperature boundary on the soil surface and the initial ground temperatures were kept as they were described within the preliminary model.

4.4.2.3.1 Results of investigation 1

The simulated Darcy velocity magnitudes for the three different modelling setups are summarised in Table 4.4. The results showed a relatively strong groundwater flow within the Thames Gravels and an extremely low velocity magnitude within the London clay for all the options.

Table 4.4: The simulated Darcy velocity magnitudes

	Velocity magnitude [m/s]		
	Scenario 1	Scenario 2	Scenario 3
Thames Gravels	2E-5	2E-5	2E-5
London Clay	5E-13	1.3E-12	N/A

A slightly faster velocity magnitude was achieved within the London Clay in Scenario 2 compared to Scenario 1. Overall, the simulated ground water velocities in all cases correspond well to typical values reported by Chiasson *et al*. (2000) as well as Diao *et al*. (2004).

4.4.2.3.2 Implication of results for a London based study

The work of Lee and Lam, (2007) addressed the fact that square borehole fields are less likely to be affected by groundwater direction, especially if the groundwater flow velocity is less than 1E-6 m/s. This was confirmed by the work of Angelotti *et al.* (2014) who simulated a vertical GHE energy injection/extraction rate to/from the ground, derived as a function of the Darcy velocity. The results were compared with the purely conductive case. For a velocity of 1E-7 m/s, negligible differences were found with respect to the null velocity case.

The 2D model results showed that within the Thames Gravels the simulated Darcy's velocity magnitudes were 2E-5 m/s. This is within the velocity range which Angelotti *et al.* (2014) concluded would have an impact on the GHEs' heat extraction or rejection rates. However, the Angelotti *et al.* (2014) conclusions were derived based on scenarios where the 100 m

deep GHEs were installed in homogenous fully saturated sandy type soils. This is not a typical case in London, where the majority of UR and GHE structures are built in the London Clay and where the more porous medium, the Thames Gravel layer, is only about 4 m in depth. The simulation results showed that in the layer of the London Clay the groundwater movement is extremely low: 1.3E-12, thus it can be established that its impact on the UR-GSHP interactions is negligible. For this reason, further more complex 3D numerical models in this thesis, where the UR and GHE structures are built in mainly clay, will neglect the simulation of groundwater movement and will assume a pure conductive heat transfer.

4.4.2.4 Investigation 2 – Groundwater movement in sands and its potential impact on UR and GSHP interactions

Although the majority of the LU tunnel network was built in London Clay, some sections of the network run through sandy type soils (Paul, 2016). Different types of earth have different heat transfer characteristics, thus could impact differently on UR and GSHP interactions. This investigation aimed to establish the potential impact of groundwater movement within sands on UR and GSHP interactions in relation to simulated Darcy velocities. The geometry and boundary conditions of the 2D model were kept as they were described previously. However, only Scenario 1 (Figure 4.9) and Scenario 2 (Figure 4.10) were considered, and the layer of London Clay was replaced with coarse and fine sands respectively.

4.4.2.4.1 Properties of sands

The thermal conductivity of soils depends upon various factors, i.e., type of soil, particle size distribution, soil structure, porosity, saturation degree, temperature, etc. The effect of porosity (n) and saturation degree (S_d) on thermal conductivity of sands (k_sand) was investigated through laboratory tests by Chen (2008), and an empirical equation of thermal conductivity expressed as a function of the two was developed as Equation 4.13. This formula was utilized during the present investigation. Other thermal and hydraulic properties were adopted from the work of Hu *et al.* (2008), Menkiti *et al.* (2015), Diao *et al*. (2004) and Chiasson *et al.* (2000) and are summarised in Table 4.5.

$$k_{sand}(n, S\_d) = 7.5^{1-n} 0.61^{n} [(1 - 0.0022) S\_d + 0.0022]^{0.78n} \quad (4.13)$$

Table 4.5: Sands thermal properties

Porous medium	Thermal Properties			Hydraulic Properties	
	Thermal conductivity	Density	Specific heat capacity	Hydraulic conductivity	Porosity
	[W/m*K]	[kg/m^3]	[J/kg*K]	[m/s]	
Sand (coarse)	k_*sand* = 2.7	1800	1550	7.3E-5	0.38
Sand (fine)				6.3E-6	0.40

4.4.2.4.2 Results of investigation 2

The simulated Darcy velocities within the sand layer that replaced the London Clay are summarised in Table 4.6. The resulting velocities did not vary significantly across the different set-ups. All the simulated values correspond well to the work of Diao *et al.* (2004) who reported velocity values of 7.3E-7 m/s within coarse and 6.3E-8 m/s within fine sand.

Table 4.6: The simulated Darcy velocity magnitudes for sands

	Velocity magnitude [m/s]	
	Scenario 1	Scenario 2
Sand (coarse)	3E-7	4.8E-7
Sand (fine)	2E-8	4.2E-8

4.4.2.4.3 Conclusions of investigation 2

As previously mentioned, for a Darcy velocity of 1E-7 m/s, negligible differences were found as regards GHE performance with respect to the null velocity case (Angelotti *et al.* 2014). Since the sandy sections of the LU tunnel network consist of more fine sands, like the Bagshot formation (Paul, 2016), further 3D simulations which consider sandy type soil characteristics, with pure conductive analysis are sufficient.

4.4.3 Parallel Running Tunnels

Within the preliminary model only a single tunnel was considered within the modelling domain. However in many cases, tunnels are running nearly parallel. Besides that, they are rarely running on a strictly horizontal line. Sometimes they do rise and then fall, even on a

short section of the network. One example of this is a section of the Central line between St Pauls and Bank stations. The tunnels are ‘stacked’ vertically one above the other at St Paul’s station. As the tunnels progress eastwards the westbound tunnel falls, and the eastbound rises. At Bank station, the tunnels are side by side. Because of the ‘rising’ and ‘falling’ alignment of the tunnels, the crown of the tunnels varies from approximately 20 to 25 m below ground level. This is illustrated in Figure 4.12.

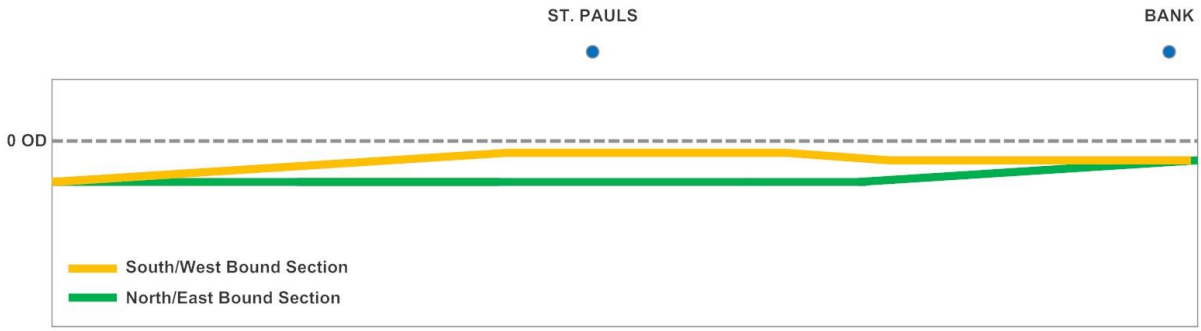

Figure 4.12: Short cross-section of the Central line between St. Pauls and Bank stations (Adapted from: TfL, (2013))

Modeling such extreme geometries adds to the model complexity by increasing its size and computational efforts, especially if more explicit 3D domains are considered. The aim of this section is to introduce an investigation into a geometrical simplifying method using the preliminary 2D model. Such methods could then be used when the thermal effects of parallel running UR tunnels on their surroundings are to be considered in further more complex models.

4.4.3.1 Investigation 3 - Tunnel Equivalent Diameter

For Investigation 3, three different tunnel geometrical options were considered as Figure 4.13, Figure 4.14 and Figure 4.15. These were based on the tunnel alignment explained for the Central line’s section between St. Pauls and Bank. Option A where the tunnels are stacked vertically one above the other at St Pauls. Option B is approximately half way between the two stations where the westbound tunnel falls and the eastbound rises. Option C is a representation of the tunnel alignment at Bank station.

During investigation 3 the following assumptions were used in the 2D model:

- The domain comprises a homogenous soil profile which is London Clay.
- Groundwater movement has been neglected.
- The surface, lateral and bottom boundaries of the domain were adiabatic.

- The temperature boundaries on the tunnel(s) surface were obtained using Equation 4.8 listed in Chapter 4.

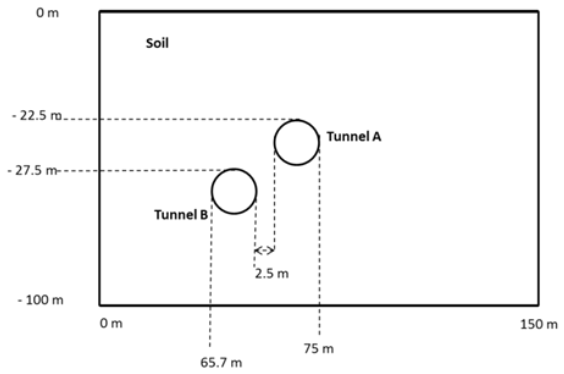

Figure 4.13: Parallel tunnels – Option A

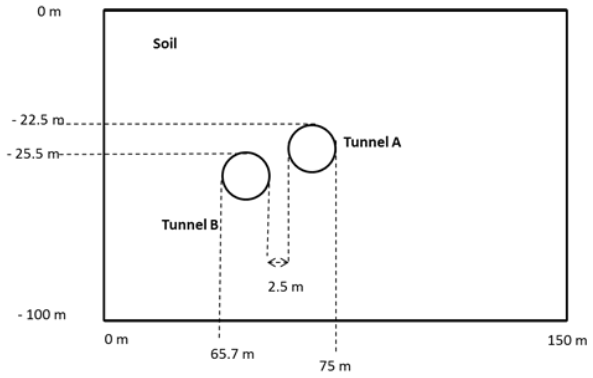

Figure 4.14: Parallel tunnels – Option B

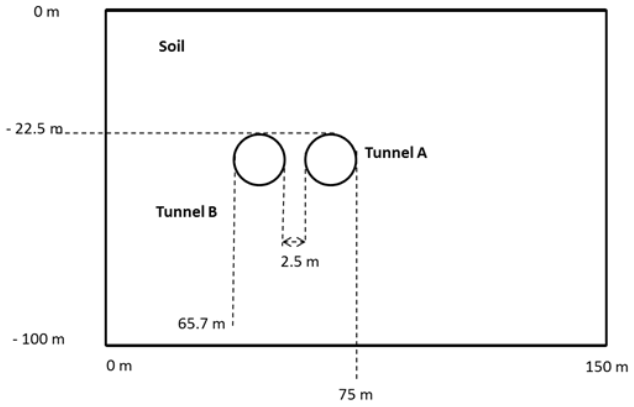

Figure 4.15: Parallel tunnels – Option C

4.4.3.1.1 Equivalent diameter (ED) simplifying method

The simplifying method used is a type of conversion called equivalent diameter (ED), which was adopted from the building services industry, converting rectangular duct geometry to an equivalent circular diameter (CIBSE, 2007). There is a mathematical relationship that can be used for such conversions. This relationship is expressed in Equation 4.14. To be able to solve that equation, first a single rectangular shape had to be achieved for the parallel running tunnel configurations, the method for which is illustrated on Figure 4.16. Following substituting into Equation 4.14, the equivalent diameters for the three different configurations

were estimated as ED-A, ED-B and ED-C. The resulting diameters with the locations of their centre point within the modelling domain are illustrated in Figure 4.17.

$$ED = \left[1.3 \times \left(\frac{(a \times b)^{0,625}}{(a+b)^{0,25}}\right)\right] \tag{4.14}$$

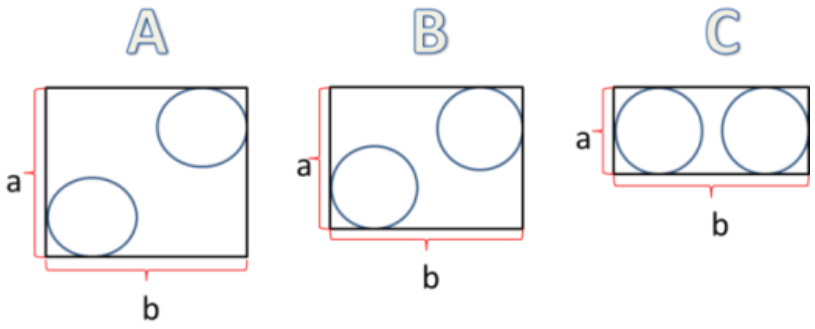

Figure 4.16: Converting tunnels for a single rectangular shape

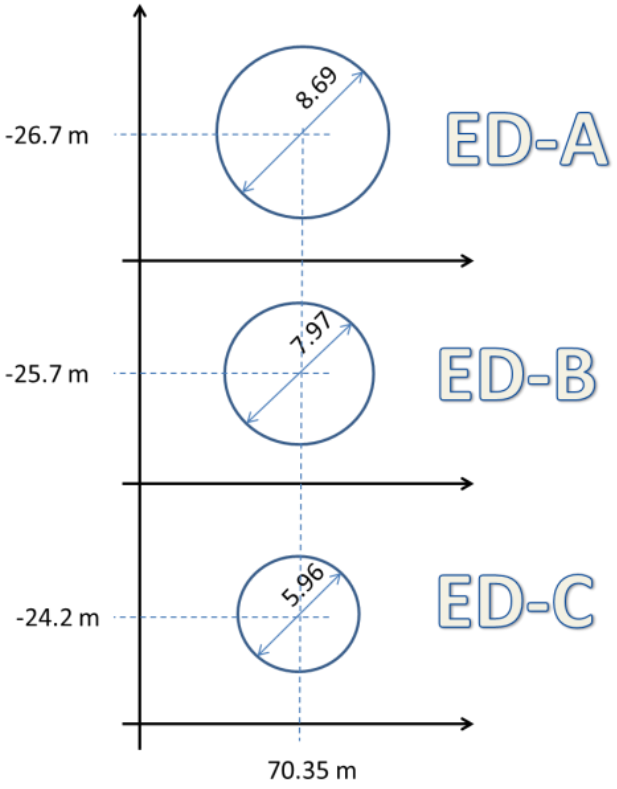

Figure 4.17: Equivalent diameters: ED-A, ED-B and ED-C

4.4.3.1.2 Results of investigation 3

The tunnel geometries within the model were then adjusted for the resulting equivalent diameters and the simulations were run again. The resulting temperature contours at specific temperatures were plotted together with the parallel tunnel scenarios for comparison. These comparisons are illustrated in Figure 4.18, Figure 4.19 and Figure 4.20 respectively.

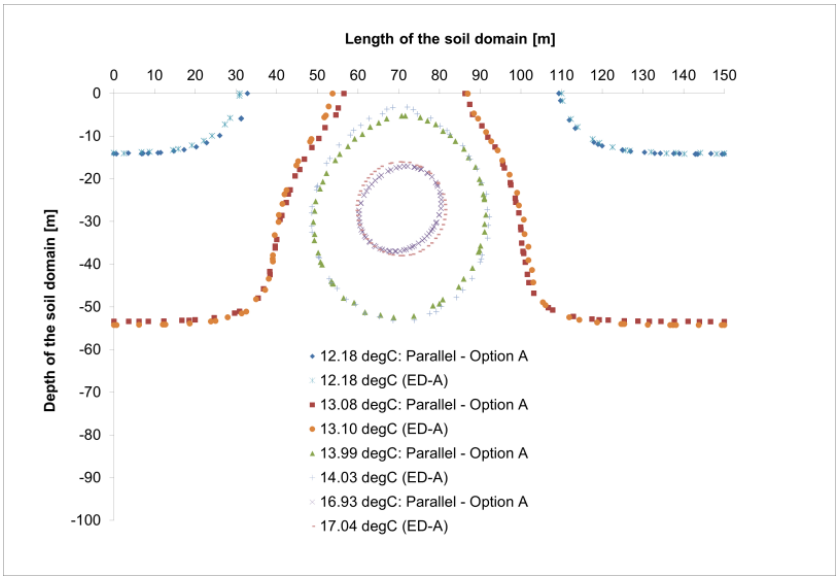

Figure 4.18: Temperature contour comparison: Parallel tunnels Option A – ED-A

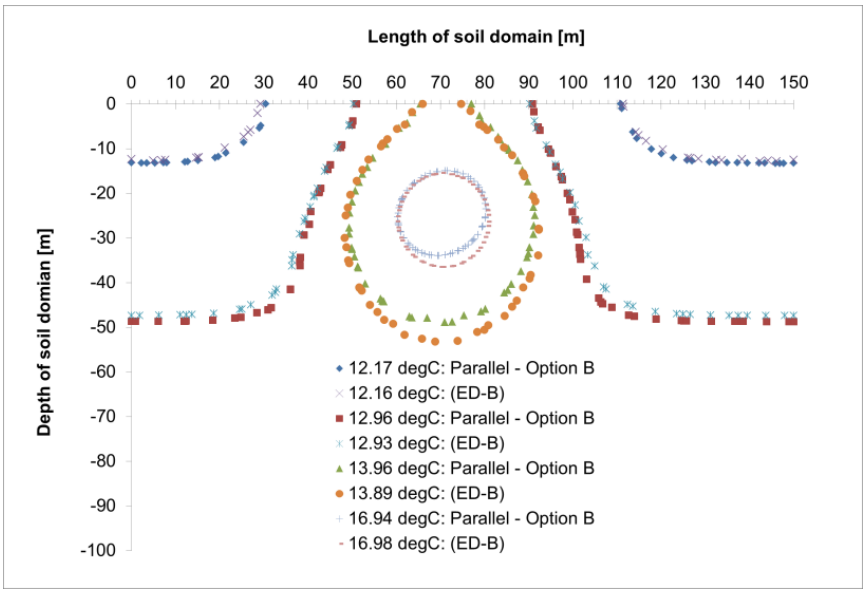

Figure 4.19: Temperature contour comparison: Parallel tunnels Option B – ED-B

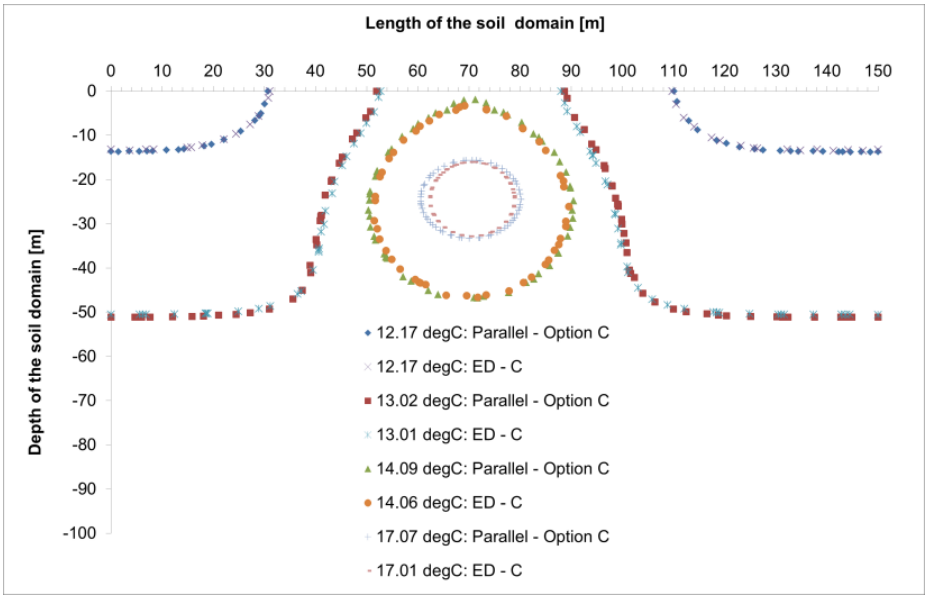

Figure 4.20: Temperature contour comparison: Parallel tunnels Option C – ED-C

4.4.3.1.3 Conclusions of investigation 3

It can be seen from the figures that the effect of the equivalent diameter configurations on their surroundings was comparable to the effect of the parallel running tunnels. Based on the results of this analysis, it is reasonable to assume that the geometry of numerical models considering parallel running tunnels could be simplified using the ED method. However, the applicability of this approach is only valid for models which do not take account of the air movement in the tunnels. It is important to note that the trains of the LU railway are running in opposite directions, causing different temperature profiles within the parallel running tunnels. The ED method does not take into account such phenomena and where the method is used this limitation and the effects of it on the results should be highlighted.

4.4.4 Earth Flux

As was seen in Figure 4.2, the ground surface temperature is affected mostly by the atmosphere and solar energy to a depth of approximately 8-10 m. When the depth is below 10 m, the ground temperature is constant throughout the year. The average annual temperature is kept constant at any given depth, and gradually increases with a gradient because geothermal heat flows from the centre of the Earth to the surface. Chapman and Pollack (1975) reported that the average continental heat flux from the interior of the Earth is 0.060 W/m^2 with the range from 0.036 to 0.092 W/m^2.

4.4.4.1 Investigation 4 – Earth flux condition on the bottom boundary

During previous investigations the lower boundary conditions were either set to be a constant temperature or an adiabatic condition. This type of model set up might be questionable when the interactions of GSHPs and URs are investigated through long term simulations. The analysis described in this section looked at temperature changes at specific points within the soil while different flux conditions were applied at the lower boundary. These flux conditions were varied between 0.036 and 0.092 W/m^2.

4.4.4.1.1 Results and conclusions of investigation 4

The resulting temperatures at the measurement points were then compared to a scenario with a zero flux condition. It was found that even the highest flux, 0.092 W/m^2, did not result in a noticeable temperature difference, in comparison to the zero flux condition. Based on this, it is practical to assume that an Earth flux condition on the bottom layer of the soil domain will not make any difference to the GSHPs and URs interactions. Consequently, a constant temperature or an adiabatic condition will be sufficient within further models.

4.4.5 Tunnel Wall

Tube tunnels in London were constructed using tunnelling shields. The tunnel wall materials that were used are either cast iron or concrete. The reliable performance of cast iron in compression and its good corrosion resistance make it a suitable material for tunnel linings. A continuous length of tunnel lining is formed of a number of rings of cast iron segments bolted together. More recent variants of the traditional grey cast iron linings are the more ductile spheroidal graphite cast iron, stronger steel, and more durable stainless steel linings. On the other hand, reinforced concrete lined tunnels are also popular, due to their good performance in compression, adequate protection from their environment, and their low maintenance requirements. Typical thermal properties of cast iron and concrete are summarised in Table 4.7. These values were adopted from the work of Ting *et al.* (2009) and Thompson (2006).

Table 4.7: Typical tunnel lining material properties

Material	**Thermal conductivity** [W/m*K]	**Density** [kg/m^3]	**Specific heat capacity** [J/kg*K]
Cast Iron	52	7272	420
Concrete	1.1	2400	880

4.4.5.1 Investigation 5 – The effect of tunnel wall on surrounding soil temperatures

4.4.5.1.1 Introduction

Previous investigations in this chapter have neglected the tunnel wall material and only considered the tunnel domain where a soil was subjected to a cylindrical cavity which has represented the tunnel. In order to establish whether the tunnel lining and its material property could have a noticeable effect on the interactions between URs and GSHPs, an analysis was carried out, which is presented in this section.

The analysis looked at temperatures at specific points of the domain during scenarios when different tunnel wall materials were considered or when the tunnel wall was neglected. The points of interest were 3, 5 and 10 m away from the centre of the tunnel in the horizontal direction within the surrounding soil. This is illustrated in Figure 4.21. The thickness of the concrete wall was set as 500 mm. This value was adopted from the work of Thompson (2006). Cast iron tunnel liners are less thick than concrete slabs, normally between 50 -100 mm (Thomas, 1977).

In the model a cast iron liner thickness of 60 mm was assumed. The temperature boundary on the inner surface of the tunnel wall was maintained as shown by Equation 4.8.

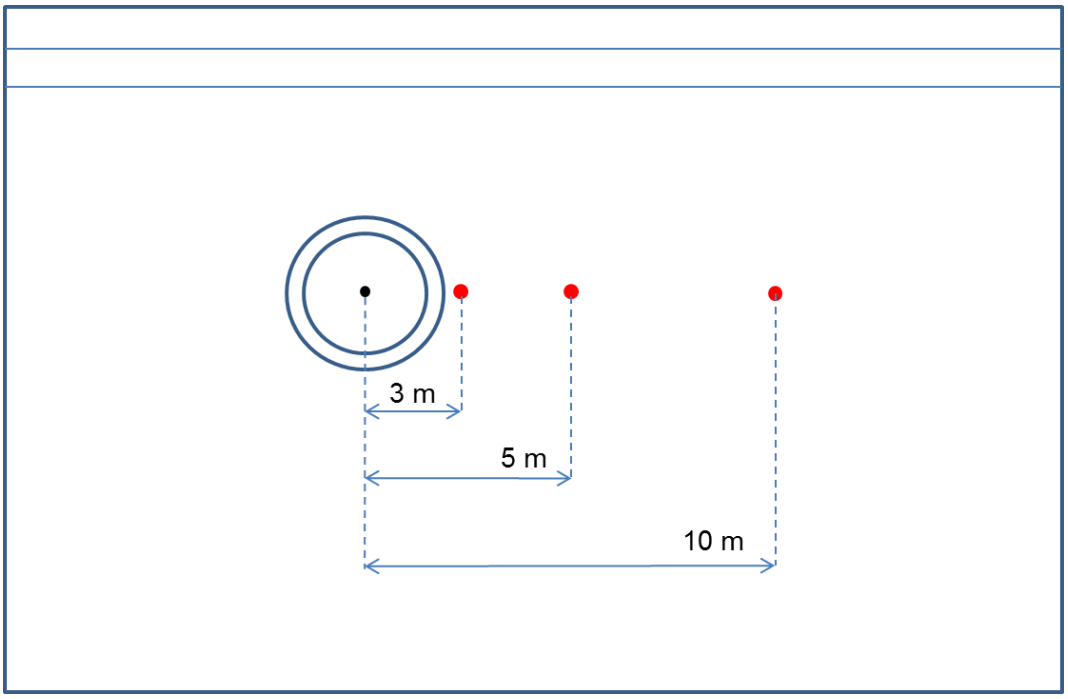

Figure 4.21: Measurement points

4.4.5.1.2 Results of investigation 5

The results showed that the temperature of the measurement points did not vary significantly for the different wall materials considered. In particular, if the tunnel was constructed using cast iron liners this resulted in an average 0.2°C higher temperature profile at each measurement point compared to if it was built using concrete slabs. The results showed that the temperature profile of the measurement points where the wall was neglected fell approximately between that of the other two scenarios. This was because clay has lower thermal conductivity that cast iron but higher than concrete.

4.4.5.1.3 Conclusions of investigation 5

Based on the results of this analysis it is practical to assume that in further models it is worth incorporating the tunnel wall, since its effect on the heat transfers within its surroundings is noticeable. Incorporating this feature into the model geometry does not come with significant additional complexities.

4.5 CONCLUSIONS

The critical literature review in Chapter 2 identified that there are a number of numerical simulation platforms exist which would be suitable for the combined analysis of URs and GSHPs. The tool which was selected and used to carry out the research detailed in this thesis is called COMSOL Multiphysics.

The tool was first used to build a preliminary 2D model, which was introduced in this chapter. The model was highly simplified to enable rapid analysis of the systems to establish key phenomena for more detailed additional research. The model predictions agreed well with previous results found in the literature and also with results gained from analytical solutions. The validated preliminary model was used to perform a study of the impact of separation of the UR and GHE. It was shown that the operation of the railway was likely to have a significant impact on the performance of the GHE. Therefore, the results demonstrated potential for UR-GSHP interactions, and expanded the understanding of such physical phenomena.

The preliminary 2D mathematical model was then used to perform five additional investigations with the aim of establishing key parameters impacting on UR-GSHP interactions. The parameters which were found to have an impact were then implemented into the more complex 3D models. In this way, the outcomes of the 2D modelling work formed the foundation of the 3D numerical model development.

Key results of these additional investigations showed an extremely low level of groundwater flow within the layer of London Clay, in which majority of the UR and GHE structures are built. Therefore, it was concluded that numerical simulations in the soil with governing equations for pure conductive heat transfer would be sufficient. Furthermore, if UR tunnels and GHEs are built in coarse sands, ground water movement could have an impact on the interactions, however if fine sands are considered a pure conductive case in further studies may be sufficient.

Results of the investigations also showed that multiple tunnel geometries which run parallel to each other could be simplified in the FE geometry of the numerical model. This simplifying method is called the equivalent diameter (ED) method. The process applies a single diameter accounting for the diameters of multiple running tunnels. Results from a comparison study in Investigation 3 showed that the temperature contours in the soil surrounding the tunnels were nearly the same when there were either multiple tunnels or the ED method was used. Therefore, it was concluded that using the ED method could potentially enhance computational efficiency of numerical models where the effect of multiple running tunnels is being investigated on their surroundings.

In addition, the results of Investigation 5 established that in further models it is worth incorporating the tunnel wall material and geometry, since its effect on the heat transfers within its surroundings is noticeable. Since the tunnel wall is normally a relatively thin layer compared to the rest of the model domain, incorporating this feature into the model geometry does not come with significant additional complexities.

Since the preliminary model presented within this chapter is a highly simplified 2D model, it cannot correctly describe URs and GHEs geometry. This is because there are complex, transient, 3D transport phenomena and extreme geometrical aspect ratios involved within both schemes. It is therefore important to further advance this research by developing 3D models, where more complex geometrical features and operational characteristics of URs and GSHPs can be more explicitly presented. The following two chapters, Chapter 5 and 6 will present the development of independent 3D UR and GHE models.

CHAPTER 5: THREE DIMENSIONAL MODEL DEVELOPMENT OF AN UNDERGROUND RAILWAY

5.1 INTRODUCTION

The results of the 2D preliminary investigation presented in Chapter 4 demonstrated that the operation of URs impacting on neighbouring GHEs. In order to further enhance understandings of the mutual impact of URs and GHEs on their surroundings, a 3D FE analysis was carried out. Although the 2D model and the related studies presented in Chapter 4 were highly simplified to enable rapid analysis of the systems, it allowed evaluation of some parameters which were likely to have some impact on UR-GSHP interactions. These parameters were implemented into the more complex 3D models.

The 3D models of URs and GHEs were developed and validated separately. This chapter introduces the development and validation of two different 3D railway models, named as UR-Model-A and UR-Model-B. Both models represent a typical deep level UR based on some definable parameters; however, the models differ in their level of complexity and their potential applicability for further investigations.

UR-Model-A utilises pre-defined tunnel air temperatures and air velocities to generate a time dependent heat flux trace on the tunnel wall. Due to the pre-defined nature of the model, the GSHP heat load cannot impact on the tunnel air temperatures. UR-Model-B does not have this limitation and it allows URs and GHEs to fully interact since it explicitly represents the air domain and the heat load from the passing trains within the tunnel. Although UR-Model-B is computationally more extensive than UR-Model-A, it can be used when the impact of the GHE array heat extraction on the tunnel air temperature is being investigated.

The advantages and disadvantages of these models and recommendations for their further use will be discussed in this chapter. The discretization of the geometries, FE mesh generation and the specifics of the system physics and boundary conditions are also explained in detail.

5.2 THE MODEL DEVELOPMENT: UR-MODEL-A AND UR-MODEL-B

5.2.1 The Model Geometry and Mesh

5.2.1.1 Model geometry

The literature review suggested that heat transfer effects in the ground are negligible after about 20 m from the wall of an UR tunnel. This was confirmed by the results of the preliminary 2D model. When the 3D model geometry was built, an extra 10 m was added to

that value to ensure that no additional effects were introduced by the boundary conditions applied at the far end of the modelling domain. Consequently, a 30 m distance was kept between the tunnel outer wall and the lateral and bottom boundaries of the soil domain. It was concluded in the previous chapter that incorporating the tunnel wall into the model geometry had some effect on the heat transfers, therefore it is worth considering it within the model geometry. The tunnel wall material was chosen to be concrete with a thickness of 500 mm. The reason for this choice was to make the model more applicable to future build tunnels which will most likely to be concrete lined. A schematic of the model cross-section is shown in Figure 5.1.

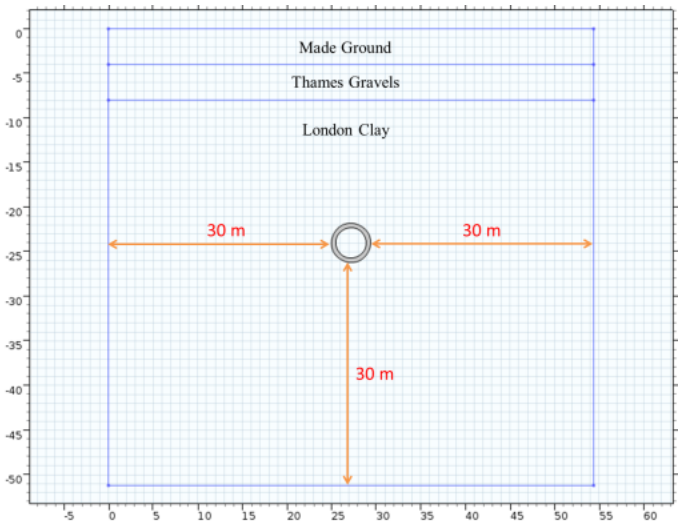

Figure 5.1: Distance between tunnel wall and lateral and bottom boundaries

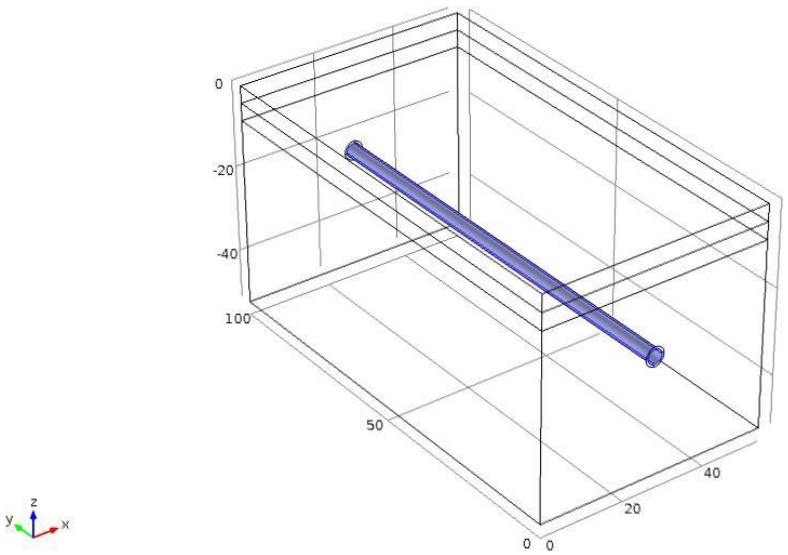

Figure 5.2: 3D geometry of the UR model

The soil/rock layers and their thermo-physical properties were kept as they were presented within Chapter 4, and were shown in Figure 4.8. The depth of the soil domain was made equal to the length of the tunnel section, 100 m. This length was chosen as it is the typical length of the LU railway's rolling stocks (Transport for London, 2016). The 3D model geometry is illustrated in Figure 5.2. The model was built in such a way that the geometrical parameters and material properties could be easily adjusted, in order to investigate different scenarios.

5.2.1.2 Mesh of the model

The FE meshes of the soil/rock domains within the model were built using tetrahedral elements. The first two soil layers, Made Ground and Thames Gravels, were more refined than the London Clay. This was because the vertical temperature gradient caused by climatic effects was considered to have a more significant effect within those layers, as shown in Figure 4.2 in Chapter 4.

In order to reduce the number of mesh elements required to solve the model, a swept mesh was created along the length of the tunnel domain. This was created by building a free triangular mesh on the centre of the tunnel inlet surface which can be considered as the source face of the swept mesh. The mesh was then swept from the source face along the domain to an opposite destination face, the outlet of the tunnel domain. The source face which was built of triangular elements was extended with a boundary layer mesh which was built with layered prism elements. The overall mesh configuration (left) and an enlarged cross-sectional view of the combined triangular and prism elements at the surface of the tunnel inlet (right) are shown in Figure 5.3.

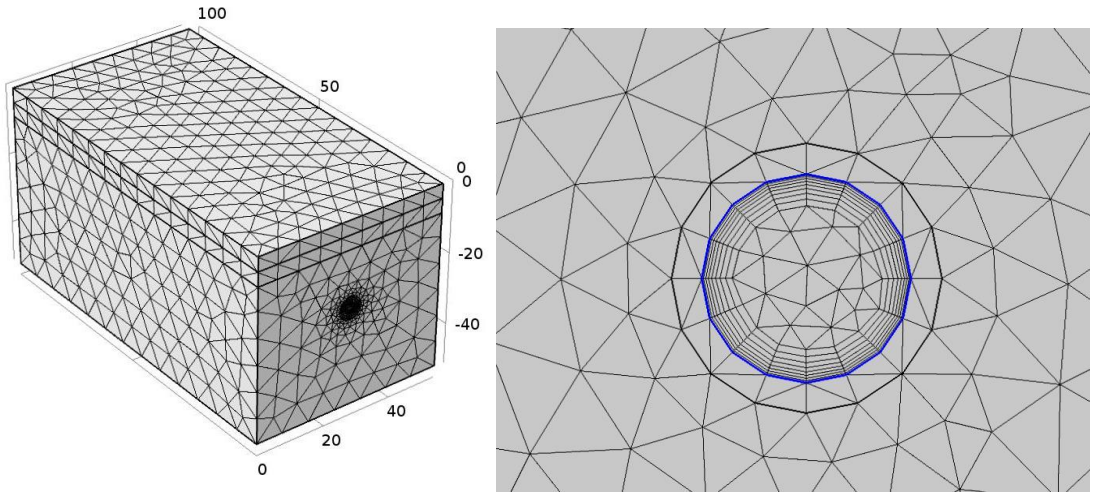

Figure 5.3: Mesh of the UR model

The mesh independency of the model generated results was achieved through an analysis which is attached in Appendix B. Three unstructured meshes made of tetrahedral elements were tested. The finest mesh contained 409913 while the coarsest mesh included 19382 domain and boundary elements. Temperature values at a specific point were compared for the three mesh configurations. Based on the results of the mesh analysis, the second finest configuration was selected with 100571 elements. Results from a model with such a mesh configuration converged to nearly the same values as the model with the finest mesh, but achieve this significantly faster. In particular, the computational time decreased from 38 min to 14 min when the number of mesh elements was reduced from the extra fine to the fine scenario.

5.2.2 Physics and Boundary Conditions

Two different UR models were developed for which the governing physics and boundary conditions applied were set based on the conclusions of the preliminary 2D investigations detailed in Chapter 4. These conditions are described within the following sub-sections. Within the soil domain of both UR models the same physics and boundary conditions were applied. However, within the rest of the model domains, different conditions were applied for the two different models. For this reason, the underlying physics and boundary conditions of UR-Model-A and UR-Model-B will be discussed separately.

5.2.2.1 Soil

Governing equations and boundary conditions applied to the soil domain were established from the results of the 2D investigations. For example, the 2D results showed that the groundwater velocity profile within the London Clay is extremely low. Therefore, applying a governing equation considering a pure conductive heat transfer (Equation 4.1) was sufficient. The temperature boundary condition at the soil surface (Equation 4.2) was kept consistent with the preliminary 2D model. The lateral boundary of the domain was assumed to be adiabatic and an initial vertical ground temperature gradient was imposed for the entire modeling domain.

5.2.2.2 UR-Model-A

5.2.2.2.1 Introduction

UR-Model-A was built with the aim of taking a step back from the wall temperature boundary condition applied within the preliminary 2D model (e.g. to allow distinguishing between tunnel air and tunnel-wall temperatures). This was achieved by replacing the fixed

temperature boundary from the preliminary 2D model (Equation 4.8) with a time dependent convective heat flux boundary condition on the inner surface of the tunnel wall.

5.2.2.2.2 Convective heat flux boundary condition on tunnel wall

This convective heat flux was defined as shown in Equation 5.1 and it is illustrated in Figure 5.4. The temperature of the tunnel wall T_{tun_wall} in Equation 5.1 is affected both by the tunnel air temperature and the temperature field computed in the surrounding soil domain. Its values were estimated through the energy balance equations solved by the model (such as Equation 4.1 and Equation 5.1). The longitudinal tunnel air temperature T_{tun_long} takes account of the non-uniform tunnel air temperature profile along the length of the tunnel which is caused by the operation of the trains.

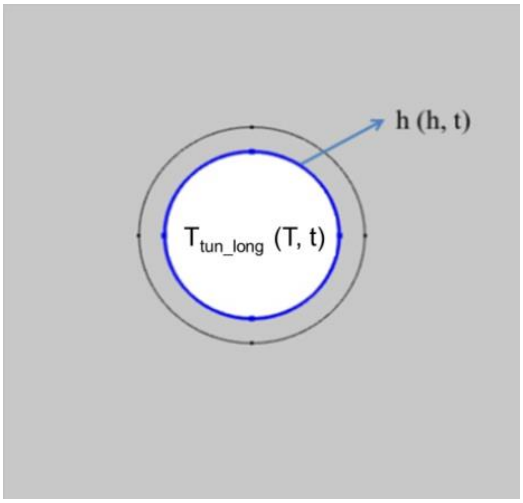

Figure 5.4: Heat flux boundary condition on the tunnel wall surface

It was important to incorporate a non-uniform temperature profile into the model, because it is likely that the UR-GSHP interactions are stronger at sections where the tunnel is warmer i.e. closer to platforms. This profile was achieved by introducing a temperature dependency into Equation 4.8. The new expression which includes a linear temperature increase of 0.5°C /100 m along the length of the tunnel (y-direction of the 3D model domain) is shown as Equation 5.2. While this increment ratio is indicative of a 100 m long breaking region of a deep level tube line in London, it can be easily adjusted within the model when different sections of the railway are to be investigated.

$$q_{tun\_wall} = h(T_{tun\_long} - T_{tun\_wall}) \quad (5.1)$$

$$T_{tun\_long} = \left(0.4 * T_{S_{surf}} + 17.5\right) + y * \left(\frac{0.5}{100}\right) \quad (5.2)$$

The heat transfer coefficient, h in Equation 5.1 depends on the fluid's material properties, the wall's surface temperature and also on the air velocity. The geometrical configuration also affects the coefficient. Heat transfer books generally contain a large set of empirical and theoretical correlations for h coefficients. The expressions are based on the Nusselt (Nu), Prandtl (Pr) and Reynolds (Re) dimensionless numbers. For the UR model presented in this chapter, a convection correlation for turbulent flow in circular tubes was utilised. The Dittus-Boelter equation which is a correlation for internal forced convection in tubes can be expressed as Equation 5.3. The Dittus-Boelter equation is a slightly different and preferred version of the Chilton-Colburn analogy, which is a classical expression for computing Nu number for fully developed (hydro-dynamically and thermally) turbulent flow in a smooth circular tube (Incropera and Lavine, 2011). For turbulent flow, the heat transfer coefficient increases with wall roughness and as a first approximation it may be computed by a correlation developed by Gnielinski (1976). The modelling work detailed in this thesis assumed that that the UR tunnels have a smooth surface and therefore used Equation 5.3 when the heat transfer coefficients were estimated. Whilst using this assumption in the model potentially causes slightly lower values when the heat transfer coefficients are estimated, it reduces the model complexity and eliminates the need for the assessment of the friction factor which is not a direct value and varies with velocity.

$$Nu = 0.023\, Re^{0.8} Pr^{n} \quad (5.3)$$

In Equation 5.3, n = 0.4 if the fluid is being heated (that is if the tunnel wall is at higher temperature than the entering air) and n = 0.3 if the air is being cooled. The numerical model has the capability to automatically adjust the equation depending on what seasonal circumstances within the railway environment are being simulated.

In UR Model A, an analytical function was used to represent the typical aerodynamic conditions within the tunnel. It was assumed that there would be no trains running between midnight and 5 a.m. For the rest of the day the operation of trains was assumed to be continuous. When Equation 5.3 was estimated, averaged bulk tunnel air velocities were assumed for periods when the trains are operating as well as for the non-operational hours.

5.2.2.2.3 Tunnel air velocities

Ting *et al.* (2009) simulated a typical tunnel segment air velocity profile, using a simulation platform called the Subway Environment Simulation (SES). Based on the SES results, a low air flow rate of 0.36 m/s was used to represent the background or residual air movement. A high air flow rate at 11 m/s was analysed to represent the maximum air movement generated just ahead of, or just behind the train currently travelling at its top speed. In recognition that the train generated air flow rate in a tunnel was cyclic, and follows approximately that of a sine-wave, an intermediate air flow rate at 6 m/s was chosen by the authors for the operational periods.

These values were implemented into UR-Model-A. The convective heat transfer coefficient, h for the non-operational and operational hours of the railway were estimated as 1.3 and 12.5 W/m^{2}K respectively. These are shown in Figure 5.5. A continuous smoothing was applied to the function of the heat transfer coefficient. The transition zone intervals for the smoothening are highlighted in blue in Figure 5.5. The smoothening not only allows a better convergence of the numerical model, but also better represents the gradual increase or decrease of the frequency of trains and the corresponding gradual changes in bulk average tunnel air velocities.

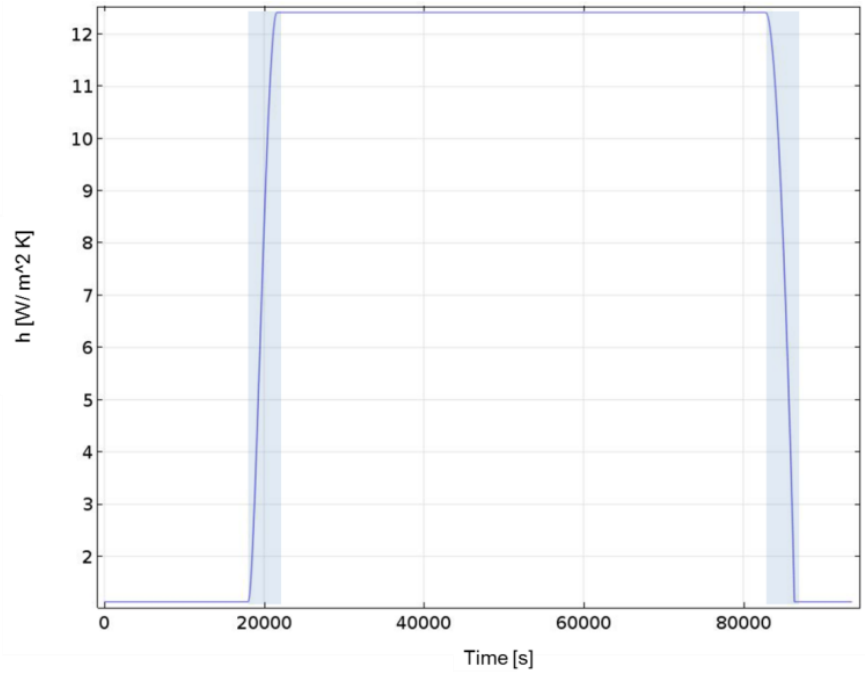

Figure 5.5: Values of the heat transfer coefficients in UR Model-A

5.2.2.2.4 In situ measurement of the LU tunnel air velocities

Measurements were conducted at LU platform at York Road London. The platform provided an ideal location for the measurements because it is disused by passengers but the trains are still passing by on regular LU operating time intervals. Tunnel air flow rates were measured at three different locations within the test site using a unidirectional anemometer. A schematic diagram of the LU test site which includes the three measurement points and the direction of train movements are shown in Figure 5.6. The equipment used and the measurement procedure are shown in Figure 5.7. The device used to measure air velocity was a unidirectional sonic anemometer (Model: Airflow Anemosonic UA30). Since the anemometer did not have a memory to save the recordings automatically, pictures were taken of its display every time a log was made. These pictures were taken both during the measurement of residual air movement and in the event of passing trains. The measured values for these two scenarios were averaged at around 0.4 m/s and 7 m/s respectively. These values are very similar to those used within the analysis presented by Ting *et al.* (2009).

Figure 5.6: Schematics of the platform area and the selected measurement points

Figure 5.7: Anemometer (left) and the measurement procedure (right)

5.2.2.2.4.1 Limitations and the use of the measured data

The measurement procedure had a number of limitations. These limitations were mainly caused by the inability to control the trains crossing patterns and their speed. For these reasons the data could not be used for validation of the UR models. However, the measurement was considered to be informative because the results showed a great variation in tunnel air velocities during the measurements. Based on this information an analysis was conducted which compared the effects of these short-term aerodynamic variations on the near ground heat transfer against the effect of the hourly averaged tunnel air velocity, which was implemented in UR-Model-A. The analysis and its results are attached as Appendix E. The result of the comparison showed that the short-term aerodynamic variation in the tunnel has negligible impact on the near ground heat transfer compared to the scenario where the average velocity was used. This is because the heat transfer in the ground is a slower process due to its thermal inertia. Hence, using the hourly averaged tunnel air velocities in the model is practical as it avoids needing to resolve the governing physics on a short term scale which in turn enhances computational efficiencies.

5.2.2.3 UR- Model-B

5.2.2.3.1 Introduction

When a train travels through a tunnel, a significant amount of thermal energy may be transferred to the tunnel environment. This thermal energy is the result of dissipation caused by aerodynamic drag, mechanical resistances and inefficiencies in the power unit (Barrow and Pope, 1987). A proportion of this energy is transferred to the tunnel wall and the train structure, the remainder being expelled from the tunnel by the induced air flow. UR-Model-B is able to take account of the heat released from the trains and allows for that heat to be transferred to the tunnel environment.

5.2.2.3.2 Train and tunnel air: physics and boundary conditions

In order to minimise the computational effort, the model uses a 1D linear element for simulating the train as a line heat source within the centre of the tunnel domain. An initial investigation, which is not detailed in this thesis, showed that the positioning of the line heat source in the model does not affect the resulting averaged tunnel air temperatures. This line heat source is so thin that it has no thickness in the model geometry. Therefore, no material properties had to be assigned to it. This source, Q_{train} is regarded as a general source with a distribution of unit power per unit length [W/m]. For the value of $Q_{\text{train,}}$ the average daily train heat dissipation rate was estimated at 284 W/m. The method used for estimating Q_{train} is

detailed in Appendix F. The material that surrounds that line heat source is air. It enters at the tunnel inlet, flows through the entire tunnel domain with a specified velocity and then leaves the tunnel at its outlet. These characteristics are illustrated in Figure 5.8.

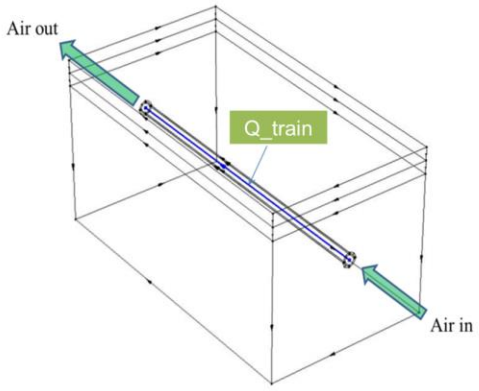

Figure 5.8: The line heat source and the locations of the entering and leaving tunnel air

The single phase air flow was assumed to be turbulent with a high Re number. The velocity of the tunnel air was assumed to be the same constant average value, as was assumed in section 5.2.2.2.3 (3.5 m/s). The equations solved for the turbulent air flow are the Reynolds-averaged Navier-Stokes (RANS) equations for conservation of momentum, the continuity equation for conversation of mass, and an algebraic equation for the scaled wall distance. The derivation of RANS equations are widely explained within the literature and are therefore not detailed here. For solving the transient heat transfer within the air domain the model uses Equation 5.4.

$$\rho C_p \frac{\partial T}{\partial t} + \rho C_p \mathbf{u} \cdot \nabla T + \mathbf{q} = Q \tag{5.4}$$

Where

$\mathbf{q} = -k\nabla T$

Two boundary conditions were assigned at the inlet of the tunnel. One is a time dependent temperature boundary T_{tun} which was assigned with Equation 4.8. The other condition specified is a net air inflow into the domain. The normal inflow velocity is specified as $\mathbf{u} = -\mathbf{n}U_0$ where $\mathbf{n}$ is the boundary normal pointing out of the domain and U_0 is the normal inflow speed in m/s. The condition applied at the outlet of the tunnel domain, $-\mathrm{n} \cdot \mathrm{q} = 0$ states that the only heat transfer occurring across the boundary is by convection. The temperature gradient in the normal direction is zero, and there is no radiation.

5.2.2.3.3 Optimization of UR-Model-B

UR-Model-B models more explicitly the UR operational characteristics than UR-Model-A, by taking account of the train heat release and the tunnel air domain. These additional model parameters have increased the number of variables required to solve the model and the number of degrees of freedom within the model. Because of that the required computational efforts have significantly increased compared to UR-Model-A. The computational time of UR-Model-B increased by 70% compared that to UR-Model-A. In order to improve computation efficiencies, model optimisation was required. This was achieved using two steps. Firstly, the problem was de-coupled by assuming that the material properties required for solving the physics of turbulent air flow within the tunnel domain do not change significantly with respect to the change in temperature expected. This allowed the physics of turbulent air flow to be solved in a preliminary stationary study. The velocity flow characteristics calculated were then transferred to a transient heat transfer study. The computational efficiency of UR-Model-B was significantly improved, and it only took about 15% longer (approximately 30 min) to compute results with it than with UR-Model-A. This model optimisation was achieved without comprising the simulation results. This is shown in Figure 5.9 which compares simulation results for a 50 years period of UR-Model-B before and after the model optimisation procedure. The average temperature of the tunnel air was compared. It can be seen in the figure that the results are identical and therefore it is practical to use the optimised version of the model within further investigations of UR-GSHP interactions.

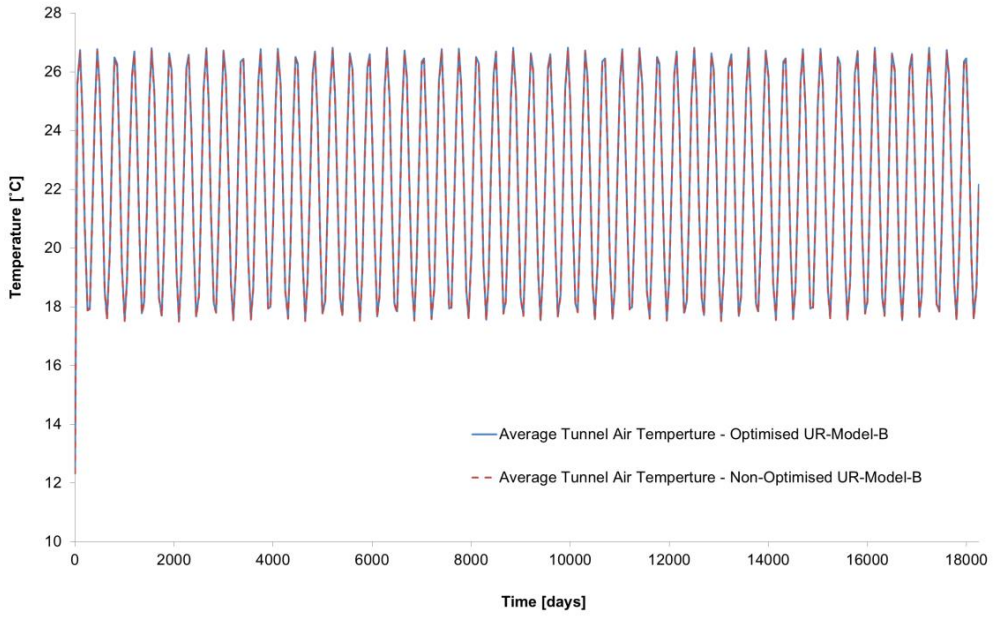

Figure 5.9: Average tunnel air temperature results from UR-Model-B before and after the model optimisation

5.3 RESULTS FROM UR-MODEL-A and UR-MODEL-B

5.3.1 Introduction

Two UR models, UR-Model-A and UR-Model-B were developed with different level of complexities. Regardless of the complexity, a common objective during the model development phase was to build UR models in a way that they were both capable of simulating the operation of URs and their impact on their surroundings. Comparisons of the simulation results from the two models are presented in the following section.

5.3.2 Results comparison

The similarity of the results from the two different railway models was established by comparing simulation results at a specific measurement section within the model domain. This section was chosen to be a circular soil segment along the length of the tunnel at 3 m radial distance from its wall. This measurement section is illustrated in Figure 5.10.

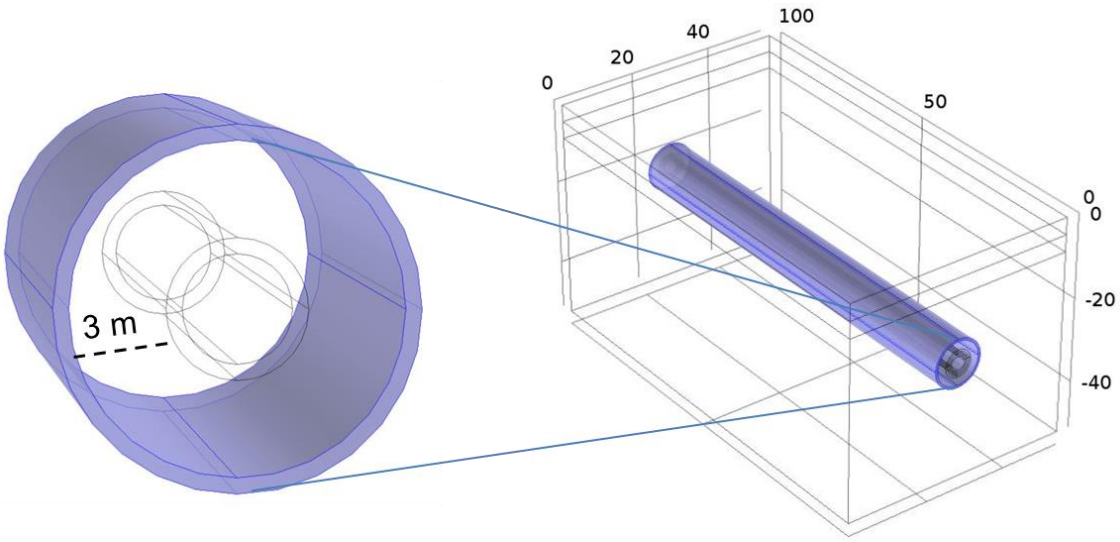

Figure 5.10: The circular soil segment in the model for measurements

The average temperature of this ground segment was compared during a long term (50 years) simulation period. The comparison results which are shown in Figure 5.11 suggest that, although the two models have different level of complexities, both have the capability to simulate the long term operational impact of an UR on its surroundings, doing so in an almost identical manner. It can be seen in the figure, that the average soil temperatures are fluctuating seasonally at 3 m distance from the wall of the tunnel. However, this fluctuation is

lower than the air temperature's variation inside the tunnel (see Figure 5.12). Whilst the seasonal variation of air temperature in the tunnel is approximately 9˚C between winter and summer peaks, the average soil temperature at 3 m distance from the wall of the tunnel only results in seasonal oscillations of about 2-3˚C.

In addition to that, it can be seen in Figure 5.11 that the temperature of the soil segment simulated with UR Model A is slightly higher when it was computed with UR Model B, especially at the early years of the simulation period. This is because of UR Model A and B vary in their level of complexities. For example, UR Model B has a constant tunnel air velocity of 3.5 m/s and also a line heat source at the centre of the tunnel. These parameters both influence the tunnel wall and hence the surrounding soil temperature. However, the results show that after a number of years of operation the difference in temperatures caused by these parameters get smaller and the soil warms up to the same extent. Therefore, both models can be used for further investigations of UR-GSHP interactions, if a long enough initial operational period of the URs is considered (approximately 50 years).

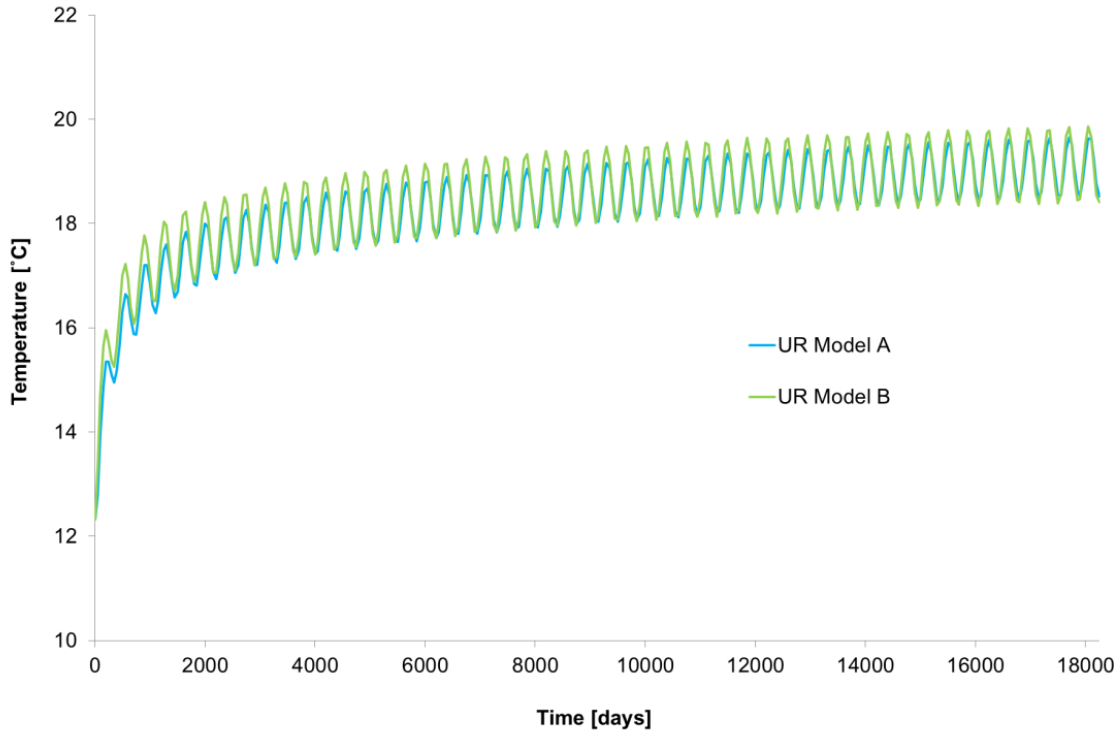

Figure 5.11: Simulation results of UR Model A and UR Model B

5.4 VALIDATIONS OF THE UR MODELS

5.4.1 UR-Model-B

The validation was started by comparing the numerically generated tunnel air temperatures of UR-Model-B with values reported in literature. The model predictions of the tunnel air temperatures are plotted in Figure 5.12.

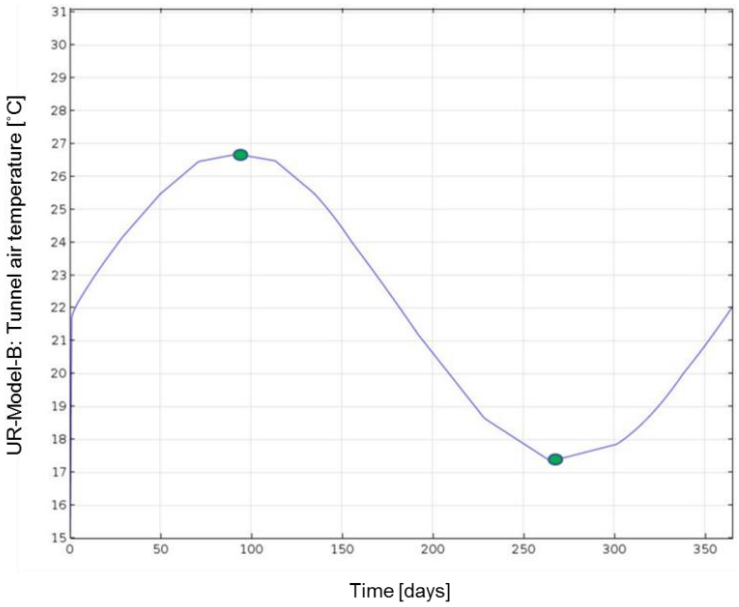

Figure 5.12: Simulated average tunnel air temperatures in UR-Model-B

The maximum and minimum values of the sinusoidal wave represent the summer and winter conditions respectively. Gilbey *et al*. (2011) reported that current winter-temperatures on LU platforms can be up to 20°C even on operational cold winter days. They also noted that tunnel temperatures are approximately 2 to 3°C cooler than the platforms. Therefore, the 17°C tunnel temperatures obtained from the simulation, during the winter season, were considered to be appropriate for the analysis of a London based interaction. The summer months are also considered to be reasonable due to matching conditions reported by Thompson *et al*. (2008).

5.4.2 UR-Model-A

Although UR-Model-A does not have an air domain, the simulated results on its surroundings compared well with the predictions of UR-Model-B. This was shown in Figure 5.11. This suggests that UR-Model-A is also capable of successfully simulating the typical conditions existing within the deep level LU railway tunnels.

5.5 CONCLUSIONS

Two different 3D UR models were introduced within this chapter, UR-Model-A and UR-Model-B. The two models have similar geometrical features, however the representations of the railway operational characteristics within the models were established using different methods. The main difference between the two models is that while UR-Model-A neglects the air domain within the model geometry, UR-Model-B explicitly represents its flow through the tunnel. UR-Model-B also represents the trains in the centre of the tunnel as a line heat source. UR-Model-A uses a time dependent convective heat flux boundary on the inner surface of the tunnel wall. This condition was developed based on hourly averaged aerodynamic profile of the railway. Such hourly variation was neglected in UR-Model-B and a constant averaged tunnel air velocity was used in the model. The results of an analysis reported in this chapter showed that despite the two models having different levels of complexity, both have the capability to simulate the long term operational impact of an UR on its surroundings and doing so in an almost identical manner. Due to its large NDF, UR-Model-B has been optimised for reaching more rapid computational times. This was achieved using two steps. Firstly, the problem was de-coupled by assuming that the material properties required for solving the physics of turbulent air flow within the tunnel domain do not change significantly with respect to the change in temperature expected. This allowed the physics of turbulent air flow to be solved in a preliminary stationary study. The velocity flow characteristics calculated were then transferred to a transient heat transfer study. It was shown that such an optimisation significantly enhanced computational efficiencies of the model (about 15% longer computation times compared to UR-Model-A) without compromising its results.

The chapter also detailed an in-situ air velocity measurement which was carried out at a disused LU station at York Road was also detailed. The results of that measurement showed that the tunnel aerodynamics highly varied in the short-term. Based on this information, a numerical investigation was conducted from which results showed that the short-term aerodynamic variation in the tunnel had no effect on the near ground heat transfer which is a slower process. Hence using the hourly averaged tunnel air velocities in UR-Model-A is practical as it avoids needing to resolve governing physics on a short-term scale.

Validation of the models was carried out by comparing the numerical results with data reported on the thermal environment of the LU. Tunnel air temperatures obtained from the simulations were within the same range as the data reported in the literature, therefore the models were considered to be appropriate for an analysis which considering London as a case study. The decision regarding which model UR-Model-A or UR-Model-B to implement

for investigations should be determined according to the objective of the analysis. The aim of the research presented in this thesis is to investigate the interactions (i.e. the mutual impact of URs and nearby GHEs on each other. For this reason, it is important to utilise a model in which the operational characteristics of the systems can be impacted on. Therefore, UR-Model-B, in which the tunnel air domain is explicitly represented, will be used in further investigations unless otherwise stated.

CHAPTER 6: THREE DIMENSIONAL MODEL DEVELOPMENT OF VERTICAL GROUND HEAT EXCHANGERS

6.1 INTRODUCTION

Chapter 6 presents the development and validation of a 3D numerical model for simulating closed-loop vertical GHEs. Two typical GHE absorber pipe arrangements were built within the model. One was with a single U-shaped and the other with a W-shaped (also called double U-shaped) GHE tube configuration. The validation of the model was carried out by comparing the numerical results with results obtained from the finite lines source (FLS) analytical solution. Both GHE models were developed in a manner that they can represent the circulation of the fluid in the GHE pipes and allow the temperature of that fluid to be changed along the length of the pipe. Being able to take account for such a physical phenomenon, the thermal interactions with nearby railway tunnels could be investigated within later chapters.

6.2 VERTICAL GHE TYPES IN THE NUMERICAL MODEL

Both single and multiple U-shaped loops GHE models were built using COMSOL Multiphysics. The geometrical dimension implemented for the two types of GHEs are illustrated in Figure 6.1.

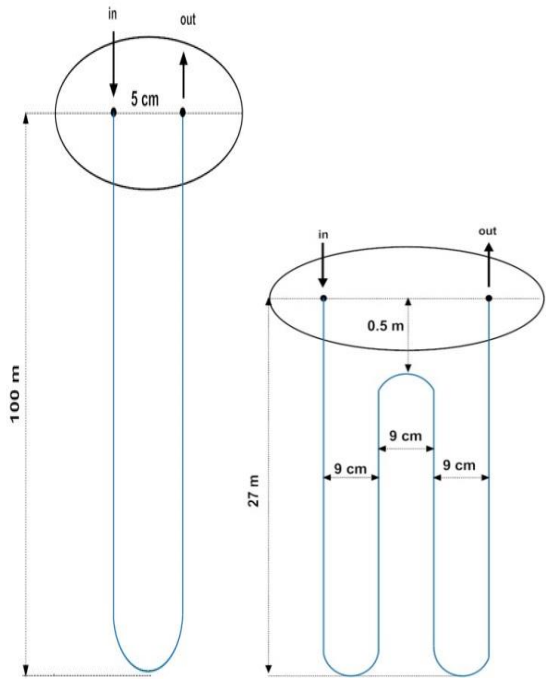

Figure 6.1: Single and multiple U-shaped GHE loops (not to scale)

These were the typically reported GHE dimensions highlighted in the literature review of this thesis (Chapter 2). Detailed model construction details are attached in Appendix G and J. For both GHE models, a mixture of water and propylene glycol with a concentration of 20% by volume was used as the heat exchange fluid. The thermal properties of the water-antifreeze solution were taken from the ASHRAE Handbook Fundamentals (ASHRAE, 2009).

6.3 GEOMETRY AND MESH OF THE GHE MODELS

6.3.1 Geometry of the GHE Models

The literature review and the results of the 2D preliminary investigation suggested that heat transfer effects in the ground were negligible after about 10 m from the wall of a single vertical GHE. When the 3D GHE model geometry was built, an extra 5 m was added to that value to ensure that no additional effects were introduced by the boundary conditions applied at the far end of the modelling domain. Consequently, a 15 m distance was kept between the GHE and the lateral and bottom boundaries of the soil domain. The soil/rock layers and their thermo-physical properties were kept as they were presented within Chapter 4 as was shown in Figure 4.8. The 3D schematics of the two different types of GHEs (borehole and energy pile) are illustrated in Figure 6.2.

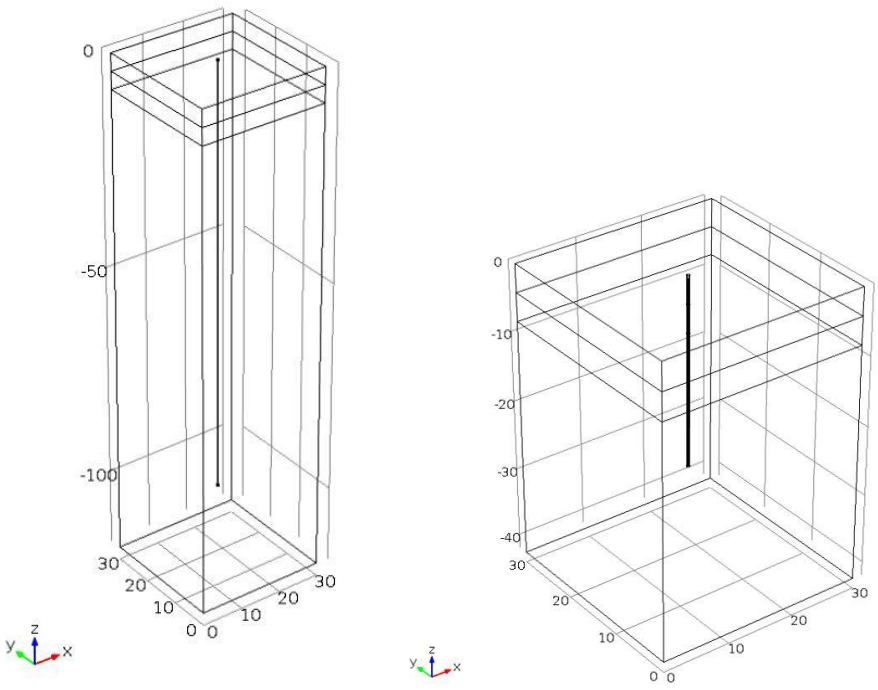

Figure 6.2: 3D geometry of vertical GHEs: BHE (left) and energy pile (right)

The dimensions and geometrical parameter values of the two different types of GHE models were adopted from the literature and are illustrated in Figure 6.1 and summarised in Table 6.1. The model was built in such a way that the geometrical parameters and material properties could be easily adjusted therefore alternative geometrical scenarios could be easily investigated.

Table 6.1: Geometrical parameter values of BHE and Energy Pile types GHE models

Parameter	**BHE** [mm]	**Energy Pile** [mm]
Diameter	150	450
Depth	100,000	27,000
Pipe inner diameter	21.5	34.0
Pipe wall thickness	2.4	3.8
Pipe shank spacing	50	90

6.3.2 Mesh of the Numerical Model

The mesh of the GHE models was built using free tetrahedral mesh elements within the entire model geometry for both types of GHE models. Figure 6.3 shows a magnified 2D cross-sectional plan view of the GHE model. It can be seen on the figure that the mesh was more refined in and around the circumference of the GHEs. In addition, the first two soil layers Made Ground and Thames Gravels were more refined than the London Clay. This was because the vertical temperature gradient caused by climatic effects was considered to have a more significant effect within those layers.

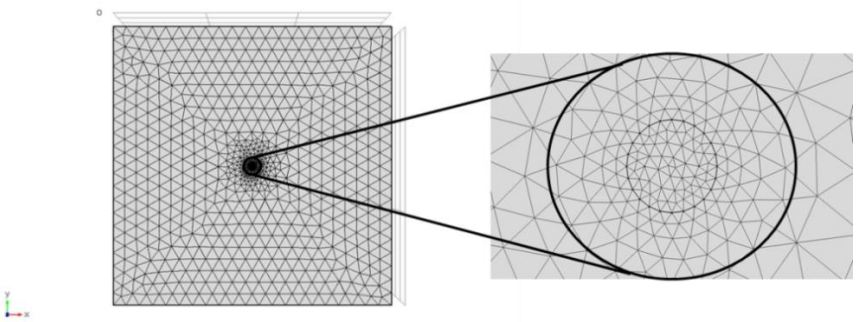

Figure 6.3: Magnified 2D cross-sectional view of the FE mesh

The mesh independency analysis is attached in Appendix B. Four unstructured meshes made of tetrahedral elements were tested for the single looped GHE. The finest mesh contained 275373 domain elements whilst the coarsest mesh included 8386. Temperature values at a specific measurement within the model domain were compared for the four different mesh configurations. Based on the analysis results, the finer mesh configuration was selected with 77969 domain elements. For the double looped GHE model the same element characteristics were built, which overall contained 173439 numbers of elements.

6.4 PHYSICS AND BOUNDARY CONDITIONS OF THE GHE MODELS

6.4.1 Introduction

Two GHE models (single and multiple U-shaped loops) were developed with different geometrical parameters. The governing physics applied are the same for both models and can be divided into two categories. One is a time dependent heat transfer problem in the volumetric domain, which is solved by calculating the temperature in each FE mesh node. The second is the transient fluid flow and forced convection problem in the GHE pipes, solved by evaluating the temperatures of the fluid and the pipe wall along the pipe axis. These are discussed in detail for each model domain (soil and GHE) in the following sub-sections.

6.4.2 Soil Domain

Governing equations and boundary conditions applied to the soil domain were established from the results of the preliminary 2D investigations. The temperature boundary condition at the soil surface (Equation 4.2) was kept. The lateral boundary of the domain was assumed to be adiabatic and an initial vertical ground temperature gradient was imposed for the entire modeling domain. The governing equation applied in the soil was considering a pure conductive heat transfer as Equation 4.1.

6.4.3 GHE

6.4.3.1 Physics

The fluid flow and the heat transfer problem in the pipes are physically modeled using linear elements, reducing the 3D flow problem to 1D as shown in Figure 6.4. This is a similar simplification to that which was used in UR-Model-B, in Chapter 5, for the representation of the trains. This simplification provides a great advantage in computational efficiency over meshing and computing 3D pipes with a finite diameter.

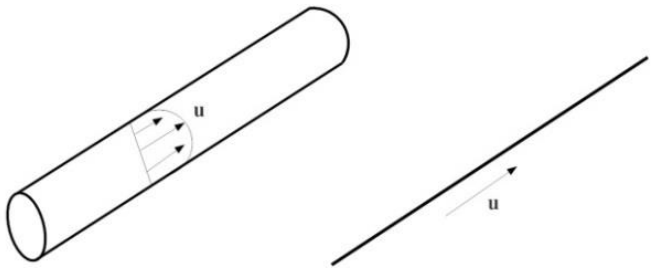

Figure 6.4: Linear pipe elements reduce the 3D flow problem to 1D

The pipe flow problem is determined by solving the momentum and continuity equations as Equations 6.1 and Equation 6.2 (Barnard *et al.*, 1966).

$$\rho_f \frac{\partial \boldsymbol{u}}{\partial t} = -\nabla p - f_D \frac{\rho_f}{2d_h} \boldsymbol{u}|\boldsymbol{u}| \tag{6.1}$$

$$\frac{\partial A_{pi}\rho_f}{\partial t} + \nabla \cdot \left(A_{pi}\rho_f \boldsymbol{u}\right) = 0 \tag{6.2}$$

Where:

$$d_h = \frac{4A}{Z} \tag{6.3}$$

The second term on the right-hand side of Equation 6.1represents the pressure drop due to viscous shear. The Darcy friction factor, f_D accounts for the continuous pressure drop along a pipe segment due to viscous shear. It is expressed as a function of the Reynolds number and the ratio of the surface roughness, e to the hydraulic diameter as shown in Equation 6.4.

$$f_D = f\left(Re, \frac{e}{d_h}\right) \tag{6.4}$$

The Darcy friction (which is valid for both laminar and turbulent flow conditions) can be estimated using the Churchill (1977) equation as follows Equation 6.5.

$$f_D = 8\left[\left(\frac{8}{Re}\right)^{12} + (C_A + C_B)^{-1.5}\right]^{1/2} \tag{6.5}$$

Where C_A and C_B are factors given as:

$$C_A = \left[-2.457\ln\left(\left(\frac{7}{Re}\right)^{0.9} + 0.27(e/d_h)\right)\right]^{16} \tag{6.6}$$

$$C_B = \left(\frac{37530}{Re}\right)^{16} \tag{6.7}$$

Where the Re is defined as the ratio of the internal forces to the viscous forces such that:

$$Re = \frac{\rho_f \boldsymbol{u} d_h}{\mu} \tag{6.8}$$

The heat transfer in pipes problem is governed by the equation for an incompressible fluid flowing in a pipe:

$$\rho_f A_{pi} C_{pf} \frac{\partial T}{\partial t} + \rho_f A_{pi} C_{pf} \boldsymbol{u} \cdot \nabla T = \nabla \cdot A_{pi} k_f \nabla T + f_D \frac{\rho_f A_{pi}}{2 d_h} |\boldsymbol{u}|^3 + q'_{wall} \tag{6.9}$$

The second term on the right hand side corresponds to friction heat dissipated due to viscous shear. The radial heat transfer from the surroundings into the pipe is given by Equation 6.10.

$$q'_{wall=(hZ)_{eff}(T_{ext}-T)} \tag{6.10}$$

In Equation 6.10, $(hZ)_{eff}$ is an effective value of the heat transfer coefficient h (W/(m^2*K)) times the wall perimeter Z (m) of the pipe and T_{ext} (K) the external temperature outside of the pipe. Figure 6.5 shows the cross-section of the pipe-fluid domains and the temperature across the pipe wall. With reference to this figure, the effective overall heat transfer

coefficient per unit length of the pipe, including internal film resistance and the wall resistance, can be deduced as Equation 6.11.

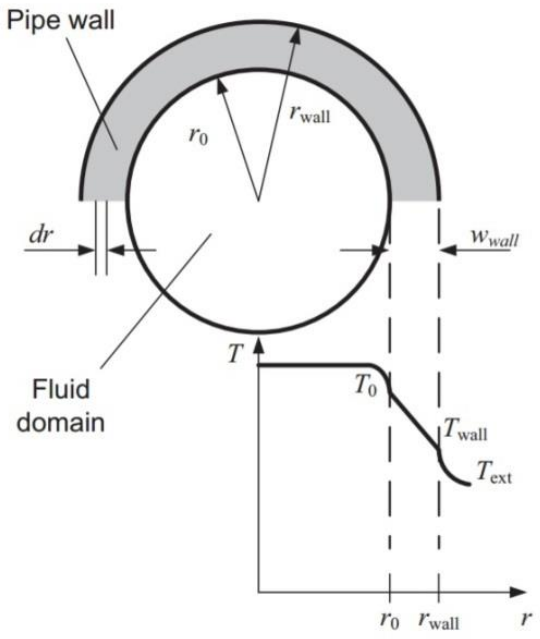

Figure 6.5: Temperature distribution across the pipe wall (Adapted from: *COMSOL Multiphysics (2017)*)

$$(hZ)_{eff} = \frac{2\pi}{\frac{2}{d_{pi\_i} h_{int}} + \frac{\ln(d_{pi\_o}/d_{pi\_i})}{k_{pi}}} \tag{6.11}$$

The internal film resistance can be calculated using Equation 6.12.

$$h_{int} = Nu \frac{k}{d_h} \tag{6.12}$$

Where, Nu is defined as the ratio of convective to conductive heat transfers across a boundary. For turbulent flow conditions, the Nusselt number can be estimated using the correlation developed by Gnielinski (1976) as follows in Equation 6.13.

$$\mathrm{Nu} = \frac{(f_D/8)(Re - 1000)P_r}{1 + 12.7(f_D/8)^{1/2}\ (Pr^{2/3} - 1)} \tag{6.13}$$

For:

$0.5 < Pr < 2000$

$3000 < Re < 6\,x\,10^6$

6.4.3.2 Heat transfer coupling

In the numerical model, the external temperature outside of the pipe T_{ext} corresponds to the temperature field computed in the surrounding volumetric domain. This provides automatic heat transfer coupling to the 3D domains considering the pipes as a line heat source.

6.4.3.3 Boundary conditions

The boundary conditions defined on the inlet point of the linear pipe element are the volume flow rate, $\dot{V}$ and a prescribed temperature T_{in} (t). The former is used to describe the flow of the circulation fluid inside the pipes, while the latter is used to define the heating or cooling of the fluid. For optimising the convergence of the model a continuous step function is used as a multiplier whilst assigning a volumetric flow rate, allowing a smooth transition from zero to the desired value.

6.5 MODEL VALIDATION

6.5.1 Validation Description

The ability of the model to calculate transient heat transfer rates was validated by comparing the numerically generated results with the results obtained from the FLS analytical solution.

The analytical solution assumes soil as a homogeneous semi-infinite medium with constant thermo-physical properties. For this reason, the model boundary conditions were modified this way. The undisturbed ground temperature was selected to be 12˚C, which is typical soil temperature below depth of 10 m in London.

The numerical simulation was performed by applying a constant heat rate of 50 W/m for 150 hrs. The magnitude of the selected heat rate is within the range recommended by Kavanaugh *et al.* (2000) for in-situ thermal response tests of soil's surrounding vertical GHEs. For the purpose of the model validation the ground surface was kept at a constant temperature both for the numerical model and the FLS solution. This was equal to the undisturbed ground temperature i.e. 12˚C.

The heat injection was accomplished by applying a temperature difference on the GHE pipe inlet boundary expressed as Equation 6.14. The temperature difference applied between the inlet and outlet of the GHE pipes, maintained the heat injection into the ground.

$$T_{pi_{in}(t)} = T_{pi_{out}(t)} + \Delta T(t) \tag{6.14}$$

The heat rate and the flow rate of the circulated fluid was selected constant and therefore ΔT was estimated using Equations 6.15 and Equation 6.16.

$$q = \dot{V}\rho_f c_{p_f}\Delta T \tag{6.15}$$

$$\Delta T = \frac{q}{\dot{V}\rho_f c_{p_f}} \tag{6.16}$$

6.5.2 COMSOL vs FLS Results Comparisons

The FLS analytical solution was used for the validation of the 3D numerical GHE model in order to capture the axial thermal effects occurring near the extremities of the GHE. The solution of the temperature excess of a point at a particular selected time can be obtained by integrating contributions of all the increments of the line source (Zeng *et al.*, 2002). This can be written as Equation 6.17. The equation was used to estimate the temperature variations at a mid-depth of the GHE, at various time/radial distance combinations starting from the wall of the GHE.

$$\Delta T(t) = \frac{q}{4k\pi}\int_0^H \left[\frac{erfc\left(\frac{\sqrt{r^2+(z-h')^2}}{2\sqrt{\alpha t}}\right)}{\sqrt{r^2+(z-h')^2}} - \frac{erfc\left(\frac{\sqrt{r^2+(z+h')^2}}{2\sqrt{\alpha t}}\right)}{\sqrt{r^2+(z+h')^2}}\right] dh \tag{6.17}$$

Figure 6.6 shows the comparison plots between the numerical and analytical values at different times: 25h, 75h and 150h. It can be seen that the numerically generated results are close to the values of the FLS analytical solution. The results of this comparison suggest that the 3D GHE model developed and introduced in this chapter of the thesis serves as a useful tool for the future analysis of UR-GSHP interactions.

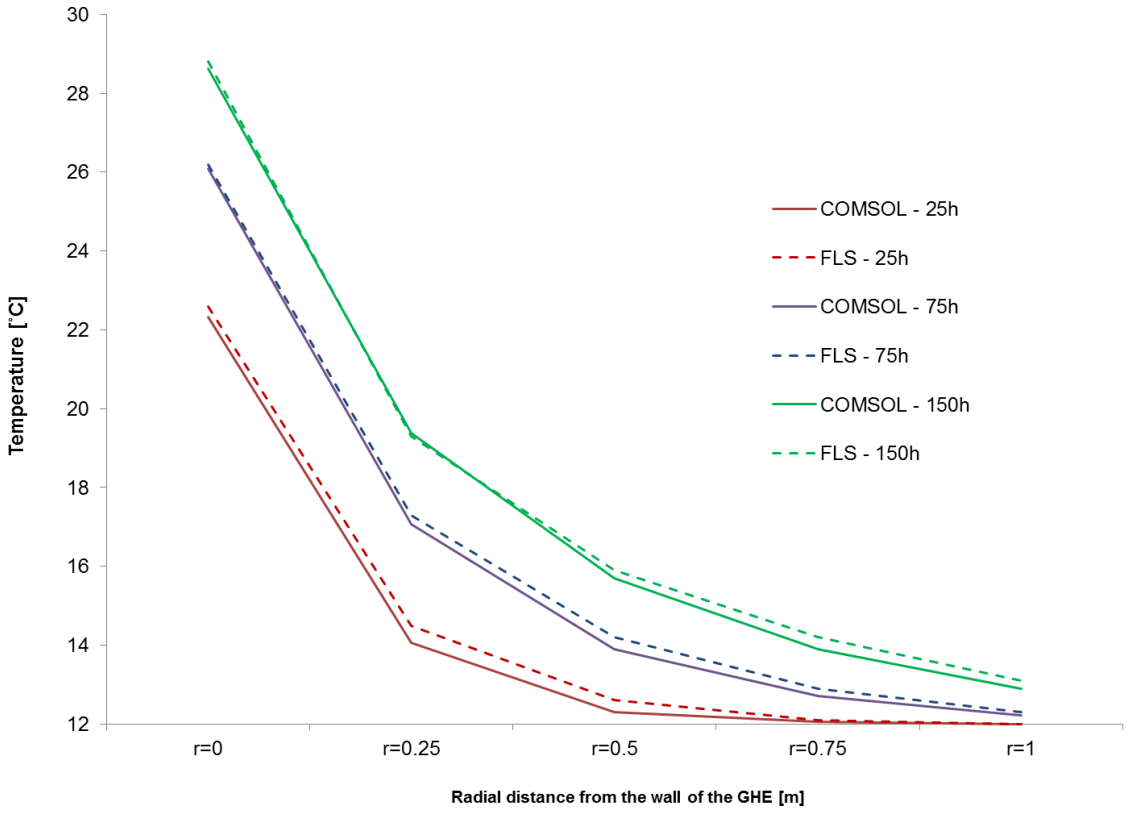

Figure 6.6: Temperature vs radial distance at mid-depth of the GHE estimated by the numerical model and by the FLS analytical solution

6.6 GHE MODEL OPTIMIZATION

When GHEs geometry is explicitly discretized within the model such that the absorber pipes as well as the small diameter borehole material (sand/bentonite) are both represented, the length scales being resolved within the numerical model differ vastly. For example, the dimensions of the GHEs are significantly smaller than that of the surrounding soil domain. Due to these different length scales, the FE mesh of the model results in a large number of degrees of freedom (NDF) and solving the model requires powerful computational resources, especially when the simulation of large GHE arrays is being considered.

6.6.1 Simplifying Assumption within GHE Models

If resources are limited, it is important to reduce the NDF of the FE mesh. This can be accomplished by reducing the number of mesh elements required to solve the model. This was achieved by assuming that the temperature profile across the thin borehole/energy pile material was not of primary interest, thus its physical geometry surrounding the linear pipe

elements could be removed from the model. The validity of the assumption rested on the fact that the overall modelling objective was to investigate UR and GSHP interactions and the temperature of the thin borehole material was not a key concern. Also, the borehole and the energy pile material have similar thermal characteristics to that of the surrounding soil. Implementing this assumption significantly reduces the number of mesh elements required to solve the model. From this point forward, all investigations which considered a GHE array, i.e. more than a single GHE, the simplification was used in order to enhance computational efficiencies.

6.7 CONCLUSIONS

In this chapter, 3D numerical models for vertical GHE simulation were introduced. Two typical types of closed-loop vertical GHE geometries, boreholes with single loop and energy piles with double loop absorber pipes were described. Both types of GHE models consist of several components. These include the pipes, grout and the surrounding soil. The lateral and bottom boundaries of the model were assumed to be adiabatic. For minimizing the computational effort, the developed numerical models use 1D linear elements for simulating the flow and heat transfer inside the GHE pipes. These linear elements were coupled with the rest of the 3D domain. The coupling method made use the external temperature outside of the pipe which corresponds to the temperature field computed in the surrounding volumetric domain.

The ability of the model to calculate transient heat transfer rates was validated by comparing numerical results against the results of the FLS analytical solution. The results of this comparison suggested that the 3D numerical GHE model could successfully simulate the operation of vertical GHEs.

The chapter also introduced a simplifying method for optimizing the GHE models for scenarios where large arrays of GHEs are considered. This method included the assumption that as the thin borehole/energy pile material was not of primary interest, its physical geometry surrounding the linear pipe elements could be removed from the model. The validity of the assumption rested on the fact that the overall modelling objective was to investigate UR and GSHP interactions and the temperature of the thin borehole material was not a key concern. By removing the borehole material from the model geometry had significantly reduced the number of finite element mesh and the NDF of the model. This in turn enhanced computational efficiencies significantly.

The next chapter will introduce a preliminary 3D investigation where the UR and GHE models were combined in order to investigate how the two systems impact on their surrounding and on each other.

CHAPTER 7: COMBINED UR-GHE MODEL; A PRELIMINARY 3D INVESTIGATION

7.1 INTRODUCTION

The work detailed in Chapter 7 aimed to combine the previously developed 3D numerical UR and GHE models within the same simulation environment and conduct a preliminary 3D investigation of the thermal interactions. The key modelling objectives of this investigation were to explore the long term thermal effects of a single UR tunnel on undisturbed ground temperatures and the thermal interactions of UR and GSHP systems based on a certain geometrical configuration and operating condition. The governing physics and the type of boundary conditions of the model were kept as described in the previous two chapters (Chapters 5 and 6). The combined model geometry and the selected operational characteristics for the analysis are described in detail. The developed combined model introduced in this chapter could then be used to conduct a parametric study on the thermal interactions of URs and GHEs which is detailed later in Chapter 8.

7.2 MODEL GEOMETRY

The model geometry contains a single UR tunnel and 40 vertical GHEs with the aspect ratio of 2x20 and a depth of 100 m. A schematic of the combined UR-GHE model is illustrated in Figure 7.1 and the dimensions of the GHEs and the UR tunnel are summarised in Table 7.1. It can be seen in Figure 7.1, that the width of the soil domain is a function of the number of GHEs in the “x” direction of the model geometry and the depth of the soil is a function of the number of GHEs in the “y” direction.

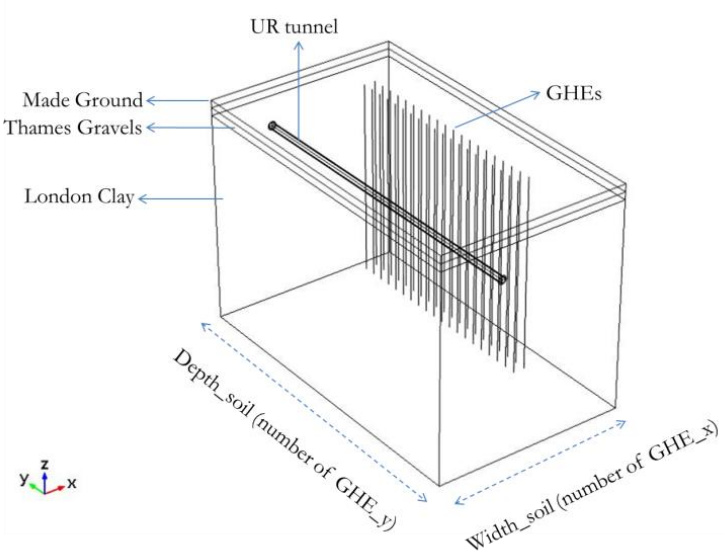

Figure 7.1: Schematic of a 3D UR-GHE model

The different ground conditions that typically exist down to 115 m below the surface within the central London area were taken into account in the building of the model. The soil layers are also illustrated in Figure 7.1 and their thermo-physical properties were summarized in Chapter 4 in Table 4.1. The overall height of the soil domain is 15 m deeper that the GHEs, i.e. 115 m. The literature suggested that after about 20 m from the wall of an UR tunnel the thermal effects are negligible, whilst for a GHE a distance of 10 m is suggested. The model domain was made deliberately larger than those values in order to ensure that that the influence of boundary conditions at the far ends of the model geometry were negligible. The proximity, which is the separation distance between the tunnel wall and the closest line of the GHE array to the tunnel, was set as 3 m. This figure was chosen because this is the minimum distance that LU allows for any structures to be constructed near the tunnels (TfL, 2013).

Table 7.1: Dimensions of GHE Array and Tunnel

Parameter	Values
GHEs	
Depth	100 m
Pipe inner diameter	21.5 mm
Pipe wall thickness	2.4 mm
Pipe shank spacing	100 mm
GHE spacing (for GHE arrays)	6 m
Tunnel	
Depth	24 m
Tunnel diameter	4.4 m
Thickness of tunnel liner (concrete)	0.5 m

7.3 ANALYSIS AND DISCUSSIONS

The developed model was used to perform two different studies. The first study investigated the effect of an UR operation on undisturbed soil temperatures. The second study then investigated the interactions of the UR and the GHE array and their impact on their surroundings. The parameters relating to the operational characteristics of the GHEs and UR are summarized in Table 7.2. A tunnel cross section and the average air velocity profile is illustrated in Figure 7.2.

Table 7.2: Operational characteristic parameters

Parameter	Values
GHEs	
Fluid flow rate	0.2 l/s
Fluid temperature at pipe inlet	5°C
UR	
Tunnel air velocity	3.5 m/s
Train heat load	287 W/m
Air temperature entering the tunnel	17-27°C

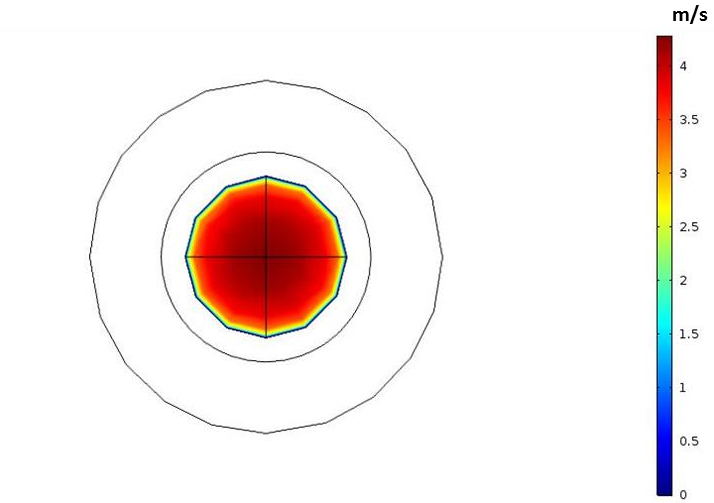

Figure 7.2: Air velocity profile at a tunnel cross section

7.3.1 Investigation 1

7.3.1.1 Introduction

Investigation 1 studied the effects of tunnel heat loads on initial ground temperatures within a block of London Clay. The operation of the GHEs was neglected during this investigation. The soil block represented a volume of soil surrounding the 40 GHEs within that soil layer. This block is highlighted blue in Figure 7.3. The horizontal distance between the wall of the tunnel and that block of soil was set as 2.9 m. The temperature of the block (T_s block) was investigated during 50 years of simulation period through two different setups as follows:

a) No tunnel heat load applied
b) With applied tunnel heat load

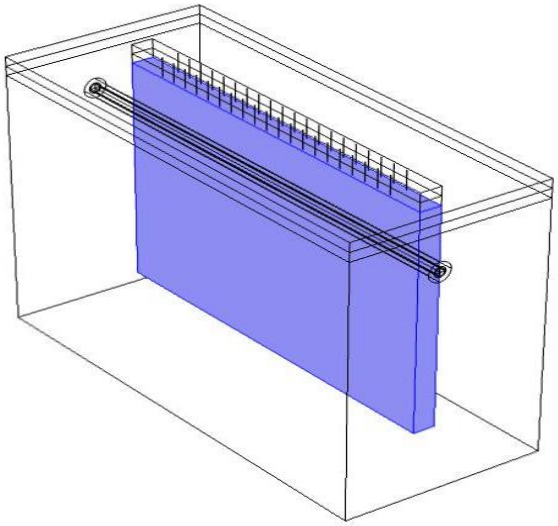

Figure 7.3: Soil block surrounding the 40 GHEs

7.3.1.2 Results

Figure 7.4 shows that when the tunnel heat load was neglected, the ground temperatures were fairly constant within the soil block. On the other hand, a gradual increase in the block temperature could be seen when the tunnel heat load was applied. At the end of the 50 year simulation period, the soil block temperature was about 1.35°C warmer than when the heat load from the tunnel was considered. Using higher than expected source temperatures could enhance performance of GSHPs operating in heating mode. The heating CoP improves by approximately 3% for each degree Celsius that the evaporating temperature is raised (Cengel and Boles, 2001).

The results of Investigation 1 also highlighted that when UR-GSHP interactions are being investigated, it is important to consider the initial effect of the UR operation on its surroundings. Starting a simulation of an UR-GSHP model from a uniform soil temperature profile would not be realistic if a London based case study is considered, since the operation of the URs over an extended period would have impacted on the surrounding soil temperature prior to the installation of the GSHP. This was shown with the red line in Figure 7.4. However, it can also be seen in the figure that after that many years of operation the warming effect of the UR on the surrounding soil is almost negligible. This has been taken as the initial ground conditions for all further time dependent studies reported in Chapter 8 of this thesis.

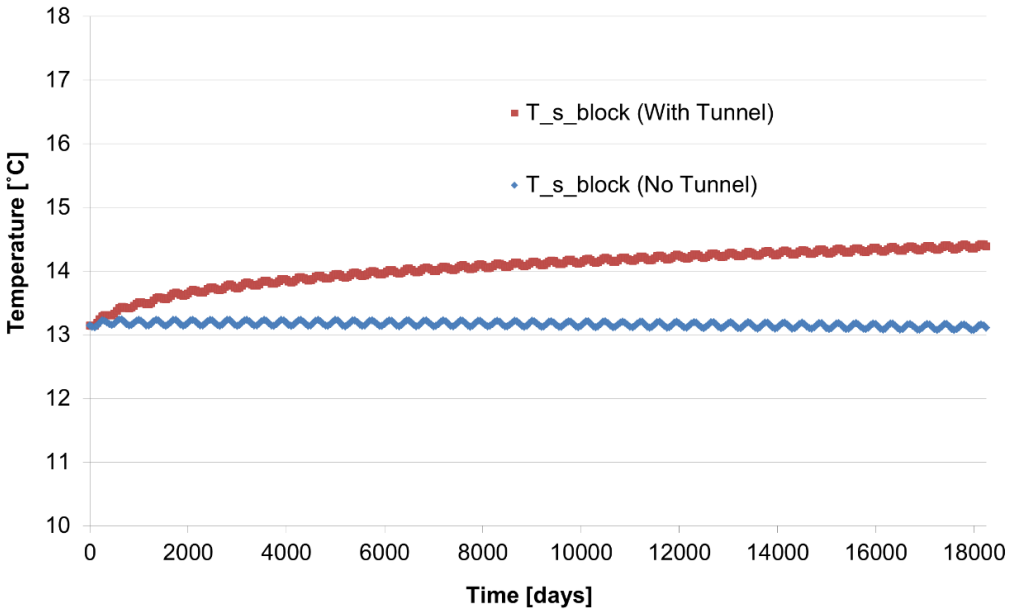

Figure 7.4: Resulting temperature of the soil block

7.3.2 Investigation 2

7.3.2.1 Introduction

Investigation 2 reflected the operation of the GHEs and aimed to study the interaction of an UR and GHEs and their mutual impact on the surrounding soil. Constant temperature and volume flow rates were specified at the GHE pipe inlets. The investigation was conducted by computing the following parameters during a 1 year simulation period:

a) The soil block temperature (T_s_block) (impact of tunnel on GHEs)
b) GHE's fluid temperature at the pipe outlet (T_p_out) (impact of tunnel on GHEs)
c) Soil temperature surrounding the tunnel (T_s_tun) (impact of GHEs on tunnel)
d) Tunnel wall surface temperature (T_w_tun) (impact of GHEs on tunnel)

7.3.2.2 Results

The results of the investigation are plotted in Figure 7.5, Figure 7.6, Figure 7.7 and Figure 7.8. The first two graphs, Figure 7.5 and Figure 7.6, show the impact of the tunnel on the GHEs (options a and b with and without the UR tunnel heat load). Then the following two graphs, Figure 7.7 and Figure 7.8, show the impact of the GHEs on the tunnel surroundings and tunnel wall surface (options c and d with and without the GHEs heat load).

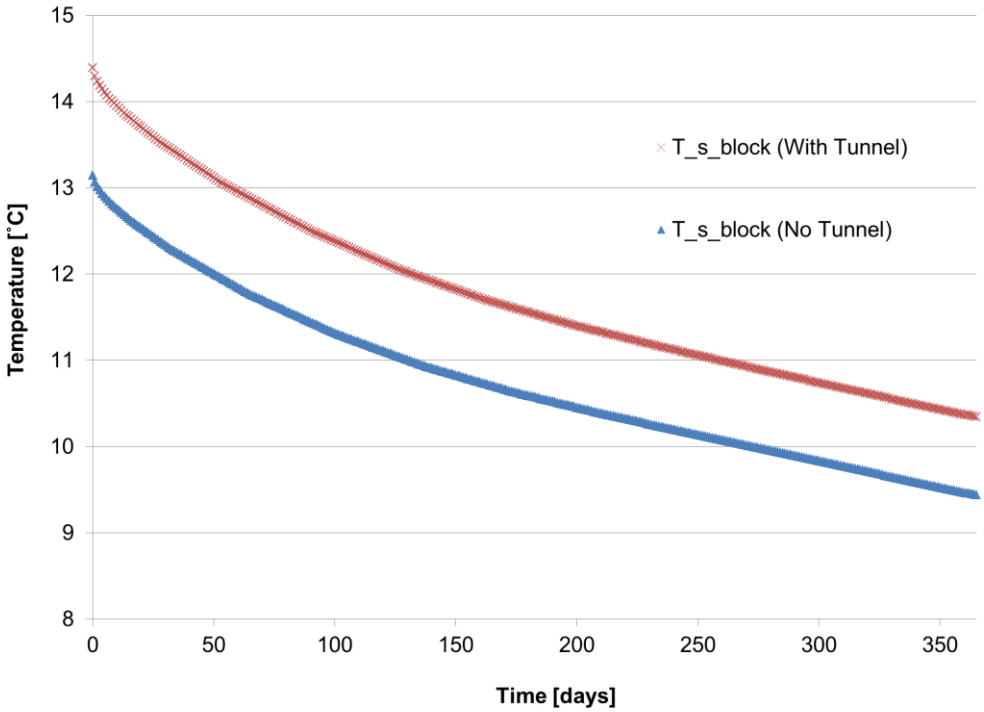

Figure 7.5: Soil block temperature with and without the tunnel load

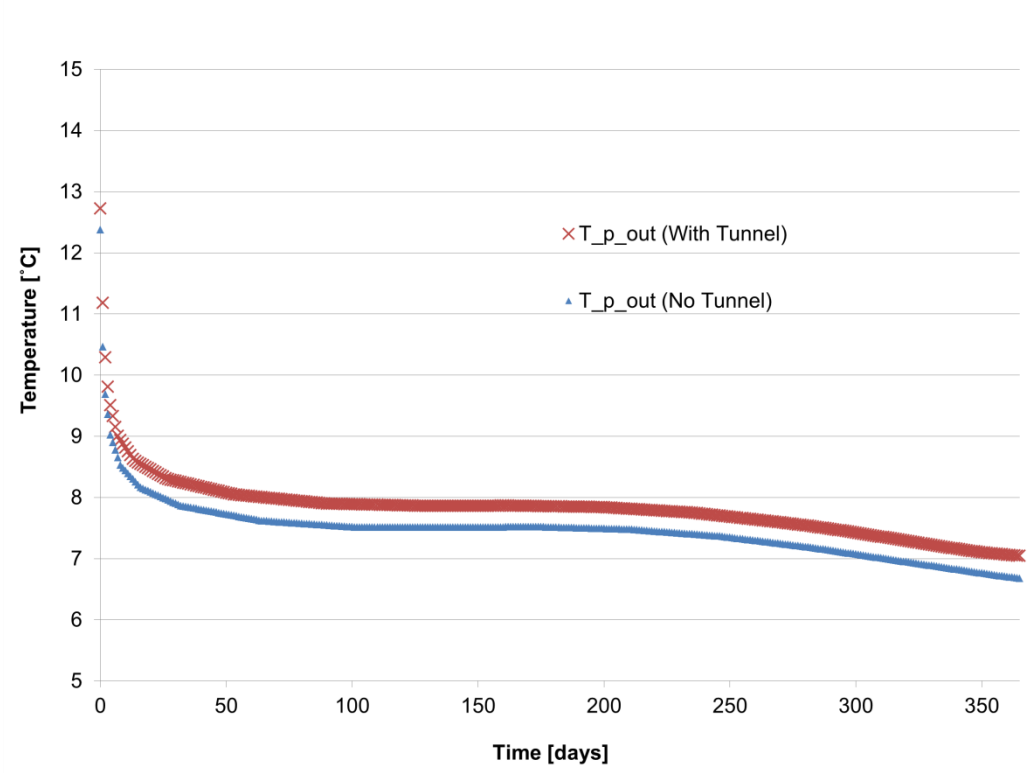

Figure 7.6: GHE's fluid temperature at the pipe outlet

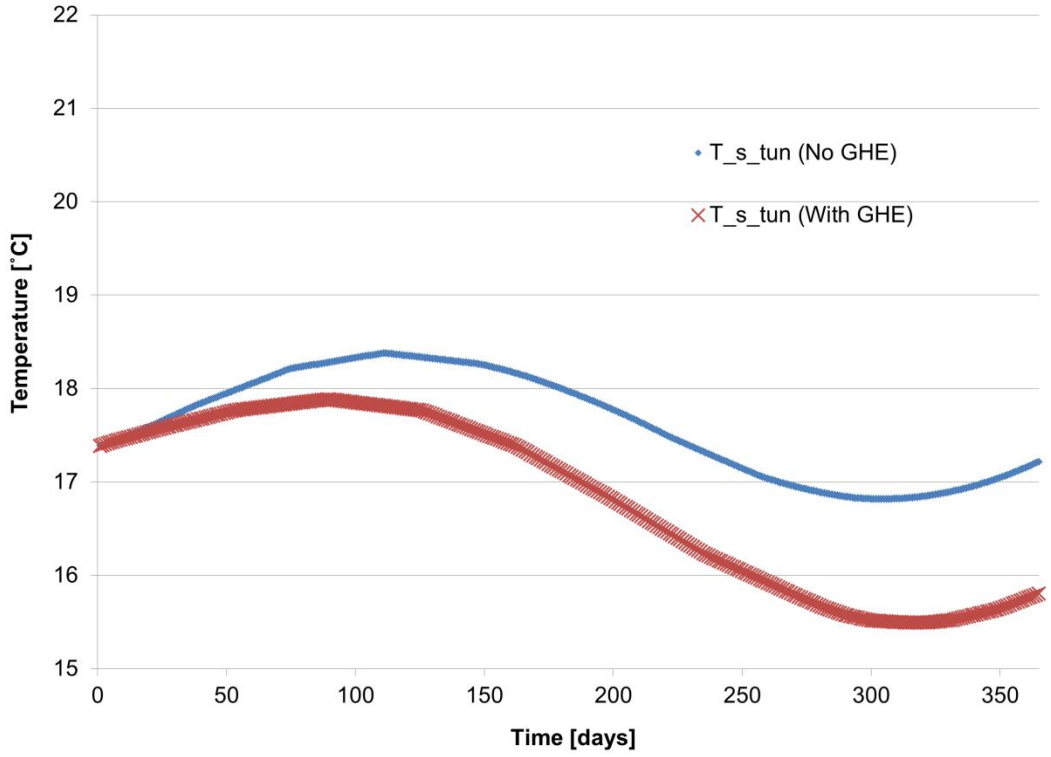

Figure 7.7: Soil temperature surrounding the tunnel

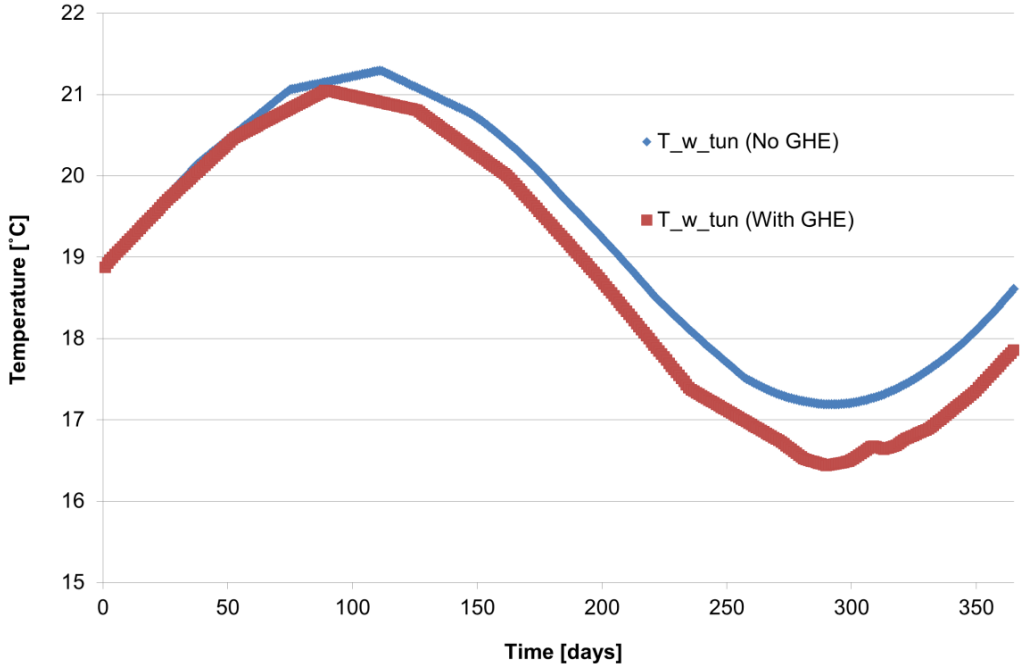

Figure 7.8: Tunnel wall surface temperature

7.3.3 Discussions on the Impact of Tunnel on GHEs

Figure 7.5 shows a similar trend of temperature decrease of the soil block for both scenarios. However, when the tunnel load is considered the temperature decrease starts from a higher initial value which results in an overall higher temperature profile of the soil. This is beneficial for GSHPs operating in heating mode, since higher temperature of the soil results in higher temperature of the circulated liquid at the GHE's pipe outlet. This is shown in Figure 7.6. The higher fluid temperature at the GHE's pipe outlet requires a smaller temperature lift from the GSHP which increases its CoP.

7.3.4 Discussions on the Impact of GHEs on Tunnel

The impact of the GHEs operation on the soil surrounding the tunnels can be seen in Figure 7.7. The impact is the most apparent at around day 300 of the simulation period, which represents the coldest part of the winter season. The average temperature of the soil during that period was reduced by approximately 1.5°C. Reducing the soil temperature surrounding the tunnels could enhance the heat sink effect of that soil which would be ultimately beneficial when the cooling effects on an UR are considered. This was confirmed by the results shown in Figure 7.8. It can be seen that the tunnel wall temperatures were reduced by about 1°C due to the operation of the nearby GHEs.

7.4 CONCLUSIONS

In this chapter, the previously developed and validated 3D UR and GHE models (introduced in Chapters 5 and 6) were combined within the same simulation environment for analysis. The geometrical parameters, governing equations and boundary conditions of the model were kept the same as for the individual 3D models. The developed combined model was used to perform two different studies which were aimed to enhance the understanding of the thermal interactions between URs and nearby GHEs. The first study investigated the effect of an UR operation on undisturbed soil temperatures. The second study then investigated the interactions of the UR and the GHE array and their impact on their surroundings.

The results clearly demonstrated that interactions occur between URs and neighboring GSHP installations. In particular, Investigation 1 showed that at the end of the 50 year simulation period, the temperature of a soil block near the tunnel was about 1.35°C warmer when the heat load from the tunnel was considered. This was concluded to be beneficial for GSHPs, since using higher than expected source temperatures could enhance performance of the systems when operating in heating mode. The results of Investigation 1 also highlighted the importance of considering the initial effect of the UR operation on its

surroundings before UR-GSHP interactions are investigated. Starting a simulation of an UR-GSHP model from a uniform soil temperature profile would not be realistic if a London based case study is considered. The operation of the URs over an extended period would have impacted on the surrounding soil temperature prior to the installation of the GSHP.

In addition, the results of Investigation 2 showed that extracting heat from the ground surrounding the tunnel was likely to enhance the heat sink effect of the soil, which could potentially have a cooling impact on the URs. This particular effect will be further explored in the following chapter.

Since the investigations presented in this chapter considered only certain geometrical configurations and operational characteristics of the systems, further research was conducted. This was taking account of a number of potential geometrical and operational parameter variations of the systems. These additional 3D parametric studies are introduced in the following chapters.

CHAPTER 8: PARAMETRIC ANALYSIS

8.1 INTRODUCTION

Chapter 8 introduces a parametric analysis, consisting of nine different studies. The analysis was conducted using the combined 3D model developed and introduced in the previous chapter, Chapter 7. The parametric analysis aimed to enhance UR-GSHP interactions by considering a number of geometrical and operational characteristic scenarios of the systems. The reason for the consideration of these factors was that GHE arrays are often vary in size, configuration and operation modes. Also tunnels are mainly running through clay in London but some section of the railway runs through fine sands. All these variations amongst others detailed in the analysis could have a potential impact on the thermal interactions. The chapter first introduces the methodology selected for carrying out the parametric analysis. Following that, it details the studies conducted and discusses their results. Based on the simulation results, a formula was developed which allowed estimation of the potential enhancement of the GHEs' heat extraction rates due to the heat load of the nearby tunnel(s). At the end of the chapter, conclusions are derived in terms of potential benefits and disadvantages of the thermal interactions of UR and GSHP.

8.2 METHODOLOGY

The selected parameters and their studied effects on the interactions were separated into two main categories. The first group of studies, named as Part 1, considered a number of different geometrical options for the UR tunnel(s) and the nearby GHE array. The second group of studies, Part 2, then examined how different GSHP operational characteristics would impact on UR-GSHP interactions. These two sets of studies and the specific key parameter variations which were examined within them are summarised in Table 8.1.

Table 8.1: Parametric studies

Study	Part 1: Geometrical Studies	Study	Part 2: operational Characteristics Studies
1	Single vs multiple tunnels	8	GSHP with balanced heating and cooling
2	GHEs in between two tunnels	9	GHE's fluid flow rate variation
3	GHE array aspect ratio		
4	Single vs double looped GHEs		
5	Proximity variation		
6	Tunnel running through fine sands		

8.2.1 UR Parameters

The parameter values related to the operation of the UR system were fixed during the parametric analysis. This is due to the fact that the operational characteristics of the deep level URs in London do not differ significantly. Typical values which were used in the studies are the same as the ones summarised in Table 7.2 in Chapter 7. In terms of the geometrical parameters of the UR railway, the only variation was to compare a single tunnel scenario with a multiple tunnel one.

8.2.2 GSHP / GHE Array Parameters

The most common use of GSHP technology revolves around domestic and commercial space heating and cooling as well as the production of hot water. For this reason both heating and balanced load systems were investigated. Although there were a large number of geometrical configurations considered through the parametric analysis, for the majority of investigations, the pipe length of the GHE array was kept the same. This allowed the comparison of the impact of nearby tunnels on GHE arrays with the same size but with different layouts and operational characteristics. The overall pipe length of this base case sized GHE array was selected as 8000 m. This equates to 40 single looped GHEs with a depth of 100 m. This is a medium sized GSHP installation that typically could be found in London (a GSHP system with a heating /cooling capacity of ~ 300 kW). Within all the geometrical type investigations (Part 1 of the parametric analysis), the GHEs operational characteristics were kept the same. That is, there were fixed temperature and volume flow rate boundary conditions applied at the inlets of the GHE, 5˚C and 0.1 l/s respectively. These are typical operating conditions for a London based GSHP system which is functioning in its heating mode (FABER MAUNSELL, 2007). These operational conditions were varied in Part 2 of the analysis.

8.2.3 Newly Defined Variables

In order to be able to characterise UR-GSHP interactions, two new geometrical variables were developed. The variables are called UR-GHE interaction proximity (Ω) and UR-GHE wall to wall distance. These new variables are described below.

8.2.3.1 Interaction proximity (Ω)

For single tunnel scenarios, Ω was defined as the distance between the geometrical centre of the UR tunnel and the geometrical centre of the GHE array. This distance is illustrated with a blue dotted line in Figure 8.1.

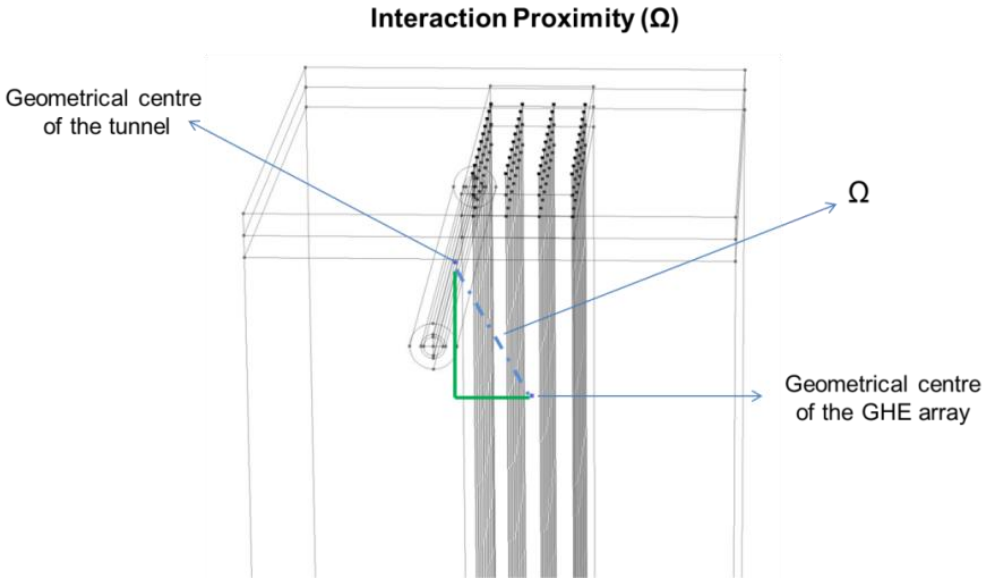

Figure 8.1: Schematic illustrating the interaction proximity of UR-GHE array

When multiple tunnels are running on one side of the GHE array, Ω should be defined as the distance between the geometrical centre of the UR tunnel (which is further away from the GHE array) and the geometrical centre of the GHE array, minus the distance between the geometrical centres of the two tunnels. This is illustrated through 2D schematic examples in Figure 8.2.

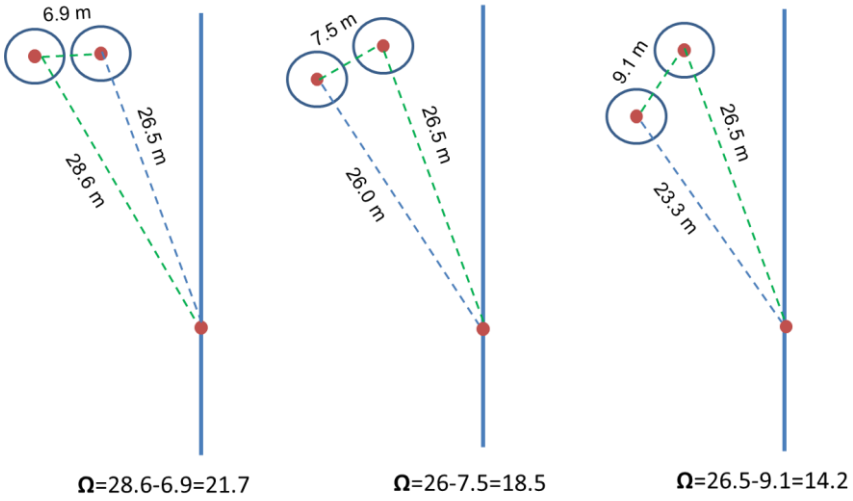

Figure 8.2: Examples of interaction proximity (Ω) when GHEs are built near multiple tunnels

The parametric analysis detailed in this chapter also investigated a geometrical scenario where the GHEs were built between multiple running tunnels. Within such geometrical configuration, the first step of defining Ω is the same as described for the earlier multiple

tunnels on one side scenario, however its value should be divided by two to take account of the surrounding effects of the tunnels on the GHEs. An example which illustrates the method of estimating Ω for these types of tunnel-GHE configurations is shown in Figure 8.3.

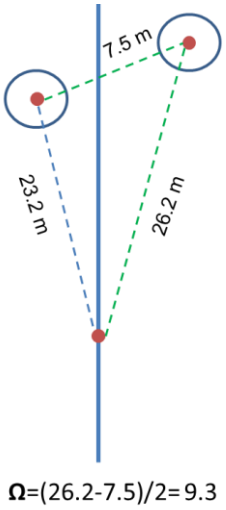

Figure 8.3: Example of interaction proximity (Ω) when GHEs are built between multiple tunnels

8.2.3.2 Wall to wall distance

The wall to wall distance was defined as the distance between the outer wall of the UR tunnel and the wall of the closest line of the GHE array. This is illustrated in Figure 8.4. For the majority of investigations, the wall to wall distance was set as 3 m. This is the minimum value in London specified by standards, which should be kept as a horizontal distance between an UR tunnel and any structures to be built near to it.

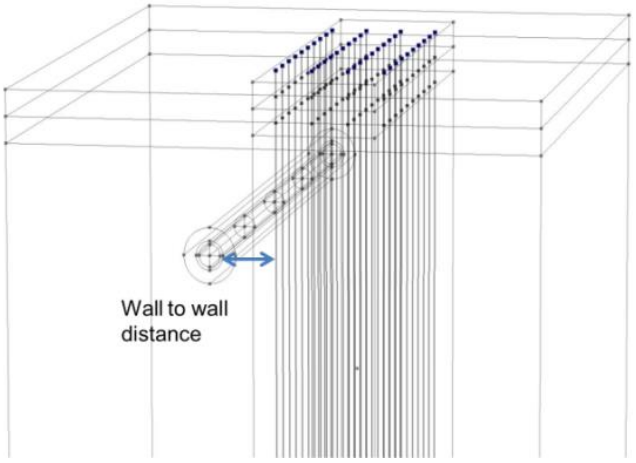

Figure 8.4: UR- GHE wall to wall distance

8.2.4 Monitored Model Outputs

In order to investigate UR-GSHP interactions the following outputs from the numerical model were monitored and analysed:

a) The impact of the tunnel heat load on the average GHE's fluid temperature at the pipe outlets [˚C].
b) The impact of tunnel heat load on the average GHEs heat extraction rate [kW].
c) The impact of the GHEs on the bulk average tunnel air temperatures [˚C].

The left side of Figure 8.5 shows the points where the fluid enters and leaves the GHEs. The heat extraction rates by the GHEs were estimated using Equation 8.1. The right side of the figure shows the bulk tunnel air domain of the model, where the average temperature was measured when the impact of the GHEs on the tunnel was investigated.

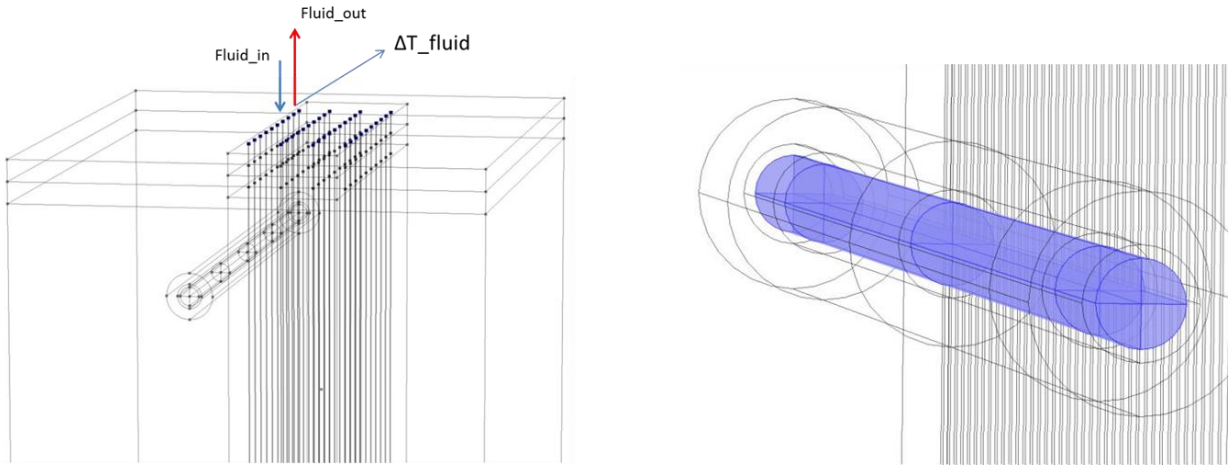

Figure 8.5: Monitored model outputs

$$Q_{GHEs} = (m_{fluid} \times cp_{fluid} \times \Delta T_{fluid}) \times Numb\_GHEs \quad (8.1)$$

8.2.5 Simulation Period and the Initial Condition of the Parametric Studies

The parametric analysis detailed in Chapter 8 was undertaken over a two years simulation period. This allowed exploration of UR-GSHP interactions on a multiple year basis. The previous chapter (Chapter 7) highlighted that starting the simulation from a uniform soil temperature profile would not have been realistic if a London based case study is considered, since the operation of the URs over an extended period would have impacted on

the surrounding soil temperature prior to the installation of the GSHP. Therefore each study within the parametric analysis was initialised by making use of results of time dependent studies where only the operation of the UR was simulated for a 50 year long period. It was shown in Chapter 7 (with the red line in Figure 7.4) that the warming effect of the UR on the surrounding soil is almost negligible after that many years, thus 50 years was considered to be a long enough initial period to take account of initial effects.

8.3 ANALYSIS, PART 1: GEOMETRICAL STUDIES

Out of the 9 different studies summarised in Table 8.1, the first 7 investigations form Part 1 of the analysis. The aim of this analysis was to investigate UR-GSHP interactions based on a number of geometrical variations, using the 3D UR-GSHP numerical model. The results from these studies are detailed in this section of the thesis. Within the majority of the investigations the simulation periods were set as two years with an initial condition set as described in section 8.2.5. In order to explore the highest potential impacts from the systems, the UR-GHE array wall to wall distance was set as 3 m within the majority of the studies. It was assumed that the GSHP operates in continuous heat extraction mode, i.e. injecting the heat exchanger fluid at 5˚C into the ground throughout the simulation period.

8.3.1 Study 1: Single vs Multiple Tunnels

8.3.1.1 Introduction of Study 1

The aim of the investigation was to establish whether the heat load from multiple running tunnels would have a larger impact on the nearby GHEs then a single tunnel.

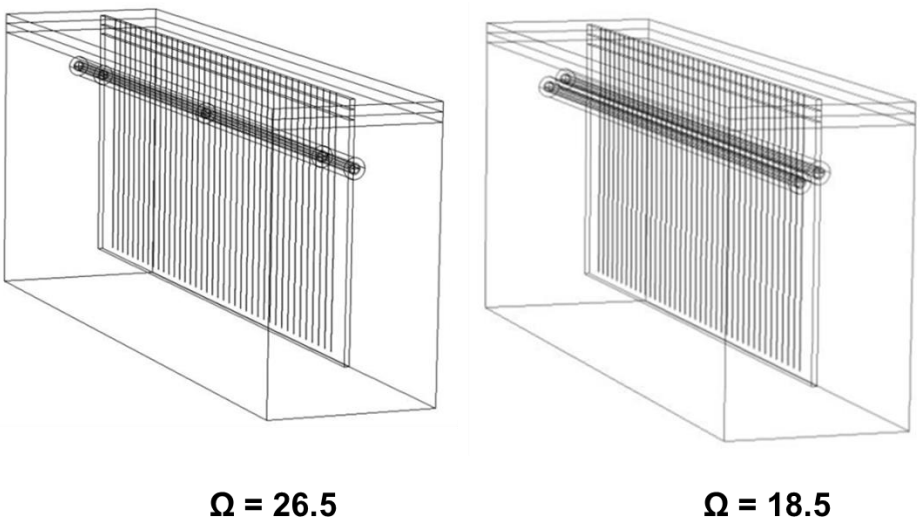

Figure 8.6: 3D schematic of single and multiple running tunnels next to 40 GHEs

The left side of Figure 8.6 shows the 3D model geometry with a single UR-tunnel and on the right side the multiple tunnels configuration is illustrated. Study 1 used the base case size GHE array, i.e. 40 vertical GHEs with a depth of 100 m. The figure also highlights the estimated values of Ω for both configurations. It can be seen that for the multiple tunnel geometry the variable Ω becomes smaller.

8.3.1.2 Results of Study 1

Figure 8.7 shows the simulated temperatures in the middle 2D cross sections of the 3D model geometries at the end of the 2 years simulation period. The left side shows the single tunnel whilst the right side shows the multiple tunnels scenario. It can be seen that the ground warms up more and the thermal plumes surrounding the tunnels are reaching longer when the heat loads of multiple tunnels are simulated. Because of this, the GHEs' fluid temperature is heated more. This is shown in Figure 8.8.

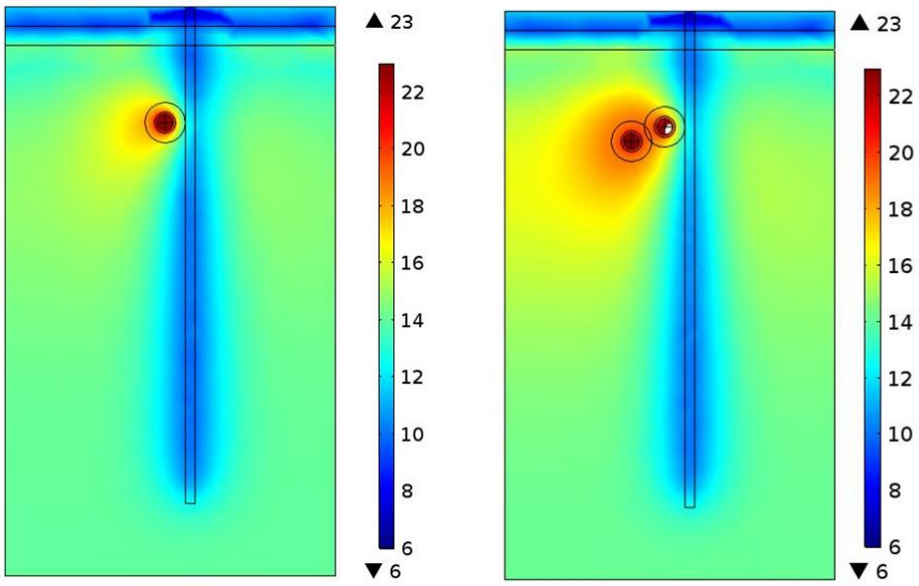

Figure 8.7: Simulated temperatures [˚C] of Study 1 at a mid-cross section at the end of year 2

Figure 8.8 shows the simulated averaged temperatures of the GHEs fluid at the pipe outlets. It can be seen that the fluid temperature increased by an average of 0.7˚C due to the tunnel heat load from a single tunnel and of 0.9˚C when a multiple tunnel heat load scenario was applied in the model. This higher temperature profile started from the beginning of the simulation, and lasted until the end of it. This shows that the initial ground temperature which is affected by the URs is an important characteristic to consider when UR-GSHP interactions are being investigated. The increment in percentage was measured as 8.9% for single and

11.5% for multiple tunnel geometry. On the other hand, the GHEs average heat extraction rate increased by 24.7% when the single and by 31.8% when the multiple tunnel heat load was applied within the model. This is shown in Figure 8.9.

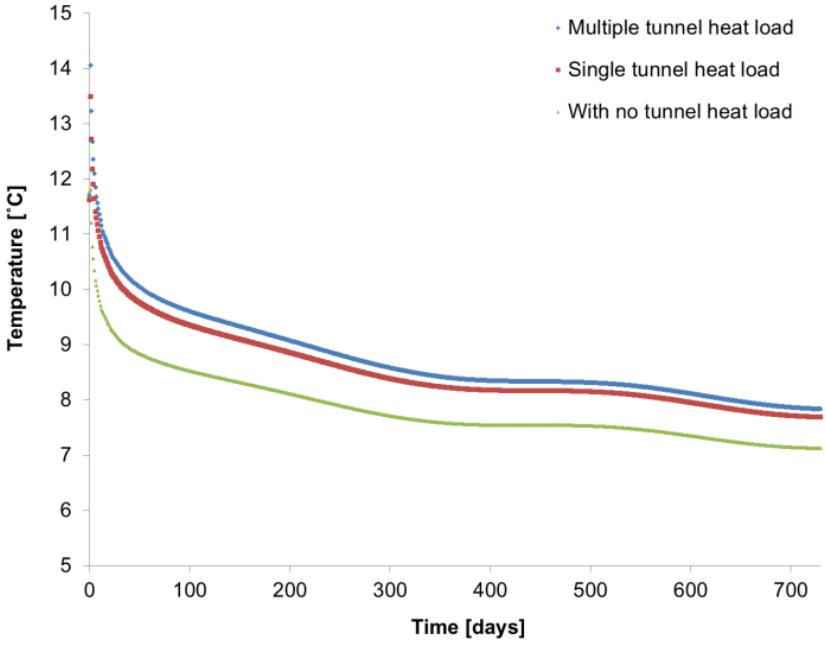

Figure 8.8: Study 1: The average GHE's fluid temperature at the pipe outlet

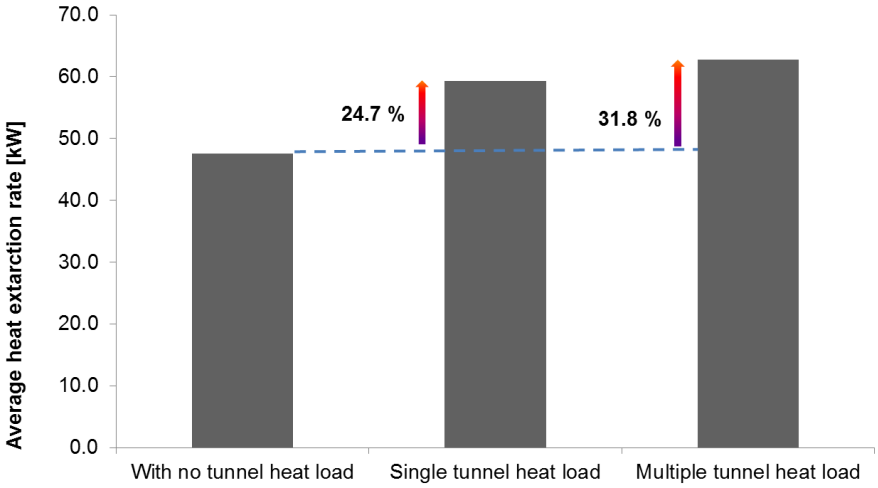

Figure 8.9: Study 1: Average heat extraction by the GHEs

8.3.1.3 Conclusions of Study 1

Based on the results of Study 1, it can be concluded that UR-GSHP interactions are stronger if the GHEs are built near multiple tunnels. However, having the multiple tunnels on one side of the GHE array does not mean that the effect from the multiple tunnels would be double that of a single tunnel scenario, because one of the tunnels in the model was built further away (which is most likely the case in real life scenarios as well) thus it would have less of an impact on the GHEs. This impact proportionality is also shown on the variable Ω. Therefore it was shown, that Ω is a useful variable to account for when UR-GSHP interaction are being investigated.

8.3.2 Study 2: GHEs in Between Multiple Tunnels

8.3.2.1 Introduction of Study 2

Study 2 aimed to explore UR-GSHP interactions in a geometrical scenario whereby the vertical GHEs are placed between multiple tunnels. It was expected that such an arrangement would increase the interactions; however in reality, such a geometrical scenario would apply to only a small range of places in London and would not be common unless part of an integrated holistic design of a new build structure, for example an UR station. The schematic of the 3D model geometry is illustrated in Figure 8.10. It can be seen in the figure that due to this geometrical arrangement the variable Ω has reduced significantly compared to the values shown in Figure 8.6.

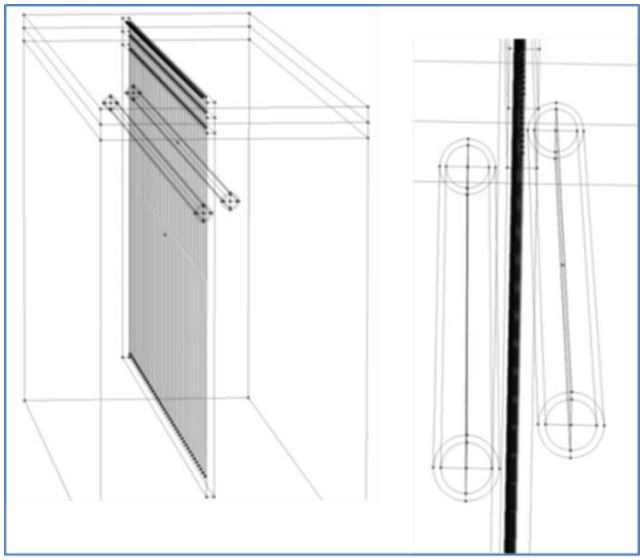

Ω = 9.3

Figure 8.10: Schematic illustration of GHEs placed between multiple running tunnels

8.3.2.2 Results of Study 2

Simulated temperatures at a 2D mid-cross section of the 3D model geometry at the end of the 2 years simulation period are shown in Figure 8.11. The left side of the figure shows the model simulated temperatures when only the GHEs operation was considered without the initial effects of the URs. It can be seen that the impact of the GHEs operation is causing a fairly linear temperature decline on its surroundings and the maximum temperatures in the soil surrounding the array are reaching at around 11˚C. However within the simulation results where the heat load from the tunnels were also accounted for (see right side in Figure 8.11), the temperature field around the GHE array is warmer (~16 to 17˚C), especially at the depths were the tunnels are operating. Because of this, the GHEs' circulated fluid temperature is heated more. This is shown in Figure 8.12.

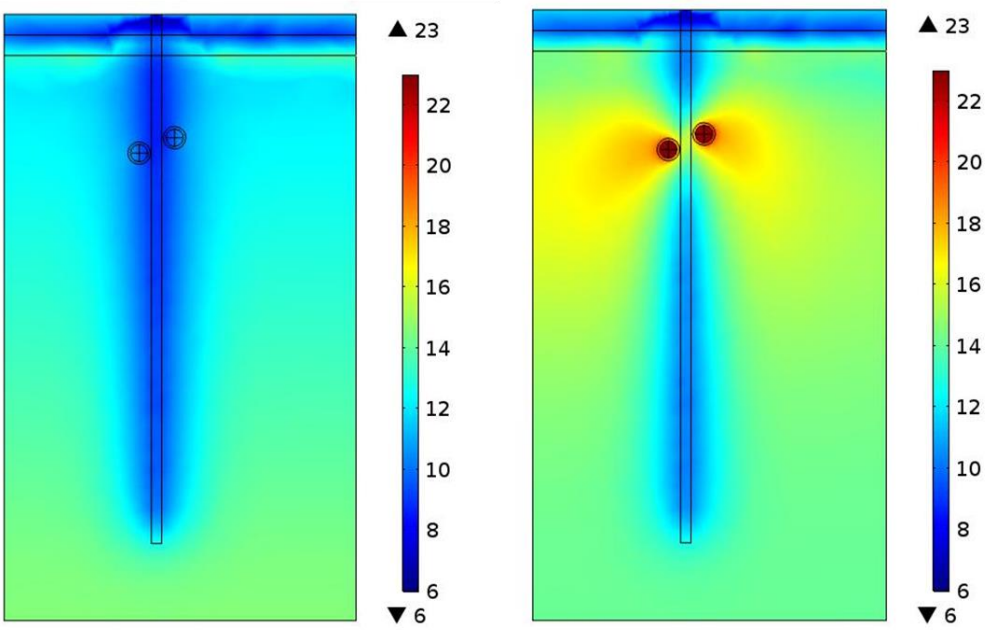

Figure 8.11: Simulated temperatures [˚C] of Study 2 at a mid-cross section at the end of year 2

The left side of Figure 8.12 shows the average fluid temperatures leaving the GHEs with and without the multiple tunnel heat loads. It can be seen that when the tunnel heat loads were applied in the model (both initially and during the two years simulation period), the temperature of the fluid leaving the pipes increased on average by approximately 1.2˚C, which equates to an increment of 14.8% compared to a scenario where the tunnel heat loads were neglected. In addition Figure 8.12 (right) shows the average heat extraction rates with and without the tunnel heat loads. It can be seen that the GHEs heat extraction rates of

the GHEs have significantly increased, by approximately 41% due to the heat loads from the tunnels.

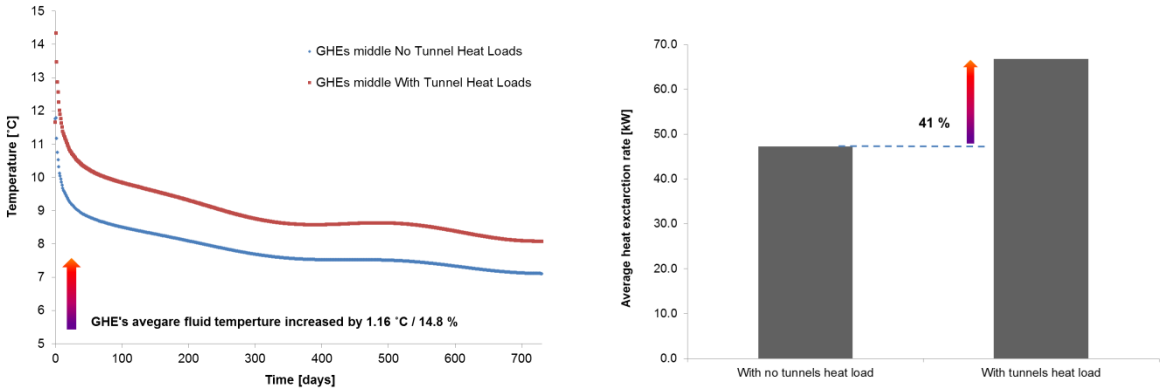

Figure 8.12: Study 2: Average GHE fluid temperature increment (left) and heat extraction rate (right)

8.3.2.3 Conclusions of Study 2

The results of Study 2 showed that if the GHE array is built between multiple tunnels, the impact on the GHEs' heat extraction rates is significant. This is due to the ground temperature increment at levels where the URs are operating. It can be concluded from the results that if such geometrical option is constructible, GSHPs which are operating in heating mode would highly benefit from the heat load of the UR tunnels.

8.3.3 Study 3: GHE Array Aspect Ratio

8.3.3.1 Introduction of Study 3

Studies 1 and 2 considered a single line of GHEs with an array aspect ratio of 1x40. However GHE arrays are often constructed with different geometrical arrangements. In order to explore how UR-GSHP interactions are influenced by the aspect ratio of a squared GHE array, two new geometrical options were constructed: option b, with GHEs having an aspect ratio of 2x20, and option c, with 4x10 GHEs. These new geometrical options, alongside the original 1x40 model geometry (option a), are illustrated in Figure 8.13. It can be seen on the figure that as the aspect ratio of the GHE array is changing, the previously introduced parameter, Ω is changing too: as the geometrical centre of the GHE array moves further away from the central point of the tunnel the Ω becomes larger. The variation in the GHEs aspect ratios as well as the change in Ω are summarised in Table 8.2. For all options, the UR-GHE wall to wall distance was kept as 3 m.

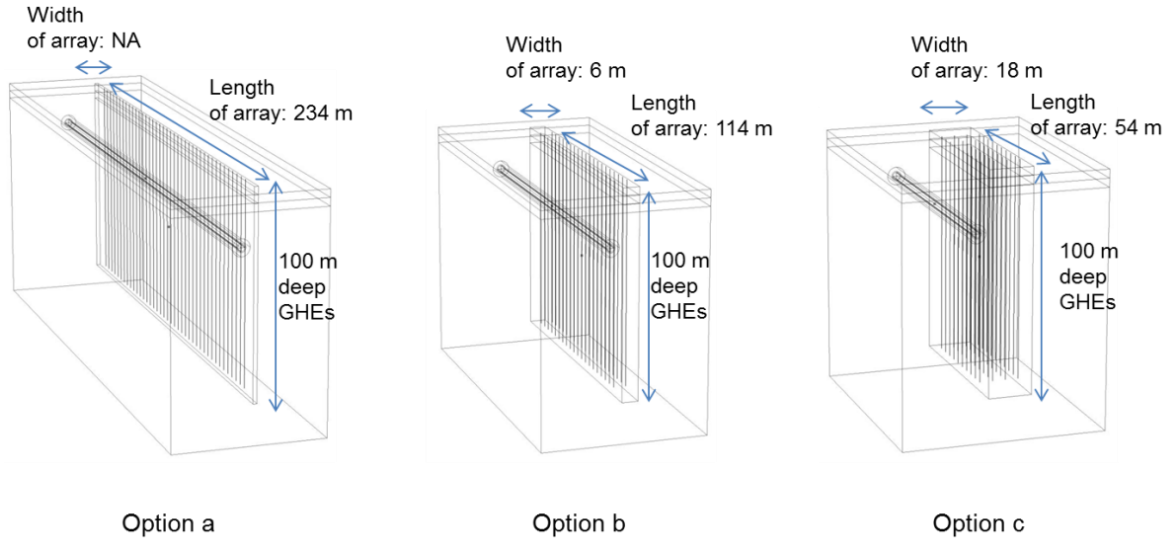

Figure 8.13: Schematics of GHE array aspect ratio options a, b and c

Table 8.2: The three different GHE array aspect ratio options

	Option a	Option b	Option c
GHE array aspect ratio	1x40	2x20	4x10
Ω (m)	26.5	27.2	29.6
Wall to wall distance (m)	3	3	3

8.3.3.2 Results of Study 3

8.3.3.2.1 Impact of tunnel on the GHEs

Study 3 first investigated the impact of the UR tunnel on the nearby GHEs. The model simulated ground temperatures surrounding the UR and GHE array at mid-cross sections at the end of the two years simulation period are illustrated in Figure 8.14. Within all three options in Figure 8.14, both the UR and GHE array heat loads were switched on during the simulations. It can be seen in the figure that a wider soil segment was affected by the operation of the GHEs as the aspect ratio of the array has changed. Since the thermal effects from the UR tunnel are only reaching to a certain radial distance from the centre of the tunnel (~20 m), the impact of on the GHE array was expected to be less when the width of it increased. Such an expectation was confirmed when the GHEs' fluid temperature and

heat extraction rates were investigated which results are shown in Figure 8.15, Figure 8.16 and Figure 8.17

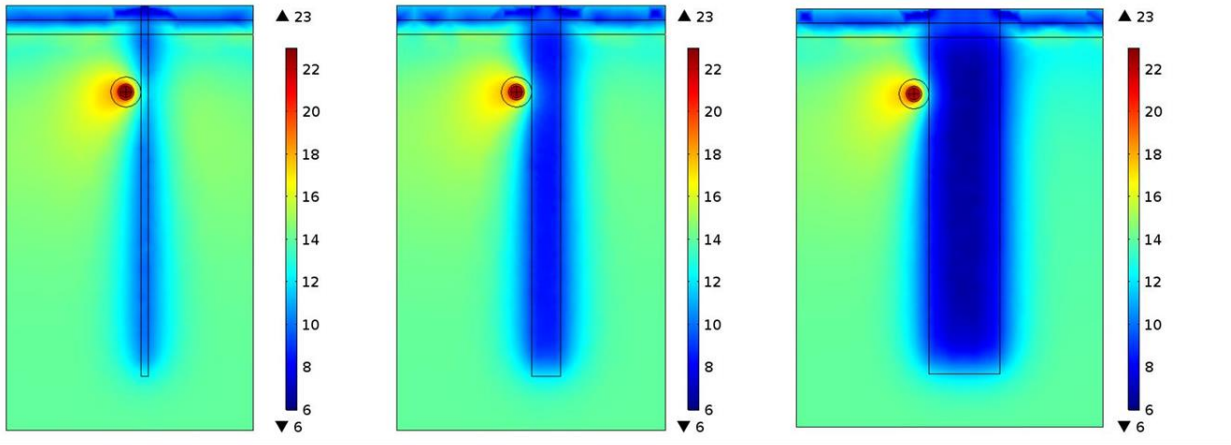

Figure 8.14: Simulated temperatures [˚C] of Study 3 at mid-cross sections at the end of year 2

The left sides of Figure 8.15, Figure 8.16 and Figure 8.17 show the average GHE fluid temperature increment at the pipe outlets due to the UR heat load. The right sides of the same figures in turn show the average heat extraction increment based on that temperature difference.

The results showed that the highest impact from the UR tunnel on the GHEs was achieved in geometrical option a, where the array has the smallest width. It can be seen in Figure 8.15, that the average temperature of the GHEs fluid leaving the pipes increased by almost 9% due to the nearby tunnel's heat load. This equates to a nearly 25% increment in the average heat extraction rates by the GHEs.

When the aspect ratio of the GHE array changed to option b, the Ω increased to 27.2 m from 26.5 m. The increased Ω resulted in less interaction between the UR tunnel and the GHEs. Figure 8.16 shows that the GHEs fluid temperature increased less than in the case of option a, by only 7.4%, and the lower fluid temperature increase resulted in a lower GHE heat extraction rate increase of 22.3%. As a result of changing the GHE array aspect ratio to option c, Ω further increased to 29.6 m. Such an increase resulted in the least UR-GSHP interactions out of the three options. This is illustrated in Figure 8.17. It can be seen that the GHE fluid temperature has only increased by 5.8% and its heat extraction was only enhanced by 18.2% due to the tunnel heat load.

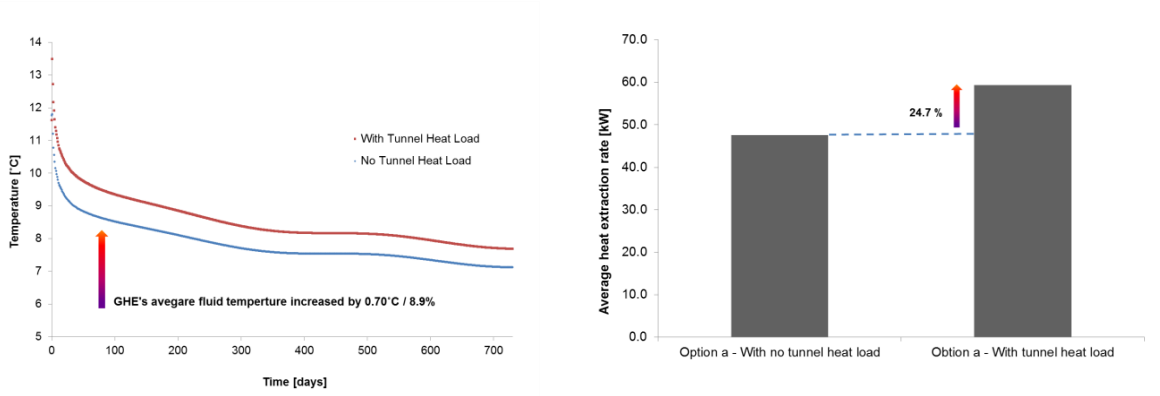

Figure 8.15: Option a – Average GHE fluid temperature increment (left) and heat extraction rate (right)

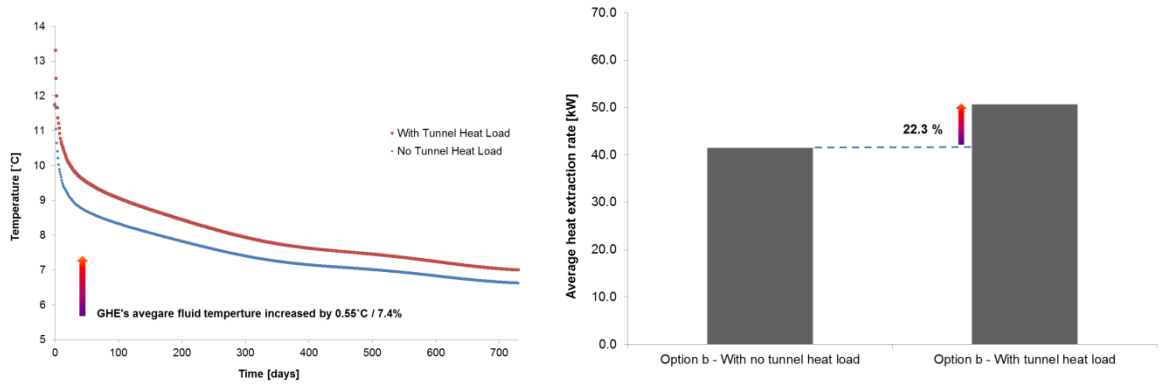

Figure 8.16: Option b – Average GHE fluid temperature increment (left) and heat extraction rate (right)

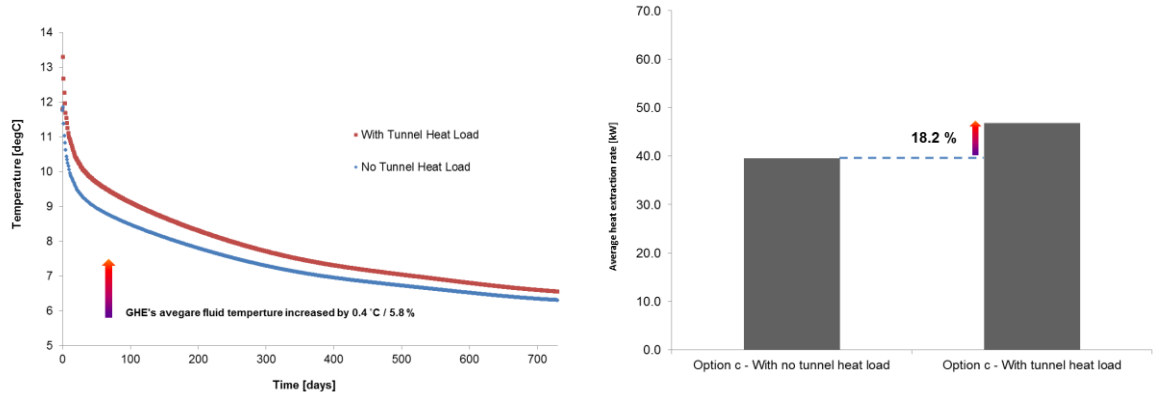

Figure 8.17: Option c – Average GHE fluid temperature increment (left) and heat extraction rate (right)

8.3.3.2.2 Impact of GHEs on UR tunnel

Study 3 also examined how the operation of the GHEs might impact on the average bulk tunnel air temperatures. The results showed that for all the geometrical options introduced above, the impacts of the GHEs on the tunnel air temperatures were negligible. It can be seen in Figure 8.14 that the tunnel air temperatures were the same for all the three options. This is because of the heat densities involved on the UR side of the model; such as the train heat load, plus the constant heat inflow with the air into the tunnel, are larger than the GHE array heat extraction rate. For this reason, in further studies, only the impact of the tunnel on the GHEs was investigated, not vice-versa, unless it is stated otherwise.

8.3.3.3 Conclusions of Study 3

Study 3 first investigated the impact of the UR tunnel on the GHEs. Based on the results, it can be concluded that the operation of the UR impacts more on GHE arrays which have smaller width. As the width of the array is smaller, the variable Ω becomes smaller too. Therefore if the aim is to increase the heat extraction rates of GSHPs in UR tunnel vicinities, the smaller the Ω, the more effective the heat addition to the GHEs. It was also discussed that the average bulk tunnel air temperatures were not affected by operation of the nearby GHEs which is most likely due to the different magnitudes of heat densities involved within the two systems.

8.3.4 Study 4: Single vs Double Looped GHEs

8.3.4.1 Introduction of Study 4

The heat exchanger pipes installed in vertical GHEs take the form of continuous loops of certain shapes. Typical vertical GHE configurations are either the single or the double looped GHE pipe systems. The schematics of these configurations were illustrated in Chapter 6 in Figure 6.1.

Study 4 aimed to investigate how UR-GSHP interactions are affected, when the GHEs are constructed in double looped configuration. The array aspect ratio and the overall GHE pipe length were kept the same as they were in the previous studies (1x40 and 8000 m). However, double looping the GHE pipes made the depth of the GHEs shorter, to 50 m. Due to the shorter depths of the GHE, the distance between the geometrical centres of the tunnel and the GHE array, i.e. the Ω decreased to 5.37 m. This is a significantly smaller distance than the ones summarised in Table 8.2, hence the interactions were expected to be stronger than in any of the geometrical options investigated in Study 3. The 3D schematic diagram of

the model geometry in Study 4 is shown in Figure 8.18. The diagram also has a magnified section of a double-looped GHE.

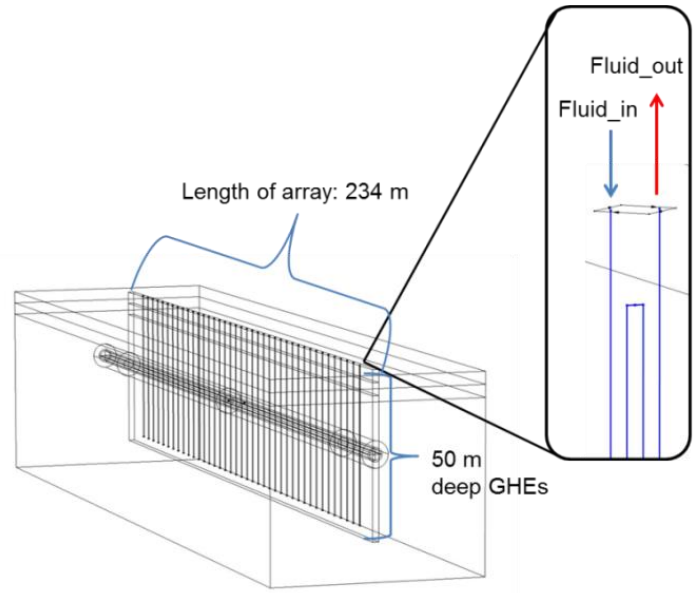

Figure 8.18: 3D schematic of the model geometry in Study 4

8.3.4.2 Results of Study 4

The left side of Figure 8.19 shows the average GHE fluid temperature increment at the pipe outlets due to the UR heat load. The right side of the same figure highlights the estimated average heat extraction increment based on the temperature increment of the GHE fluid due to the tunnel heat load.

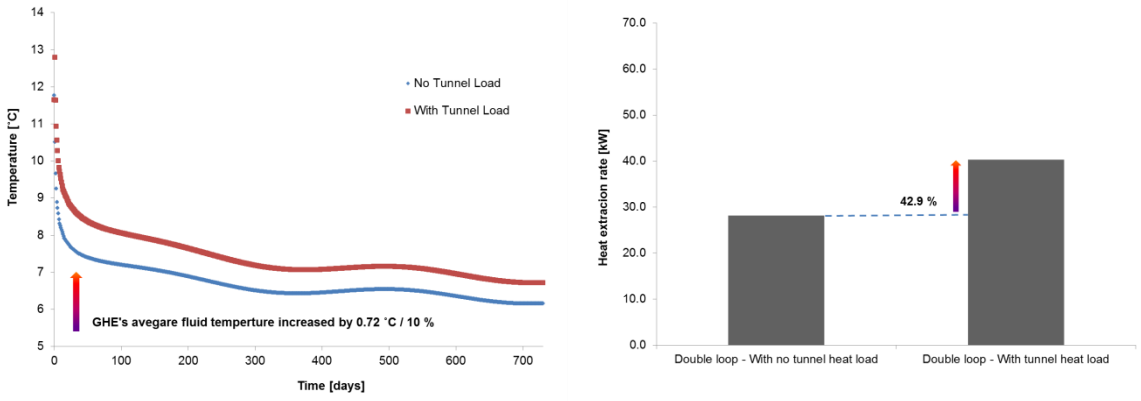

Figure 8.19: Double loop - Average GHE fluid temperature increment (left) and heat extraction rate (right)

It can be seen in Figure 8.19, that the average fluid temperature leaving the pipes is lower than it was when the deeper single looped GHEs were simulated in the previous studies. This is because the soil temperatures are higher at greater depths which resulted by the geothermal gradient condition imposed on the soil domain by Equation 4.3 in Chapter 4. On the other hand, when the tunnel heat load was applied, the heat extraction rate of the GHEs significantly increased, by almost 43%, compared to the scenario when the tunnel heat load was neglected. This is a substantial increase and it is about 18% higher than the increment obbserved in option a, in Study 3. The reason for this is that altough the length of the GHE pipes were kept the same 8000 m as within Study 3, the double looped configuration appied in Study 4 reduced the overall depth of the GHE array. This in turn reduced the varible, hence enhanced UR-GSHP interactions.

8.3.4.3 Conclusions of Study 4

The results of Study 4 showed that the heat extraction rates of double looped GHEs, (which are normally shorter in depth than single looped ones) can be significantly improved if the array is built near UR tunnels. This is because the geomnetrical centre of the GHE array moves closer to the UR tunnel's centre point, i.e. the Ω becomes smaller. The results also confirmed that the geothermal gradient has an impact on the GHEs' fluid temperture since ground is warmer at greater depths. Study 4 has considered a 50 m deep looped GHE array configuration the heat extraction rate of which improved by ~ 43% due to the UR tunnel heat load.

8.3.5 Study 5: Proximity Variation

8.3.5.1 Introduction of Study 5

Within studies 1 to 4, a fixed UR-GHE wall to wall distance, 3 m was used. This was set based on the fact that structures are normally not allowed to be built any closer than 3 m to the UR tunnels in London (TfL, 2013). Therefore, these previous studies have explored UR-GHE interactions by considering geometrical options with the largest interaction potential possible. Study 5 aimed to explore to what extent the interactions are affected by moving the GHE array further away from the wall of the UR tunnel, i.e. increasing both the wall to wall distance as well as the variable, Ω. The base case scenario, to which the newly built geometrical options were compared, was the same as option a, in Study 3. The wall to wall distance was then gradually increased in order to investigate how the UR-GSHP interactions were affected by horizontally separating the systems. The base case scenario, option a, and the other four wall to wall distance options (options b to e) are illustrated in Figure 8.20.

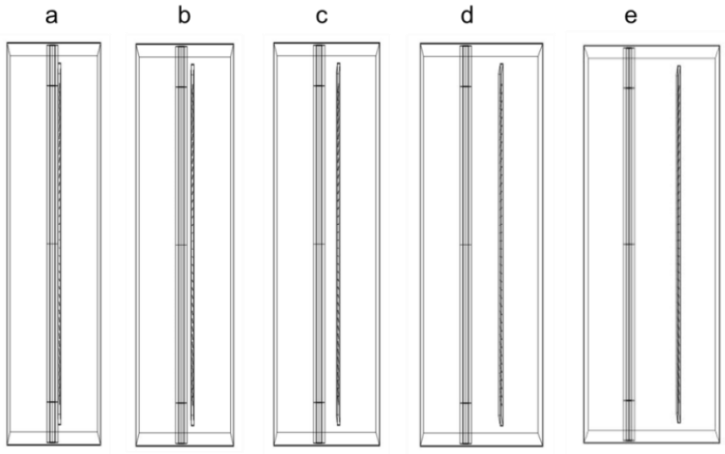

Figure 8.20: Study 5: UR-GHE wall to wall distance variations

Study 5 also aimed to establish at what wall to wall distance and ultimately at what Ω, the UR-GSHP interactions would become negligible. Table 8.3 summarises the set wall to wall distance values and the corresponding Ω for each geometrical option.

Table 8.3: Study 5: Summary of the wall to wall distances and corresponding UR-GHE distance factors

Geometrical option	**a**	**b**	**c**	**d**	**e**
Wall to wall distance (m)	3	6	12	24	35
Ω (m)	26.5	27.2	29.6	36.9	45.4

8.3.5.2 Results of Study 5

Simulated temperature results at 2D mid-cross sections for the five different geometrical arrangements are illustrated in Figure 8.21. For each plot, the results are representing the end of the two years simulation period with considering both the UR and GHE array operation. It can be seen that as the wall to wall distance is increasing (and therefore Ω is increasing too) the UR impact on the GHE array becomes smaller. As it was previously highlighted in Study 3, the thermal effects from the UR tunnel are only reaching to a certain radial distance from the centre of the tunnel (~20 m), thus the impact on the GHE array is less if the wall to wall distance and the Ω is larger. This lesser impact was confirmed by the results in the GHEs' fluid temperature variation in Figure 8.22. It can be seen in the figure that the average temperature of the GHEs fluid leaving the pipes is getting lower as the UR-GHE wall to wall distance and Ω increase. However, it can be seen that in option b, the impact from the tunnel was almost as high as it was in option a. This suggests that at a 6 m

radial distance from the wall of the UR tunnel the thermal impact from it are still relatively large. The results also suggest that after about 24 m from the wall of the tunnel the impact on the GHEs is small and after about 35 m it is almost negligible.

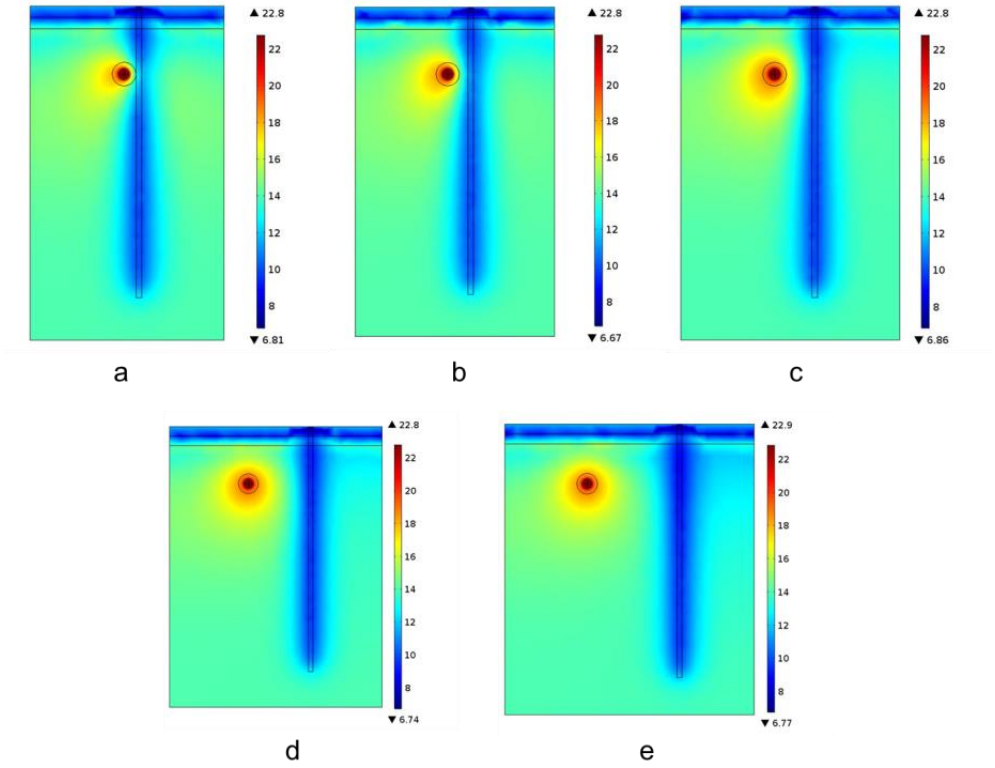

Figure 8.21: Simulated temperatures [˚C] of Study 3 at mid-cross sections at the end of year 2

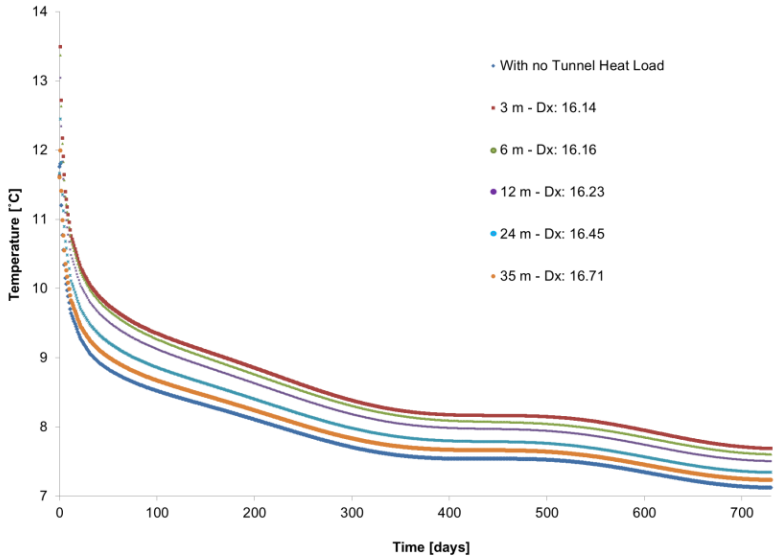

Figure 8.22: Average GHE fluid temperature leaving the pipes at different wall to wall distance scenarios

In the context of the GHEs heat extraction performance, Figure 8.23 illustrates the average heat extraction rate for each geometrical option studied. It can be seen that the GHEs were extracting less heat as their horizontal distance increased from the tunnel. The results showed that constructing the GHE array at 6 m distance from the wall of the tunnel could still result in a significant (above 20%) heat extraction rate improvement compared to a scenario where there was no additional heat source available from a nearby UR tunnel. On the other hand, the results suggest that after about 30 m from the tunnel wall, the GHEs heat extraction rates would only improve by less than 5%.

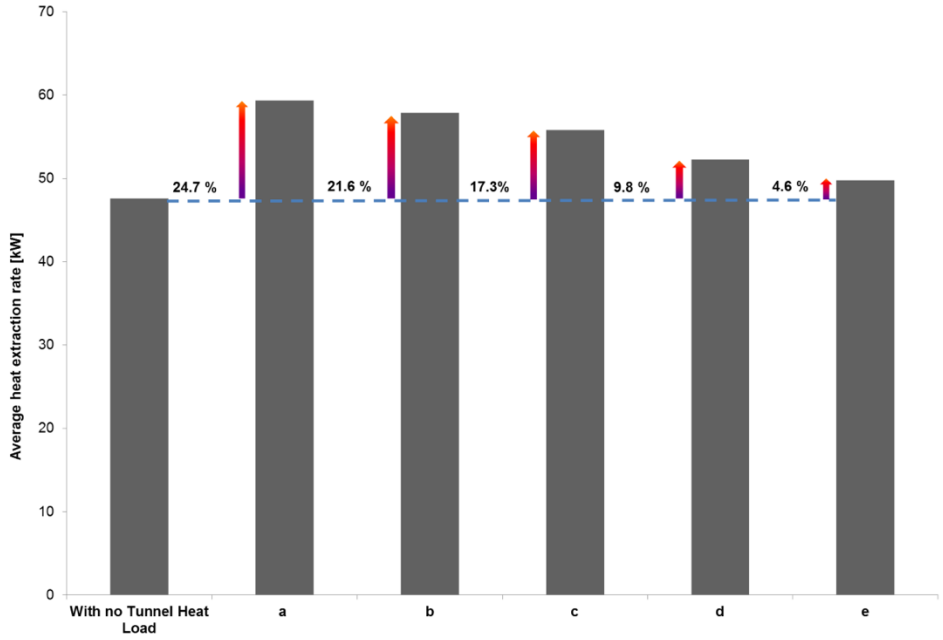

Figure 8.23: Study 5: The average heat extraction rates and the improvements in percentage

8.3.5.3 Conclusions of Study 5

It can be concluded from the results of Study 5, that UR-GSHP interactions are unlikely to occur if the GHE array is built further than ~ 20 m from the wall of the UR tunnel. Therefore, if the aim is to enhance the heat extraction rates of urban GSHP systems, constructing the GHEs as close as possible to the UR tunnel is essential. The optimal wall to wall distance for heat recovery purposes is 3 m, however even at 6 m distance from the wall of the tunnel the thermal effects on the GHE array are still significant and it would enhance the GHE array heat extraction performance substantially.

8.3.6 Study 6: Tunnel Running Through Fine Sands

8.3.6.1 Introduction of Study 6

Chapter 4, highlighted that the majority of the LU tunnel network was built in London Clay, however some sections of the network run through sandy type soils (Paul, 2016). Different types of earth have different heat transfer characteristics, and thus could have a unique impact on UR-GSHP interactions. Study 6 aimed to explore UR-GSHP interactions in a scenario where the UR tunnel was constructed in fine sands. The sand material properties used were the same as the ones summarised in Chapter 4 in Table 4.5. The model geometry of Study 6 is illustrated in Figure 8.24. It can be seen in the figure, that the model geometry used the base case GHE array configuration, i.e. the 1x40 single looped GHEs (option a in Study 3). Chapter 4 also discussed that the sandy sections of the LU tunnel network mainly consist of more fine sands, like the Bagshot formation (Paul, 2016). Investigation 2 in Chapter 4 showed that in such fine sands the low velocity magnitude of the groundwater movement (<1E-7 m/s) is unlikely to have an impact on the UR-GSHP interactions. For this reason Study 6 neglects groundwater movement and represents a pure conductive analysis.

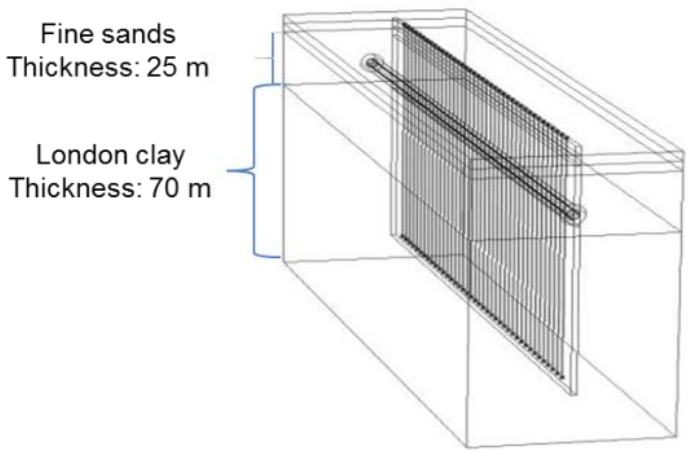

Figure 8.24: Study 6: Model geometry. UR tunnel runs through fine sands

8.3.6.2 Results of Study 6

First simulation results from Study 3, where the UR tunnel was built in London Clay were compared with the results of Study 6. The simulated temperatures at the mid-cross section of the models from Study 3 (option a) and Study 6 are illustrated in Figure 8.25. It can be

seen in the figure that when the UR tunnel was built in fine sands, which is material with higher thermal conductivity than the London Clay, the thermal plumes reach a larger radial distance, causing a higher thermal impact on the surrounding ground temperatures. This is in turn impacts more on the nearby GHEs. This was established with the results shown in Figure 8.26.

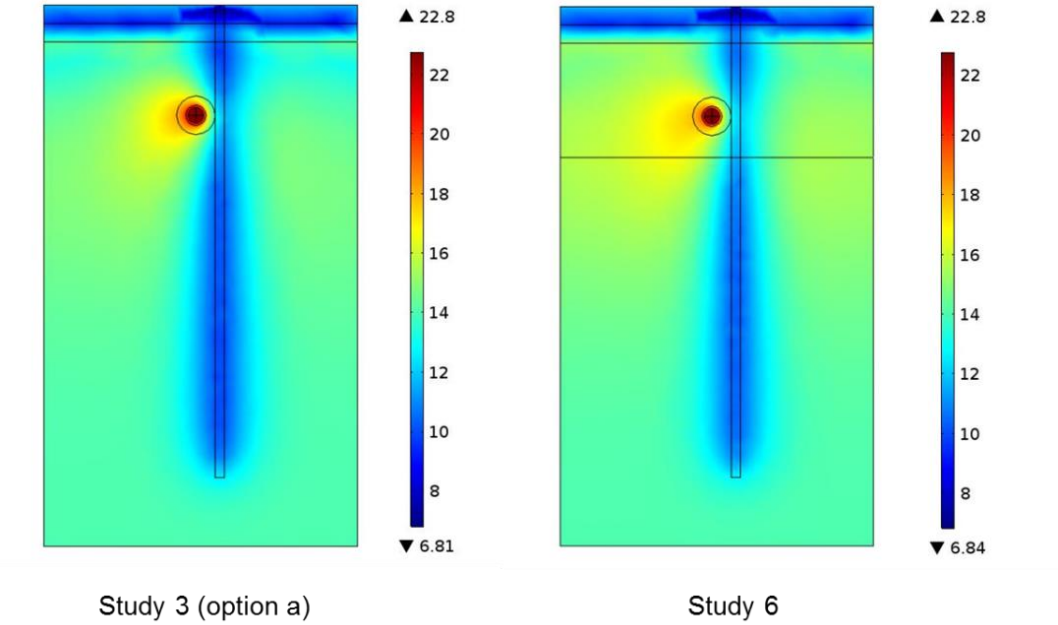

Figure 8.25: Simulated temperatures [˚C] of Study 3 (option a) (left) and Study 6 (right) at mid-cross sections at the end of year 2

The left side of Figure 8.26 shows the average fluid temperature leaving the GHEs with and without the UR tunnel heat load. It can be seen in the figure that if the UR tunnel was built in a soil consisting of fine sands, the impact of the tunnel heat load on the GHEs would be higher than if the tunnel was built in London Clay (see results for option a in Study 3). In particular, the average temperature of the GHEs fluid increased by more than 13% due the tunnel heat load. This is almost a 5% higher increment compared to a scenario when the tunnel was built in London Clay (see Figure 8.15 (left)). This is due to different thermal characteristics of the fine sands. For example, the thermal conductivity of fine sands is almost double the conductivity of London Clay. The right side of Figure 8.26 shows the average heat extraction rates of the GHEs with and without the UR tunnel heat load. It can be seen that the average heat extraction rates of the GHEs increased by approximately 35% when the tunnel heat load was modelled. This is a more than 10% higher increment compared to option a in Study 3, where the tunnel was built in London Clay (see Figure 8.15 (right)).

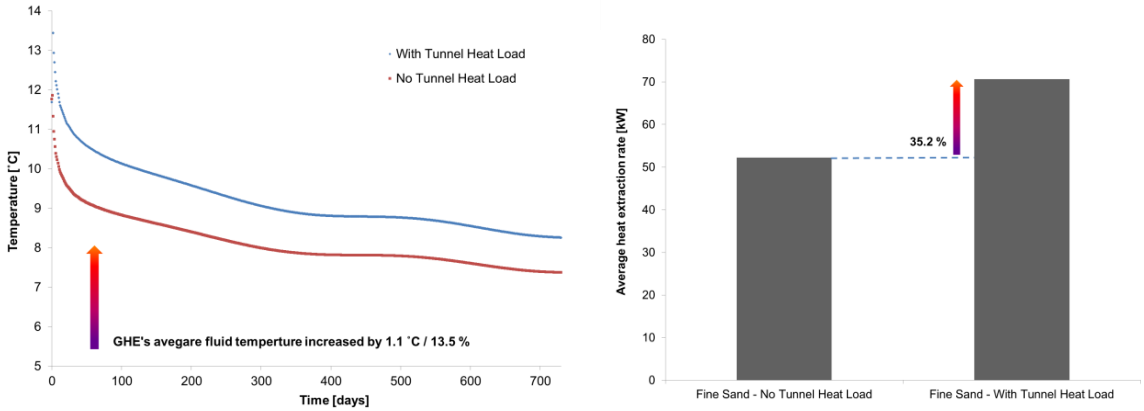

Figure 8.26: Study 6: Average GHE fluid temperature increment (left) and heat extraction rate (right)

8.3.6.3 Conclusions of Study 6

Due to the different thermal characteristics of the tunnel surrounding soil material, which consisted of fine sands, the impact of the UR tunnel on the nearby GHEs was higher than if the tunnel was built in London Clay. Based on this information a conclusion can be drawn that UR-GSHP interactions are stronger and the GHE heat extraction performance improves if the soil material in which the UR tunnel is built has a higher thermal conductivity than London Clay. Study 6 considered a London base scenario where some sections of the LU railway network are running through fine sands. Based on the results of Study 6, it can be concluded that at those sections where such material characteristics dominate, UR-GSHP interactions will be stronger.

8.3.7 Study 7: Size of the GHE Array

8.3.7.1 Introduction of Study 7

The previous studies investigated UR-GSHP interactions by considering a typical medium sized GHE array. However, GSHP installations in London and elsewhere commonly serve larger commercial buildings as well. Larger building heat demands are associated with the requirement of larger GHE arrays, thus increased length of the heat absorber pipes. Study 7 aimed to explore UR-GSHP interactions when a relatively large array, consisting of 160 GHEs, was built in the model geometry. The size of this array is almost equivalent to the GSHP installation at LSBU serving the building with 600 kW of heating and cooling. The depths of the GHEs within the model were kept the same: 100 m, and the aspect ratio of the array was constructed as 4x40. A 2D plan view of the model geometry and the 3D schematics are shown in Figure 8.27.

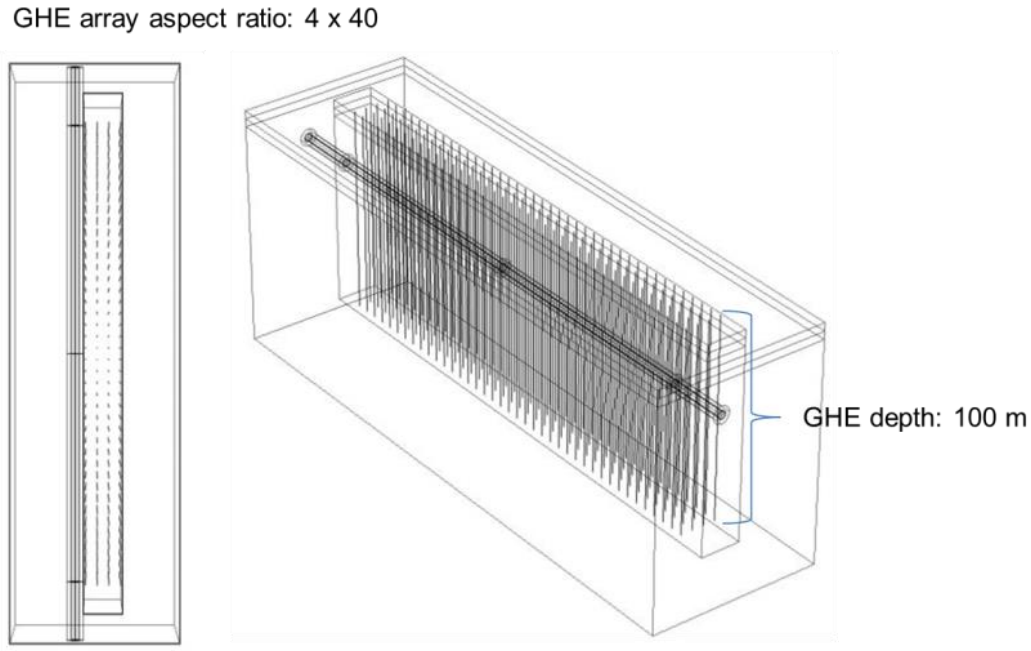

Figure 8.27: Study 7: 2D plan view (left) and 3D model geometry (right)

The wall to wall distance was kept as 3 m. The Ω within Study 7 became 29.6 m since the geometrical centre of the GHE array moved further away from the centre of the UR tunnel. Since the size of the GHE array in study 7 is significantly larger than in the previous studies (Study 1 to Study 6), the potential impact of the array on the tunnel air temperatures were also investigated.

8.3.7.2 Results of Study 7

8.3.7.2.1 Impact of tunnel on the GHEs

First the UR tunnel heat load on the nearby array was investigated. Simulation results are shown in Figure 8.28. It can be seen in the figure that the initial part of the time dependent study (i.e. 50 years with only UR operation) causes a radial temperature increment, reaching even to the regions where the large 4x40 GHE array are installed. These regions are highlighted with red dotted lines in Figure 8.28. Therefore, it was expected that even for a large GHE array as considered in Study 7, the heat accumulated and stored in the ground due to the operation of the UR will increase the temperature of the GHEs' fluid. This was confirmed when the GHEs' fluid temperate with and without the UR tunnel heat load was investigated. Results of this investigation are shown in Figure 8.29.

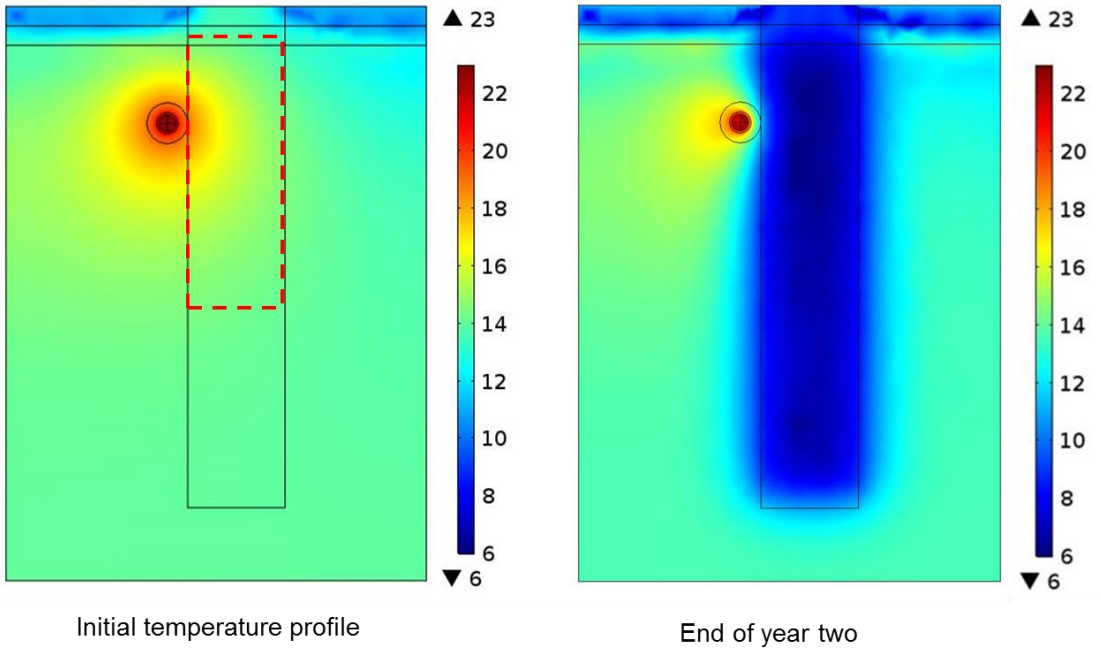

Figure 8.28: Initial temperatures (left) and simulation results at the end of the two years (right)

The left side of Figure 8.29 shows that the GHEs' fluid temperature increase due to the tunnel heat load was 0.47˚C. This increase was similar to that which was observed in Study 3, in the case of option c (see Figure 8.17 (left)). The similarity of the results was due to the fact the values of Ω were the same in both models. The average heat extraction rates of the GHEs increased by approximately 20%. This was again similar to the result obtained in Study 3, (see Figure 8.17 (right)).

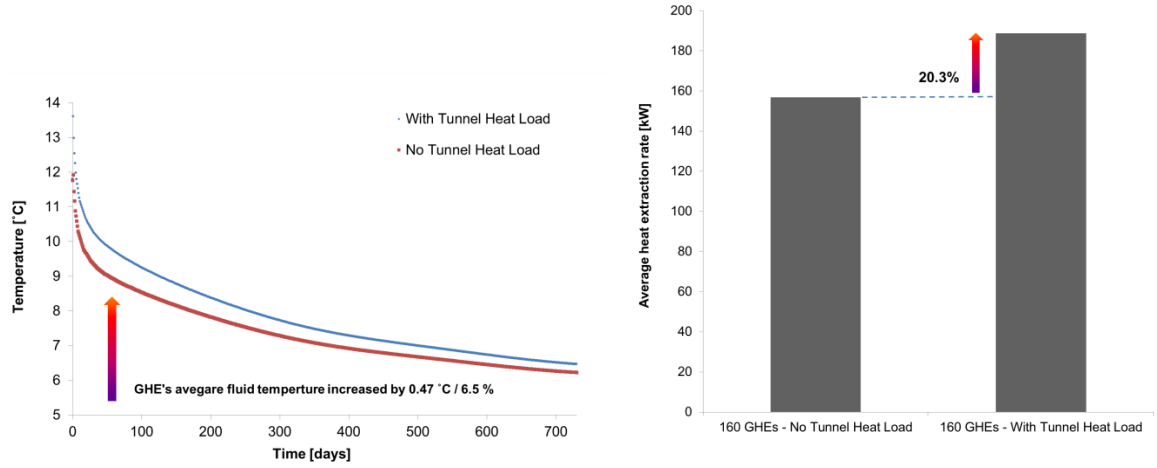

Figure 8.29: Study 7: Average GHE fluid temperature increment (left) and heat extraction rate (right)

8.3.7.2.2 Impact of the GHEs on UR tunnel

Within the previously conducted studies it was highlighted that the GHE array heat extraction rate was not large enough to have an impact on the UR-tunnel air temperature. Due to the increased size of GHE array utilised in Study 7, the potential impact of the GHE array on the UR tunnel was explored again. As can be seen in the simulation results illustrated in Figure 8.28 (right), although the soil surrounding the UR tunnel has cooled down due to the heat extraction of the large GHE array, the temperature of the tunnel air has not been impacted on. This is also shown in Figure 8.30.

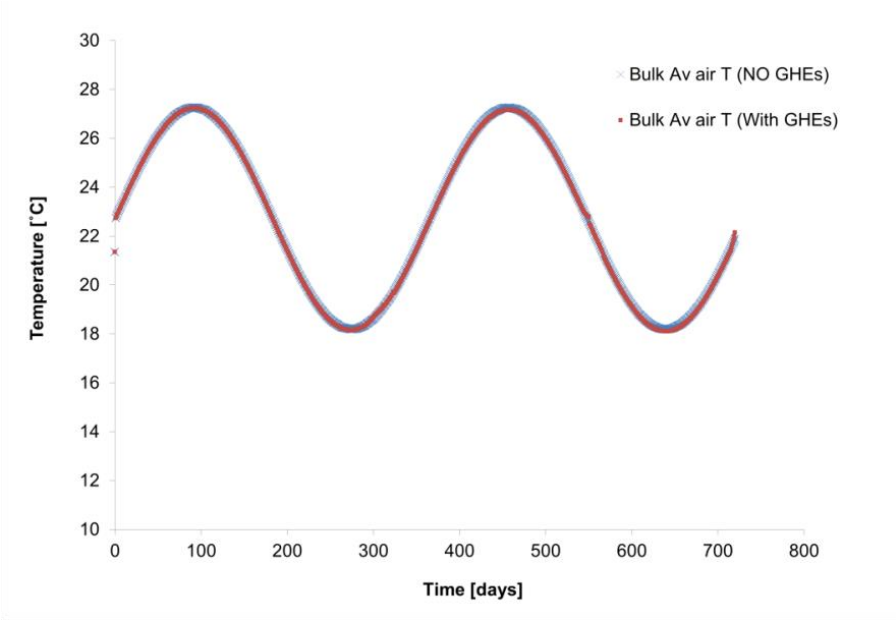

Figure 8.30: Study 7: Average tunnel air temperature with and without the GHEs operation

Figure 8.30 shows the average bulk tunnel air temperature with and without the operation of the nearby GHEs. It can be seen in the figure, that although the size and therefore the heat extraction rate of the GHE array was significantly larger than in the previous studies, its impact on the tunnel air was still negligible. This is because of the continuous heat generation by the trains in the tunnel plus the constant heat flow through the incoming air is still involves larger heat densities that the heat extraction rate of the nearby GHE array.

8.3.7.3 Conclusions of Study 7

The results of Study 7 showed that even a large GHE array which was considered in the study could be impacted on by the heat load of UR tunnels. The results illustrated that the thermal effects in the soil surrounding the UR were reaching to a radial distance where the

large 40x40 GHE array was built in the model. It was also shown that these thermal effects were strong enough to have an impact on the GHEs' fluid temperature. However, the interactions between the two systems would still remain a one way influence, since the tunnel air temperature would not change due to the heat extraction of the nearby GHEs. Based on the results of Study 7, it can be concluded that even large GHE array's heating related operational efficiencies can be improved if the system is being installed near UR tunnels.

8.3.8 Summary and Conclusions of Analysis Part 1: Geometrical Studies

The developed UR-GHE model was used to perform seven different studies, investigating different geometrical options which could potentially influence UR-GSHP interactions. The key aim of these studies was to explore how the waste generated in the ground by the operation of URs could potentially enhance the heat extraction rates of nearby GSHP installations. For this reason, part 1 of the analysis assumed a single operational characteristic of the GSHP system, namely a system which operated in heating mode only throughout the set simulation period. The mass flow rate and the temperature of the GHEs' fluid were kept the same for all the seven studies. At the beginning of the analysis new variables were introduced, namely interaction proximity, Ω and UR-GHE wall to wall distance.

The results of these investigations are summarised in Table 8.4 and showed that the new parameter, Ω is key variable when UR-GSHP interactions are being investigated. As Ω becomes smaller the impact of the UR on the nearby GHEs would become larger. Whilst the impact of the GHEs on the UR tunnel was negligible throughout the analysis, the results showed that the heat extraction rate of GHEs built near UR tunnels could be significantly enhanced. For the model configurations investigated in part 1, the GHE heat extraction rates due to the tunnel(s) heat load improved between approximately 5 and 43%.

The results from the studies where the tunnels are built in London Clay (which is the most common case in London) were plotted on a graph which is shown in Figure 8.31. It can be seen in the figure that an almost linear relationship can be derived, when the Ω, as a single variable, was compared against the improvement in the GHEs average heat extraction rates due to the tunnel heat load. This relationship can be described with a formula as Equation 8.2. This formula is one of the key contributions to knowledge within this PhD and it could potentially be used as a designer aid to provide guidance to engineers working in fields where UR-GSHP interactions occur.

Table 8.4: Summary of Analysis Part 1: Geometrical Studies

	ANALYSIS PART 1: GEOMETRICAL STUDIES				
	Number of tunnel (s)	Overall GHE pipe length [m]	Single/Double U-tube GHEs	Interaction Proximity [Ω]	Improvement on the GHEs average heat extraction rates due to the tunnel (s) heat load
Study 1	2	8000	Single	26.5/18.5	24.7/31.8 %
Study 2	2	8000	Single	9.3	41 %
Study 3		8000			
a	1		Single	26.5	24.7 %
b	1		Single	27.2	22.3 %
c	1		Single	29.6	18.2 %
Study 4	1	8000	Double	5.4	42.9 %
Study 5		8000			
a	1		Single	26.5	24.7 %
b	1		Single	27.2	21.6 %
c	1		Single	29.6	17.3 %
d	1		Single	36.9	9.8 %
e	1		Single	45.4	4.6 %
Study 6	1	8000	Single	26.5	35.2 %
Study 7	1	32000	Single	29.6	20.3 %

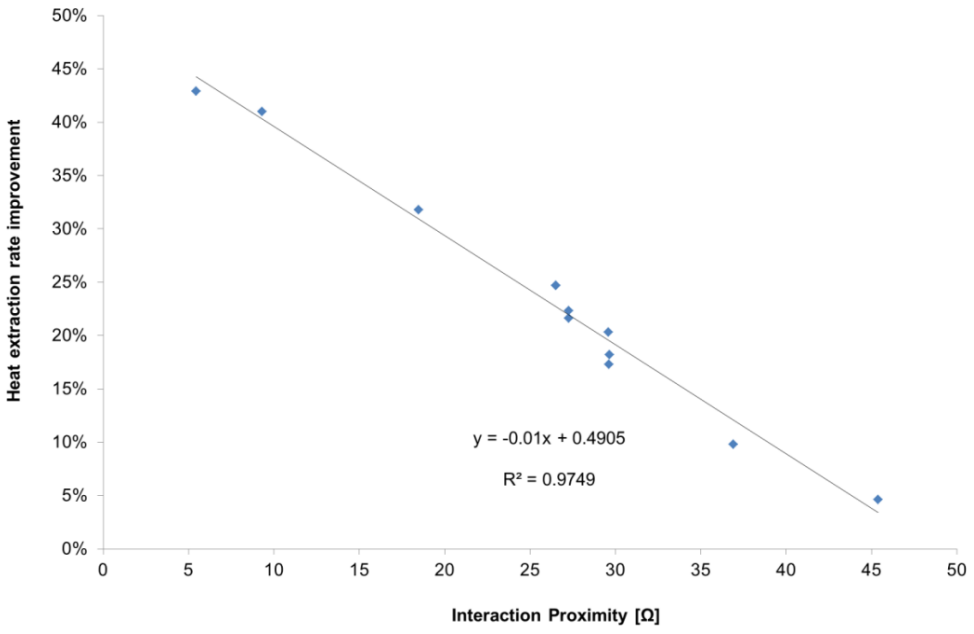

Figure 8.31: GHEs heat extraction improvement in relation to Ω

$$GHE_{Heat\ extraction\ improvement\ \%} = -0.01\ \Omega + 0.4905 \quad (8.2)$$

8.4 ANALYSIS, PART 2: OPERATIONAL CHARACTERISTICS STUDIES

Out of the nine studies summarised in Table 8.1, the last two, Study 8 and Study 9 form part 2 of the parametric analysis. These studies investigated UR-GSHP interactions based on variations in the operational characteristics of the GSHP system. The geometrical parameters and the operational characteristics of the UR were kept the same as in part 1 of the analysis. The GHE array geometry was also kept the same throughout the investigations. The base case sized array, 1x40 GHEs with a depth 100 m, was utilised (option a in Study 3). Part 1 of the analysis concluded that the size of the GHE array had a negligible impact upon the UR tunnel air temperature. Therefore, the remaining simulations were conducted with a GHE arrangement to minimise the number of required simulations. For the purposes of this study the GHE layout is 1x40.

8.4.1 Study 8: GSHP with Balanced Heating and Cooling

8.4.1.1 Introduction of Study 8

The most common use of GSHP technology revolves around domestic and commercial space heating and cooling and the production of hot water. For this reason, Study 8 aimed to explore how UR-GSHP interactions would be affected if the GSHP near the tunnels would operate in an annually balanced heating and cooling mode, depending on the seasonal energy requirements of the building to which the system is connected. In order to establish a possible annual heating and cooling pattern for a London GSHP installation, measured data was used from a GSHP installation at LSBU (Yebiyo *et al.*, 2016).

In particular, the average monthly temperatures entering the GHE pipes were obtained and used to assist in developing a continuous function. The function developed could then be used within the numerical model as a boundary condition at the GHE pipes inlet. The formula developed is shown as Equation 8.3.

The measured average monthly fluid temperatures entering the GHE pipes at LSBU, and the values for the same predicted by Equation 8.3 are plotted in Figure 8.32. It can be seen in the figure that the values generated by the formula correspond well to the values measured at the site.

$$T_{Pi_{in}} = a_{in_{var}} \times sin\left(\frac{2 \times \pi \times t}{year}\right) + T_{av_{in}} \qquad (8.3)$$

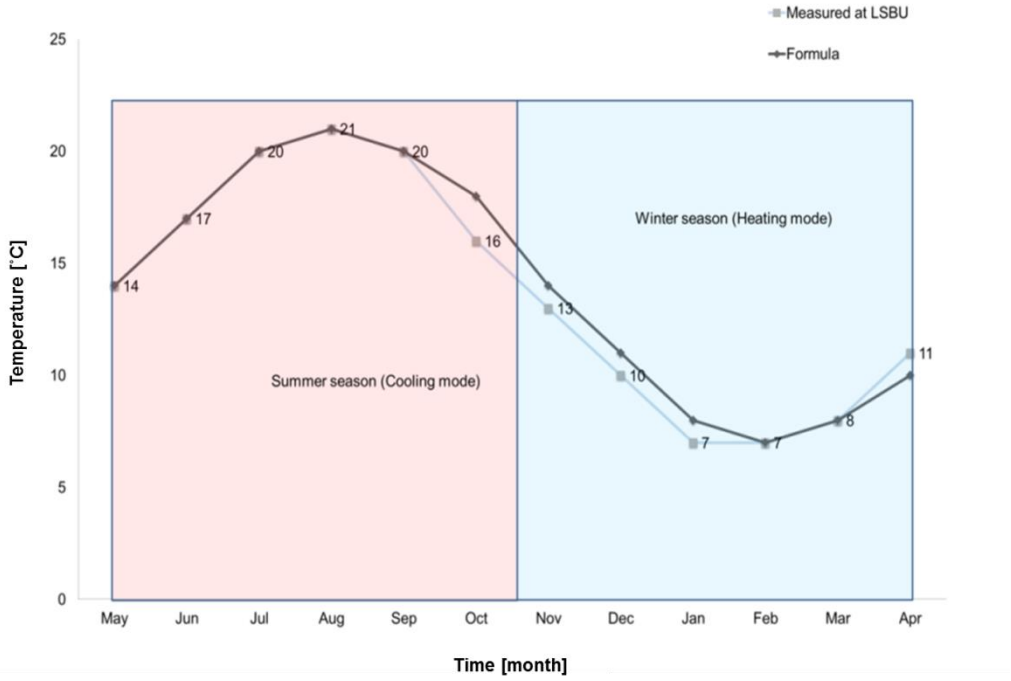

Figure 8.32: Average monthly GHE pipe inlet temperatures; measured and formula predicted

8.4.1.2 Results of Study 8

Figure 8.33 shows both the entering and leaving temperatures of the GHEs' fluid with and without the tunnel heat load. The green dotted line in in the figure is the GHEs inlet-fluid temperature variation generated by Equation 8.3. The red and blue lines are GHE fluid temperatures at the pipe outlets with and without the tunnel load respectively. The red and blue arrows in the figure show the differences between the fluid temperature entering and leaving the GHE pipes at the summer/winter peak periods. It can be seen that the average temperature of the GHEs fluid at the pipe outlets has increased by 5% over the two years when the tunnel heat load was simulated in the model. Since study 8 assumed continuous operation of the GSHP system, it can be seen in the figure that the GHEs fluid temperature remained higher even during the summer season (approx. between day 160 and 320), when the GHEs were injecting heat into the ground. Increasing the fluid temperature during the heating months would have a positive impact on the GSHP performance since the GHEs would extract more heat due to the tunnel heat load. This is illustrated in Figure 8.34 (left). However, the increased fluid temperatures during the summer months resulted in almost 34% less heat rejection into the ground for the scenario when the UR tunnel heat load was simulated. This is because of the 0.7˚C increment in the GHEs' fluid temperature, resulting in a smaller temperature difference between the inlet and outlet of the fluid during the summer months.

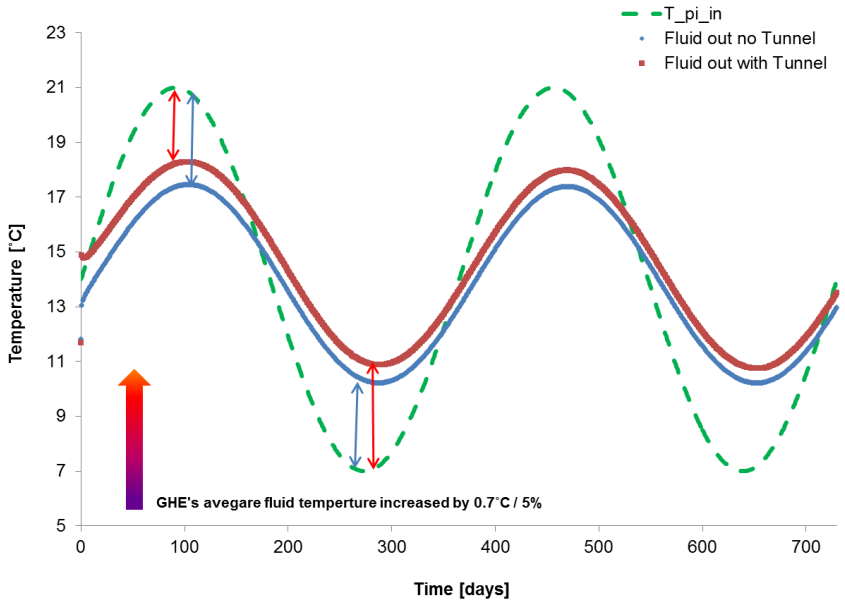

Figure 8.33: GHE fluid temperature entering/leaving the pipes, with and without the tunnel heat load

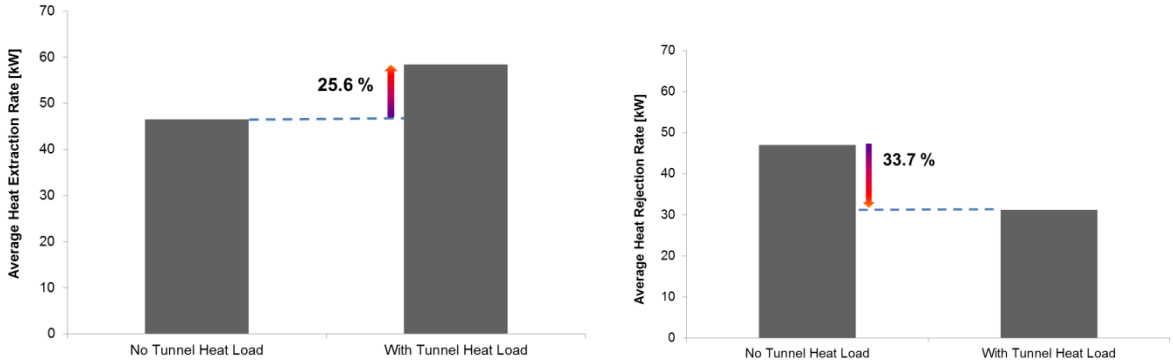

Figure 8.34: Average heat extraction (left) and heat rejection (right) by the GHEs

8.4.1.3 Conclusions of Study 8

Based on the results of Study 8 it can be concluded that constructing a GSHP system which operates in both heating and cooling modes near UR tunnels, could enhance heating related operating efficiencies of the system. However if the fluid circulation is continuous between the seasons, the increment in the temperature of the GHEs' fluid would remain during the summer months, which in turn would impact negatively on the heat rejection of the GSHP system. Such negative impact is recommended to be considered when GSHP systems with both heating and cooling modes are being designed in urban environments near UR tunnels.

8.4.2 Study 9: GHE's Fluid Flow Rate Variation

8.4.2.1 Introduction of Study 9

Study 9 aimed to explore how UR-GSHP interactions are affected by varying the GHEs circulated fluid's flow rate. The effects of three typical GHE fluid flow rates: 0.1, 0.2 and 0.3 l/s were compared. The numerical model in Study 9 used the base case geometrical scenario, option a, from Study 3. The impact of the GHEs flow rate variation on the tunnel air temperature was found to be negligible, therefore it was not included in the discussion section of the results analysis. The simulation period was kept as two years.

8.4.2.2 Results of Study 9

Figure 8.35 and Figure 8.36 show the average GHE fluid temperature and heat extraction increments for the different flow ranges without and with the tunnel heat load respectively. It can be seen that the percentage increases were within the same ranges in both figures. By decreasing the GHEs fluid flow rate from 0.3 to 0.2 l/s, the average fluid temperature at the pipe outlets increased by approximately 40% within both tunnel load scenarios. The increment in both figures was about 66% when the fluid flow rate was reduced from 0.2 to 0.1 l/s.

In the context of heat extraction, it can be seen that when the fluid flow rates were increased, the GHEs heat extraction rates increased as well. The increments with and without the tunnel heat load were within the same ranges: approximately 20% increase from fluid flow rate 0.1 to 0.2 l/s and about 7% from 0.2 to 0.3 l/s.

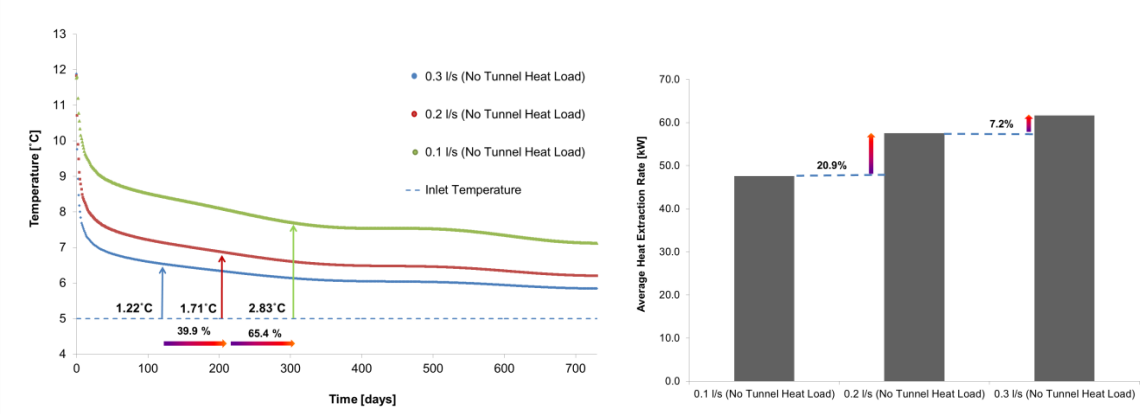

Figure 8.35: Study 9: Average GHE fluid temperature increment (left) and heat extraction rate (right) without tunnel heat load

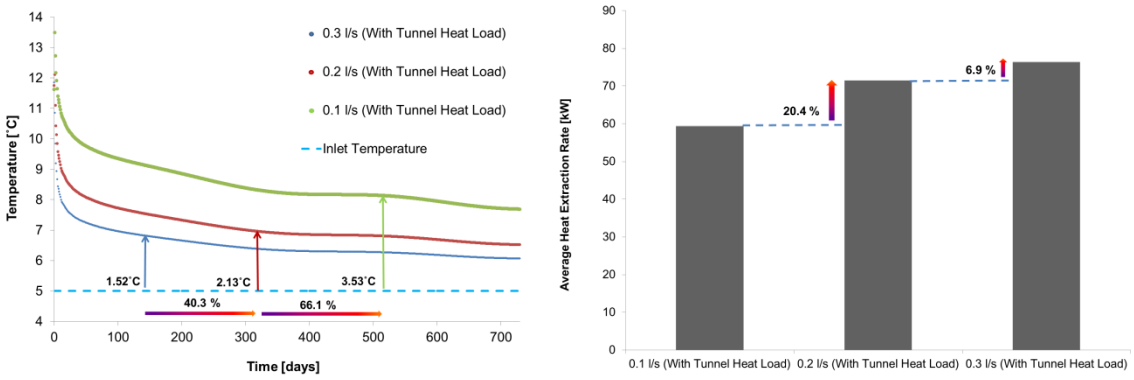

Figure 8.36: Study 9: Average GHE fluid temperature increment (left) and heat extraction rate (right) with tunnel heat load

In addition, Figure 8.37 compares the increment in heat extraction rates with and without the tunnel heat load for the different fluid flow options. Although for all three options the increments were in a similar range, the highest, 24.7%, was achieved when the fluid was circulated at the lowest flow rate 0.1 l/s.

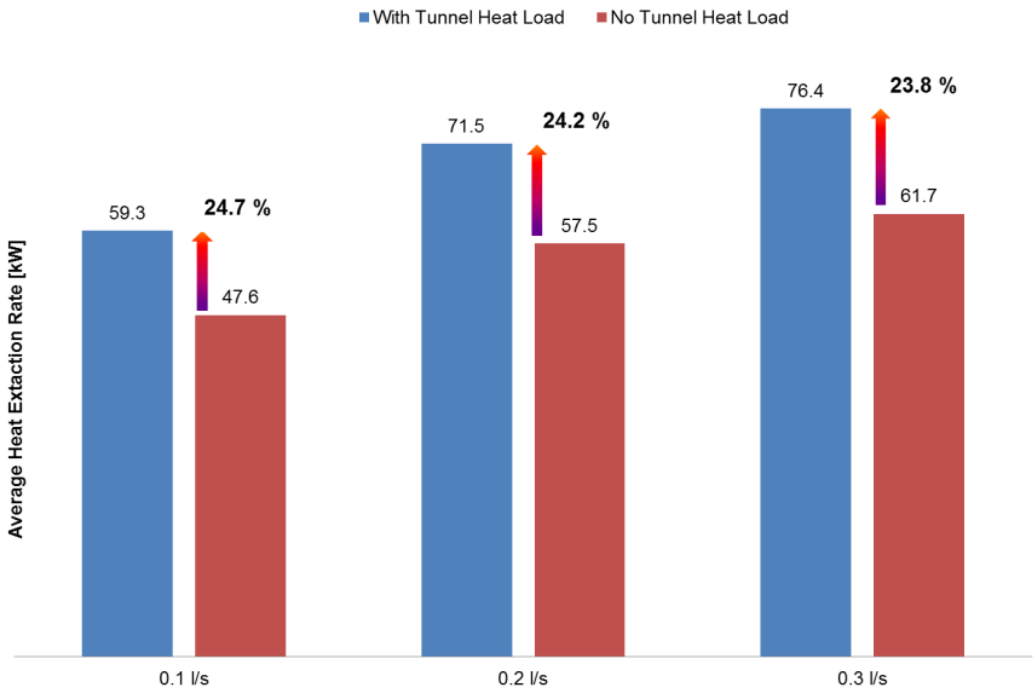

Figure 8.37: GHEs average heat extraction rates with and without the tunnel heat load at different flow rates

This suggests that the UR-GSHP interactions are somewhat stronger when the GHEs fluid circulates at a lower flow rate. The reason behind this is that at lower flow rate of the fluid,

there is a greater temperature increment along the length of the GHE pipes. This can be seen in Figure 8.38 which illustrates the fluid temperature variations along the two legs of the U-shaped GHE pipes at the end of year 1 of the simulation period, with and without the tunnel heat load. It can be seen in the figure that the UR tunnel heat load caused the largest temperature increment when the lowest fluid flow rate of 0.1 l/s was simulated.

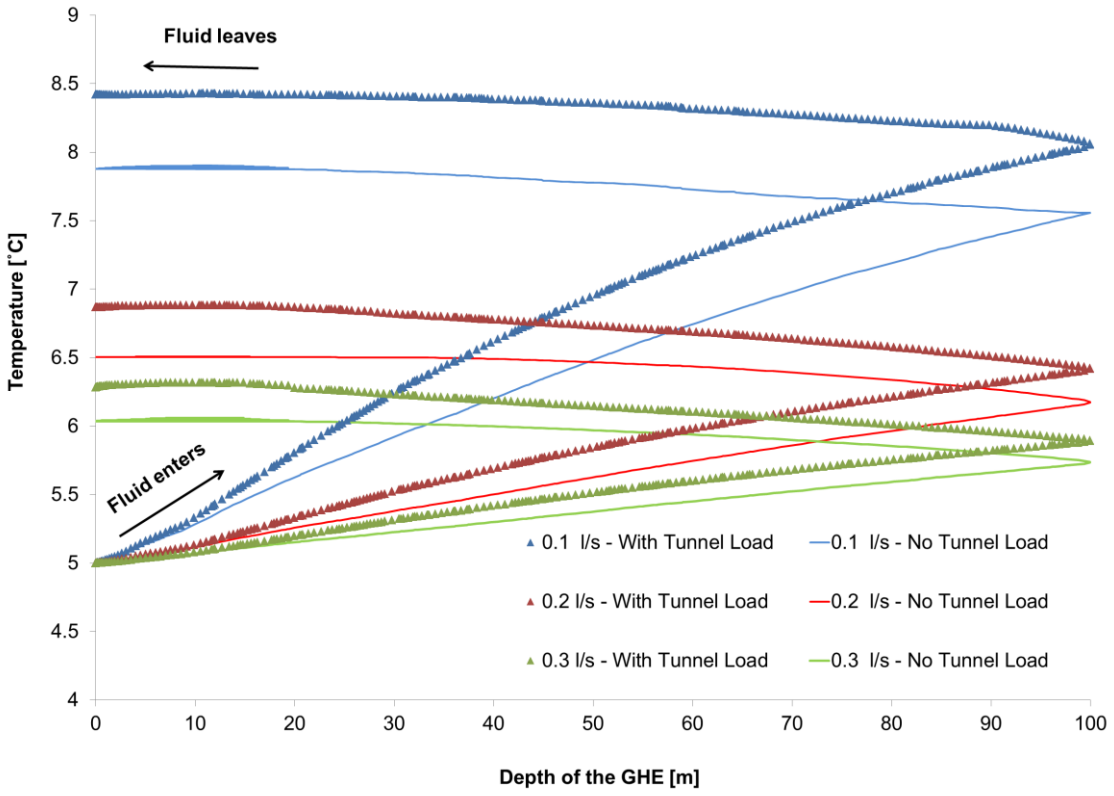

Figure 8.38 GHE fluid temperature profile with and without the tunnel heat load at different flow rates

8.4.2.3 Conclusions of Study 9

The results of Study 9 showed that the flow rate of the GHEs' fluid would have an impact on UR-GSHP interactions. It can be concluded that at lower flow rates the fluid warms up more, hence the GHEs' heat extraction rates improve if it's built near UR tunnels. However, the lower fluid flow rates in general results in lower heat extraction rates, therefore it is important to select an optimal value for the fluid flow rate when the GSHP system is being designed near UR tunnels.

8.4.3 Summary and Conclusions of Analysis Part 2: Operational Characteristics Studies

The developed 3D model was used to perform two different studies which investigated the effects of different GSHP operational characteristics on UR-GSHP interactions.

Table 8.5 summaries the studies with the key parameters and conclusions derived from them. The results showed that the different operational characteristics of the GSHP systems simulated have negligible impacts on the UR tunnel air temperatures. It was also shown that higher GHE fluid flow rates would enhance UR-GSHP interactions.

Table 8.5: Summary of Analysis Part 2: Operational Characteristics Studies

	Model Geometry	GSHP in Heating or Cooling mode	Circulated fluid flow rate [l/s]	Improvement on GHEs average heat extraction rate due to the tunnel heat load [%]	Reduction on GHEs average heat rejection rate due to the tunnel heat load [%]	Impact of GHEs on UR tunnel air temperature
Study 8	Option a (Study 3)	Heating and cooling	0.1	25.6	33.7	None
Study 9	Option a (Study 3)	Heating only	0.1, 0.2, 0.3	11.8, 13.9, 14.7	NA	None

8.5 CONCLUSIONS

Chapter 8 introduced a parametric analysis, aimed at enhancing the understanding of UR-GSHP interactions by considering a number of geometrical and operational characteristic scenarios of the systems. The nine different studies introduced in this chapter used the previously introduced, combined 3D, UR-GSHP numerical model.

The results of the parametric analysis showed that the impact of the GHEs on the UR tunnel air temperatures is negligible. This is due to the fact that the magnitudes of heat densities involved in the tunnel environment are much stronger than the heat extraction or rejection rates of the nearby GHEs. These large energy magnitude differences could be seen in the literature review section of this thesis. In addition, the conclusions of the preliminary 2D modeling work in Chapter 4 also suggested that the heat load of the UR is likely to have a stronger impact on the GHE than the GHE's impact upon the UR. This was confirmed with the simulation results presented in Chapter 8.

However, it was shown that the performance of a GSHP can be significantly improved if the ground heat exchanger (GHE) array is installed near to the UR tunnel. It was shown that the improvement on the GHEs average heat extraction rate due to the heat load from the UR tunnel can be high as ~ 40%, depending on the size and shape of the GHE array and its proximity to the UR tunnel(s). The results also suggested that the UR-GSHP interactions are stronger when the GHEs fluid circulates at a lower flow rate. An analysis showed that the reason for this is that at lower flow rate of the GHEs' fluid, there is a greater temperature change along the GHEs' pipes.

The key contribution to knowledge from this chapter is a formula which was developed from the results of the parametric studies. The formula can assist in determining the potential improvements of GHEs heat extraction rates due the heat load from a nearby UR tunnel(s). Therefore, it could be used as a designer aid by engineers who are working on fields where UR-GSHP interactions occur. Figure 8.39 summarises the key conclusions derived from the parametric analysis presented in Chapter 8.

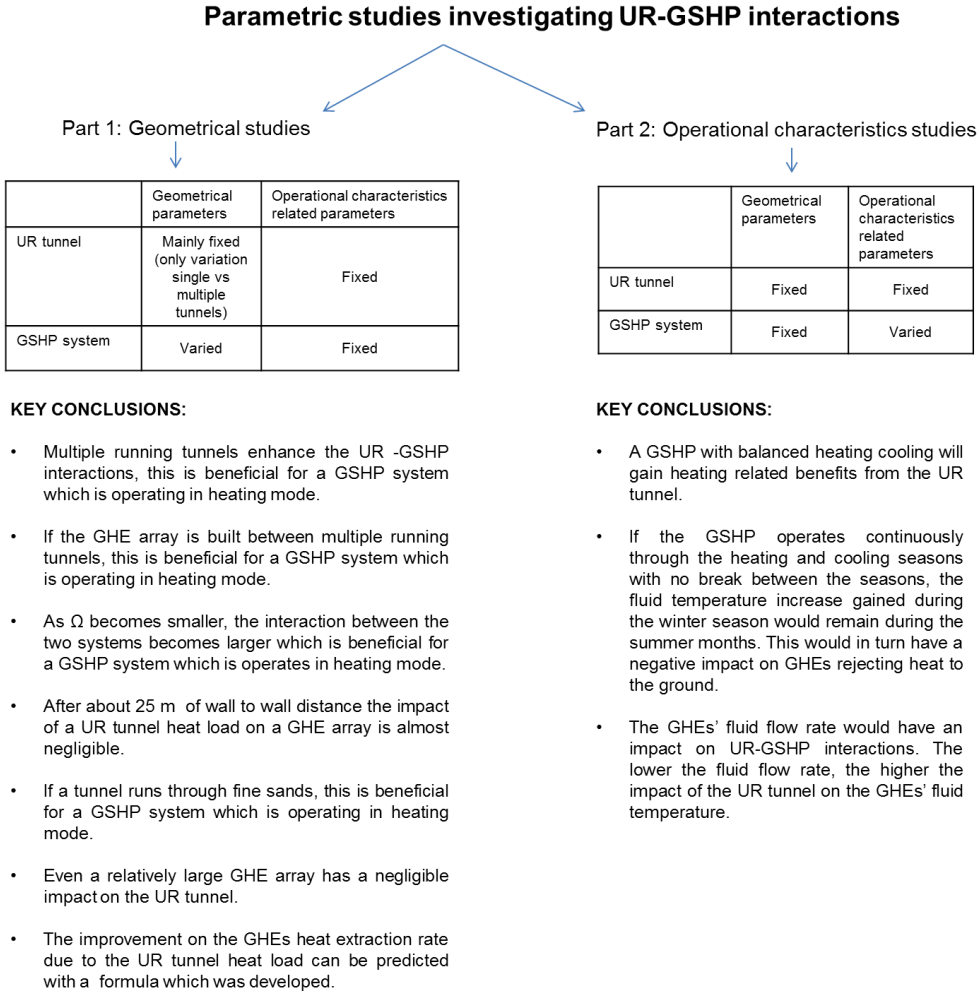

	Geometrical parameters	Operational characteristics related parameters
UR tunnel	Mainly fixed (only variation single vs multiple tunnels)	Fixed
GSHP system	Varied	Fixed

	Geometrical parameters	Operational characteristics related parameters
UR tunnel	Fixed	Fixed
GSHP system	Fixed	Varied

Figure 8.39: Summary of parametric analysis conclusions

CHAPTER 9: CONCLUSIONS AND SCOPE FOR FURTHER WORK

9.1 INTRODUCTION

This thesis has described an investigation into the thermal interactions of URs with nearby vertical GHEs of GSHPs. The research detailed in the thesis mainly involved mathematical modelling of ground source heating and cooling in the context of underground railways and infrastructure. The motivation for this work was the utilisation of waste heat energy generated by urban URs with localised GSHP installations. Understanding the thermal interactions between URs and nearby GSHPs would help to identify how the energy generated and eventually dissipated to the ground by urban UR railway systems could contribute towards sustainable city planning.

A critical review of the published work provided the basis for a series of numerical and analytical investigations into the thermal interactions of URs with nearby vertical GHEs. The numerical modelling part of the research was conducted using 2 main sections. These were: a preliminary 2D and a more complex 3D investigation.

This chapter describes the key conclusions drawn first from the literature review, second from the initial 2D numerical modelling, and third from the 3D numerical models which were also used to conduct parametric studies. These conclusions include the fundamental results from each section and the implications that these have for the overall situation. The chapter concludes with a look at what further work should be performed to continue the progress in this field of research.

9.2 CONCLUSIONS FROM THE LITERATURE SURVEY

The literature review has shown that due to their high operating efficiencies, concerns about carbon emissions, and the highly incentivised nature of GSHPs, the technology has become an increasingly common choice for heating and cooling many types of buildings. There are many examples for large scale GSHP installations operating in urban settings. The review highlighted two central London GSHP installations (K2 building in Keyworth street and One New Change Building in Bank) which are well designed systems operating at high system efficiencies in the centre of the city. The review also highlighted that the vertical type GHEs typically extract heat from the soil between 18 and 100 W/m per liner depth of the GHE depending on the GHE type, the geology, mean undisturbed ground temperature and the hours of system operation.

The literature review revealed that the implementation of these systems in urban environments could have further benefits. In such locations ground source heat is potentially available from alternative sources such as sewers, electricity cable tunnels and underground railways (URs).

Comprehensive research has been conducted to identify major heat sources in URs. Most of the past research has categorised these sources into: (i) the sources generated in the trains (i.e. heat load of passengers) and (ii) the heat gains in the tunnel (i.e. operation of the trains). Data in previous publications has shown that at peak operating hours the passenger heat gain would be around 4.5 kW sensible and 10.5 kW latent heat gains per 100 passengers per car in busy sections of the LU network. In terms of the heat gains in the tunnels and platforms due to the operation of the trains, an equivalent continuous steady state heating effect of between 300 and 350 W/m depending on the train type, speed, loading and service frequency has been identified.

The literature review also revealed that the soil that surrounds typical deep level UR tunnels such as the LU contains significant quantities of heat energy. This is due to the heat sink effect that the soil provides to the tunnels. Previous research showed that the heat absorbed by the earth surrounding an UR accounts for 30% of the total heat release, and contains approximately 4,500 GJ of heat energy per km of tunnel. This energy is low-grade and ranges in temperature from approximately 20 to 30°C. This is due to the large amount of heat energy being generated and eventually dissipated to the wall of the tunnels. For example, it was shown in the literature review that in 2005 the heat input into the Victoria Line alone was approximately 3 million kWh heat/year/single track tunnel mile. The review also showed that despite the relatively high proportion of heat entering the tunnel walls, the temperature difference between the air and tunnel walls is relatively small, approximately 1.2°C.

The low-grade energy dissipated into the ground could give an opportunity for a year-round heat supply for nearby users of heat through GSHPs. It was shown that there are more and more installations in the city of London and some of them are relatively close to the LU tunnels. One example is the One New Change installation which operates with a heating capacity of 1.6 MW. Some of its vertical GHEs are located at only 7 m distance from the wall of the LU's Central Line tunnels.

The review showed that there is a comprehensive literature available regarding how to extract heat directly from URs, for example by placing heat exchangers within existing ventilation shafts. The literature however somehow lacks in terms of the potential for

recovering heat through the ground surrounding the UR tunnels via localised GHEs. In order to explore this potential in detail, the interactions of GSHPs with neighbouring UR tunnels first had to be understood, which was the key objective of this research. Investigation of such interactions required mathematical modelling.

The literature review looked at a number of modelling approaches which have been developed separately for UR and GSHP schemes with a different level of complexity. The review helped to establish that some of these approaches could potentially be used for the separate or combined analysis of the two systems. For example, some analytical solutions such as the finite line source (FLS) method or the infinite cylindrical source (ISC) method could be used to estimate some aspects of the operational performance of vertical GHEs and UR tunnels. However, both UR and GSHP modelling involves complex geometrical aspect ratios and a transient phenomenon, therefore use of numerical solution methodologies was preferable. The literature review showed that a number of numerical simulation platforms exist which are suitable for such combined analysis. Within the research detailed in this thesis a commercial numerical simulation platform, COMSOL Multiphysics was utilised.

The critical literature survey also revealed that investigating UR-GSHP interactions using London as a case study is a practical choice, since the tunnels of the LU railway run beneath a significant part of the central area of the city. Simultaneously, GSHP installations are becoming increasingly common in the city, and thus GHEs will eventually get closer in proximity to the tunnels.

The use of secondary heat sources in London (i.e. the heat from URs) is highly promoted by the London Mayor. These secondary heat sources could be connected to existing or future heat networks through heat pumps. One example for such a scheme is the Bunhill heat network in Islington, London where the low grade heat from a LUL ventilation shaft and a nearby electricity transformer is boosted with heat pumps which are connected to the existing heat network. The literature showed that similar schemes are expected to become popular in the future in order to achieve the carbon emission reduction targets of UK Government.

9.3 CONCLUSIONS FROM THE PRELIMINARY 2D MODELLING

Chapter 4 introduced an initial 2D model which was highly simplified to enable rapid analysis of the systems to establish key phenomena for more detailed additional research. The model predictions agreed well with previous results found in the literature and also with results gained from analytical solutions.

In particular the temperature distribution within the soil from the surface was validated against an analytical equation presented by Brandl (2006). The numerical simulation results agreed well with the analytical solution. Similarly, the radial heat transfer from the wall of the tunnel into the soil was validated against an analytical equation (1D steady state heat equation for cylindrical sources). Comparison results showed that the numerical results and the results of the analytical solution are nearly identical (~ plus or minus 0.02˚C temperature difference).

The validated 2D mathematical model was used to perform a number of investigations with the aim of establishing key parameters impacting on the thermal interactions between UR-GSHPs. Those parameters which were found to have a potential impact were then implemented into more complex 3D models which were detailed in later chapters. Thus the outcomes of the 2D modelling work formed the foundation of the 3D numerical model development.

One of the key conclusions from the preliminary 2D modelling was that for a London based case study where the majority of URs and vertical GHEs are built in London Clay, simulation of groundwater movement could be neglected and assuming a pure conductive heat transfer during the simulations was sufficient. The reason for that was that the hydraulic conductivity of the London Clay is extremely low (~2.2E-10 m/s) and it is a type of soil material which has a relatively high porosity (~0.47).

The results from these initial investigations also showed that the heat load of the UR is likely to have a stronger impact on the GHE than the GHE's impact upon the UR. This could be beneficial depending on the application requirements.

In addition, it was also concluded that it is possible to use a model geometry simplification strategy called the equivalent diameter (ED) method. It was shown that by applying the ED method in 2D cross-sectional numerical models it is possible to represent the effect of parallel running tunnels on their surroundings using a single diameter without compromising the results significantly.

Finally, the 2D simulation results showed that incorporating the tunnel wall into the model geometry could have an impact on the temperature distribution from the centre of the tunnel into the soil. Adding the material does not increase the model complexity therefore it was recommended to incorporate it in future 3D models.

9.4 CONCLUSIONS FROM THE 3D MODEL DEVELOPMENTS

Chapter 5 and 6 described the development and validation of 3D UR and GHE numerical models.

Chapter 5 presents the development of two different UR models (UR-Model A and UR-Model-B). The two UR models have different levels of complexity. Whilst one of the models neglects the tunnel air domain (UR-Model-A), thus enabling rapid analysis of the system, the other model explicitly represents tunnel air and the heat load from the trains (UR-Model-B), which allows more detailed investigations. However, representing the tunnel air domain and its related physics such as the turbulent air flow and the related boundary conditions have significantly increased the number of degrees of freedom (NDF) of the model. Because of that computational efficiency of the model was reduced and so it had to be optimised to achieve more rapid computational times without compromising the results. This was achieved using two steps. Firstly, the problem was de-coupled by assuming that the material properties required for solving the physics of turbulent air flow within the tunnel domain do not change significantly with respect to the change in temperature expected. This allowed the physics of turbulent air flow to be solved in a preliminary stationary study. The velocity flow characteristics calculated were then transferred to a transient heat transfer study. It was shown that such an optimisation significantly enhanced computational efficiencies of the model (about 15% longer computation times compared to UR-Model-A) without compromising its results. The validation of the model predicted results was carried out by comparing the numerical results with data reported on the thermal environment on the LU. The comparison showed good agreement between the simulated and site-measured data.

Chapter 5 finally concluded that the decision regarding which UR model to implement for investigations should be made according to the objective of the analysis. Since the research detailed in this thesis aimed to explore the mutual impact of URs and nearby GHEs, the use of UR-Model-B was chosen for further analysis.

Following that, Chapter 6 introduced the method used for the 3D numerical GHE model development. The numerical model of the GHE uses a combination of 1D and 3D physics, such that the fluid flow and heat transfer inside the pipes were simulated using 1D linear elements. The external temperature outside of the 1D pipe elements corresponds to the temperature field computed in the surrounding volumetric domain. This provided automatic heat transfer coupling to the 3D domains. The ability of the 3D GHE model to calculate transient heat transfer rates was validated by comparing numerical results against the FLS analytical solutions. Analysis results of the numerical and analytical models were compared

by several temperature-radial distances at the mid-depth of the GHE at various times. In addition, the numerical results of the absorber pipes' wall heat transfer rates were compared to typical values reported in literature. Results from these verifications suggested that the GHE model developed can successfully simulate the operation of vertical GHEs.

Finally, Chapter 6 concluded that if large GHE arrays are being investigated, a model optimisation strategy is suggested. Such optimisation could be achieved by assuming that the temperature profile across the thin borehole/energy pile material was not of primary interest, thus its physical geometry surrounding the linear pipe elements could be removed from the model. The validity of the assumption rested on the fact that the overall modelling objective was to investigate UR and GSHP interactions and the temperature of the thin borehole material was not a key concern. Also, the borehole and the energy pile material have similar thermal characteristics to that of the surrounding soil. Implementing this assumption significantly reduces the number of mesh elements required to solve the model which in turn enhances computational efficiencies.

9.5 CONCLUSIONS FROM THE 3D NUMERICAL INVESTIGATIONS

Chapter 7 introduced a preliminary 3D investigation of UR-GSHP interactions. The model geometry in this initial study combined the previously developed and validated UR and GHE models. The aim of the study was to investigate how the two systems impact on their surroundings and on each other. This preliminary 3D study included two investigations. Investigation 1 aimed to explore the impact of the tunnel heat load on a surrounding soil block with a specific volume using a 50 year simulation period. The results showed that the soil block temperature was about 1.35°C warmer than when the heat load from the tunnel was considered. This showed the potential for enhancing the performance of nearby GSHPs operating in heating mode. The results of Investigation 1 also highlighted the importance of considering the initial effect of the UR operation on its surroundings before UR-GSHP interactions are investigated. Starting a simulation of an UR-GSHP model from a uniform soil temperature profile would not be realistic if a London based case study is considered. The operation of the URs over an extended period would have impacted on the surrounding soil temperature prior to the installation of the GSHP. The results of Investigation 2 showed that extracting heat from the ground surrounding the tunnel would be likely to enhance the heat sink effect of the soil, which could potentially have a cooling impact on the URs. Overall, the results of the investigations detailed in Chapter 7 clearly demonstrated that interactions occur between URs and neighboring GSHP installations.

The investigations presented in Chapter 7 considered only certain geometrical configurations

and operational characteristics of the systems, therefore further research was conducted to take account of a number of potential geometrical and operational parameter variations of the systems. These additional 3D parametric studies were detailed in Chapter 8.

Findings from the parametric studies showed that the impact of the operation of an UR tunnel on nearby GHEs can be significant, especially in the case of GSHPs only extracting heat from the ground. The improvement on the GHEs average heat extraction rate due to the heat load from the UR tunnel can be high as 40%, depending on the size and shape of the array and its proximity to the tunnel.

The results also showed that even a relatively large GHE array would have a negligible impact on the UR tunnel air temperatures. This is most likely due to the fact that the heat densities involved on the UR side of the model are significantly larger than the GHE array heat extraction/rejection rates. Differences in large energy magnitudes between URs and vertical GHEs were highlighted in the literature review section of this thesis. In addition, the conclusions of the preliminary 2D modeling work in Chapter 4 also suggested that the heat load of the UR is likely to have a stronger impact on the GHE than the GHE's impact upon the UR. This was confirmed with the simulation results presented in Chapter 8.

The results from the parametric studies were used to develop a formula which can assist in predicting the approximate heat extraction improvements of GHEs based on a single variable called the interaction proximity (Ω). This variable is the geometrical distance between the UR and the nearby GHEs. The formula developed is one the key contributions to knowledge from this research. It could potentially be used as a designer aid to provide guidance to engineers working in fields where UR-GSHP interactions occur.

9.6 SCOPE FOR FURTHER WORK

9.6.1 Tests and Experiments

The research detailed in this thesis involved numerical modelling of ground source heating and cooling in the context of URs and infrastructure. The numerical models developed were validated against analytical equations and against data which was available in literature or was provided by LUL to support the progress of the research. Further in situ experiments and real life case studies would be required to test the applicability of the model and the conclusions driven from this thesis.

9.6.2 Different Case Studies

One of the key contributions to knowledge of this research was a formula which allows estimating the approximate improvement of GHEs which are built near UR tunnels. This formula was developed based on the results of a London based case study (scenarios only where the tunnels are built in London Clay). In order to make the developed formula more general and be applicable to other cities metro systems, further research would be required.

9.6.3 GHE Arrays with Irregular (Circular, Triangular) Shapes

This research has provided a formula for estimating the potential enhancement on the GSHPs heat extraction rates due to a heat load from an UR tunnel. The formula was developed considering only typical squared GHE arrays. The interactions of more unusual geometrical GHE layouts, such as circular and triangular arrays, with URs are recommended to be investigated.

9.6.4 Non-Thermal Aspects of UR-GSHP interactions

The research detailed in this thesis only investigated the thermal interactions of UR with localised GSHPs. Further research is suggested on other aspects of the interactions, for example how the vibration from the trains in the tunnels might impact on the nearby installed GHE array. Geotechnical aspects such as potential deformations of the structures caused by their interactions are also recommended to be investigated.

9.6.5 Detailed Survey for Mapping the Locations with the Greatest Potentials

The research conducted assumed a generic deep level LU tunnel section and its interaction with a nearby GHE array. It was assumed that there were no geographical limitations for the combined analysis of the systems. In order to make the most practical use of the research outcomes, a detailed geographical survey of the LU network and its surroundings would need to be conducted. Gathering such data would allow the development of a map which would identify locations with the greatest energy recovery potential through GSHPs in London.

9.6.6 The flexibility of integration into DHNs

Heat networks in urban settings can be an effective way of supplying low carbon heat to buildings. The outcomes of this research showed that the extraction rates of GSHPs built near to tunnels can be significantly improved. This suggests that urban GSHP based heat networks could be an environmentally friendly alternative to gas fired CHP based networks.

GSHP based heat networks are not yet common in the UK. The technical and non-technical flexibility of the integration of such systems should be established.

9.6.7 Carbon and Cost Savings against Conventional GSHPs and Other Heating Systems

The research work detailed in the thesis showed that the heat extraction of GSHPs operating in heating mode can be increased if the system is built in close proximity to UR tunnels. Further research would need to establish the carbon and cost savings associated with waste heat recovery through GSHPs. These should be compared to savings associated with regular GSHP systems as well as with conventional non-renewable heating systems in London.

9.6.8 Heat Recovery Potential from Other Types of Urban Subterranean Structures

The outcomes of this research showed that the waste heat generated by URs in London could enhance the heat extraction rates of nearby installed GSHP systems. The literature survey revealed that other subterranean infrastructure systems such as sewers, electricity cable tunnels and water mains could also potentially provide a year-round heat supply. However, the potential for heat recovery from such structures has not yet been established and an investigation of this would be needed. A successful study demonstrating the technical and non-technical challenges of subterranean heat recovery will lead to many opportunities for energy recovery applications across London and elsewhere.

REFERENCES

Abdelaziz, S. L., Ozudogru, T. Y., Olgun, C. G. and Martin II, J. R. (2014) Multilayer finite line source model for vertical heat exchangers, *Geothermics*, 51, pp. 406–416. DOI:10.1016/j.geothermics.2014.03.004.

AccuWeather (2017) London January Weather 2017 - AccuWeather Forecast for Greater London United Kingdom, *AccuWeather*. Available from: http://www.accuweather.com/en/gb/london/ec4a-2/january-weather/328328 [Accessed 11 April 2017].

Adam, D. and Markiewicz, R. (2009) Energy from earth-coupled structures, foundations, tunnels and sewers, *Géotechnique*, 59 (3), pp. 229–236. DOI:10.1680/geot.2009.59.3.229.

Al-Khoury, R. and Bonnier, P. G. (2006) Efficient finite element formulation for geothermal heating systems. Part II: transient, *International Journal for Numerical Methods in Engineering*, 67 (5), pp. 725–745.

Al-Khoury, R., Bonnier, P. G. and Brinkgreve, R. B. J. (2005) Efficient finite element formulation for geothermal heating systems. Part I: steady state, *International Journal for Numerical Methods in Engineering*, 63 (7), pp. 988–1013. DOI:10.1002/nme.1313.

Ampofo, F., Maidment, G. and Missenden, J. (2004a) Underground railway environment in the UK Part 2: Investigation of heat load, *Applied Thermal Engineering*, 24 (5–6), pp. 633–645. DOI:10.1016/j.applthermaleng.2003.10.018.

Ampofo, F., Maidment, G. and Missenden, J. (2004b) Underground railway environment in the UK Part 2: Investigation of heat load, *Applied Thermal Engineering*, 24 (5–6), pp. 633–645. DOI:10.1016/j.applthermaleng.2003.10.018.

Angelotti, A., Alberti, L., La Licata, I. and Antelmi, M. (2014) Borehole Heat Exchangers: heat transfer simulation in the presence of a groundwater flow, in: *Journal of Physics: Conference Series*. IOP Publishing,501, pp. 012033.

ANSYS (2017) Simulation Driven Product Development | ANSYS. Available from: http://www.ansys.com/ [Accessed 31 March 2017].

ASHRAE (2009) *ASHRAE Handbook: Fundamentals*. American Society of Heating, Refrigeration and Air-Conditioning Engineers.

Bandos, T. V., Montero, Á., Fernández, E., Santander, J. L. G., Isidro, J. M., Pérez, J., Córdoba, P. J. F. de and Urchueguía, J. F. (2009) Finite line-source model for borehole heat exchangers: effect of vertical temperature variations, *Geothermics*, 38 (2), pp. 263–270. DOI:10.1016/j.geothermics.2009.01.003.

Barla, M. and Perino, A. (2014) Energy from geo-structures: a topic of growing interest, *Environmental Geotechnics*. DOI:10.1680/envgeo.13.00106.

Barnard, A. C. L., Hunt, W. A., Timlake, W. P. and Varley, E. (1966) A Theory of Fluid Flow in Compliant Tubes, *Biophysical Journal*, 6 (6), pp. 717–724.

Barrow, H. and Pope, C. W. (1987) A simple analysis of flow and heat transfer in railway tunnels, *International Journal of Heat and Fluid Flow*, 8 (2), pp. 119–123.

BBC (2009) BBC NEWS | England | London | Map reveals hotspots of the Tube. Available from: http://news.bbc.co.uk/1/hi/8218059.stm [Accessed 12 March 2017].

BBC (2016) Hottest day of 2016 recorded at Gravesend in Kent, *BBC News*.

Bendelius, A. G. (1976) Aerodynamic and thermodynamic evaluation for the Atlanta subway system, in: *Proceedings of the Second International Symposium on the Aerodynamics and Ventilation of Vehicle Tunnels*. pp. C1-1–20.

Bernier, M. A. (2001) SYMPOSIUM PAPERS-AT-01-8 Pumping Design and Performance Modeling of Geothermal Heat Pump Systems-Ground-Coupled Heat Pump System Simulation, *ASHRAE Transactions-American Society of Heating Refrigerating Airconditioning Engineering*, 107 (1), pp. 605–616.

BGS (2017) BGS Reference and research reports - Ground source heat pumps. Available from: http://www.bgs.ac.uk/reference/gshp/gshp_report.html [Accessed 31 March 2017].

Bortoloni, M., Bottarelli, M. and Su, Y. (2017) A study on the effect of ground surface boundary conditions in modelling shallow ground heat exchangers, *Applied Thermal Engineering*, 111, pp. 1371–1377. DOI:10.1016/j.applthermaleng.2016.05.063.

Brandl, H. (2006) Energy foundations and other thermo-active ground structures, *Géotechnique*, 56 (2), pp. 81–122. DOI:10.1680/geot.2006.56.2.81.

Brown, J. M. B. and Vardy, A. E. (2006) Practical evaluation of convective heat exchanges between deep tunnels and the surrounding ground, in: Slovenia.

Brown, J. M. B., Vardy, A. E. and Tijsseling, A. S. (2005) Response of wall heat transfer to flows along a cylindrical cavity and to seepage flows in the surrounding medium, *Journal of Water Resources*, 26 (2), pp. 57–68.

Busby, J., Lewis, M., Reeves, H. and Lawley, R. (2009) Initial geological considerations before installing ground source heat pump systems, *Quarterly Journal of Engineering Geology and Hydrogeology*, 42 (3), pp. 295–306. DOI:10.1144/1470-9236/08-092.

Carslaw, H. and Jaeger, J. C. (1946) *Conduction of Heat in Solids*. Oxford, UK: Claremore Press.

Cengel, Y. A. and Boles, M. A. (2001) *Thermodynamics: An Engineering Approach*. 4th edition. Boston: Mcgraw-Hill College.

Chapman, D. S. and Pollack, H. N. (1975) Earth and Planetary Science Letters 28, Global Heat Flow: A New Look, Earth Planet.

Chen, S., Mao, J. and Han, X. (2016) Heat transfer analysis of a vertical ground heat exchanger using numerical simulation and multiple regression model, *Energy and Buildings*, 129, pp. 81–91. DOI:10.1016/j.enbuild.2016.07.010.

Chiasson, A. C., Rees, S. J. and Spitler, J. D. (2000) A preliminary assessment of the effects of ground-water flow on closed-loop ground-source heat pump systems, *ASHRAE Transaction*, 106 (1), pp. 380–393.

Churchill, S. W. (1977) Friction-factor equation spans all fluid-flow regimes, *Chemical Engineering*, 84 (24), pp. 91–92.

CIBSE (2007) *CIBSE Guide C: Reference Data*.

Cockram, I. J. and Birnie, G. R. (1976) The ventilation of London's underground railways, in: *Proceedings of the Second International Symposium on the Aerodynamics and Ventilation of Vehicle Tunnels, Paper H*.2, pp. 11–27.

COMSOL (2017) COMSOL Multiphysics® Modeling Software. Available from: https://www.comsol.com/ [Accessed 31 March 2017].

Constructionenquirer (2014) Northern line extension green light for spring start I Construction Enquirer. Available from: http://www.constructionenquirer.com/2014/11/13/northern-line-extension-go-ahead-for-spring-start/ [Accessed 20 April 2015].

CTP (2009) *Tunnel Ventilation Modelling Manual* (No. RS_UIP1189/TCXA-029/D0252).

Cui, P., Yang, H. and Fang, Z. (2008) Numerical analysis and experimental validation of heat transfer in ground heat exchangers in alternative operation modes, *Energy and Buildings*, 40 (6), pp. 1060–1066. DOI:10.1016/j.enbuild.2007.10.005.

DECC (2012) Renewable Heat Incentive (RHI) - Increasing the use of low-carbon technologies - Policies - GOV.UK. Available from: https://www.gov.uk/government/policies/increasing-the-use-of-low-carbon-technologies/supporting-pages/renewable-heat-incentive-rhi [Accessed 6 October 2014].

DECC (2013) The Future of Heating: Meeting the challenge. Available from: https://www.gov.uk/government/uploads/system/uploads/attachment_data/file/190149/16_04-DECC-The_Future_of_Heating_Accessible-10.pdf [Accessed 6 October 2014].

Deerman, J. D. and Kavanaugh, S. P. (1991) Simulation of vertical u-tube ground-coupled heat pump systems using the cylindrical heat source solution. Available from: http://www.techstreet.com/products/1717186 [Accessed 22 October 2014].

Diao, N., Li, Q. and Fang, Z. (2004) Heat transfer in ground heat exchangers with groundwater advection, *International Journal of Thermal Sciences*, 43 (12), pp. 1203–1211. DOI:10.1016/j.ijthermalsci.2004.04.009.

DTR (2017) ThermoTun Software - Overview. Available from: http://www.thermotun.com/thermotun/overview/overview.htm [Accessed 31 March 2017].

Environmental Agency (2014) *Management of the London Basin Chalk Aquifer*. Available from:https://www.gov.uk/government/uploads/system/uploads/attachment_data/file/320038/2014_London_GWL_Report.pdf [Accessed 22 February 2015].

EQUA (1995) *IDA*. Available from: http://equa.se/en/tunnel [Accessed 18 May 2017].

ERRAC and UITP (2012) Metro, light rail and tram systems in Europe, *UITP - Advancing Public Transport*. Available from: http://www.uitp.org/metro-light-rail-and-tram-systems-europe [Accessed 10 October 2014].

European Commission (2009) Decision No 406/2009/EC on the effort of Member States to reduce their greenhouse gas emissions to meet the Community's greenhouse gas emission reduction commitments up to 2020. Official Journal of the European Union. Available from: http://eur-lex.europa.eu/LexUriServ/LexUriServ.do?uri=OJ:L:2009:140:0136:0148:EN:PDF [Accessed 2 October 2014].

FABER MAUNSELL (2007) *Specification for Ground Source Heat Pump Installation, London South Bank University, Keyworth II*.

Fan, R., Jiang, Y., Yao, Y., Shiming, D. and Ma, Z. (2007) A study on the performance of a geothermal heat exchanger under coupled heat conduction and groundwater advection, *Energy*, 32 (11), pp. 2199–2209. DOI:10.1016/j.energy.2007.05.001.

Federal Transit Administration (2002) *Subway Environmental Simulation Computer Program SES Version 4.1, Part I User's Manual*. Washington, DC.

Florides, G. and Kalogirou, S. (2007) Ground heat exchangers—A review of systems, models and applications, *Renewable Energy*, 32 (15), pp. 2461–2478. DOI:10.1016/j.renene.2006.12.014.

Franzius, J. N. and Pralle, N. (2011) Turning segmental tunnels into sources of renewable energy, *Proceedings of the Institution of Civil Engineers - Civil Engineering*, 164 (1), pp. 35–40. DOI:10.1680/cien.2011.164.1.35.

Gilbey, M. and Thompson, J. (2009) Temperature control on the London Underground, SME Annual Meeting & Exhibit and CMA's 111th National Western Mining Conference in: Denver, Colorado, USA.

Gilbey, M., Thompson, J. and Duffy, S. (2011) The Potential for Heat Recovery from London Underground Stations and Tunnels, in: *CIBSE Technical Symposium*. Leicester UK.

Gnielinski, V. (1976) New equations for heat and mass-transfer in turbulent pipe and channel flow, *International Chemical Engineering*, 16 (2), pp. 359–368.

GOV.UK (2015, October 19) Policy 5.5 Decentralised energy networks, *London City Hall*. Available from: https://www.london.gov.uk//what-we-do/planning/london-plan/current-london-plan/london-plan-chapter-five-londons-response/poli-0 [Accessed 25 March 2017].

Gunn, M. (2015) London South Bank University Lecture notes.

HAL (2016) London Tunnel Water Ring Main Design and Analysis of a Tunnel Ring Main and Pump Out Shafts | Hydraulic Analysis Limited. Available from: http://hydraulic-analysis.com/case-studies/london-tunnel-water-ring-main-design-and-analysis-of-a-tunnel-ring-main-and-pump-out-shafts/ [Accessed 22 May 2017].

Halliday, S. (2013) *The Great Stink of London: Sir Joseph Bazalgette and the Cleansing of the Victorian Metropolis*. Stroud: History Press Limited.

Headon, J., Banks, D., Waters, A. and Robinson, V. K. (2009) Regional distribution of ground temperature in the Chalk aquifer of London, UK, *Quarterly Journal of Engineering Geology and Hydrogeology*, 42 (3), pp. 313–323. DOI:10.1144/1470-9236/08-073.

Hein, P., Kolditz, O., Görke, U.-J., Bucher, A. and Shao, H. (2016) A numerical study on the sustainability and efficiency of borehole heat exchanger coupled ground source heat pump systems, *Applied Thermal Engineering*, 100, pp. 421–433. DOI:10.1016/j.applthermaleng.2016.02.039.

Hellström, G. (1991) *Ground heat storage: thermal analyses of duct storage systems* (dissertation). Lund University, Lund, Sweden. Available from: http://lup.lub.lu.se/record/2536279 [Accessed 2 December 2016].

Hight, D. W., McMillan, F., Powell, J. J. M., Jardine, R. J. and Allenou, C. P. (2003) Some characteristics of London clay, *Characterisation and Engineering Properties of Natural Soils*, 2, pp. 851–946.

Hu, Z., Li, X., Zhao, X., Xiao, L. and Wu, W. (2008) Numerical analysis of factors affecting the range of heat transfer in earth surrounding three subways, *Journal of China University of Mining and Technology*, 18 (1), pp. 67–71. DOI:10.1016/S1006-1266(08)60015-2.

Incropera, F. P. and Lavine, A. S. (2011) *Fundamentals of heat and mass transfer*. John Wiley & Sons.

Ingersoll, L. and Plass, H. (1948) Theory of the ground heat pipe heat source for the heatpump, *Transactions of the American Society of Heating and Ventilating Engineers.* Available from: http://www.citeulike.org/user/fghorow/article/4097264 [Accessed 17 March 2015].

Kavanaugh, S. P., Xie, L. and Martin, C. (2000) Investigation of methods for determining soil and rock formation thermal properties from short-term field tests, *Final Report for ASHRAE TRP-1118*.

Koohi-Fayegh, S. and Rosen, M. A. (2012) Examination of thermal interaction of multiple vertical ground heat exchangers, *Applied Energy*, 97, pp. 962–969. DOI:10.1016/j.apenergy.2012.02.018.

Lazzari, S., Priarone, A. and Zanchini, E. (2010) Long-term performance of BHE (borehole heat exchanger) fields with negligible groundwater movement, *Energy*, 35 (12), pp. 4966–4974. DOI:10.1016/j.energy.2010.08.028.

Lee, C. K. and Lam, H. N. (2008) Computer simulation of borehole ground heat exchangers for geothermal heat pump systems, *Renewable Energy*, 33 (6), pp. 1286–1296. DOI:10.1016/j.renene.2007.07.006.

Lee, C. and Lam, H. (2007) Effects of groundwater flow direction on performance of ground heat exchanger borefield in geothermal heat pump systems using 3-D finite difference method., in: *Proceedings of Building Simulation Conference*. Beijing, China.

Lei, T. (1993) Development of a computational model for a ground-coupled heat exchanger, *ASHRAE Transaction*, 99.

Lightfoot, T. (2016) Private communication.

London Infrastructure Plan 2050 | London City Hall [no date]. Available from: https://www.london.gov.uk/what do we do/business-and-economy/better-infrastructure/London-infrastructure-plan-2050 [Accessed 26 April 2016].

London.gov.uk (2016) Scenarios to 2050: London Energy Plan, *London City Hall*. Available from: https://www.london.gov.uk//what-we-do/environment/energy/scenarios-2050-london-energy-plan [Accessed 26 March 2017].

Loveridge, F. (2012) *The Thermal Performance of Foundation Piles used as Heat Exchangers in Ground Energy Systems*. University of Southampton.

Lund, J., Sanner, B., Rybach, L., Curtis, R. and Hellstrom, G. (2004) Geothermal (Ground-Source) Heat Pums a World Overview. Geo - Heat Center. Available from:

http://file.seekpart.com/keywordpdf/2011/5/24/2011524112558636.pdf [Accessed 10 October 2014].

MathWorks (2017) MathWorks - Makers of MATLAB and Simulink. Available from: https://uk.mathworks.com/ [Accessed 31 March 2017].

Mavroulidou, M., Gunn, M. J. and Woods, R. I. (2005) Numerical modelling of groundwater pumping processes, *Proceedings of the Institution of Civil Engineers-Geotechnical Engineering*, 158 (2), pp. 83–93.

Menkiti, C. O., Davis, J. A., Semertzidou, K., Abbireddy, C. O. R., Hight, D. W., Williams, J. D. and Black, M. (2015) The geology and geotechnical properties of the Thanet Sand Formation–an update from the Crossrail Project, in: *Crossrail Project: Infrastructure design and construction*. ICE Publishing, pp. 63–77.

MIKE (2016) FEFLOW. Available from: https://www.mikepoweredbydhi.com/products/feflow [Accessed 31 March 2017].

Mimouni, T., Dupray, F., Minon, S. and Laloui, L. (2013) Heat Exchanger Anchors for Thermo-Active Tunnels. Available from: http://infoscience.epfl.ch/record/190673 [Accessed 28 October 2014].

Molina-Giraldo, N., Blum, P., Zhu, K., Bayer, P. and Fang, Z. (2011) A moving finite line source model to simulate borehole heat exchangers with groundwater advection, *International Journal of Thermal Sciences*, 50 (12), pp. 2506–2513. DOI:10.1016/j.ijthermalsci.2011.06.012.

Mortada, A., Choudhary, R. and Soga, K. (2015) Thermal Modeling and Parametric Analysis of Underground Rail Systems, *Energy Procedia*, 78, pp. 2262–2267.

Mott MacDonald (2017) Global engineering, management and development consultants - Mott MacDonald. Available from: https://www.mottmac.com/ [Accessed 11 April 2017].

Mount, S. C. (1947) Ventilation and Cooling in London's Tube Railways, *Institution of Heating and Ventilating Engineers Journal*, pp. 354–374.

Muraya, N., O'Neal, D. and Heffington, W. (1996) Thermal interference of adjacent legs in a vertical u-tube heat exchanger for a ground-coupled heat pump, *ASHRAE Transaction*, 102 (Paper number 3980), pp. 12–21.

National Grid (2017) Home, *LPT*. Available from: http://www.londonpowertunnels.co.uk/ [Accessed 12 March 2017].

Nera Economic Consulting, Renewable Heat Technologies for Carbon Abatement: Characteristics and Potential, Final Report to the Committee on Climate Change July 2009 - Google Search (2009). Available from: https://www.google.co.uk/webhp?sourceid=chrome-instant&ion=1&espv=2&ie=UTF-8#q=Nera+Economic+Consulting%2C+Renewable+Heat+Technologies+for+Carbon+Abatement:+Characteristics+and+Potential%2C+Final+Report+to+the+Committee+on+Climate+Change+July+2009 [Accessed 9 January 2017].

Ninikas, K., Hytiris, N., Emmanuel, R., Aaen, B. and Younger, P. L. (2016) Heat recovery from air in underground transport tunnels, *Renewable Energy*, 96, Part A, pp. 843–849. DOI:10.1016/j.renene.2016.05.015.

Northon, K. (2017, January 18) NASA, NOAA Data Show 2016 Warmest Year on Record Globally, *NASA*. Available from: http://www.nasa.gov/press-release/nasa-noaa-data-show-2016-warmest-year-on-record-globally [Accessed 24 February 2017].

Ozudogru, T. Y., Olgun, C. G. and Senol, A. (2014) 3D numerical modeling of vertical geothermal heat exchangers, *Geothermics*, 51, pp. 312–324.

Pahud, D. and Matthey, B. (2001) Comparison of the thermal performance of double U-pipe borehole heat exchangers measured in situ, *Energy and Buildings*, 33 (5), pp. 503–507. DOI:10.1016/S0378-7788(00)00106-7.

Paul, J. D. (2009) Geology and the London Underground, *Geology Today*, 25 (1), pp. 12–17. DOI:10.1111/j.1365-2451.2009.00699.x.

Paul, J. D. (2016) High-resolution geological maps of central London, UK: Comparisons with the London Underground, *Geoscience Frontiers*, 7 (2), pp. 273–286.

Paurine, A. and Maidment, G. (2015) The potential use of the mains water loop for cooling, heat and energy networks, *ResearchGate*. Available from: https://www.researchgate.net/publication/282849000_The_potential_use_of_the_mains_water_loop_for_cooling_heat_and_energy_networks [Accessed 12 March 2017].

Rees, S. J. and He, M. (2013) A three-dimensional numerical model of borehole heat exchanger heat transfer and fluid flow, *Geothermics*, 46, pp. 1–13. DOI:10.1016/j.geothermics.2012.10.004.

Revesz, A., Chaer, I., Thompson, J., Mavroulidou, M., Gunn, M. and Maidment, G. (2016) Ground source heat pumps and their interactions with underground railway tunnels in an urban environment: A review, *Applied Thermal Engineering*, 93, pp. 147–154. DOI:10.1016/j.applthermaleng.2015.09.011.

Rivera, J. A., Blum, P. and Bayer, P. (2017) Increased ground temperatures in urban areas: Estimation of the technical geothermal potential, *Renewable Energy*, 103, pp. 388–400. DOI:10.1016/j.renene.2016.11.005.

Sadokierski, S. and Thiffeault, J.-L. (2008) Heat Transfer in Underground Rail tunnels. Available from: http://arxiv.org/pdf/0709.1748.pdf [Accessed 17 March 2015].

Secretary of State for Energy and Climate Change (2009) The UK Renewable Energy Strategy. HM Government. Available from: https://www.gov.uk/government/uploads/system/uploads/attachment_data/file/228866/7686.pdf [Accessed 17 March 2015].

Stylianou, I. I., Florides, G., Tassou, S., Tsiolakis, E. and Christodoulides, P. (2017) Methodology for estimating the ground heat absorption rate of Ground Heat Exchangers, *Energy*, 127, pp. 258–270. DOI:10.1016/j.energy.2017.03.070.

TfL (2013) Civil Engineering – Common Requirements, Category 1 Standard.

The Greater London Authority and Buro Happold (2013) *LONDON'S ZERO CARBON ENERGY RESOURCE*. Available from: http://www.london.gov.uk/sites/default/files/031250%20GLA%20Secondary%20Heat%20-%20Summary%20Report.pdf. [Accessed 11 December 2015].

The Stationery Office (2008) Climate Change Act 2008. Available from: http://www.legislation.gov.uk/ukpga/2008/27/pdfs/ukpga_20080027_en.pdf [Accessed 2 October 2014].

Thermal Dynamics Inc. (2017) GLD Software - Windows™-based revolutionary geothermal HVAC software design package. Available from: http://www.groundloopdesign.com/ [Accessed 20 May 2017].

Thomas, H. S. (1977) Measuring the structural performance of cast Iron tunnel linings in the laboratory, *Ground Engineering*, 10 (5). Available from: https://trid.trb.org/view.aspx?id=73541 [Accessed 4 March 2017].

Thompson, J. (2014) Dynamo - Enhancing Tunnel Ventilation Modelling, *Parsons Brinckerhoff - Network*, 78, pp. 63–66.

Thompson, J. (2006) *Sustainable cooling of underground railways through enhancement of the heat sink effect*. PhD thesis, London South Bank University, London, UK.

Thompson, J., Missenden, J. F., Gilbey, M. and Maidment, G. G. (2009) Response of wall heat transfer to steady and transient flows along a cylindrical cavity, in: New Brunswick, New Jersey, USA.

Thompson, J., Gilbey, M. and Maidment, G. (2008) Geothermal cooling of underground railways-the opportunity, in: UK, London: The Institute of Refrigeration, Volume 105.

Thompson, J. and Maidment, G. (2010) Alternative geothermal heating sources, heat pumps and their application, in: *1st IIR International Conference on the Cold Chain and Sustainability*. Cambridge, UK.

Thornton, J. W., McDowell, T. P., Shonder, J. A., Hughes, P. J., Pahud, D. and Hellstrom, G. A. (1997) Residential vertical geothermal heat pump system models: calibration to data, *Transactions-American Society of Heating Refrigerating And Air Conditioning Engineers*, 103, pp. 660–674.

Tideway (2016) Tideway | Reconnecting London with the River Thames, *Tideway*. Available from: http://www.tideway.london [Accessed 12 March 2017].

Ting, Y. S., Gilbey, M. J., Drake, S. N., Missenden, J. F. and BHR Group Limited (2009) CFD estimation of heat transfer enhancement on a cooling pipe in underground railway tunnels, in: pp. 629–644.

Transport for London (2016) Rolling stock, *Transport for London*. Available from: https://www.tfl.gov.uk/corporate/about-tfl/what-we-do/london-underground/rolling-stock [Accessed 17 January 2017].

TRNSYS (2017) Welcome | TRNSYS: Transient System Simulation Tool. Available from: http://www.trnsys.com/ [Accessed 20 May 2017].

Vardy, A. E. (2001) User Manual, ThermoTun/5.2. Dundee Tunnel Research.

VDI (2009) Thermal use of the underground - Ground source heat pump systems, VDI 4640 Part 2. The Association of German Engineers.

Weibo, Y., Mingheng, S. and Zhengian, C. (2009) A Variable Heat Flux Line Source Model for Boreholes in Ground Coupled Heat Pump, in: *Power and Energy Engineering Conference, 2009. APPEEC 2009. Asia-Pacific*. pp. 1–4.

Wilson, G. and Grace, H. (1942) The settlement of London due to underdrainage of the London clay., *Journal of the Institution of Civil Engineers*, 19 (2), pp. 100–127. DOI:10.1680/ijoti.1942.13846.

Winterling, R., Nicholson, D. P., Winter, A., Chen, Q. and de Silva, M. (2014) The design of thermal tunnel energy segments for Crossrail, UK, *Proceedings of the ICE - Engineering Sustainability*, 167, pp. 118–134.

Yebiyo, M., Maidment, G., Paurine, A. and Day, T. (2016) *Optimisation of inter-seasonal ground source heat pumps with predictive behavioural control.* PhD thesis, London South Bank University London, UK.

Zanchini, E., Lazzari, S. and Priarone, A. (2012) Long-term performance of large borehole heat exchanger fields with unbalanced seasonal loads and groundwater flow, *Energy*, 38 (1), pp. 66–77. DOI:10.1016/j.energy.2011.12.038.

Zeng, H. Y., Diao, N. R. and Fang, Z. H. (2002) A finite line-source model for boreholes in geothermal heat exchangers, *Heat Transfer—Asian Research*, 31 (7), pp. 558–567.

APPENDIX A: 2D MODEL STRUCTURE INFORMATION

1. USED PRODUCT

COMSOL Multiphysics
Heat Transfer Module

2. GLOBAL SETTINGS

Name	Basic 2D model
COMSOL version	COMSOL 5.2a (Build: 229)
Unit system	SI

3. COMPUTATION INFORMATION

CPU	Intel(R) Core(TM) i7-4800MQ CPU @ 2.70GHz, 4 cores
Operating system	Windows 7

4. STUDY TYPE: Time dependent

Times	Unit
range(0,1,(365*5))	d

5. PARAMETERS

Name	Expression	Value	Description
width_s	150[m]	150 m	Random
height_s	100[m]	100 m	Random
diam_bhe	0.75[m]	0.75 m	CEREB
radius_bhe	diam_bhe/2	0.375 m	
depth_bhe	-27[m]	−27 m	CEREB
radius_tunnel	1.70 [m]	1.7 m	(Sadokierski and Thiffeault, 2008)
crosssection_tunnel	pi*radius_tunnel^2	9.0792 m²	
Av_air	11.7[degC]	284.85 K	(Headon et al., 2009)
amp	13	13	(Headon et al., 2009)
year	31536000[s]	3.1536E7 s	
k_clay	1.3 [W/(m*K)]	1.3 W/(m·K)	Thompson J (Thesis)
rho_clay	1920 [kg/m^3]	1920 kg/m³	Thompson J (Thesis)
cp_clay	790 [J/(kg*K)]	790 J/(kg·K)	Thompson J (Thesis)
geo_grad	0.026 [K/m]	0.026 K/m	(Busby, 2009)

Name	Expression	Value	Description
Earth_flux	0.075 [W/m^2]	0.075 W/m²	(Zheng, 2013)
made_ground	2[m]	2 m	(Paul, 2009)
Thames_alluvium	2[m]	2 m	(Paul, 2009)
Rivert_depos	4[m]	4 m	(Paul, 2009)
London_clay	92[m]	92 m	(Environmental Agency, 2014)
k_madeg	3.2 [W/(m*K)]	3.2 W/(m·K)	(CTP, 2009)
rho_madeg	1800 [kg/m^3]	1800 kg/m³	(CTP, 2009)
cp_madeg	6889 [J/(kg*K)]	6889 J/(kg·K)	calculated using CTP diffusivity info
k_alluvium	1.25 [W/(m*K)]	1.25 W/(m·K)	(CTP, 2009)
rho_alluvium	1800 [kg/m^3]	1800 kg/m³	(CTP, 2009)
cp_alluvium	1076 [J/(kg*K)]	1076 J/(kg·K)	calculated using CTP diffusivity info
k_terrace	0.95 [W/(m*K)]	0.95 W/(m·K)	(CTP, 2009)
rho_terrace	2000 [kg/m^3]	2000 kg/m³	(CTP, 2009)
cp_terrace	920 [J/(kg*K)]	920 J/(kg·K)	calculated using CTP diffusivity info
hydcond_clay	2.2E-10 [m/s]	2.2E−10 m/s	(Diao et al., 2004)
hydcond_gravel	3.0E-3 [m/s]	0.003 m/s	(Diao et al., 2004)
porosity_clay	0.47	0.47	(Diao et al., 2004)
porosity_gravel	0.31	0.31	(Diao et al., 2004)
distx_b	100	100	Randomly selected
distx_t	50 - radius_tunnel	48.3 m	Randomly selected
depth_t	-24[m]	−24 m	Thompson et al.,(2008)
height_bhe	depth_bhe* - 1	27 m	CEREB
load_ampl	18[W/m]	18 W/m	CEREB
add	17.5[degC]	290.65 K	
point_x	((distx_b + radius_tunnel) + distx_t)/2	75 m	

6. VARIABLES

Geometric entity level	Entire model

Name	Expression	Unit
T_surf	amp*sin((2*pi*t)/year) + Av_air	K

Name	Expression	Unit
T_initial	Av_air - geo_grad*(y)	K
BHE_load1	load_ampl*sin((2*pi*t)/year)	W/m
T_tunnel	(0.36*(T_surf - 273)) + add	K

7. GEOMETRY

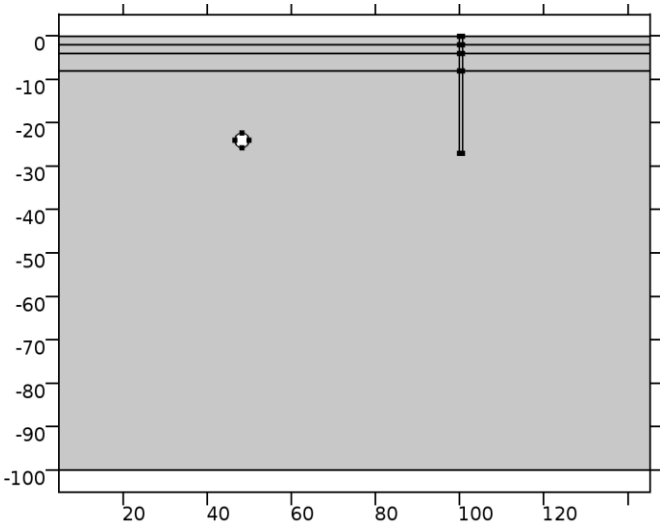

Units

Length unit	m
Angular unit	deg

Geometry statistics

Description	Value
Space dimension	2
Number of domains	7
Number of boundaries	30
Number of vertices	25

Soil

Position

Description	Value
Position	{0, -100}
Layers on bottom	Off
Layers on top	On

Layer name	Thickness (m)
Made Ground	made_ground
Thames Alluvium	Thames_alluvium
River terrace deposits	Rivert_depos

Size

Description	Value
Width	width_s
Height	height_s

Tunnel

Position

Description	Value
Position	{distx_t, depth_t}

Size and shape

Description	Value
Radius	radius_tunnel

BHE

Position

Description	Value
Position	{distx_b, depth_bhe}

Size

Description	Value
Width	diam_bhe
Height	height_bhe

8. MATERIALS

Made Ground

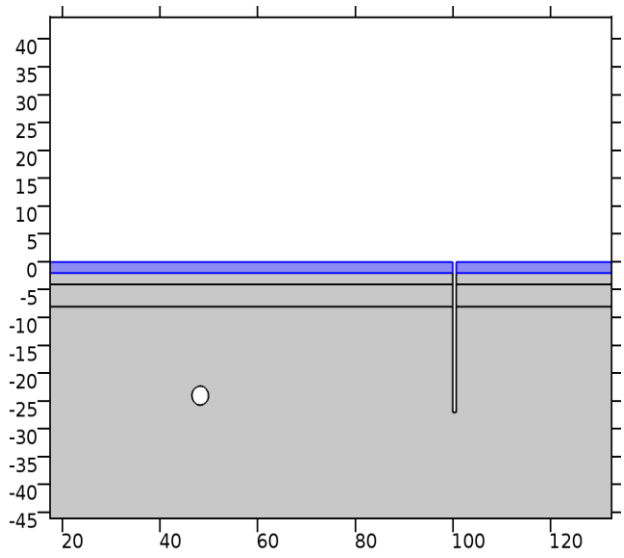

Selection

Geometric entity level	Domain
Selection	Domains 4, 7

Material properties

Name	Value	Unit
Thermal conductivity	k_madeg	W/(m·K)
Density	rho_madeg	kg/m³
Heat capacity at constant pressure	cp_madeg	J/(kg·K)
Ratio of specific heats	1	1

Thames Alluvium

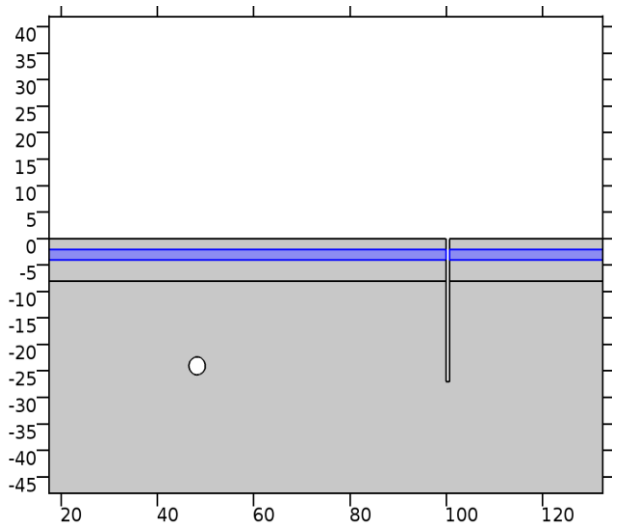

Selection

Geometric entity level	Domain
Selection	Domains 3, 6

Material properties

Name	Value	Unit
Thermal conductivity	k_alluvium	W/(m·K)
Heat capacity at constant pressure	cp_alluvium	J/(kg·K)
Density	rho_alluvium	kg/m³
Ratio of specific heats	1	1

River Terrace Deposits

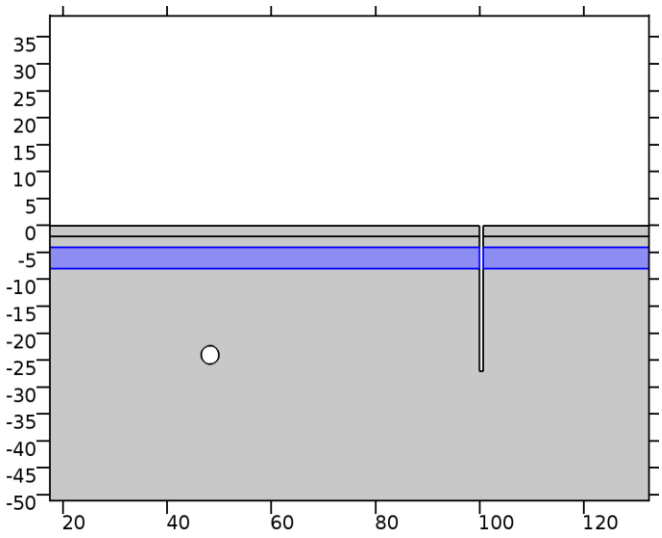

Selection

Geometric entity level	Domain
Selection	Domains 2, 5

Material properties

Name	Value	Unit
Thermal conductivity	k_terrace	W/(m·K)
Density	rho_terrace	kg/m³
Heat capacity at constant pressure	cp_terrace	J/(kg·K)
Ratio of specific heats	1	1

London Clay

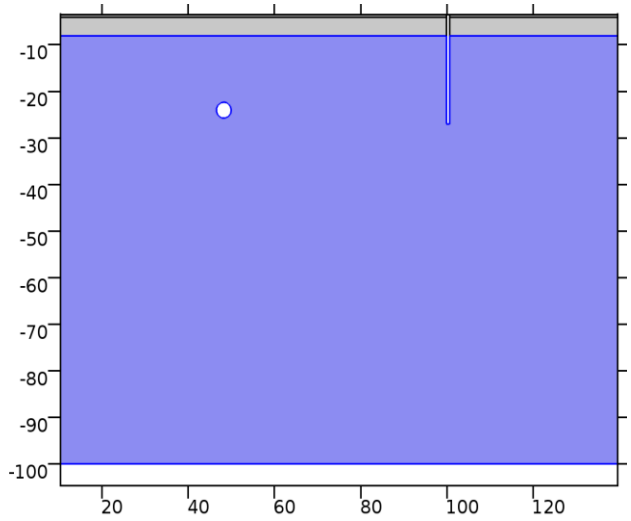

Selection

Geometric entity level	Domain
Selection	Domain 1

Material properties

Name	Value	Unit
Thermal conductivity	k_clay	W/(m·K)
Density	rho_clay	kg/m³
Heat capacity at constant pressure	cp_clay	J/(kg·K)
Ratio of specific heats	1	1

9. PHYSICS: HEAT TRANSFER IN POROUS MEDIA

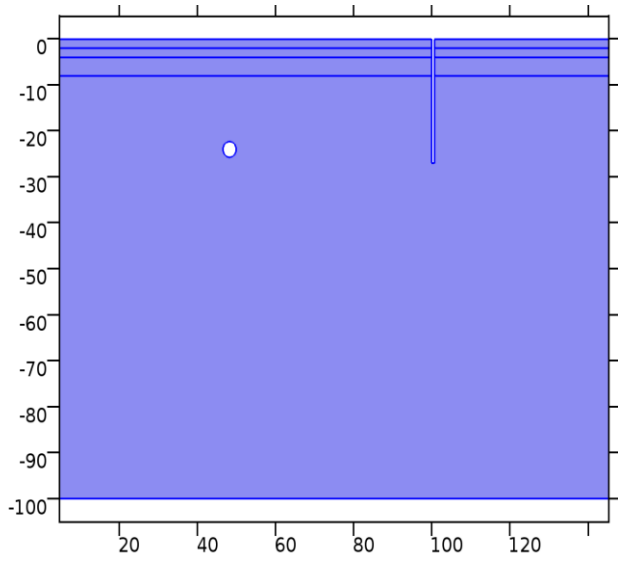

Selection

Geometric entity level	Domain
Selection	Domains 1–7

10. BOUNDARY CONDITIONS

Initial condition: Temperature gradient

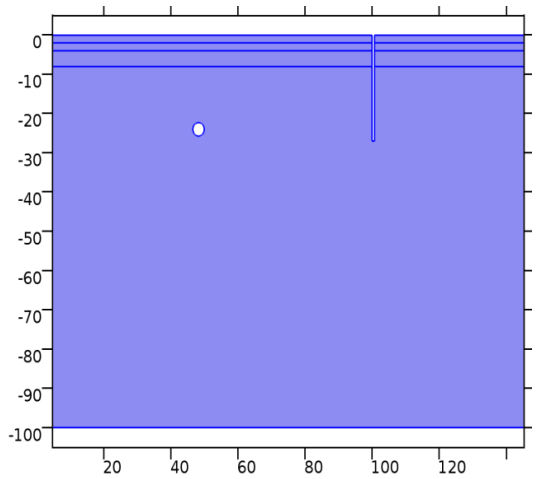

Selection

Geometric entity level	Domain
Selection	Domains 1–7

Settings

Description	Value
Temperature	T_initial
Temperature	User defined

Thermal Insulation

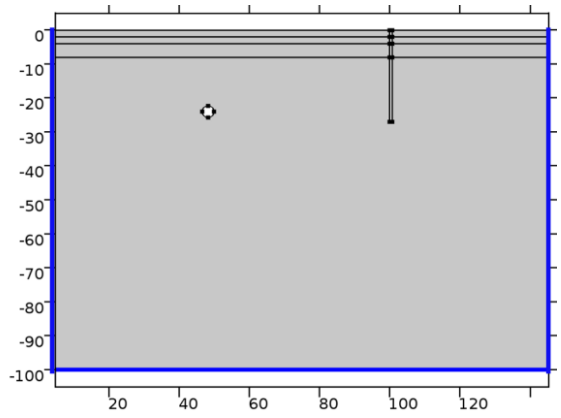

Selection

Geometric entity level	Boundary
Selection	Boundaries 1–3, 5, 7, 23–26

Heat Flux

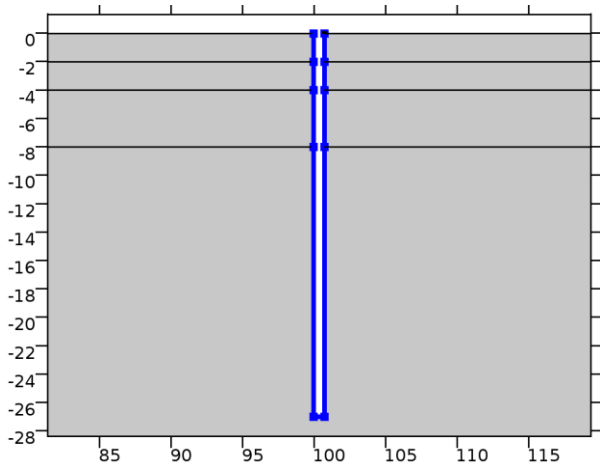

Selection

Geometric entity level	Boundary
Selection	Boundaries 10–16, 18, 20

Settings

Description	Value
Heat flux	General inward heat flux
Inward heat flux	BHE_load/(2*pi*radius_bhe)

Temperature 1

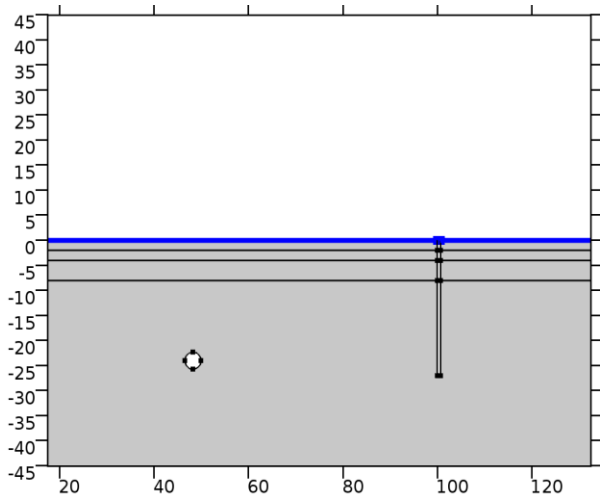

Selection

Geometric entity level	Boundary
Selection	Boundaries 9, 22

Settings

Description	Value
Temperature	T_surf
Constraint method	Elemental
Temperature	User defined

Temperature 2

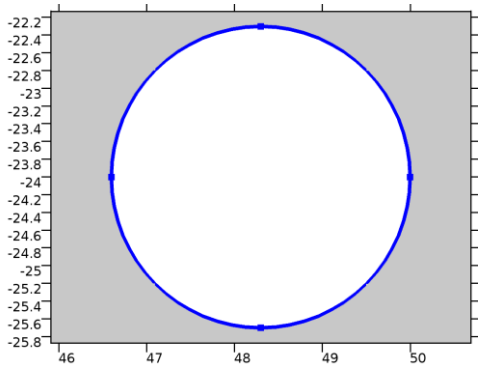

Selection

Geometric entity level	Boundary
Selection	Boundaries 27–30

Settings

Description	Value
Temperature	T_tunnel
Constraint method	Elemental
Temperature	User defined

11. MESH

Mesh statistics

Description	Value
Minimum element quality	0.5318
Average element quality	0.9279

Description	Value
Triangular elements	1807
Edge elements	311
Vertex elements	25

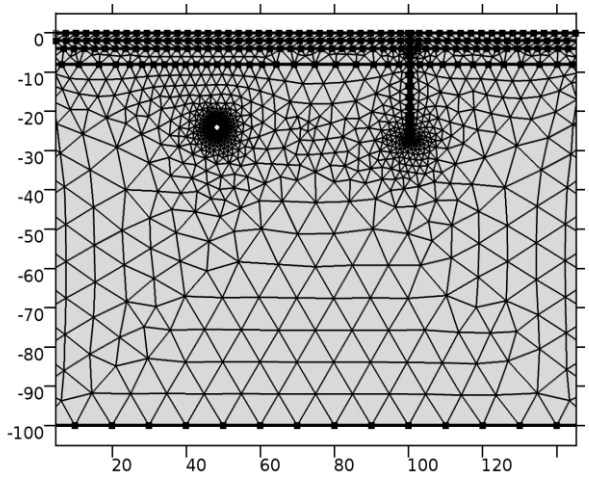

Mesh Refinement

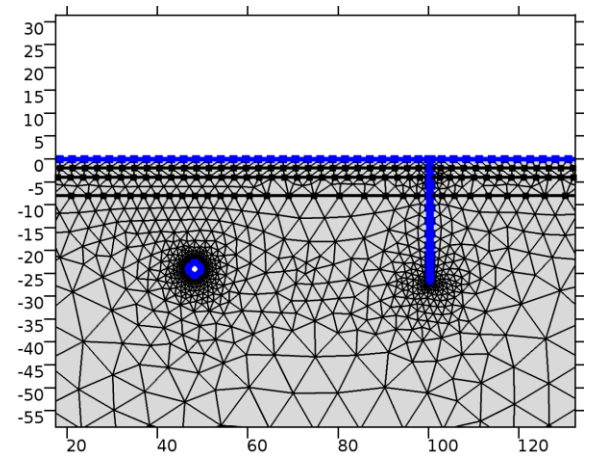

Selection

Geometric entity level	Boundary
Selection	Boundaries 9–16, 18, 20, 22, 27–30

APPENDIX B: MESH ANALYSIS

Appendix B includes three different mesh independency analyses. One is for the 2D preliminary model and the other two is for the 3D UR and GHE models independently.

2D Preliminary Model

The blue point on Figure A represents the middle point between the tunnel and GHE walls. The temperature of that point during a 2 years simulation period was measured and compared. The tested mesh configurations were included an extremely coarse, a coarser, a fine and an extra fine configuration. The structures of these configurations and the simulation results from each of these at day 240 of the simulation period are shown in Figures B, C, E and D. The overall results of the analysis are illustrated in Figure F. It can be seen in the figure that the results gained through the fine mesh configurations are almost identical with the results of the extra fine set-up.

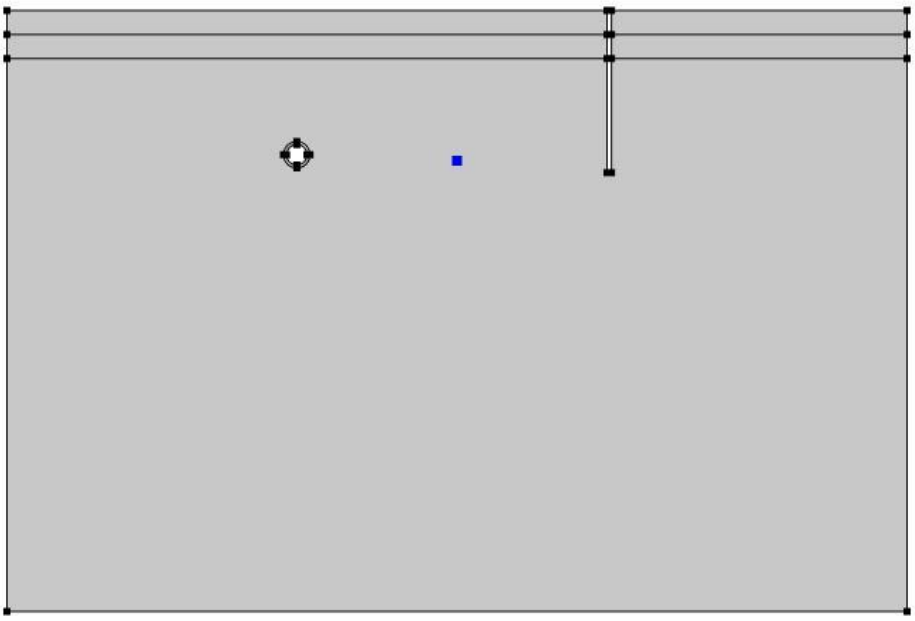

Figure A: Measurement point

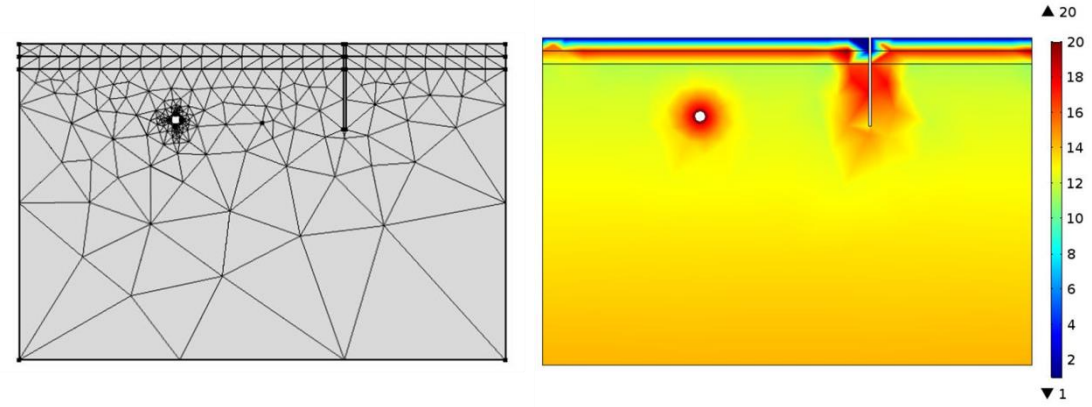

Figure B: Extremely coarse mesh structure with 426 elements (left) and simulated temperatures [˚C] at day 240 (right)

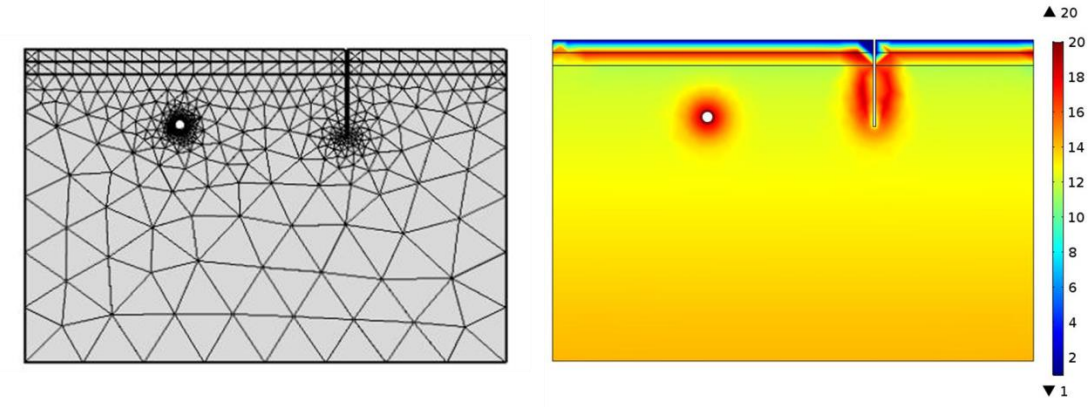

Figure C: Coarser mesh structure with 863 elements (left) and simulated temperatures [˚C] at day 240 (right)

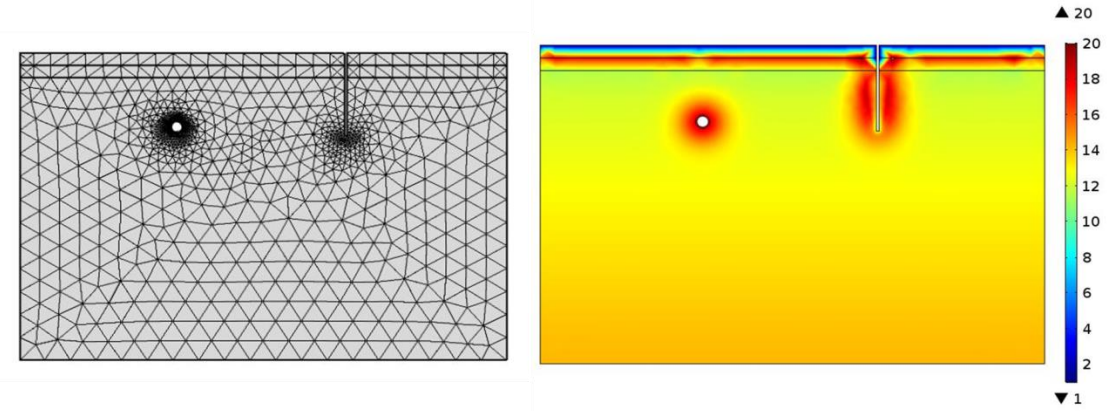

Figure D: Fine mesh structure with 1807 elements (left) and simulated temperatures [˚C] at day 240 (right)

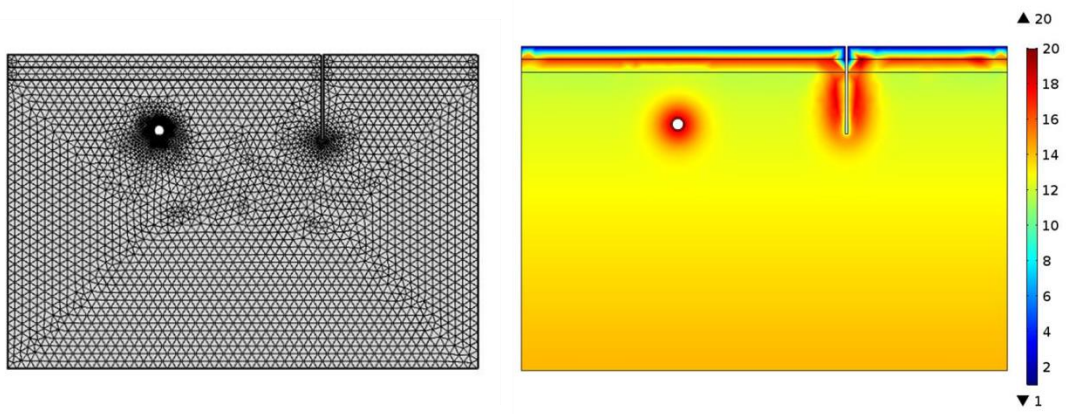

Figure E: Extra fine mesh structure with 5926 elements (left) and simulation results at day 240 (right)

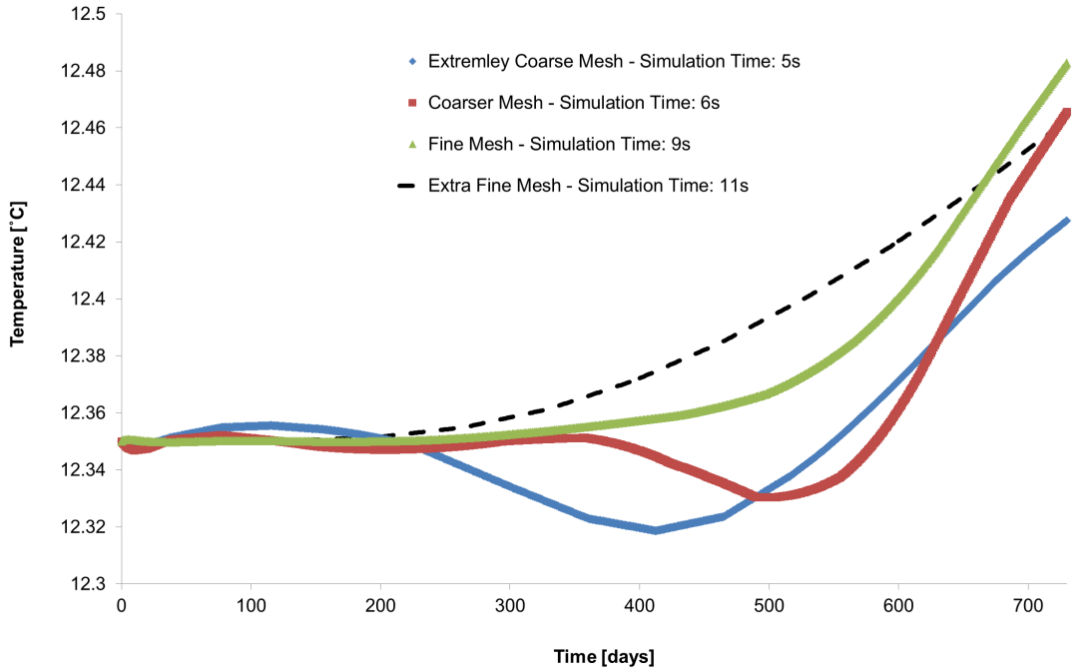

Figure F: Simulation results at the measurement points for the different mesh configurations

3D UR Model

The red point on Figure G represents a measurement point within the 3D UR model domain. The temperature of that point during a 2 years simulation period was measured and compared for three different mesh configurations, which are illustrated in Figure H. It can be seen on the figure that the tested configurations were included a coarse, a fine and an extra fine meshes. Simulation results of the measurement point are illustrated in Figure I. It can be seen that the results from a model with a fine mesh configuration converged to nearly the same values as the model with the extra fine mesh, but being able to achieve that

significantly faster. In particular, the computational time decreased from 38 min to 14 min when the number of mesh elements was reduced from the extra fine to the fine scenario.

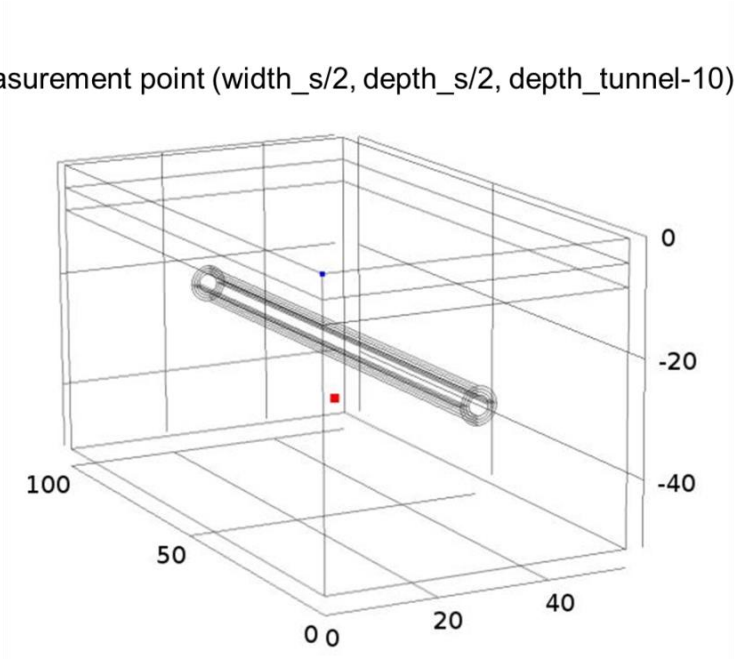

Figure G: Measurement point

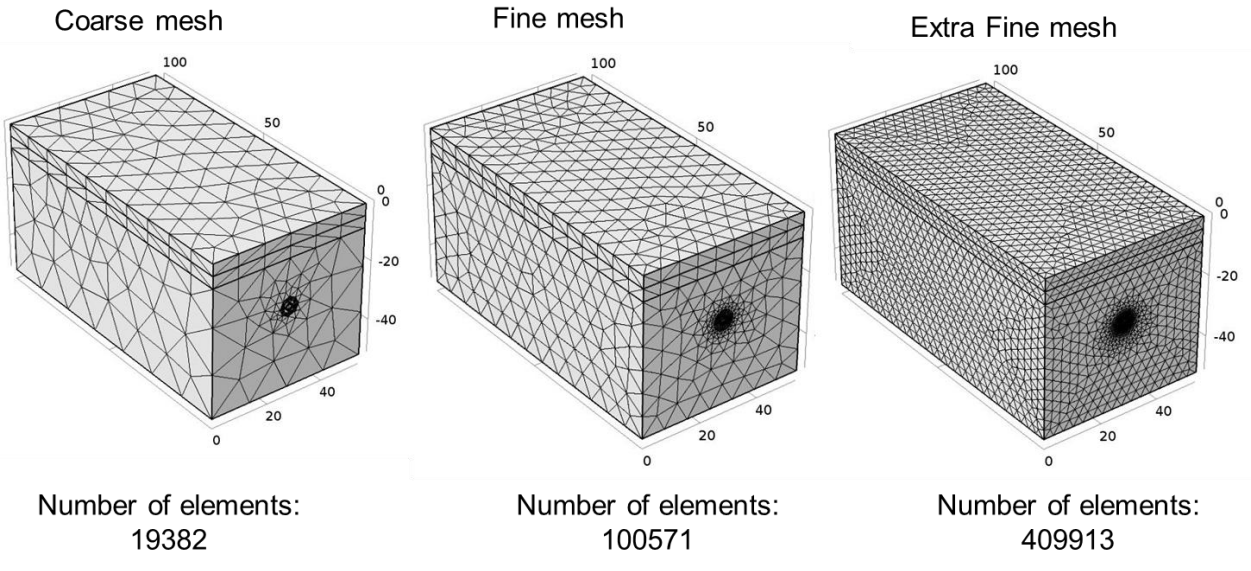

Figure H: The three different 3D UR model mesh configurations compared

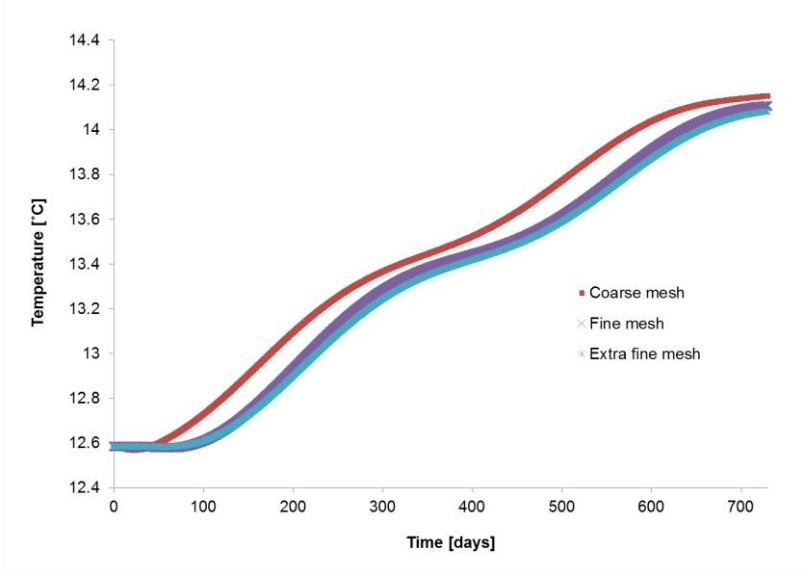

Figure I: Simulation results at the measurement point for the three different mesh configurations

3D GHE Model

Four unstructured meshes made of tetrahedral elements were tested for the 3D single looped GHE model. These configurations are illustrated in Figure J. It can be seen in the figure that the finest mesh contained 275373 while the coarsest mesh included 8386 domain elements. Temperature values at a specific point which is illustrated in Figure K were compared for the four different mesh configurations. The results of these comparisons are illustrated in Figure L.

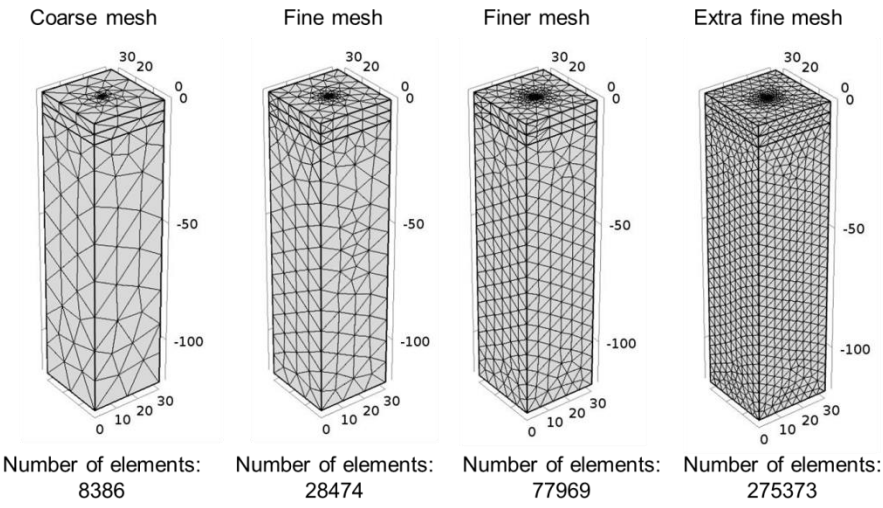

Figure J: The four different mesh configurations for the 3D GHE model

The results in Figure L show that when the model was constructed with finer mesh elements, the simulation converges to almost the same values of the ones generated by the extra fine mesh configuration. This was achieved with a significantly lower number of mesh elements and with substantial reduction in computational time, i.e. from 1 hour 20 min from the extra fine to 33 min in the finer mesh configuration.

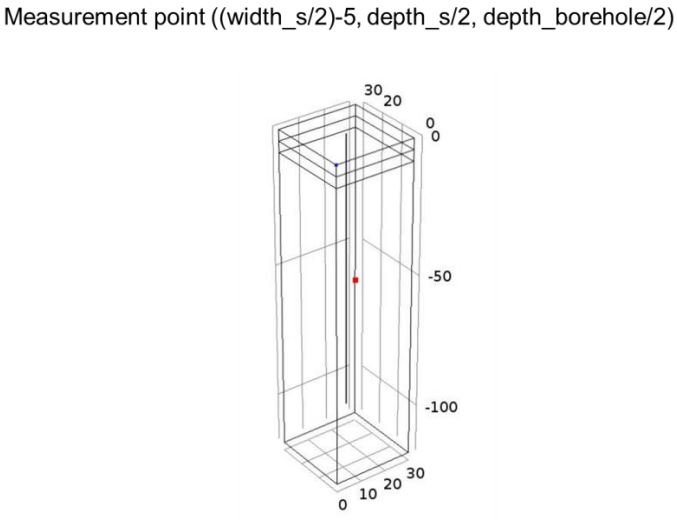

Figure K: Measurement point

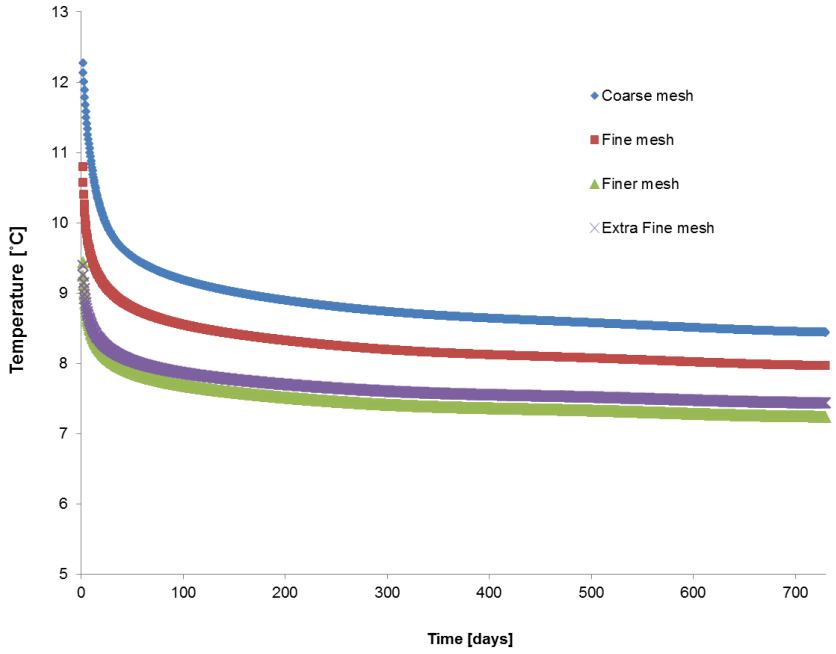

Figure L: Simulation results at the measurement point for the four different mesh configurations

APPENDIX C: 3D UR MODEL-A STRUCTURE INFORMATION

1. USED PRODUCT

COMSOL Multiphysics
Heat Transfer Module

2. GLOBAL SETTINGS

Name	UR MODEL A
COMSOL version	COMSOL 5.2a
Unit system	SI

3. COMPUTATION INFORMATION

CPU	Intel(R) Core(TM) i7-4800MQ CPU @ 2.70GHz, 4 cores
Operating system	Windows 7

4. STUDY TYPE: Time dependent

Times	Unit
range(0,1,(365*5))	d

5. PARAMETERS

Name	Expression	Value	Description
width_s	(25*2) + diam_tun	54.4 m	
depth_s	100[m]	100 m	
Av_air	11.7[degC]	284.85 K	(Headon et al., 2009)
amp	13	13	(Headon et al., 2009)
year	31536000[s]	3.1536E7 s	
geo_grad	0.026 [K/m]	0.026 K/m	(Busby, 2009)
add	17.5[degC]	290.65 K	
MadeG_layer	4	4	Combined CTP
ThamesGravel_layer	4	4	Combined CTP
ClayorSand_layer	43.2	43.2	Conference paper
k_madeg	2.2 [W/(m*K)]	2.2 W/(m·K)	Combined CTP
cp_madeg	3982 [J/(kg*K)]	3982 J/(kg·K)	Combined CTP
rho_madeg	1800 [kg/m^3]	1800 kg/m³	CTP
k_gravels	0.95 [W/(m*K)]	0.95 W/(m·K)	CTP

Name	Expression	Value	Description
cp_gravels	920 [J/(kg*K)]	920 J/(kg·K)	CTP
rho_gravels	2000 [kg/m^3]	2000 kg/m³	CTP
perm_gravel_a	3.0E-3 [m/s]	0.003 m/s	(Diao et al., 2004)
porosity_gravel	0.31	0.31	(Diao et al., 2004)
k_clay	1.3[W/(m*K)]	1.3 W/(m·K)	Jolyon thesis
rho_clay	1920 [kg/m^3]	1920 kg/m³	Jolyon thesis
cp_clay	790 [J/(kg*K)]	790 J/(kg·K)	Jolyon thesis
dH	1	1	Hydraulic head
radius_tunnel	1.7 [m]	1.7 m	(Sadokierski and Thiffeault, 2008)
depth_tdeep	-24[m]	−24 m	
Tun_outerradius	radius_tunnel + thick_lining	2.2 m	
thick_lining	0.5[m]	0.5 m	
distx_tunnel	width_s/2	27.2 m	
depth_tunnel	-24[m]	−24 m	
h0	5[W/m^2/K]	5 W/(m²·K)	Reference heat transfer coefficient
T_av	11.7[degC]	284.85 K	Average annual temperature
T_A	13[degC]	286.15 K	Annual temperature fluctuation
t_step	3[h]	10800 s	
diam_tun	Tun_outerradius*2	4.4 m	
maxe_size	5	5	

6. VARIABLES

Geometric entity level	Entire model

Name	Expression	Unit
T_surf	amp*sin((2*pi*t)/year) + Av_air	K
T_initial	Av_air - geo_grad*(y)	K
T_tunnel	(0.36*(T_surf - 273)) + add	K

7. GEOMETRY

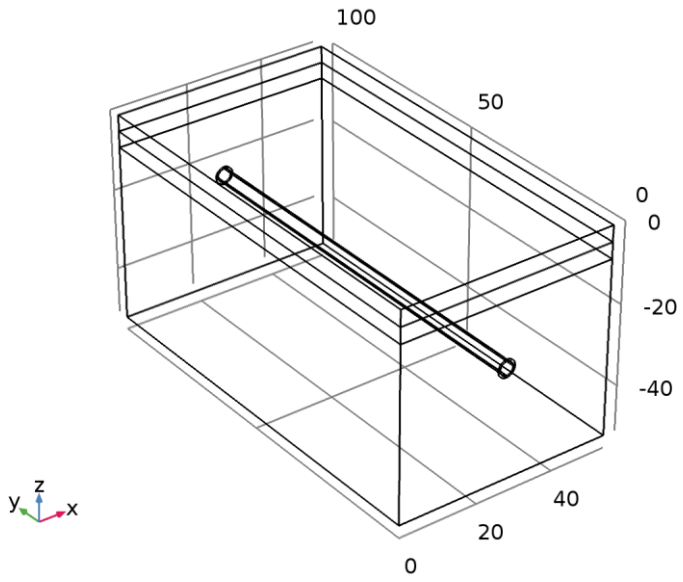

Units

Length unit	m
Angular unit	deg

Geometry statistics

Description	Value
Space dimension	3
Number of domains	5
Number of boundaries	28
Number of edges	52
Number of vertices	32

Work Plane 1: Rectangle

Settings

Description	Value
Plane	xy - plane

Position

Description	Value
Position	{0, 0}

Size

Description	Value
Width	width_s
Height	depth_s

Extrusion 1

Settings

Description	Value
Work plane	Work Plane 1

Distance from plane

Distances (m)
MadeG_layer
MadeG_layer+ThamesGravel_layer
MadeG_layer+ThamesGravel_layer+ClayorSand_layer

Description	Value
Reverse direction	On

Displacements

Displacements xw (m)	Displacements yw (m)
0	0
0	0
0	0

Twist angles

Twist angles (deg)
0
0
0

Work Plane 2: Circle 1

Settings

Description	Value

Description	Value
Plane	xz - plane

Position

Description	Value
Position	{distx_tunnel, depth_tunnel}

Size and shape

Description	Value
Radius	Tun_outerradius

Work Plane 2: Circle 2

Settings

Description	Value
Plane	xz - plane

Position

Description	Value
Position	{distx_tunnel, depth_tunnel}

Size and shape

Description	Value
Radius	radius_tunnel

Extrusion 2

Settings

Description	Value
Work plane	Work Plane 2

Distance from plane

Distances (m)
depth_s

Description	Value
Reverse direction	On

Displacements

Displacements xw (m)	Displacements yw (m)
0	0

Twist angles

Twist angles (deg)
0

8. MATERIALS

Made Ground

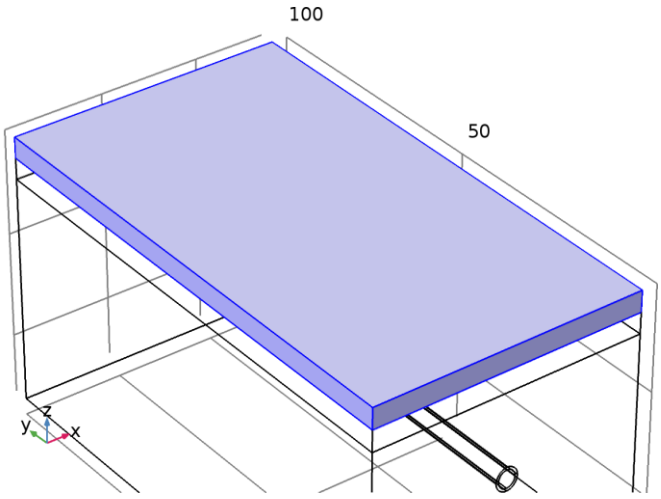

Selection

Geometric entity level	Domain
Selection	Domain 3

Material properties

Name	Value	Unit
Thermal conductivity	k_madeg	W/(m·K)
Density	rho_madeg	kg/m³

Name	Value	Unit
Heat capacity at constant pressure	cp_madeg	J/(kg·K)

Thames Gravels

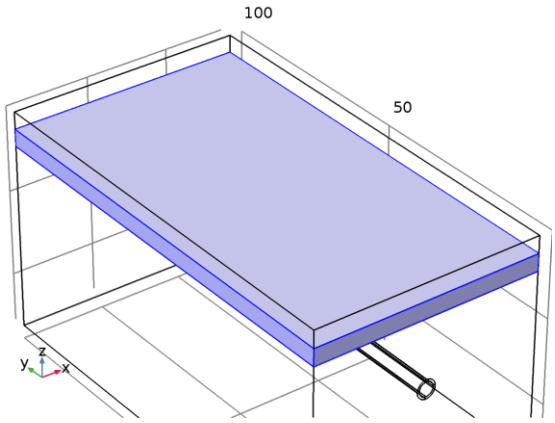

Selection

Geometric entity level	Domain
Selection	Domain 2

Material Properties

Name	Value	Unit
Thermal conductivity	k_gravels	W/(m·K)
Density	rho_gravels	kg/m³
Heat capacity at constant pressure	cp_gravels	J/(kg·K)
Porosity	porosity_gravel	1

London Clay

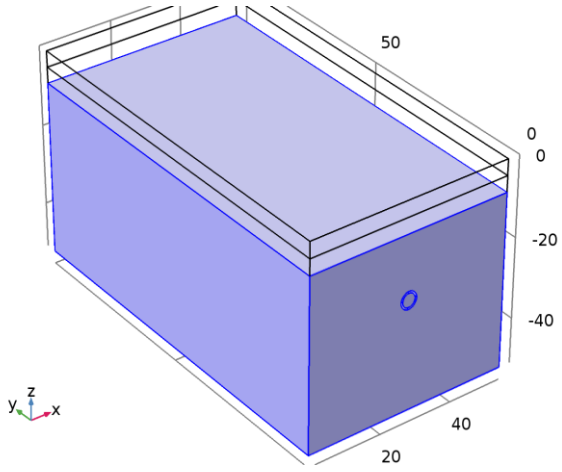

Selection

Geometric entity level	Domain
Selection	Domains 1, 5

Material Properties

Name	Value	Unit
Thermal conductivity	k_clay	W/(m·K)
Density	rho_clay	kg/m³
Heat capacity at constant pressure	cp_clay	J/(kg·K)

Tunnel Liner

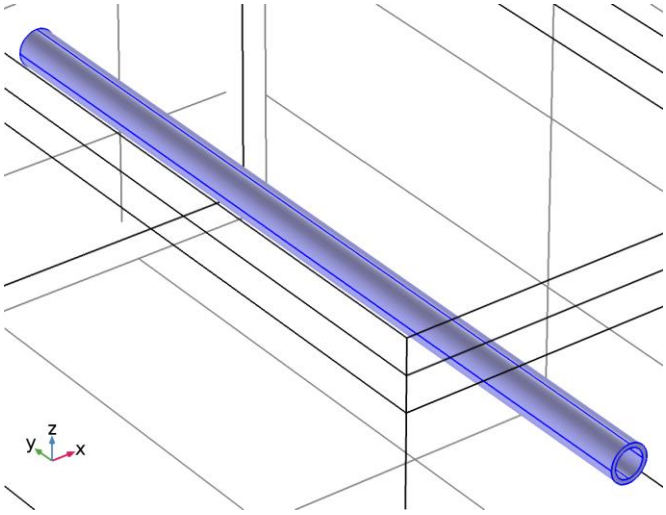

Selection

Geometric entity level	Domain
Selection	Domain 4

Material properties

Name	Value	Unit
Thermal conductivity	1.1	W/(m·K)
Density	2400	kg/m³
Heat capacity at constant pressure	880	J/(kg·K)

9. PHYSICS: HEAT TRANSFER IN POROUS MEDIA

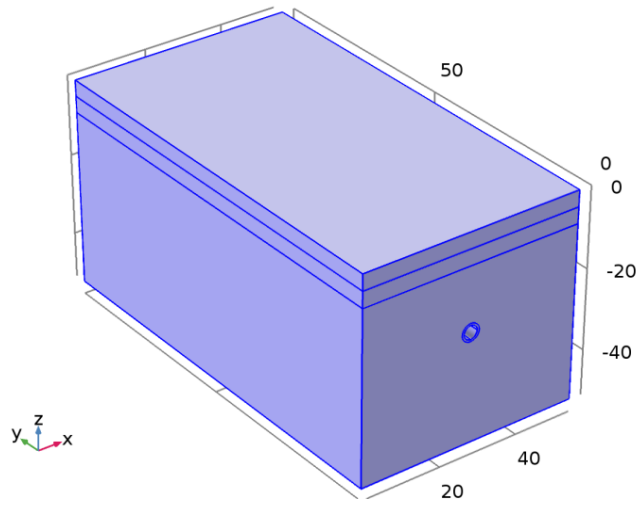

Selection

Geometric entity level	Domain
Selection	Domains 1–4

10. BOUNDARY CONDITIONS

Initial condition: Temperature gradient

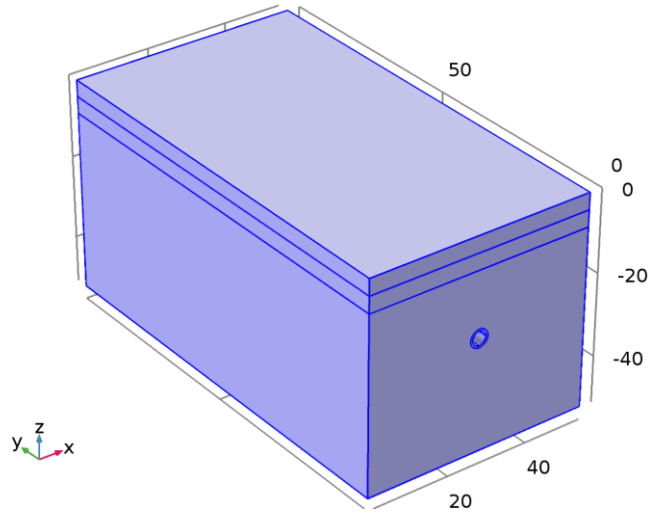

Selection

Geometric entity level	Domain
Selection	Domains 1–4

Settings

Description	Value
Temperature	T_initial
Temperature	User defined

Thermal Insulation

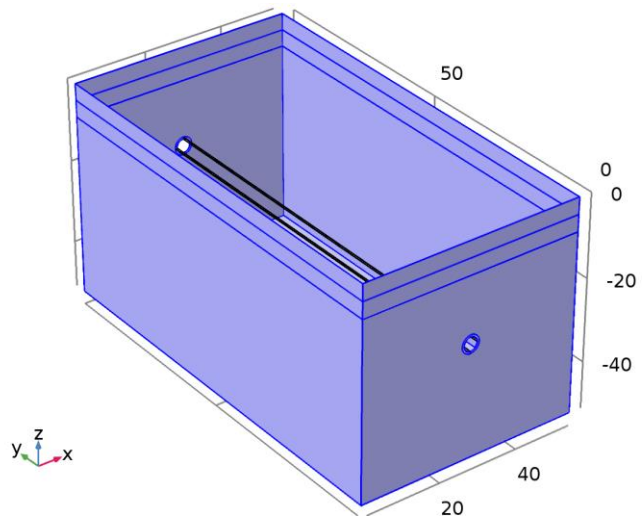

Selection

Geometric entity level	Boundary
Selection	Boundaries 1–5, 7–8, 11–13, 16–17, 26–28

Temperature

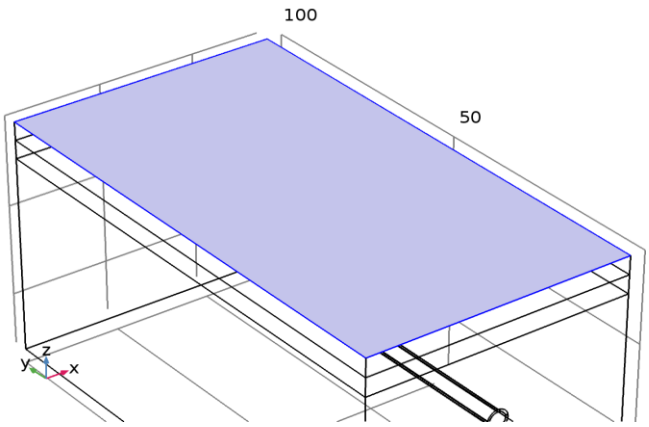

Selection

Geometric entity level	Boundary
Selection	Boundary 10

Settings

Description	Value
Temperature	T_surf
Temperature	User defined

Heat Flux

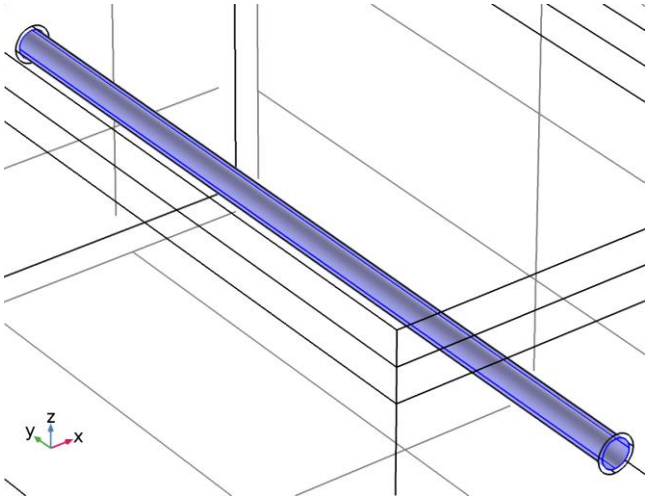

Selection

Geometric entity level	Boundary
Name	Inner wall
Selection	Boundaries 18–19, 23–24

Settings

Description	Value
Heat flux	Convective heat flux
Heat transfer coefficient	User defined
Heat transfer coefficient	pw1(t)
External temperature	T_a(T_av, T_A, t, y)
External temperature	User defined

APPENDIX D: 3D UR MODEL-B STRUCTURE INFORMATION

1. USED PRODUCT

COMSOL Multiphysics
Heat Transfer Module

2. GLOBAL SETTINGS

Name	UR MODEL B
COMSOL version	COMSOL 5.2a
Unit system	SI

3. COMPUTATION INFORMATION

CPU	Intel(R) Core(TM) i7-4800MQ CPU @ 2.70GHz, 4 cores
Operating system	Windows 7

4. STUDY TYPE: Time dependent

Times	Unit
range(0,1,(365*5))	d

5. PARAMETERS

The majority of the parameters are the same as listed in APPENDIX A. The new ones are the following:

Name	Expression	Value	Description
Av_train_heat	284[W/m]	284 W/m	Estimated (see Appendix D)
Av_tun_air_vel	3.5[m/s]	3.5 m/s	Data from LUL

6. GEOMETRY

Differences compared to UR Model-A:

- Air domain fully represented in the tunnel
- A line runs through in the centre of the tunnel which represents the trains

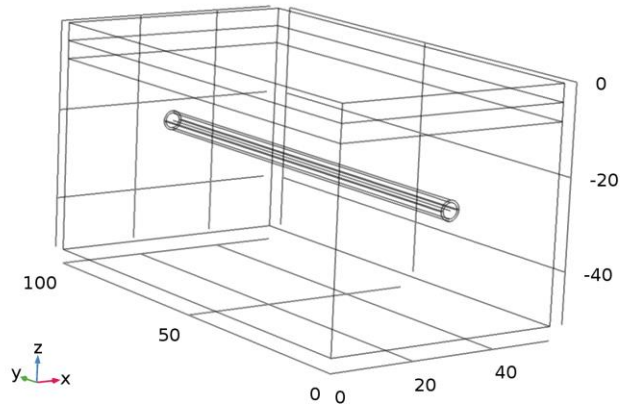

Units

Length unit	m
Angular unit	deg

Geometry Statistics

Description	Value
Space dimension	3
Number of domains	5
Number of boundaries	28
Number of edges	53
Number of vertices	34

7. MATERIALS

Differences compared to UR Model-A: New domain: Air in the middle of the tunnel

- New material: Air

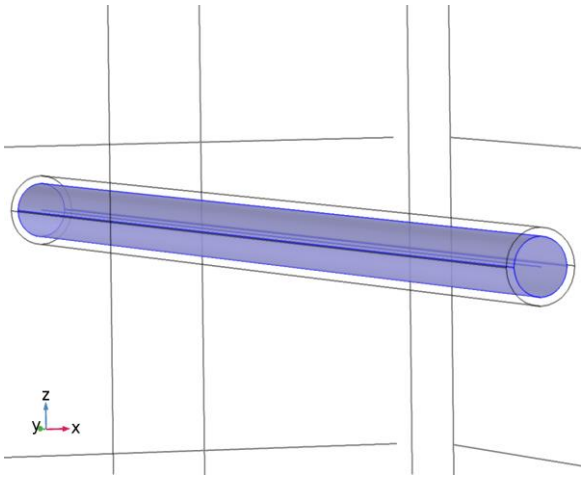

Selection

Geometric entity level	Domain
Selection	Domain 5

Material properties: COMSOL Built in Material Properties for Air

Name	Material	Value	Unit
Dynamic viscosity	Air	eta(T[1/K])[Pa*s]	Pa·s
Ratio of specific heats	Air	1.4	1
Heat capacity at constant pressure	Air	Cp(T[1/K])[J/(kg*K)]	J/(kg·K)
Density	Air	rho(pA[1/Pa],T[1/K])[kg/m^3]	kg/m³
Thermal conductivity	Air	k(T[1/K])[W/(m*K)]	W/(m·K)

8. PHYSICS

Differences compared to UR Model-A:

- Turbulent Air flow: Entire Air domain

Selection

Geometric entity level	Domain
Selection	Domain 5

Settings

Description	Value
Compressibility	Incompressible flow
Turbulence model type	RANS
Turbulence model	Algebraic yPlus
Reference pressure level	1[atm]
Include gravity	Off
Reference temperature	293.15[K]
Streamline diffusion	On
Crosswind diffusion	On

Initial values

Description	Value
Velocity field, x component	0
Velocity field, y component	0

Description	Value
Velocity field, z component	0
Pressure	0
Reciprocal wall distance	spf2.G0
Wall distance in viscous units	spf2.yPlusinit

Wall

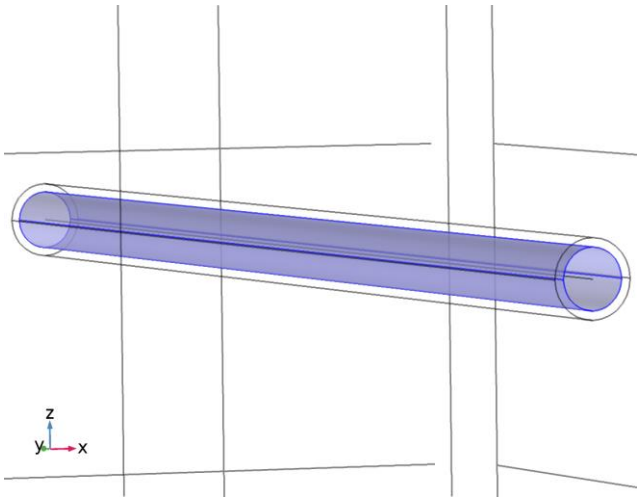

Selection

Geometric entity level	Boundary
Selection	Boundaries 18–19, 23–24

Settings

Description	Value
Boundary condition	No slip
Apply reaction terms on	Individual dependent variables
Use weak constraints	Off
Constraint method	Elemental

9. BOUNDARY CONDITIONS

Differences compared to UR Model-A:

- Temperature boundary condition was added at the tunnel inlet
- Outflow condition at the tunnel outlet
- Air velocity boundary condition was added at the tunnel inlet
- Outlet condition at the tunnel outlet

- Line heat source was added at the centre of the tunnel

Temperature boundary at tunnel inlet

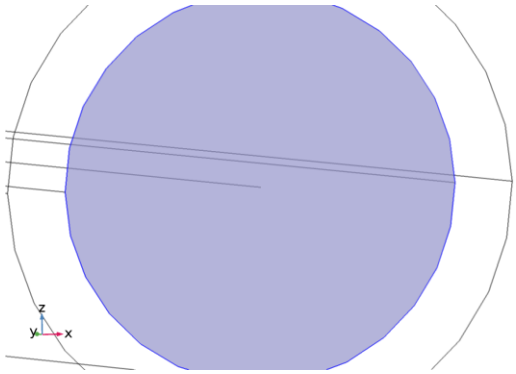

Selection

Geometric entity level	Boundary
Selection	Boundary 20

Settings

Description	Value
Temperature	T_tunnel*step1(t/t_step) + T_initial*(1 - step1(t/t_step))
Temperature	User defined

Outflow condition at the tunnel outlet: this condition states that the only heat transfer occurring across the boundary is by convection. The temperature gradient in the normal direction is zero.

Selection

Geometric entity level	Boundary
Selection	Boundary 21

Air velocity at tunnel inlet

Selection

Geometric entity level	Boundary
Selection	Boundary 20

Settings

Description	Value
Boundary condition	Velocity
Velocity field componentwise	Normal inflow velocity
Normal inflow velocity	Av_tun_air_vel
Use weak constraints	Off
Constraint method	Elemental

Outlet at the tunnel outlet

Selection

Geometric entity level	Boundary
Selection	Boundary 21

Settings

Description	Value
Boundary condition	Pressure
Pressure	0
Normal flow	Off
Suppress backflow	On
Use weak constraints	Off
Apply reaction terms on	All physics (symmetric)
Constraint method	Elemental

Line Heat Source (Train)

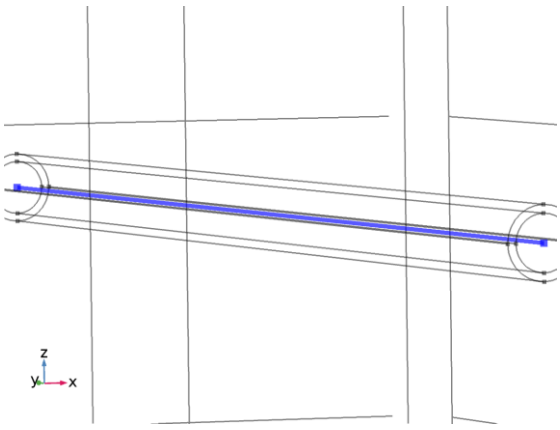

Selection

Geometric entity level	Edge
Selection	Edge 33

Settings

Description	Value
Heat source	General source
Line heat source	Av_train_heat

APPENDIX E: TUNNEL AIR VELOCITY ANALYSIS

Introduction

The investigation detailed in Appendix E studied the effect of tunnel air velocity on the surrounding soil heat transfer. In particular, the thermal effects of short-term (variation in every minute within an hour) and averaged constant tunnel air velocities on the tunnel wall and nearby soil were investigated and compared. The simulation period within the analysis was set at two weeks, thus the thermal effects on the tunnel surroundings were evident. The thermal effects were observed by numerically computing the average temperature of the inner wall surface, and of circular soil segments at 0.5 and 1 m away from the wall of the tunnel. These surface and soil segment locations are illustrated in Figure A.

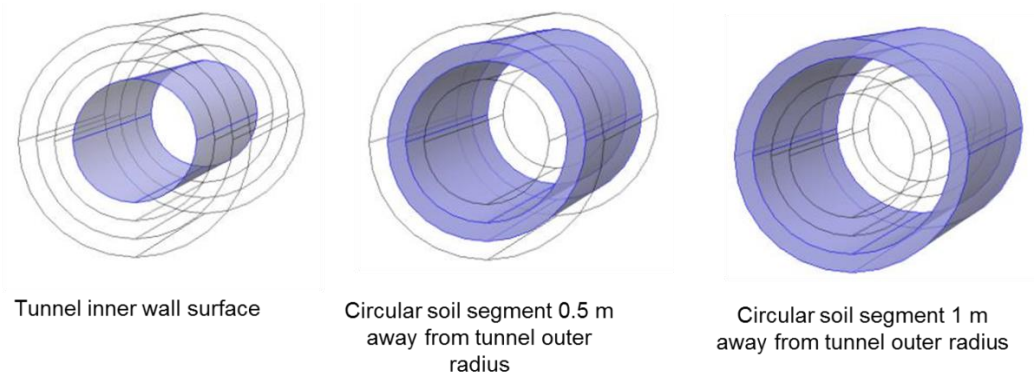

Figure A: Measurement segments

Short-term variation – Variation in an hour

It was assumed that there are 14 trains running per hour on average during a typical operational day. Based on that assumption an hourly tunnel air velocity profile was created and implemented into the numerical model. The profile is illustrated in Figure B. It can be seen on the figure that it was assumed that when trains are passing the air velocity is the highest, 10 m/s and before the next train runs through it goes down to 0.5 m/s.

Long term variation – Hourly averaged (Variation in a day)

The plot of the hourly averaged air velocities are shown in Figure C. The values were selected based on the work of Ting *et al.* (2009) as described in Chapter 5.

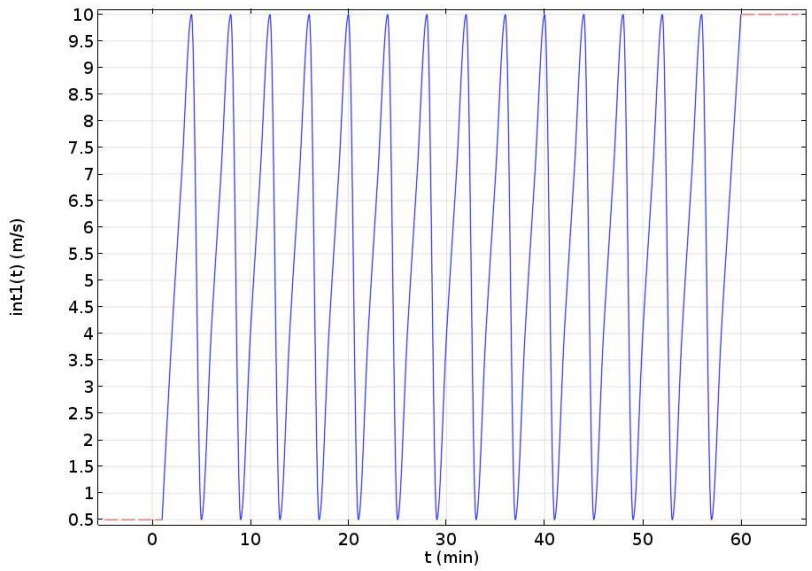

Figure B: Short time variation of tunnel air velocities

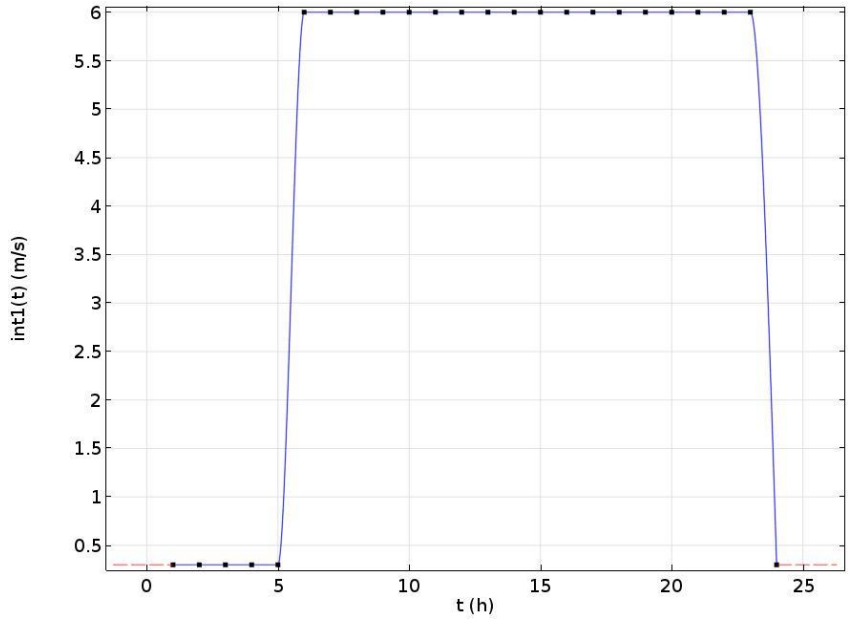

Figure C: Hourly averaged tunnel air velocities

Results

It can be seen in Figure D that when the short term velocity variation was simulated the tunnel wall surface had a smoother temperature increment that when the hourly averaged values were used. This is because the operation of the trains was assumed to be continuous for each hour and each day when the short term velocity fluctuations were simulated. It can be seen that even after 0.5 m away of the wall of the UR tunnel, this effect is much lower

and in about 1 m distance it is almost negligible. The results showed that the conductive heat transfer process in the ground is a much slower progression that the convective transfers at the air wall interface.

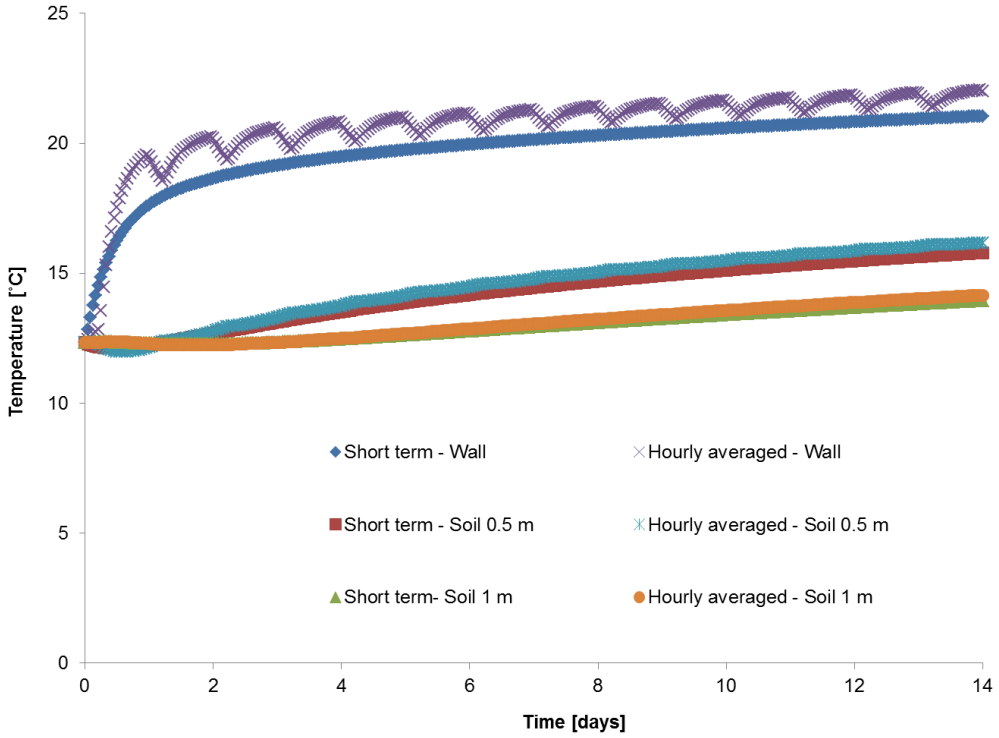

Figure D: Average temperatures at the different measurement segments due to the short term and hourly averaged tunnel air velocity variations

Analysis conclusions

Based on the results of this analysis it can be concluded that with UR-Model A, the hourly averaged air velocity set-up is a practical choice when UR-GSHP interactions are being investigated. This is because the GHEs are not likely to be constructed closer than 3 m to the UR tunnels and at this distance from the wall of the tunnel the short-term and hourly averaged air fluctuations will have no impact on the heat transfers. Simplifying the model by using the hourly averaged tunnel air velocities, the simulation time was reduced by more than 50%. This is a substantial increment in terms of computational efficiencies and therefore using the hourly averaged tunnel air velocities in UR-Model-A is a practical choice.

APPENDIX F: 3D UR MODEL-B TRAIN HEAT LOAD ESTIMATION

In UR Model-B which is presented in chapter 5, a line runs through the centre of the UR within the model geometry. This line represents the operation of the trains which was achieved by assigning a certain heat dissipation rate in W/m to it. The heat dissipation is a highly varying phenomena due to the high train frequency during normal operating hours. In order to reduce this level of complexity within the model an average continuous heat rate was assumed. This value was derived based on detailed discussions with the lead of LU's tunnel ventilation modeling team, Tony Lightfoot (Lightfoot, 2016). Typical trains per hour (TPH) ratios were used to generate hourly averaged heat dissipation rates. The TPH values which were assumed based on Lightfoot (2016) are illustrated in the left side of Figure A. It can be seen in the figure that the highest train frequency is during the morning rush (6-9 am) and evening peak (5-9 pm) hours. Using this assumption the TPH values were converted into hourly averaged heat train heat dissipation rates. This conversion was achieved by using the following assumption in an excel spreadsheet:

*IF(TPH=10,200,(TPH/10)*200)*

The excel formula assumes that the TPH of 10 equates to a typical train heat dissipation rates of 200 W/m. This value was also obtained from Lightfoot (2016). The resulting averaged W/m values from the excel formula are illustrated in the right side of Figure A. It can be seen that the heat dissipation from the trains shows a similar trend to the train frequency and it peaks at around 480 W/m during the rush hours. Based on these values the average daily train heat load was estimated and implemented into the model. This average daily value is 284 W/m, as is highlighted with the green dotted line in Figure A (right). Removing the short term variation in train heat dissipation rates significantly improved computational efficiencies.

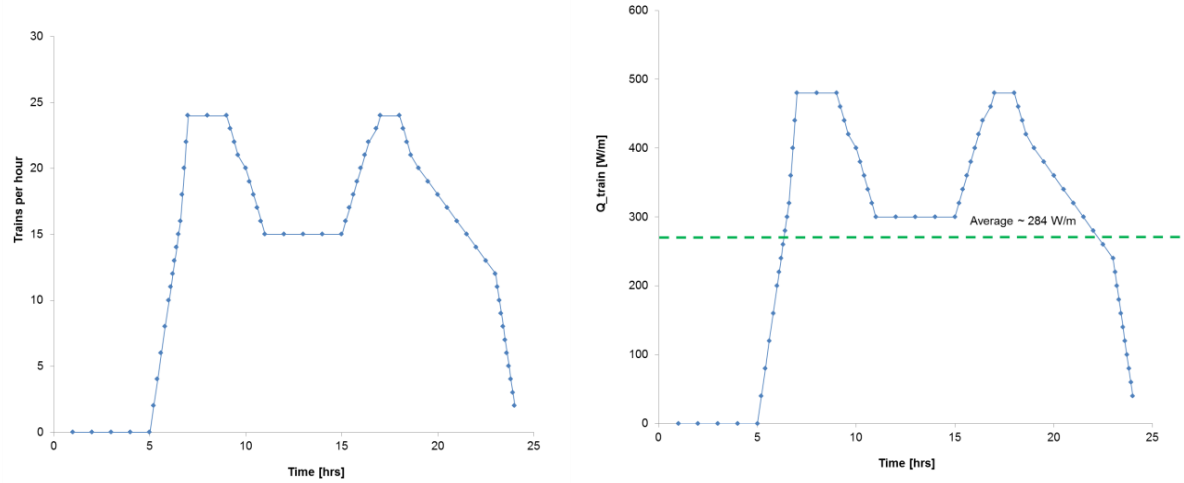

APPENDIX G: 3D GHE MODEL STRUCTURE INFORMATION (SINGLE LOOPED)

1. USED PRODUCT

COMSOL Multiphysics
Heat Transfer Module
Pipe Flow Module

2. GLOBAL SETTINGS

Name	GHE MODEL
COMSOL version	COMSOL 5.2a
Unit system	SI

3. COMPUTATION INFORMATION

CPU	Intel(R) Core(TM) i7-4800MQ CPU @ 2.70GHz, 4 cores
Operating system	Windows 7

4. STUDY TYPE: Time dependent

Times	Unit
range(0,1,(365*5))	d

5. PARAMETERS

Name	Expression	Value
width_s	30[m]	30 m
depth_s	30[m]	30 m
Pipe_inner_dimater	21.5[mm]	0.0215 m
Pipe_wall_thickness	2.4[mm]	0.0024 m
Pipe_outer_diameter	Pipe_inner_dimater + Pipe_wall_thickness	0.0239 m
Spacing_borehole	5[cm]	0.05 m
Borehole_diam	150[mm]	0.15 m
Borehole_radius	Borehole_diam/2	0.075 m
Pipe_radius	Pipe_outer_diameter/2	0.01195 m
Borehole_sand_bentonite_cond	1[W/(m*K)]	1 W/(m·K)
Borehole_sand_bento	1600 [J/(kg*K)]	1600 J/(kg·K)

Name	Expression	Value
nite_cp		
Borehole_sand_bentonite_rho	1500 [kg/m^3]	1500 kg/m³
Dynam_vis_fluid	0.00202	0.00202
Density_fluid	1020.91 [kg/m^3]	1020.9 kg/m³
Depth_borehole	-100[m]	−100 m
cond_lin_pipe	0.39[W/(m*K)]	0.39 W/(m·K)
circ_fluid_flowrate	20[dm^3/min]	3.3333E−4 m³/s
Density_circ_fluid	1020.91[kg/m^3]	1020.9 kg/m³
Specific_heat_circ_fluid	3962[J/(kg*K)]	3962 J/(kg·K)
cond_circ_fluid	0.48[W/(m*K)]	0.48 W/(m·K)
pipe_wall_thick	2.4[mm]	0.0024 m
pipe_cond	0.39[W/(m*K)]	0.39 W/(m·K)

6. GEOMTERY

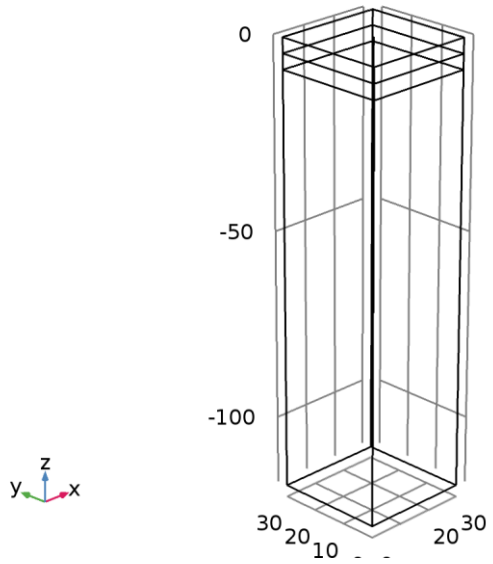

Units

Length unit	m
Angular unit	deg

Geometry statistics

Description	Value
Space dimension	3
Number of domains	6
Number of boundaries	32
Number of edges	63
Number of vertices	40

Work Plane 1: Rectangle

Position

Description	Value
Position	{0, 0}

Size

Description	Value
Width	width_s
Height	depth_s

Work Plane 2: Circle

Position

Description	Value
Position	{width_s/2, depth_s/2}

Size and shape

Description	Value
Radius	Borehole_radius

Extrusion

Distances (m)
Depth_borehole

Work Plane 3: Point 1 and Point 2

Point 1

Description	Value
Point coordinate	{(width_s/2) - (Spacing_borehole/2), depth_s/2}

Point 2

Description	Value
Point coordinate	{(width_s/2) + (Spacing_borehole/2), depth_s/2}

Extrusion

Distances (m)
Depth_borehole+5[cm]

Bézier Polygon 1 (b1)

Polygon segments

Description	Value
Control points	{{(width_s/2) - (Spacing_borehole/2), width_s/2, (width_s/2) + (Spacing_borehole/2)}, {depth_s/2, depth_s/2, depth_s/2}, {Depth_borehole+5[cm], Depth_borehole, Depth_borehole+5[cm]}}
Degree	2
Weights	{1, 1/sqrt(2), 1}
Type	Open curve

7. MATERIAL

Soil layers material properties are the same as with the UR models. New materials:

- Borehole surrounding the GHE pipes (Sand Bentonite)
- Circulated liquid
- GHE pipe wall

Borehole (Sand Bentonite)

Selection

Geometric entity level	Domain
Selection	Domains 4–6

Material properties

Property	Value
Thermal conductivity	Borehole_sand_bentonite_cond
Density	Borehole_sand_bentonite_rho
Heat capacity at constant pressure	Borehole_sand_bentonite_cp

Circulated fluid

Selection

Geometric entity level	Edge
Selection	Edges 30–33, 48–50

Material properties

Name	Value	Unit
Dynamic viscosity	Dynam_vis_fluid	Pa·s
Density	Density_circ_fluid	kg/m³
Thermal conductivity	cond_circ_fluid	W/(m·K)
Heat capacity at constant pressure	Specific_heat_circ_fluid	J/(kg·K)
Ratio of specific heats	1	1

8. PHYSICS

Differences compared to UR Model-A and B:

- Non-Isothermal Pipe Flow
- Pipe wall heat transfer

Non-Isothermal Pipe Flow

Selection

Geometric entity level	Edge
Selection	Edges 30–33, 48–50

Pipe properties

Selection

Geometric entity level	Edge

Selection	Edges 30–33, 48–50

Settings

Description	Value
Pipe shape	Circular
Inner diameter	Pipe_inner_dimater
Friction model	Churchill
Surface roughness	Thermoplastics (0.0015 mm)

Pipe wall heat transfer

Selection

Geometric entity level	Edge
Selection	Edges 30–33, 48–50

Settings

Description	Value
Wall thickness	pipe_wall_thick
Thermal conductivity	pipe_cond

Description	Value
Internal film heat transfer model	Automatic

9. BOUNDARY CONDITIONS

Differences compared to UR Model-A and B:

- Temperature boundary at the GHE pipe inlet
- Heat Outflow at the pipe outlet

Temperature boundary at the pipe inlet

Selection

Geometric entity level	Point
Selection	Point 16

Settings

Description	Value
Temperature	[degC]
Volumetric flow rate	circ_fluid_flowrate

Heat outflow at the pipe inlet

Selection

Geometric entity level	Point
Selection	Point 28

Settings

Description	Value
Pressure	101325[Pa]

APPENDIX J: 3D GHE MODEL STRUCTURE INFORMATION (DOUBLE LOOPED)

The only differences in the double looped GHE model compared to the single looped model are the model geometry and the corresponding model mesh. The physics and boundary conditions are the same, therefore not detailed here.

1. USED PRODUCT

COMSOL Multiphysics
Heat Transfer Module
Pipe Flow Module

2. GLOBAL SETTINGS

Name	GHE MODEL
COMSOL version	COMSOL 5.2a
Unit system	SI

3. COMPUTATION INFORMATION

CPU	Intel(R) Core(TM) i7-4800MQ CPU @ 2.70GHz, 4 cores
Operating system	Windows 7

4. STUDY TYPE: Time dependent

Times	Unit
range(0,1,(365*5))	d

5. PARAMETERS

Name	Expression	Value
Pipe_inner_dimater	21.5[mm]	0.0215 m
Pipe_wall_thickness	2.4[mm]	0.0024 m
Pipe_outer_diameter	Pipe_inner_dimater + Pipe_wall_thickness	0.0239 m
Pipe_radius	Pipe_outer_diameter/2	0.01195 m
Depth_borehole	-27[m]	−27 m
Pile_diameter	45[cm]	0.45 m
Pile_radius	Pile_diameter/2	0.225 m
Spacing_pile_x	10[cm]	0.1 m

Name	Expression	Value
Spacing_pile_y	20[cm]	0.2 m
Pipe_inner_diam_pile	34[mm]	0.034 m
Pipe_wall_thick_pile	3.8[mm]	0.0038 m

6. GEOMETRY

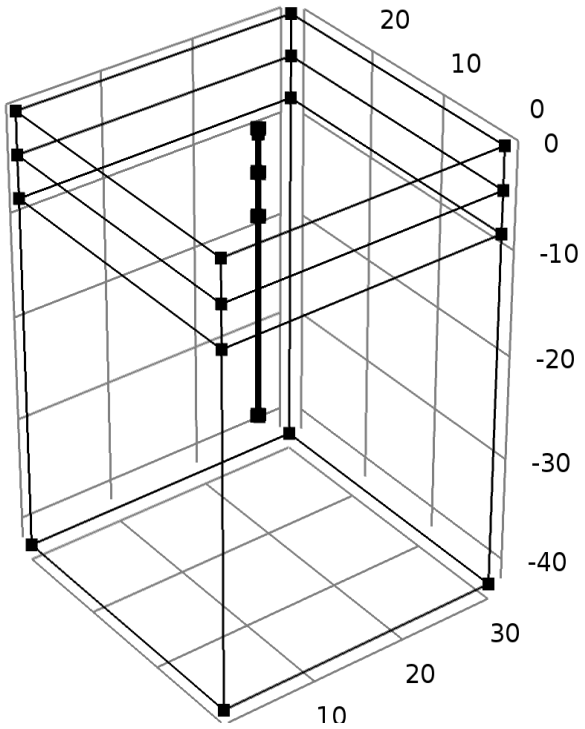

Units

Length unit	m
Angular unit	deg

Geometry Statistics

Description	Value
Space dimension	3
Number of domains	6
Number of boundaries	32
Number of edges	71
Number of vertices	48

Point 1: Inlet

Description	Value
Point coordinate	{(width_s/2) - 0.135, depth_s/2}

Point 2: Outlet

Description	Value
Point coordinate	{(width_s/2) + 0.135, depth_s/2}

Bézier Polygon 1

Polygon Segments

Description	Value
Control points	{{(width_s/2) - 0.135, (width_s/2) - 0.09, (width_s/2) - 0.045}, {depth_s/2, depth_s/2, depth_s/2}, {Depth_borehole+5[cm], Depth_borehole, Depth_borehole+5[cm]}}
Degree	2
Weights	{1, 1/sqrt(2), 1}
Type	Open curve

Bézier Polygon 2

Polygon Segments

Description	Value
Control points	{{(width_s/2) + 0.135, (width_s/2) + 0.09, (width_s/2) + 0.045}, {depth_s/2, depth_s/2, depth_s/2}, {Depth_borehole+5[cm], Depth_borehole, Depth_borehole+5[cm]}}
Degree	2
Weights	{1, 1/sqrt(2), 1}
Type	Open curve

Bézier Polygon 3

Polygon Segments

Description	Value
Control points	{{(width_s/2) - 0.045, (width_s/2) - 0.045}, {depth_s/2, depth_s/2}, {Depth_borehole+5[cm], Depth_borehole-(Depth_borehole+0.5)}}

Description	Value
Degree	1
Weights	{1, 1}
Type	Open curve

Bézier Polygon 4

Polygon Segments

Description	Value
Control points	{{(width_s/2) - 0.045, (width_s/2), (width_s/2) + 0.045}, {depth_s/2, depth_s/2, depth_s/2}, {Depth_borehole-(Depth_borehole+0.5), Depth_borehole-(Depth_borehole+0.45), Depth_borehole-(Depth_borehole+0.5)}}
Degree	2
Weights	{1, 1/sqrt(2), 1}
Type	Open curve

Bézier Polygon 5

Polygon Segments

Description	Value
Control points	{{(width_s/2) + 0.045, (width_s/2) + 0.045}, {depth_s/2, depth_s/2}, {Depth_borehole-(Depth_borehole+0.5), Depth_borehole+5[cm]}}
Degree	1
Weights	{1, 1}
Type	Open curve